# Bayesian Methods for the Construction of Robust Chronologies


Sharen Woon Yee Lee

Linacre College

University of Oxford

Thesis submitted in partial fulfilment
of the requirements for the degree of

*Doctor of Philosophy*

Trinity Term 2012

# Abstract

# Bayesian Methods for the Construction of Robust Chronologies

Sharen Woon Yee Lee
Linacre College
Oxford

Doctor of Philosophy
Trinity Term 2012

Bayesian modelling is a widely used, powerful approach for reducing absolute dating uncertainties in archaeological research. It is important that the methods used in chronology building are robust and reflect substantial prior knowledge. This thesis focuses on the development and evaluation of two novel, prior models: the trapezoidal phase model; and the Poisson process deposition model. Firstly, the limitations of the trapezoidal phase model were investigated by testing the model assumptions using simulations. It was found that a simple trapezoidal phase model does not reflect substantial prior knowledge and the addition of a non-informative element to the prior was proposed. An alternative parameterisation was also presented, to extend its use to a contiguous phase scenario. This method transforms the commonly-used abrupt transition model to allow for gradual changes. The second phase of this research evaluates the use of Bayesian model averaging in the Poisson process deposition model. The use of model averaging extends the application of the Poisson process model to remove the subjectivity involved in model selection. The last part of this thesis applies these models to different case studies, including attempts at resolving the Iron Age chronological debate in Israel, at determining the age of an important Quaternary tephra, at refining a cave chronology, and at more accurately modelling the mid-Holocene elm decline in the British Isles. The Bayesian methods discussed in this thesis are widely applicable in modelling situations where the associated prior assumptions are appropriate. Therefore, they are not limited to the case studies addressed in this thesis, nor are they limited to analysing radiocarbon chronologies.

# Acknowledgements

Thanks are due to numerous people for various aspects of the work presented in this thesis. This work has been funded by a Natural Environment Research Council studentship on the Response of Humans to Abrupt Environmental Transitions (RESET) project. Thanks are also due to Linacre College for providing the funding for attending various research related trips for the duration of this work. I am indebted to my supervisor, Professor Christopher Bronk Ramsey, for his endless guidance, encouragement, patience, and expertise in my subject area, which have been inspirational for the course of my study in Oxford.

In terms of academic input, I would especially like to thank Fiona Brock, Michael Dee, Thomas Higham, Christine Lane, Mark Pollard, Richard Staff, and Rachel Wood, from the Research Laboratory of Archaeology and the History of Art, for ideas and assistance throughout this process. More specifically, I would like to thank Geoff Nicholls, for stimulating discussions regarding the trapezoidal phase model and Alex Bayliss for suggesting interesting case studies. I would also like to thank the following colleagues: Nick Barton and Simon Collcutt, for providing information for the Taforalt chronology; Amihai Mazar, for his help with the Iron Age chronology; and Mark Hardiman, for his help with the Cape Riva data set. I would also like to thank J. Andrés Christen and Maarten Blaauw, who organised a very enjoyable and informative Paleochronology Workshop in August 2010, to which I had the privilege of attending. Additionally, I would like to thank members of the RESET team.

On a more personal level, I would like to thank two very good friends, Stephen English, who offered to tutor me in using the `C++` language in exchange for home-made food; and Robert Spanton, who was only a phone call away whenever an I.T. problem arose, of which I took full advantage.

Finally, I must thank my parents, whose love has given me the energy to never give up and achieve my goals, my younger brother, Michael, whose passion and focus towards his own studies have been most inspirational, and John Russell, whose support was unconditional.

# Contents

# List of Figures

# List of Tables

# Chapter 1

# Introduction

Establishing an absolute chronology is very important in addressing archaeological and palaeoenvironmental questions. Different methods of dating, relative and absolute, offer ways to better understand the timing of different archaeological and historical events. Relative dating methods provide the relationship between a group of events and absolute dating methods provide means to measure how old a sample is. However, these methods are not without their associated problems. The former techniques do not provide a calendar time scale, and the latter techniques have their own sources of uncertainty associated with quality assurance, reliability of individual determinations, and the transformation from the scientific time scale to the calendar scale. Radiocarbon dating is the most commonly used scientific dating method, producing absolute dates on the calendar scale after calibration. Buck et al. (1991, 1992) introduced the use of a Bayesian approach, combining radiocarbon determinations (likelihoods) with relative dating information (prior), to provide more precise, accurate, and relevant archaeological information in relation to timing than absolute dates alone (for example, temporal constraints to a groups of groups of events). This approach used in analysing radiocarbon data has also been extended to analysing data from other scientific dating methods (Bronk Ramsey, 2009a; Blaauw and Christen, 2011).

Over the recent decades, Bayesian methods have become popular among archaeol-

ogists and researchers wishing to build chronologies. New models are being developed to more appropriately represent relative dating information (for example, Bronk Ramsey, 2008; Karlsberg, 2006; Blaauw and Christen, 2011).

## 1.1 Research objectives

Some of the mathematical functions of current Bayesian prior models used in archaeological research generate a bias and do not reflect substantial prior knowledge. One example is the uniform prior model described in Buck et al. (1991), which has a bias towards wider date ranges (i.e. the overall span of the model is lengthened by likelihoods with large uncertainties). This was overcome by the introduction of a non-informative prior described in Nicholls and Jones (2001). Another potential problem is that, with numerous different models available, the researcher is faced with the crucial task of model selection. This includes identifying and isolating possible outliers. As a result of this, Christen (1994b) devised an approach of down-weighting outlying ages in model runs, and this method has recently been extended to account for outliers in the calendar scale (Bronk Ramsey, 2009b). Other methods of identifying outliers are also available using pseudo Bayes' factors (Bronk Ramsey, 1995). This still leaves researchers with the non-trivial task of choosing the most suitable prior model for analysing data.

Recent literature introduced robust prior models for chronology construction. They include: the trapezoidal phase prior (Karlsberg, 2006); and the Poisson process deposition model (Bronk Ramsey, 2008). The former models non-abrupt groups (or phases) of related data; and the latter models deposition sequences using an underlying random (Poisson) process. It is the non-abruptness and the randomness that make these models robust. The research presented in this thesis aims to test and identify possible bias in the former phase model, before further development and evaluation. A novel chronological framework is also devised to extend the use of the current trapezoidal phase prior with new parameters. A model averaging ap-

proach is introduced to the latter deposition prior to remove subjectivity in model selection. Its use is also thoroughly evaluated. These two methods are then used to explore different archaeological and palaeoenvironmental case studies. The methods and frameworks described in this thesis are suitable for modelling chronologies dated using any absolute dating techniques; they are not limited to analysing radiocarbon data.

With respect to the precision of data in each of the presented case studies, the resulting chronologies are heavily reliant on the quality of the radiocarbon determinations (likelihoods); as well as the relative information (prior), obtained from various relevant literature and provided by collaborators. This thesis focuses on testing and developing novel Bayesian techniques in archaeological chronology construction. Whilst every effort has been made to ensure that the radiocarbon determinations used are of good quality, the performance of the scientific methods, and the types of material used in dating, as well as assessing the archaeological evidence that underpins the historical chronologies, are beyond the scope of this work.

## 1.2 Thesis outline

This thesis comprises 4 main parts. An account of the background to the research is presented in Part I. This includes highlighting the problems in chronology construction (Chapter 2), describing the theory of the approach to overcoming those problems (Chapter 3), as well as discussing methods of robust chronologies construction (Chapter 4). The development and evaluation of recently developed Bayesian methods are presented in Part II, focusing on two techniques: the trapezoidal phase prior model (Chapter 5); and the Poisson process deposition model (Chapter 6). Applications of the methods to both archaeological and palaeoenvironmental case studies are described in Part III, where comparisons are made between the improved and the old methods using data from different case studies (Chapters 7–9). Finally, concluding remarks are made in Part IV and possible avenues of future research suggested

(Chapter 10).

All references are listed at the end of the thesis, followed by appendices containing (A) computer program listings for the experimental part of Chapter 5 and the first 2 sections in Chapter 7, using the theory and methods described in Chapter 3; (B) data, from literature and collaborators, used in Part III; and (C) the `chronology query language` (`CQL`) used in `OxCal` (Bronk Ramsey, 2009a), outlining the structure of various models in this thesis.

# Part I

# Background

# Chapter 2

# Chronology building and associated complications

When studying the past, it is often essential to know the timing of a particular period or event in order to put it into context with other information. An event, for the purpose of this thesis, is a date of interest. In archaeology, an event can be related to the time when an artefact was used or the death of an organism. In geology, it can be a volcanic eruption or an abrupt environmental change. It can also be a deposition event. Individual events can be dated relatively, by observing the relative ordering of multiple objects; or absolutely, via the use of scientific measurements. Multiple events form the building blocks of any chronology (Bronk Ramsey, 1998). This chapter discusses the different methods of dating, their limitations, and solutions.

## 2.1 Dating

Determining the relationship between multiple events is often the initial step in most archaeological research. This process is known as relative dating, where events are put into sequences. Deposits from an excavation can be put into a stratigraphic sequence, and artefacts can be put into a typological sequence. Understanding that an event occurred before another is a crucial step in chronology construction.

Ultimately, however, it is useful to know the absolute age in calendar years of the different parts of the relative sequence and methods of absolute dating are needed. Absolute dating depends on the existence of a regular, time-dependent process (Renfrew and Bahn, 2008, p.137). It provides a measured age (also known as the 'absolute age') of a sample based on its physical and chemical properties. The absolute age is independent of any chronologies or dating techniques. Different absolute dating methods are used for different types of samples, measuring different physical and chemical properties, and cover different parts of the calendar scale.

Both relative and absolute dating are widely used to construct chronologies in archaeology and environmental science. There are many different types of relative and absolute dating methods, and sometimes, absolute dating can provide information that can be used relatively. This chapter discusses a selection of these methods, which provide building blocks for the chronologies constructed in the later parts of this thesis.

### 2.1.1 Typology

In archaeology, typology (Brainerd, 1951; Robinson, 1951) is the classification of artefacts according to their characteristics (or types). A type is a series of attributes, for example, decorations, material, and shape, which distinguishes one group of artefacts from all other groups of artefacts. The underlying assumption of typology is that each type with the same style belongs to a certain period and originated from the same region or culture. Archaeologists often use this relative method to date a site, or strata at a site, and identify trade routes. This method forms the backbone of many chronological systems, including the hotly debated Iron age chronology in the Levant, which is discussed in Section 7.3.

### 2.1.2 Tephrochronology

Tephra is volcanic ash from an eruption. Tephrochronology is a technique which uses tephra to provide chronology for a site of interest. Following an eruption, tephra particles become airborne and get deposited downwind of the volcanic source. Deposition of tephra layers is instantaneous (within the uncertainty of absolute dating) and often widespread (e.g. Lowe, 2011). It provides tephra horizons. They can be visible or non-visible to the naked eye. Non-visible tephra is also known as microtephra or cryptotephra (Lowe and Hunt, 2001).

Tephra particles from different volcanic eruptions have different chemistry. They can, in many cases, be distinguished by their unique chemical fingerprint. Tephra horizons provide a basis for absolute dating, either directly using argon isotopes (e.g. Laacher See Tephra (LST); van den Bogaard, 1995) or indirectly using carbon isotopes (e.g. Cape Riva tephra; Eriksen et al., 1990; Pichler and Friedrich, 1976) or via the counting of annual increments (e.g. LST; Brauer et al., 1999). Tephra horizons are important because they provide independent, physical links for correlation between different sites. Once dated directly, the tephra becomes a time marker for different records.

### 2.1.3 Annual increments

Yearly cycles, i.e. the rotation of the earth around the sun once a year, cause regular annual fluctuations in climate. This changes certain features of the environment, which are recorded, for example in trees, lake sediments, and ice cores, and can be measured to create a chronology. The counting of annual increments (or laminations) can be relative, if the chronology does not date to present day, i.e. a floating chronology; or it can be absolute, if the chronology dates to present day.

### 2.1.4 Potassium-argon and argon-argon dating

Potassium-argon (K-Ar) dating is an absolute dating technique used for establishing the age of volcanic rocks. $^{40}$K is an unstable (radioactive) nuclide that undergoes beta decay to both $^{40}$Ca (88.8%) and $^{40}$Ar (11.2%) (Faure, 1986).

$$^{40}\mathrm{K} \rightarrow ^{40}\mathrm{Ca} + \mathrm{e}^{-} + \bar{\nu}_e$$

The conversion of $^{40}$K to $^{40}$Ar is achieved via positron ($e^+$) emission and electron ($e^-$) capture. In both cases, an electron neutrino ($\nu_e$) is produced.

$$^{40}\mathrm{K} \rightarrow ^{40}\mathrm{Ar} + \mathrm{e}^{+} + \nu_e$$

$$^{40}\mathrm{K} + \mathrm{e}^{-} \rightarrow ^{40}\mathrm{Ar} + \nu_e$$

The age of the sample is determined by measuring the radioactive decay of the unstable potassium isotope, $^{40}$K, with a half-life of 1250 million years (Steiger and Jäger, 1977), to $^{40}$Ar.

Argon-argon ($^{40}$Ar/$^{39}$Ar) dating was developed as a replacement for K-Ar dating to improve reliability. In $^{40}$Ar/$^{39}$Ar dating, the stable form of $^{39}$K is converted to $^{39}$Ar and the amount of $^{39}$Ar is measured at the same time as $^{40}$Ar. This approach is considered more reliable because only Ar isotopes are measured and has the advantage of being able to date very small samples, for example, tephra (Lowe and Walker, 1997, p.249).

### 2.1.5 Radiocarbon dating

Carbon is one of the most important building blocks of life. It is an element found in all organic compounds. It has two naturally occurring stable isotopes, $^{12}$C and $^{13}$C, which make up 99% and 1% of carbon respectively. Unstable, radioactive $^{14}$C (also known as radiocarbon) make up $10^{-10}$% of carbon in nature. The numbers refer to the atomic mass of the different isotopes and it is the existence of the unstable

radioactive $^{14}$C that enables radiocarbon dating. It is the most widely used method of dating and forms the majority of the supporting data for the chronologies in this thesis, hence, it is discussed in more detail below.

#### 2.1.5.1 Background and basic principles

The radioactive isotope of carbon, $^{14}$C, is continually formed in the upper atmosphere. Cosmic rays undergo transformation when entering the atmosphere and produce neutrons (n). Neutrons participate in a nuclear reaction with the nitrogen in the atmosphere to form $^{14}$C and a proton (p):

$$\mathrm{n} + {}^{14}\mathrm{N} \rightarrow {}^{14}\mathrm{C} + \mathrm{p}$$

Upon formation, the $^{14}$C reacts with oxygen, oxidises rapidly to $^{14}$CO and slowly to $^{14}CO_2$ (Weinstock, 1969). The $^{14}CO_2$ is mixed throughout the atmosphere, exchanges with the ocean, and may also enter the food chain via photosynthesis. $^{14}$C is unstable and goes through beta decay to produce $^{14}$N, an electron ($e^-$) and a antineutrino ($\bar{\nu}_e$):

$$^{14}\mathrm{C} \rightarrow {}^{14}\mathrm{N} + \mathrm{e}^- + \bar{\nu}_\mathrm{e}$$

The amount of atmospheric $^{14}$C is, in principle, in equilibrium with the amount of $^{14}$C in a living organism. Once the organism dies, the uptake of $^{14}$C stops.

There are two ways of radiocarbon dating: radiometric and using accelerator mass spectrometry (AMS). The former was first developed by Libby and his group. It detects the beta particle emitted during radioactive decay of the sample. Radiocarbon decays at a constant rate and the half-life was first measured to be 5568±30 years (Arnold and Libby, 1949; Libby et al., 1949; Libby, 1955), also known as Libby's half life. This was later replaced by the 'Cambridge' half life of 5730±40 years (Godwin, 1962). Libby's half-life continues to be cited by convention and the difference is accounted for in calibration. In contrast, AMS directly measures the proportion of $^{14}$C atoms relative to $^{12}$C or $^{13}$C atoms in the sample. Both methods use modern

standards such as oxalic acid and background samples containing very low levels ($<10^{-15}$ $^{14}C/^{12}C$) of carbon, which is insufficient $^{14}C$ for dating, as reference materials. Although measured differently, the absolute dates produced by both methods can be interpreted in the same way.

Whilst being very popular and useful, radiocarbon dating, like many other dating methods, is not without its issues and these are discussed below.

#### 2.1.5.2 Radiocarbon samples

The selection of samples is one of the most important first steps in dating. Any organic remains can be radiocarbon dated. Single entity, short-lived, and articulated samples provide confidence that they do indeed relate securely to the context dated, and hence are preferred. After selecting the appropriate samples, they are chemically treated to remove both modern and ancient contaminations before they can be dated. The dating of animal, plant (including charcoal), and insect remains provides the age of death of the organism. However, older dates were often radiometric, needing larger sample size, so bulk materials were often used. The dating of bulk sediment (peat) samples can be problematic.

Peat is an accumulation of different organic matter at various stages of degradation and humification. It can, like other organic material, be troublesome to date. Peat has three chemical components: humins, which is acid and alkali insoluble; humic acids, which is acid insoluble, alkali soluble; and fulvic acids, which is acid and alkali soluble (Shore et al., 1995; Cook et al., 1998). Humin is the solid residue of the plant remains and is usually regarded as the most representative of the original vegetation, although it may still be contaminated with in-wash or intrusive carbon (e.g. Dugmore et al., 1995; Waller et al., 2006). Humic and fulvic acids are soluble (can be separated on the basis of pH) and more mobile. Fulvic acid is often found to be younger than both other corresponding fractions (Shore et al., 1995). The more mobile components are likely to leach downwards and some studies find humic acids to be younger than the humins (Williams, 1989). Some find that humins provide ages closest to the

those obtained from macrofossills (McGeehin et al., 2001), which would be the ideal material to date if found in sediments, and represents the 'true age' (Bartley and Chambers, 1992); other argue that humic acid dates are the most reliable (Johnson et al., 1990). The different fractions may also provide statistically indistiguishable dates (Cook et al., 1998). Different grain size fractions of peat deposit has also been investigated. Studies have found that the humin dates get older with increasing grain size (Nilsson et al., 2001; Brock et al., 2011) and the humic acid dates can be both older or younger than the humins of the corresponding grain size (Brock et al., 2011). Blaauw et al. (2004) found that bulk peat samples yield the same results as above ground plant remains. Considering all of the above case studies, it is difficult to conclude which fraction provides the most reliable radiocarbon age. The limited availability of radiocarbon dated chronologies using short-lived plant remains means that, unfortunately, some of the environmental case studies in this thesis had been dated using bulk peat sediments.

#### 2.1.5.3 Calibration

A radiocarbon measurement is an estimate of radiocarbon content based on a set of physical measurements (Renfrew and Bahn, 2008, p.146). Unfortunately, it does not reflect the true calendar age of the sample. This is because the level of atmospheric radiocarbon fluctuates slightly from year to year due to changes in the carbon cycle and in atmospheric conditions caused by sunspot activity and changes in the geomagnetic field. This leads to difficulty in estimating the calendar age of a sample directly. The first step in interpreting the result from radiocarbon dating is calibration. It is this calibration process that makes radiocarbon an absolute dating method. It is essential for determining the calendar age of a sample, and for comparing the radiocarbon ages with other records dated using other absolute dating techniques.

Radiocarbon calibration curves are needed in order to estimate the calendar age of a sample. The most recent consensus terrestrial and marine radiocarbon curves are IntCal09 and Marine09 respectively (Reimer et al., 2009). The amount of radio-

carbon in ocean water differs from that in the atmosphere, hence the need for two curves. This is because the process of carbon exchange between the atmosphere and living organisms in the deep water is slower. Samples from a marine environment tend to be 400 years older on average than terrestrial samples from the same period (Stuiver and Braziunas, 1993). IntCal09 is made up of dendrochronologically dated records up to 12,550 years before present (BP) and various marine sediments and coral records for 12,550-50,000 years BP. Whilst being very useful, IntCal09 is not without the uncertainties arising from marine correction. Contiguous terrestrial varved lake records (Stuiver, 1971; Kitagawa and van der Plicht, 1998, 2000; Wohlfarth and Possnert, 2000; Staff et al., 2010) would eliminate these uncertainties. The process and statistics involved in calibration will be discussed in Section 3.4.1. In this thesis, radiocarbon determinations are cited as "BP", where BP stands for years before 1950 AD; dates "BC", "BCE", "AD", or "CE" are historical dates on the calendar scale; "cal BC", "cal BCE", "cal AD", or "cal CE" are calibrated radiocarbon or modelled ages on the calendar scale.

Calibration of radiocarbon determinations adds an extra level of complication when it comes to interpreting radiocarbon chronologies. Due to the oscillations in the calibration curves, a calibrated age is often a multi-modal distribution spanning several centuries, giving an imprecise estimation. Calibration aside, other sources of uncertainty (e.g. contaminated, residual, or intrusive samples) would result in inaccurate estimations.

## 2.2 Accuracy and precision

A common analogy for accuracy and precision is bullets on a target. Multiple firings close to the bullseye is considered accurate and precise, far away and scattered from the bullseye is imprecise and inaccurate. In terms of dating, accuracy refers to the degree to which the measurement matches the true date of the sample, and precision refers to the degree of refinement in a measurement.

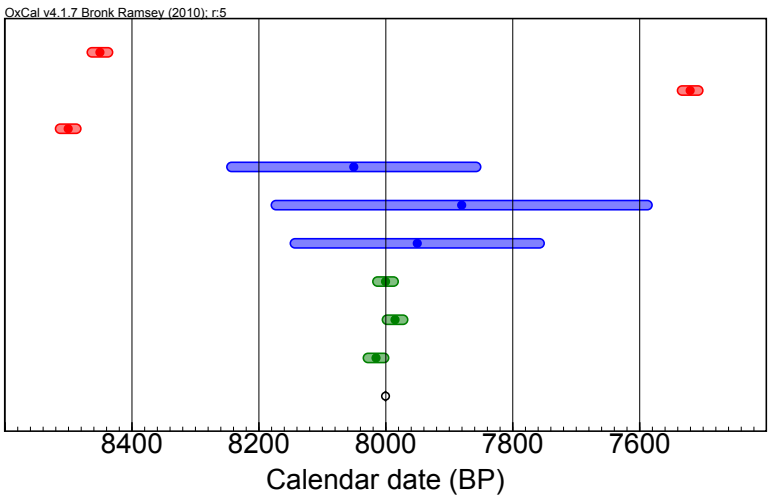


Figure 2.1: Accuracy and precision in dating (Lowe and Walker, 1997; Walker, 2005). The 'true' age of sample is 8000 BP (white dot). See text for details.

Figure 2.1 shows multiple measurements of the same sample, which has a 'true' age of 8000 BP (marked by the white dot). The measurements in red are precise with small standard errors. They are, however, inaccurate because they are far away from 8000 cal BP. The measurements in blue are close to 8000 cal BP but with large standard errors, hence they are accurate but imprecise. The measurements in green have small errors and are close to 8000 cal BP, and thus are accurate and precise.

If only one measurement is made, it is difficult to determine if said measurement is accurate. This is often the case in archaeology and environmental science, where the availability of sample materials is limited, absolute dates are expensive to obtain, and preservation and contaminations are often problems of concern. Small and old samples often have large associated uncertainties. Calibration adds another level of uncertainty because the resulting calendar age is often multi-modal.

Bayesian statistics provides a solution to this problem. Using a Bayesian framework, one could construct a chronology with both absolute and relative dating information (Buck et al., 1991, 1992). The resulting output often provides more accurate and refined chronologies, a simulated example is shown in Figure 2.2.

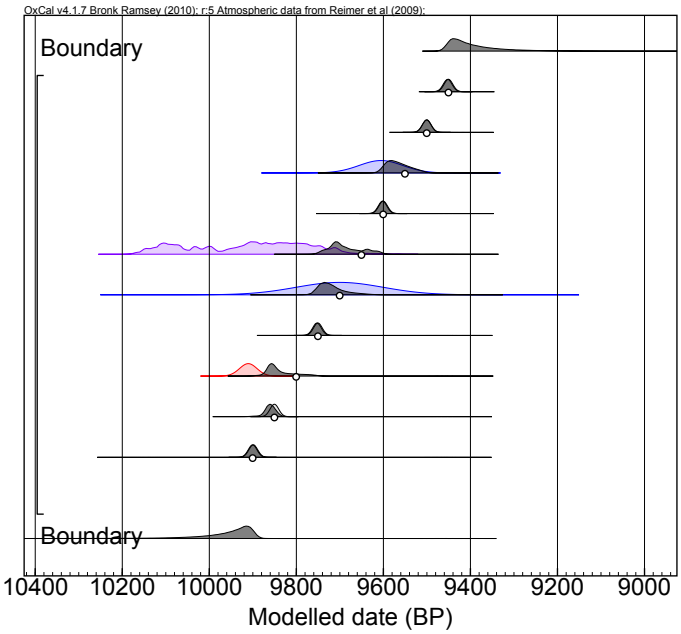


Figure 2.2: Figure showing a chronology (in grey) after applying a Bayesian framework with order constraints (see Section 3.4.3). The 'true' chronology is marked by the white dots. The inaccurate (red) and imprecise (blue) Gaussian ages and radiocarbon age (purple) are more accurate and precise after modelling.

## 2.3 The Bayesian solution

Bayesian inference provides a tool for combining results from relative dating (also known as prior) information, obtained from archaeological and / or environmental evidence; and absolute dating (also known as likelihood) information, measured directly from samples from the same context, to enhance the precision and accuracy of chronologies. The employment of Bayesian statistics in archaeology is discussed in more detail in Section 3.4. In recent decades, this technique has been made freely available, and easily accessible, to a wide community of researchers wishing to build chronologies via the use of chronology building software such as `OxCal` (Bronk Ramsey, 1995, 2001, 2009a) and `BCal` (Buck et al., 1999), which have a wide range of different models; and `Bpeat` (Blaauw and Christen, 2005), `Bchron` (Haslett and Parnell, 2008; Parnell et al., 2008), and `Bacon` (Blaauw and Christen, 2011), which have individual statistical models within each package.

The availability of different models provides researchers with the freedom of using

specific models for different event scenarios. Until recently, one was unable to address archaeological questions involving processes with slow transitions (e.g. Housley et al., 1997; Zeidler et al., 1998; Van Strydonck et al., 2004; Blackwell and Buck, 2003; Buck and Bard, 2007). Karlsberg (2006) introduced a prior, in the shape of a trapezoid, for modelling such transitional processes. However, the trapezoidal prior is not without its limitations. Chapter 5 discusses its limitations, proposes and evaluates two important developments, making the model more robust and allowing its use in a contiguous / abutting phase scenario.

The freedom of model selection often poses a dilemma for researchers because multiple priors might be suitable for modelling the same event scenario. Since the choice of prior (relative) information is subjective, and the output from a Bayesian model is heavily dependent on the choice of prior, the output may be biased if the wrong model is chosen. A method called Bayesian model averaging removes the need for subjective model input. This technique is currently employed in outlier analysis (Christen, 1994b; Bronk Ramsey, 2009b). It is a very powerful approach and can also be used for choosing the suitable prior model for a data set. The model averaging approach is discussed in further detail in Section 4.3.2.2 and the application of the method to an age-depth model is evaluated in Section 6.4.

# Chapter 3

# Bayesian statistical modelling

There are two approaches to statistics: the frequentist (also known as classical) approach; and the Bayesian approach. The former makes inferences based on the data obtained. It does so by calculating the likelihood probability distribution from the situation. The Bayesian approach makes inferences, *posterior* probability, by combining *prior* information with *likelihood* function(s). It uses Bayes' theorem, which is described below. Both frequentist and Bayesian statistical approaches have been used in chronology construction (e.g. Grimm et al., 1993; Bennett, 1994; Boreux et al., 1997; Buck et al., 1991, 1992; Bronk Ramsey, 1995; Blaauw, 2010). The former can sometimes produce (erroneously) narrow error ranges and the latter takes into account the uncertainties in dating, improving the accuracy and precision of absolute age measurements. This thesis features modelling (primarily radiocarbon) chronologies with the latter approach, thus, only Bayesian inference will be discussed from this point forward. The methods of Bayesian calculations described in this chapter are used in the experimental parts of Chapter 5, for investigating the limitations of a recently developed prior model; and in Chapter 7, for addressing archaeological questions. The computer program listings are available in appendix A.

## 3.1 History

Bernoulli (1713) (in Bernoulli (2006)) first articulated the issue of using inference to solve inductive problems. Reverend Thomas Bayes provided an answer to Bernoulli's problem in a paper published posthumously by Bayes and Price (1763). The paper discusses the inference of the parameters of a binomial distribution using observational data. Early forms of Bayesian inference were called "inverse probability" (Stigler, 1986). The present day version of the theorem was finalised by Laplace (1812) (in Langou (2009)).

## 3.2 Bayes' theorem

Bayes' theorem, named after Thomas Bayes, states that

$$p(x|y) = \frac{p(y|x) \times p(x)}{p(y)}$$

where

- $p(x)$ is the prior knowledge about the values of parameter $x$ before obtaining the data $y$. In terms of archaeology, this is the relative information obtained from excavations.
- $p(y|x)$ is the likelihood of obtaining the observations if the parameters were known. These are the probability density functions obtained from absolute dating.
- $p(y)$ is the (marginal) probability of obtaining the observed data integrated over all possible values of the parameters.
- $p(x|y)$ is the posterior distribution incorporating the prior knowledge and the likelihood, thus what we seek to obtain.

$p(y)$ can also be thought of as the normalising constant. Bayes' theorem can also be written as

$$p(x|y) \propto p(y|x) \times p(x) \tag{3.1}$$

or in words: The posterior *it proportional to* the likelihood *times* the prior.

### 3.2.1 *A priori*

*A priori* is a Latin phrase that means "from what comes before". It relates to the information or knowledge available before the observations are made. This is a familiar concept and is applied in everyday life.

The use of prior information forms the fundamental difference between frequentist statistics and Bayesian statistics. Prior information is usually formulated as a single numerical statement or as a probability density function. This information is usually deduced from relevant literature or is elicited by experts in the field. In terms of archaeology, prior information could include related, for example, ceramic or regional, groups (or phases) and stratigraphic information obtained from excavations.

Prior modelling is important for a small sample populations. It becomes less important as the sample population increases. Archaeological and environmental materials are usually scarce and their sample sizes often limited. Thus, chances to experiment with the samples are restricted. Prior knowledge, therefore, becomes very important.

There are a number of different types of prior information used within the Bayesian framework; informative prior, non-informative prior, conjugate prior, and improper prior.

#### Informative prior

An informative prior expresses specific, definitive, information about a variable. Informative priors arise from knowledge of the data obtained from previous studies. This is the most obvious form of prior information used in a Bayesian framework. In

terms of archaeology, this is the relative information.

#### Non-informative prior

A non-informative prior expresses vague or general information about a variable. Non-informative priors can express objective information such as the "variable is positive" or "the variable is less than some limit". The application of non-informative priors can make a significant difference to some data sets (e.g. Nicholls and Jones, 2001). In Chapter 5, a non-informative prior element is introduced to remove the existing bias in the trapezoidal phase prior.

#### Conjugate prior

As its name suggests, a conjugate prior "conjugates" itself to the likelihood function. A conjugate prior provides a first approximation to the adequate prior distribution.

#### Improper prior

An improper prior has an integral that does not equal one. It can sometimes be used as a non-informative prior. Such a distribution can be used in Bayesian statistics as long as the posterior distribution is not also improper.

### 3.2.2 *Likelihood*

The likelihood function is the information brought by an observation. It is the probability of obtaining a particular set of data. In archaeology, the probability density functions obtained from absolute dating, for example, calibrated ages in a radiocarbon chronology, form the likelihood functions.

### 3.2.3 *A posteriori*

*A posteriori* is a Latin phrase that means "from what comes later". It relates to the information which is held after observations are made. It is derived from combining *a priori* information with likelihood functions.

## 3.3 Bayesian calculations

Although the idea of using Bayesian inference to address inductive problem was suggested centuries ago, its use was restricted by the limited computing power that was available at the time. This is because the calculation of eq. 3.1 is not always straightforward. The advances in computing power in recent decades allowed the use of simulation techniques to facilitate Bayesian calculations and Markov Chain Monte Carlo is the most commonly used simulation technique in chronology construction in archaeology.

### 3.3.1 Markov Chain Monte Carlo methods

Markov Chain Monte Carlo (MCMC) is a general form of Monte Carlo method. Monte Carlo methods are a class or computational algorithms that rely on repeated random sampling to generate results. They are used when simulating physical and mathematical systems, where it is impossible to compute an exact result with a deterministic algorithm. They are, therefore, useful for modelling phenomena with significant uncertainty in inputs. They are used to generate a posterior distribution when this distribution cannot be analytically calculated.

Monte Carlo methods refer to a large and widely used class of approaches and these approaches tend to follow a particular pattern (Gilks et al., 1996):

- Define a domain of possible inputs
- Generate inputs randomly from the domain
- Perform a deterministic computation using the inputs
- Aggregate the results of the individual computations into the final result

In order to explain MCMC in greater detail, it is broken down into two stages:

### Monte Carlo integration

Monte Carlo integrations are algorithms for the approximate evaluation of definite, usually multidimensional, integrals. Random numbers, $\{X_j : j = 1, \ldots, n\}$, are chosen over some simple domain, $f(X)$, which is a superset of the (complicated unknown) function, $\pi(.)$, of interest. Deterministic computations are performed to check to see if the points chosen are within $f(X)$, before the distribution of $\pi(.)$ is estimated. The law of large numbers (Bernoulli, 1713, 2006) ensures that the approximation can be made as accurate as desired by increasing the sample size $n$. In the case of MCMC, $n$, the number of repeated computations (iterations), is under the control of the analyst.

The Markov chain is a method of Monte Carlo integration, which is frequently employed in archaeological research.

### Markov chain

A Markov chain is a random process where all information about the future state is contained in the present state, i.e. the future states depend only on the present state, and is independent of the past states. The description of the present state fully captures all the information that could influence the future evolution of the process. The development of the Markov chain is a stochastic process, where all state transitions are determined by random chance.

Suppose a sequence of random variables, $\{X_0, X_1, X_2, \ldots\}$, is generated such that for each time, the state $X_j \geq 0$, the next state, $X_{j+1}$, is sampled from a distribution $p(X_{j+1}|X_j)$, which depends only on the current state of the chain, $X_j$. That is, at any given state, let this be $X_t$, the next state $X_{t+1}$ does not depend further on the history of the chain $\{X_0, X_1, \ldots, X_{j+1}\}$. This sequence is called a Markov chain. Subject to the regularity conditions, the chain will gradually 'forget' its initial state and will eventually converge to a unique stationary distribution, $\pi(.)$, which does not depend on $t$ or $X_0$. As $t$ increases, the sample points $\{X_j\}$ will look increasingly like dependent samples from $\pi(.)$. MCMC can be applied to a wide field, although its performance varies depending on the complexity of the problem (Gilks et al., 1996).

It is difficult to determine the number of steps needed to converge to a stationary distribution within an acceptable error. Reaching the stationary distribution quickly starting from an arbitrary position indicates a good Markov chain. Some MCMC methods are explained in more detail below.

#### 3.3.1.1 Gibbs sampler

Gibbs sampling, also known as Gibbs sampler, was introduced in the context of image processing by German and German (1984). The key to the Gibbs sampler is that only univariate conditional distributions are considered - the distributions when all of the random variables but one are assigned fixed values. Such conditional distributions are easier to simulate than complex joint distribution and usually have simple forms.

If one wishes to compute one of both marginal distributions, $p(x)$ and $p(y)$ of a bivariate random variable $(x, y)$, it is easier to consider a sequence of conditional distributions, $p(x|y)$ and $p(y|x)$, than it is to obtain the marginal by integration of the joint density $p(x, y)$. The Gibbs sampler starts with some initial value $y_0$ for $y$ and obtains $x_0$ by generating a random variable from the conditional distribution $p(x|y = y_0)$. The sampler then uses $x_0$ to generate a new value of $y_1$, drawing from the conditional distribution based on the value $x_0$, $p(y|x = x_0)$.

The process is repeated $n$ times, generating a Gibbs sequence of length $k$, where a subset of points $(x_j, y_j)$ for $1 \leq j \leq m \leq n$ are taken out from the full joint distribution. To obtain the desired total of $m$ sample points, one samples the chain after a sufficient number of iterations to remove the effects of the initial sampling values and at set time points. The Gibbs sequence converges to a stationary distribution that is independent of the starting values, and this stationary distribution is the target distribution we are trying to simulate.

The Gibbs sampler is particularly useful in high dimensional problems, when it is possible to sample from each of the one dimensional conditional distributions. It takes advantage of hierarchical structure. Suppose that there are $k$ parameters $t_a, \ldots, t_k$ of interest, denoted by $t$, and we wish to make inference about their joint posterior

distribution, $p(t|x)$, as well as their marginal posterior distributions $p(t_i|x)$. Then the Gibbs sampler can be used to sample from the conditional distributions in the following way (Gilks et al., 1996):

1. Choose arbitrary starting values $t^0 = \{t_1^0, t_2^0, \ldots, t_k^0\}$
2. Generate a series of random values $t^{(1)}, t^{(2)}, \ldots, t^{(t)}$ in the following way:
   - draw $t_1^{(1)}$ from $p(t_1|x, t_2^{(0)}, \ldots, t_k^{(0)})$,
   - draw $t_2^{(1)}$ from $p(t_2|x, t_1^{(1)}, t_3^{(0)}, \ldots, t_k^{(0)})$,
   - draw $t_3^{(1)}$ from $p(t_3|x, t_1^{(1)}, t_2^{(1)}, t_4^{(0)}, \ldots, t_k^0)$,
     $\vdots$
   - draw $t_k^{(1)}$ from $p(t_k|x, t_1^{(1)}, t_2^{(1)}, \ldots, t_{k-1}^{(1)})$.

   This completes one iteration of the algorithm.
3. Repeat step 2 for $n$ iterations.

The idea behind the Gibbs sampler is to draw samples from the posterior distributions $p(t_i|x)$ using Markov Chains which have the stationary distribution, $\phi(t_i) = p(t_i|x)$. In particular, as $n \to \infty$, $t_i^{(h)}$ tends to a random quantity whose density is $p(t_i|x)$. Thus for large $h$, the values $(t_1^{(h)}, \ldots, t_k^{(h)})$ are approximately a random sample from $p(t|x)$.

The Gibbs sampler is a special case of Metropolis-Hastings sampling wherein the random value is always accepted. It was originally introduced to solve archaeological problems by Buck et al. (1991, 1992).

#### 3.3.1.2 Metropolis-Hastings algorithm

The Metropolis-Hastings algorithm was constructed by Metropolis et al. (1953), originally for physics and generalised by Hastings (1970) in a more statistical setting. It applies to a wide variety of problems, since its main restriction is that the distribution of interest be known up to a constant. This algorithm allows an infinite number of proposal distributions,, that yield a Markov Chain, to converge to a distribution of interest.

For the Metropolis-Hastings algorithm, at each time $j$, the next state $\{X_{j+1}\}$ is chosen by first sampling a candidate point $Y$ from a proposal distribution $q(.|X_j)$. The candidate point $Y$ is then accepted with probability $\alpha(X_j, Y)$ where

$$\alpha(X_j, Y) = min\left(1, \frac{\pi(Y)q(X|Y)}{\pi(X)q(Y|X)}\right) \tag{3.2}$$

If the candidate point is accepted, the next state becomes $X_{j+1} = Y$ and if the candidate point is rejected, the chain does not move, i.e. $X_{j+1} = X_j$.

The Metropolis-Hastings algorithm can be summarised as (Gilks et al., 1996, p.7):

Initialise $X_0$; set $t = 0$

Repeat {

Sample a point $Y$ from $q(.|X_t)$
Sample a uniform $(0, 1)$ random variable $U$
If $U \leq \alpha(X_j, Y)$ set $X_{j+1} = Y$
otherwise set $X_{j+1} = X_j$
Increment $t$

}

The proposal distribution $q(.|.)$ can have any form and the stationary distribution of the chain will be $\pi(.)$. Once a sample from the stationary distribution has been obtained, all subsequent samples will be from that distribution. In this case, only symmetric proposals, having the form $q(Y|X) = q(X|Y)$ for all $X$ and $Y$ (Gilks et al., 1996, p.9), are used. Hence, the ratio of $q(X|Y)/q(Y|X)$ from eq. 3.2 is always 1 and can be ignored. This applies to all of the Bayesian calculations described in Chapter 5. In cases where the proposal distribution is not symmetric, $q(Y|X) \neq q(X|Y)$, the ratio of $q(X|Y)/q(Y|X)$, must be account for.

**Single-component Metropolis-Hastings**

Instead of updating the whole of $X$ *en bloc*, it is often more convenient and computationally efficient to divide $X$ into components $\{X_1, X_2, \ldots, X_i\}$ of possibly differing

dimension, and then update these components one by one. This was the framework for MCMC originally proposed by Metropolis et al. (1953), and it is referred as *single-component Metropolis-Hastings*.

An iteration of the single-component Metropolis-Hastings algorithm comprises $h$ updating steps. A fixed updating order is normally assumed, although it is not necessary. Random permutations of the updating order are quite acceptable. The $i$th update of $X$ at iteration $j$ may depend of the current values of any of the components of $X$, i.e. $X_{(i)}^{j} = \{X_1^j, X_2^j, \ldots, X_{i-1}^j, X_{i+1}^{j-1}, X_{i+2}^{j-1}, \ldots, X_h^{j-1}\}$, where $X_{(i)}$ denotes all $X$ except the $i$th element.

The single-component Metropolis-Hastings algorithm is the method used to construct the trapezoidal prior model described in Chapter 5 for efficiency.

## 3.4 Bayesian statistics in Archaeology

Bayesian statistical tools are now routinely used by many researchers who wish to construct a formal model, incorporating *a priori* knowledge and suitable data (*likelihoods*), to arrive at *a posteriori* inferences. More than two decades ago, tools were developed for formal chronology building (Naylor and Smith, 1988). Initially, attention was focused on the calibration and interpretation of radiocarbon data; very soon after that, it became apparent that the Bayesian statistical framework is ideally suited to the integration of relative chronological information from a range of different sources, in particular stratigraphic sequences and historical evidence, with absolute dating information (Buck et al., 1991, 1992, 1994; Bronk Ramsey, 1995; Litton and Buck, 1996; Buck and Christen, 1998).

There are two main types of prior information one could build into a Bayesian model for analysing chronological records: groupings (or phases) and sequential information. The former allows the researcher to group together related data; this can be samples from the same culture, region, or even sediment blocks, using mathematical functions. The latter allows the ordering of data to be constrained and this is par-

ticularly useful in sedimentary records. The two types of prior information can also be used together for more complex models. Other assumptions also include regional offsets and the probability of a particular sample being an outlier.

### 3.4.1 Radiocarbon age calibration

When a sample is dated using radiocarbon, we are interested in obtaining the unknown calendar age at which the organic material ceased metabolising. Let this calendar age be $x_i$, measured in calendar years BP (cal BP). This calendar age has a uniform prior

$$p(x_i) \sim U(-\infty, \infty)$$

(Bronk Ramsey, 2009a) which is an improper prior. However, it can be used because the posterior for this age is not improper. If measured using carbon isotopes, this sample will have a known radiocarbon determination, $y_i$, which is a realisation of the random variable $Y$. $Y$ can be represented as

$$Y = r(x_i) + \epsilon$$

, where the radiocarbon concentration is $r(x_i)$ and $\epsilon$ is the uncertainty associated with the experimental error in the dating process. Both $r(x_i)$ and $\epsilon$ are provided by the radiocarbon laboratory. The associated error, $\epsilon$, is represented as normally distributed with mean 0 and $\sigma_i(x_i)$, as the standard deviation.

$$\epsilon \sim N(0, \sigma_i^2(x_i))$$

$Y$ is modelled using a Gaussian distribution and depends upon the unknown parameter $x_i$. The counts of radioactive decay of the unstable carbon isotopes have a Poisson distribution which is approximated by the Gaussian distribution

$$Y \sim N(r(x_i), \sigma_i^2(x_i)) \tag{3.3}$$

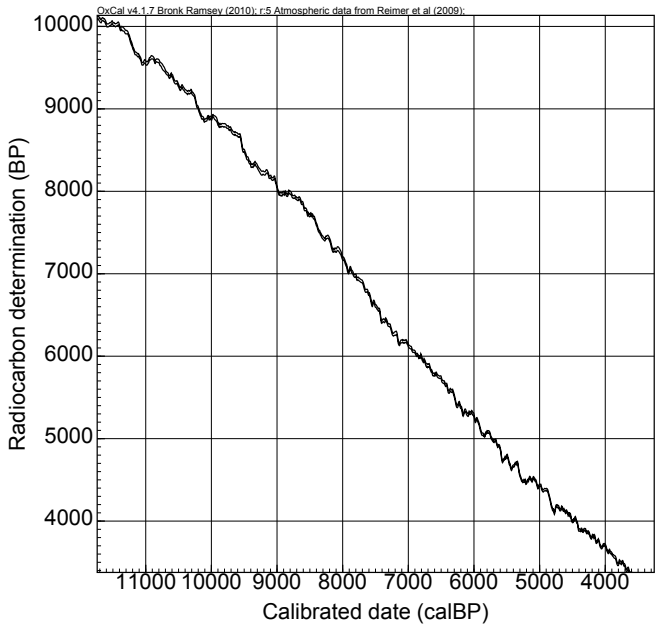


Figure 3.1: A section of the high precision radiocarbon calibration curve IntCal09 (Reimer et al., 2009) for calibrating terrestrial dates.

where $r(x_i)$ represents the radiocarbon calibration curve with uncertainty modelled as (Christen, 1994a,b)

$$\sigma_i^2(x_i) = s_i^2 + s^2(x_i) \tag{3.4}$$

Using a Bayesian framework, the unknown calendar age can be calculated using information provided by the measured radiocarbon determination and the calibration curve. A likelihood distribution based on equations 3.3 and 3.4 is obtained

$$p(y_i|x_i) \propto \frac{1}{s_i^2 + s^2(x_i)} exp(-\frac{(r_i - r(x_i))^2}{2(s_i^2 + s^2(x_i))}) \tag{3.5}$$

In the absence of informative prior information, the convention is to assume that the prior value for $x_i$ is equally likely to lie anywhere over the range of the calibration. This is usually represented using a uniform prior for $x_i$, implying that the posterior density (calibrated radiocarbon age distribution), $p(x|y)$, is essentially equivalent to the likelihood. Due to the non-linear nature of the calibration curve (Fig. 3.1), the likelihood distribution can often be non-symmetric and multi-modal, which can make interpretation difficult (Fig. 3.2).

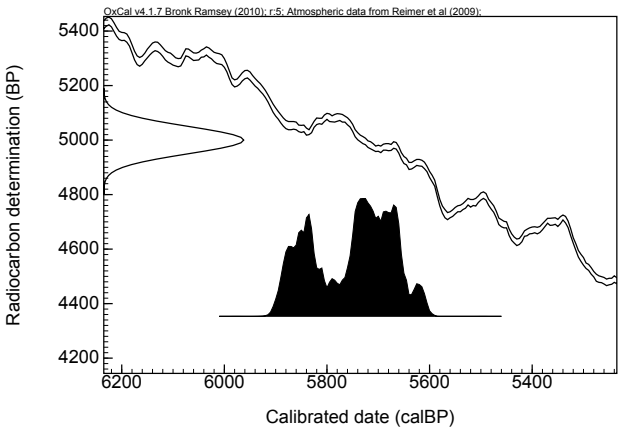


Figure 3.2: Calibration of a radiocarbon determination. The Gaussian distribution on the right is the uncalibrated radiocarbon determination. The irregular oscillating diagonal line is the calibration curve at one standard error and the black distribution at the bottom is the posterior density of unmodelled data.

### 3.4.2 Groupings / Phases

Grouping is very important in the modelling of archaeological data. If group information is not specified, the data is assumed to be unrelated and independent; and the output from the model will reflect that assumption (Nicholls and Jones, 2001). The most frequently used prior assumption is that a group (or phase) of events is uniformly distributed (Buck et al., 1992) between two `boundary` parameters. Let $\{x_i, i = 1, \ldots, n\}$ be the events in a single uniform phase model on the calendar scale. For a single phase within two `boundary` parameters, $t_a$ and $t_b$, where $t_a < t_b$, the prior for the group is

$$p(\mathbf{t}) \propto p_H(t_a, t_b) \prod_{i=1}^{n} \frac{p_H(t_a, x_i, t_b)}{(t_b - t_a)} \tag{3.6}$$

where $n$ is the number of events in the group.

The uniform phase model can be used singly, to model one group of data; or it can be used in a multiple phase scenario, to model multiple groups of related data. The relationships between multiple phase can be defined as: *overlapping*, where the phases are independent of each other; *sequential*, where hiatuses exist between the phases, and that the end of the earlier phase is constrained to be before the start of the later phase; and *contiguous* (or *abutting*), where the phases are directly adjacent

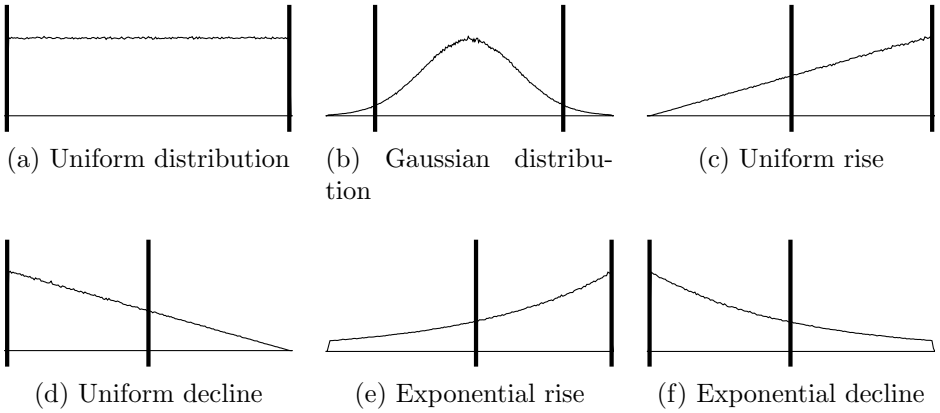

(a) Uniform distribution (b) Gaussian distribution (c) Uniform rise

(d) Uniform decline (e) Exponential rise (f) Exponential decline

Figure 3.4: Phase models defined with different mathematical functions. The black vertical lines are the model (`boundary`) parameters.

to each other, and that the end of the earlier phase is the start of the later phase, indicating a direct transition of one phase to the next (Bronk Ramsey, 1995, 2009a; Buck et al., 1999). The different multiple phase scenarios are illustrated in Figure 3.3.

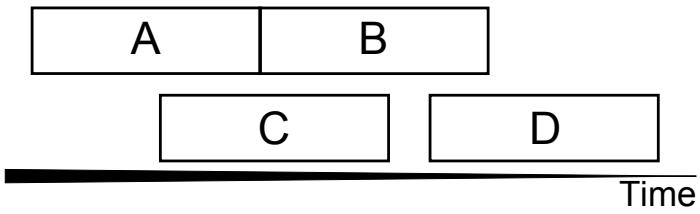


Figure 3.3: Figure illustrating different multiple phase scenarios. Phases A and B are *contiguous*, at the same time *overlapping* with phase C. Phase D is *sequential* to phase C.

Other non-uniform groupings, with different mathematical functions are also available (Bronk Ramsey, 2009a):

- **Gaussian distribution**, suggesting a steady rise in deposition followed by a steady decline in deposition (Fig. 3.4b)
- **Exponential distribution**, suggesting an exponential rise (Fig. 3.4e) or an exponential decline (Fig. 3.4f)
- **Ramped distribution**, suggesting a uniform rise (Fig. 3.4c) or a uniform decline in deposition (Fig. 3.4d)

The model parameters of the above phase priors are suitable for modelling events associated with significant phase activity, i.e. the density of the model parameter is

not zero; and the majority of the phase priors, apart from the Gaussian model, are only suitable for the modelling of abrupt processes. Karlsberg (2006) introduced a trapezoidal phase prior for modelling processes with slow transitions, which is a more realistic prior for archaeological research. The development and evaluation of this prior model is discussed in Chapter 5.

### 3.4.3 Deposition models

Sequential prior information is not limited to constraining multiple phases of data. Individual events can also be constrained according to stratigraphy. The simplest deposition model allows the ordering of events to be defined (Buck et al., 1991; Bronk Ramsey, 1998, 2008). Let $\{x_i, i = 1, \ldots, n\}$ be the events in a dated record on the calendar scale, which occurred in a specific order between the bottom $t_a$, and the top of the sequence $t_b$. The prior for this is (Bronk Ramsey, 2008)

$$p_H(\mathbf{t}, \mathbf{x}) = \begin{cases} 1 & t_a < x_i < x_{i+1} < \ldots < x_n < t_b \\ 0 & \text{otherwise} \end{cases} \tag{3.7}$$

For each $x_i$, an associated $z_i$ for its depth in the sequence can also be assigned, however, this information is not essential for this simple model. The only assumption in this model is that deposition is monotonic. The prior probability for any single event occurring at time $x'$ is given by (Bronk Ramsey, 2008)

$$p(x'|t_a, t_b) = \begin{cases} \dfrac{1}{(t_b - t_a)} & t_a < x' < t_b \\ 0 & \text{otherwise} \end{cases} \tag{3.8}$$

The overall prior probability becomes

$$p(\mathbf{x}|t_a, t_b) \propto \prod_{i=0}^{n} \frac{1}{(t_b - t_a)} \tag{3.9}$$

For any interpolated point $x'$, the time of deposition must lie somewhere between $x_i$

and $x_{i+1}$, hence, there is a uniform prior for $x$ over the range $x_i$ to $x_{i+1}$

$$p(x') = \begin{cases} \dfrac{1}{x_{i+1} - x_i} & x_i < x' < x_{i+1} \\ 0 & \text{otherwise} \end{cases} \tag{3.10}$$

With this simplest assumption, one can also build in known age gaps (with or without uncertainties) between deposits, this method is known as wiggle matching (Christen, 1994b; Christen and Litton, 1995; Bronk Ramsey et al., 2001; Bronk Ramsey, 2008; Blaauw and Christen, 2005) and is suitable for modelling dendrochronological samples, ice cores, or varved lake sediments. The depth profile of a record can also be built in (Haslett and Parnell, 2008; Parnell et al., 2008), with assumptions on accumulation rates (Blaauw and Christen, 2011) or relating to the coarseness of sediments (Bronk Ramsey, 2008). A model assuming uniform deposition rate, although not recommended, can also be used for modelling for the sequence (Bronk Ramsey, 2008). In a uniform deposition model, the time ($x$) at any particular depth ($z$) is defined through linear interpolation over the range $z_i \leq z \leq z_{i+1}$

$$x = x_i + (x_{i+1} - x_i)\frac{(z - z_i)}{(z_{i+1} - z_i)} \tag{3.11}$$

The uniform deposition model is not recommended because its assumption is unrealistic. One can never assume a constant sedimentation rate over decades, let alone centuries. However, this is the most-used assumption within the palaeo-community. Random deposition is a more realistic depiction of the complex sedimentation for many case studies. The development and the evaluation of a prior for random deposition with an underlying Poisson process is discussed in Chapter 6.

### 3.4.4 Bayesian modelling packages

Bayesian calculations are complex and often difficult to compute. It has only been made accessible in archaeological research in the past two decades. Statictical pack-

ages with user friendly interfaces have been made available to aid chronology construction. Recent chronology building software include: OxCal (Bronk Ramsey, 2009a), BCal (Buck et al., 1999), Bacon (Blaauw and Christen, 2011), BChron (Haslett and Parnell, 2008; Parnell et al., 2008), and Bpeat (Blaauw and Christen, 2005).

Bpeat (Blaauw and Christen, 2005) and Bchron (Haslett and Parnell, 2008; Parnell et al., 2008) use a piecewise linear process to construct age-depth models. The latter has an additional function which uses a Gamma (random) process to add a number of monotonic increments between dated points to account for the uncertainty. Bacon (Blaauw and Christen, 2011) constructs age-depth models using a stepwise autoregressive Gamma process. Priors for step-size (similar to the step-size parameter in OxCal; in Section 6.2), accumulation rate, and memory effect, need to be defined. The memory effect provides the coherence in accumulation rates along the depth profile. All of these models contain functions for formal outlier analysis, which is explained in further details in Section 4.3.

Results of Bayesian models are often reproducible even when implemented in different packages with different prior information (Blaauw and Christen, 2011; Hua et al., in press). This is because correct definitions of prior models, including model parameters, yields similar posterior results due to the random sampling of MCMC.

The statistical package used for modelling and presenting results in this thesis is OxCal (using versions later than 4.1.7; Bronk Ramsey, 2009a). The experimental part of Chapter 5 and trapezoidal phase model were implemented independently using the computing language C++ (computer program listings are available in appendix A.2).

#### 3.4.4.1 The OxCal modelling program

The Bayesian modelling program, OxCal, is made up of three modules. The program is written in the computing language C++ for fast computations and integrated in a html format to provide a user friendly interface. This forms the project manager. Users can input the specifics of a model into the program using Chronological Query Language (CQL; Bronk Ramsey, 1998). The CQL takes the format

`command (inputs) {further information};`

The analysis module takes information provided by the `CQL` and performs the model run. The underlying algorithm for Bayesian calculations uses the Metropolis-Hastings approach. A convergence checker is also available and runs are stopped automatically after the model has reached satisfactory convergence. Posterior probability distributions are then generated and confidence intervals are calculated for the output module. The output module allows the users to view the posterior of the model run in a tabular or graphical form.

The main components of a model are **events**, which can be in the form of:

- a radiocarbon determination; `R_Date("name",`$\mu$`,`$\sigma$`);`
- a calendar date; `C_Date("name",expression);` or
- an unknown date; `Date("name",expression);`

, where the $\mu$ and $\sigma$ of a radiocarbon determination are provided by the radiocarbon laboratory. The date `expressions` are ranges specified by the user. They can be in the form of a uniform distribution (e.g. `U(-100,-50)`, where the date is uniformly distributed between 100 and 50 BC) or a Gaussian distribution (e.g. `N(`$\mu$`,`$\sigma$`)`, where the $\mu$ and $\sigma$ are provided by the dating laboratory).

Individual events can also be combined using the `Combine` command, where a prefix of `R` or `C` specifies whether radiocarbon determinations or calendar dates are combined, respectively. The `CQL` for combine events are

- `R_Combine(){};` for combining `R_Date`s
- `C_Combine(){};` for combining `C_Date`s and
- `Combine(){};` for combining `Date`s.

The function automatically performs a $\chi^2$ test and produces a weighted average of a set of dates for the model run. If there are several determinations $r_i$ with standard errors $s_i$, a combined determination $r_c$ is calculated with standard error $s_c$ (Ward and

Wilson, 1978; Bronk Ramsey, 2009a)

$$\begin{aligned} r_c &= \frac{\sum \frac{r_i}{s_i^2}}{\sum \frac{1}{s_i^2}} \\ s_c &= (\sum \frac{1}{s_i^2})^{-\frac{1}{2}} \\ T &= \sum \frac{(r_i - r_c)^2}{s_i^2} \end{aligned} \tag{3.12}$$

This is performed for the combination of radiocarbon determinations, before the weighted average is calibrated. This way, the uncertainty on the calibration curve is not understated, since only the measurements are averaged. For the other two combine functions, the ages on the calendar scale are combined. The use of the latter two combine functions cross reference the defined parameters within the functions to the same parameter.

Events can be simulated using the `Simulate` command, again, the prefix `R` or `C` defines whether a radiocarbon date or a calendar date is simulated. The `CQL` for simulated events are:

- `R_Simulate("name",calendar date, uncertainty);` for a simulated (calibrated) radiocarbon date
- `C_Simulate("name",calendar date, uncertainty);` for a simulated calendar date

For each simulated radiocarbon date, the program generates a radiocarbon determination with randomly sampled errors from the calibration curve, given the calendar age $c_i$ and the expected laboratory error $s_i$. The function `R_Simulate(`$c_i$`,`$s_i$`)` calculates a likelihood function as

$$p(y_i|x_i) \propto \frac{exp[-\frac{(r(c_i)-r(x_i)-\epsilon)^2}{2(s_i^2+s^2(x_i))}]}{\sqrt{(s_i^2+s^2(x_i))}} \tag{3.13}$$

(Bronk Ramsey, 2001, 2009a), where $\epsilon \sim N(0, s_i^2)$ and $x_i$ is the modelled calendar age.

The events in a model can be grouped into phases (Section 3.4.2). These are the relative information obtained from the archaeology. A `Phase` is constrained by a start and an end `boundary` parameters. The groupings supported in `OxCal` version 4.1.7

are illustrated in Figure 3.4. Users can access these models by altering the prefix of the `Boundary` command, for example, a `Sigma_Boundary` results in an S-shaped (part Gaussian) model and a `Tau_Boundary` results in an exponential model. The `CQL` for a single uniform phase model is

```
Sequence(){
    Boundary();
    Phase(){
        R_Date(...);
        ⋮
        R_Date(...);
    }
    Boundary();
};
```

where `Sequence()` is the command for defining the order of each of the parameters; the `Boundary()` parameters defines the uniform phase prior; and `Phase()` specifies the grouping for individual event parameters, in this case, the `R_Date()` parameters.

Events can also be sorted to their chronological order. This is known as a `Sequence` model, which is a deposition model (Section 3.4.3). Again, users can access different deposition models by altering the prefix of the `Sequence` command, for example, a `U_Sequence` results in a model with uniform deposition. The depths of samples, `z`, although not needed for modelling, can also be specified for visual purposes. The `CQL` for a simple `Sequence` model is

```
Sequence(){
    Boundary();
    R_Date(...){ z=...; };
    ⋮
    R_Date(...){ z=...; };
    Boundary();
};
```

, where, same as the phase model, `Sequence()` is the command for defining the order of each of the parameters. The `Boundary()` parameters are used to remove bias towards wider date ranges (Nicholls and Jones, 2001) in a sequence of `R_Date()` parameters.

Other useful commands include: `Span`, which generates a posterior for the length of a phase model; `Interval`, which generates a posterior between two neighbouring constraints; `Difference`, which generates a posterior between any two constraints; `Order`, which generates an order matrix of the model parameters; and `Prior`, which allows the input of a probability density function. Another useful feature of `OxCal` is the ability to `cross reference`, which allows unrelated constraints to be applied to the same events, for example, a synchronous marker can be used to correlate multiple chronologies. `cross referencing` also allows the same constraints to be applied to more than one related events, for example, multiple groups of samples from different areas are relatively dated to the same period.

Model convergence relates to the degree to which a truly representative solution set has been generated. It is important for reliability. `OxCal` has an inbuilt test for model convergence, which gives indication of model stability. A convergence integral of over 95% indicates a stable algorithm and reliable posterior outputs.

Outlier analysis is performed via the methods described in Section 4.3. Offsets in both the radiocarbon and the calendar scales can be accounted for via the use of a model averaging approach. The `CQL` for formal outlier analysis is

- `Outlier_Model("name",distribution,magnitude,type);` for the specifics of the model, and
- `Outlier("name",probability);` for individual events

where `distribution` specifies the distribution for the outliers and `magnitude` specifies the scaling of the outliers, given in powers of 10. There are three outlier `types`: `t` for outliers on the calendar scale, `r` for outliers on the radiocarbon scale (which are only applicable to radiocarbon determinations) and `s` for outliers in the uncertainty of the radiocarbon determinations. `Probability` specifies the probability that the

particular event is likely to be an outlier. Multiple `type`s of `Outlier_Model` can also be used in the same model run and this is demonstrated in Sections 7.3 and 8.2.

These different command functions in `OxCal` allow very complex models to be built to the specification defined by the archaeology. It also allows the input and the modelling of probability density functions obtained from within the program or from an external source. The results from independent programming in Chapter 5 and the first two sections of Chapter 7 are presented using the `OxCal` interface via the use of the `Prior` function.

A typical `OxCal` output is shown in Figure 3.5. It is very similar to outputs from other chronology building software, with calibrated (or modelled) dated along the $x$-axis. The radiocarbon likelihoods are in white, overlaid by the posterior distributions in black. The height of the probability density functions are normalised. The square brackets underneath the probability density functions indicate their highest probability at 68.2% and 95.4% ranges. 68.2% and 95.4% correspond to the $1\sigma$ and $2\sigma$ ranges of a Gaussian distribution and this latter notation is used in some literature (e.g. Parker et al., 2002) to highlight the probability ranges. The use of the $\sigma$ notations is not strictly correct since the probability density functions from a Bayesian model are usually not Gaussian, thus, the probability ranges are quoted in percentages throughout this thesis.

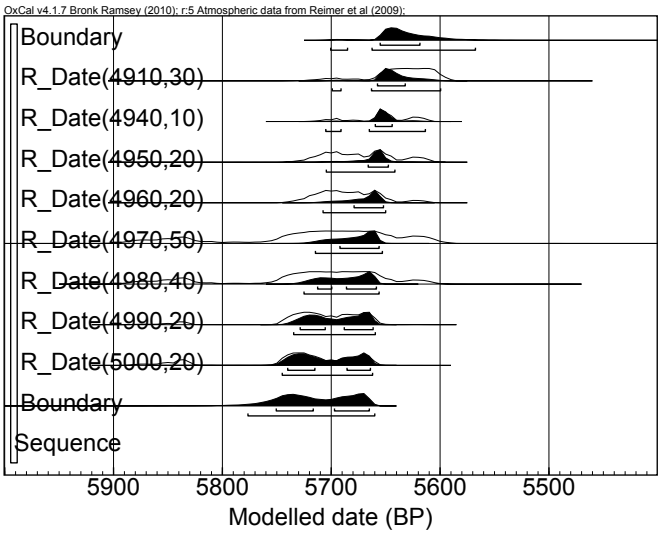


Figure 3.5: A typical `OxCal` output with the model definitions on the left. The brackets underneath the distributions highlight the 68.2% and 95.4% probability ranges.

# Chapter 4

# Constructing a robust chronology

The first step in chronology construction is to define the research question. After the question has been defined, researchers can select samples for dating, assess assumptions, and build simulations before using this information to build a Bayesian model. These steps are recommended by Bayliss (2009) and are shown in Figure 4.1. Each of these steps play an important role in ensuring that the final age model is reliable. The work presented in this thesis focuses on further developing the prior models used in Bayesian modelling, making two models: the trapezoidal phase prior (Chapter 5); and the Poisson process prior (Chapter 6), in particular, more robust and suitable for previously unexplored scenarios. However, other steps in Figure 4.1 are not to be dismissed and thus are also taken into consideration. Whilst every effort has been made to ensure that the absolute dating information used is of good quality; the performance of the scientific dating method, and the types of material used in dating, as well as assessing the archaeological evidence that underpins the historical chronologies, are beyond the scope of this work. This chapter discusses the Bayesian methods used in ensuring a robust chronology.

A Bayesian framework is employed in analysing archaeological data because there is obvious prior information available, for example, from excavations and annual laminations, and this prior information helps to reach more precise, and usually more coherent, results with uncertain inputs. Having uncertain inputs means that one

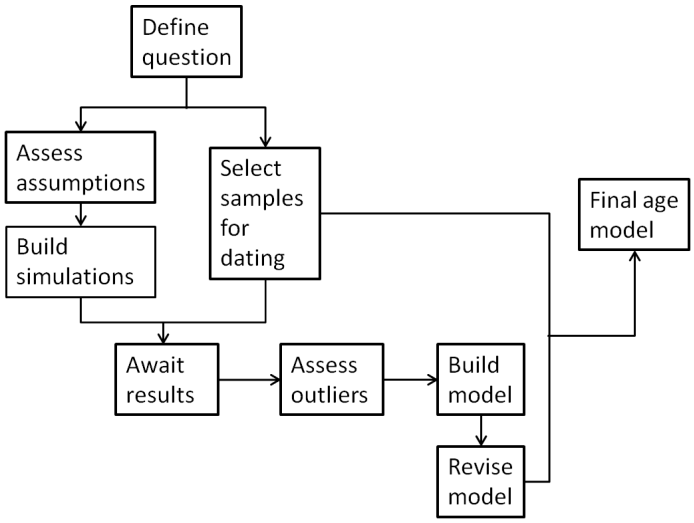


Figure 4.1: Steps in chronology building, adapted from Bayliss (2009).

should be critical with the results obtained from any Bayesian estimations, especially when the amount of likelihood information from absolute dating is limited, which is often the case in archaeology. Posterior estimates become less sensitive to the prior information if more likelihood information is available. Limited likelihood information means that the posterior outputs are largely influenced by the prior information, and this prior information is subjective.

When constructing a Bayesian model, its robustness should be assessed. Robustness testing can be performed by varying the prior information, also known as **sensitivity testing**, by constructing **simulations** with known results, and by evaluating model outputs via the use of **outlier analysis**. It is a very important process in assessing model reliability. This is because

> "essentially, all models are wrong, but some are useful"

(Box and Draper, 1987, p.424). Performing robustness tests helps to better understand the nature of the data and the prior. It is this understanding that helps to ensure that the modelled results are reliable.

## 4.1 Sensitivity testing

If multiple prior models are suitable for modelling one process, and that the selection of prior involves an arbitrary decision, a sensitivity analysis should be performed. Sensitivity analyses of arbitrary assumptions are critical when engaging in model evaluation.

In a recent paper by Vanpaemel (2010), the author summarised very clearly the sensitivity of the prior and the posterior measures to the prior information.

> "Prior and posterior measures differ in their sensitivity to the prior. In a prior measure, the parameter values that generate the model's predictions are drawn from the prior distribution over the parameters. Consequently, the predictions and the model evaluation relying on these predictions are, by design, sensitive to the prior. In a posterior measure, the prediction-generating parameter values are drawn from the posterior distribution, which is the data-updated version of the prior distribution. In principle, the posterior distribution, and hence the posterior predictions, is affected by the exact choice of the prior. However, as data provide sufficient information, they overwhelm the prior, and the posterior is hardly influenced by the prior. Thus unlike prior measures, posterior measures are not always sensitive to the prior."

In terms of archaeological research, the prior measures are often the `boundary` parameters in a phase model, and researchers rely heavily on these model parameters (marginal likelihoods) to draw inference on the date of an event, or the temporal constraints of a process or a historical period (e.g. Needham et al., 1997; Blockley et al., 2008c; Mazar and Bronk Ramsey, 2008; Finkelstein and Piasetzky, 2010b). The sensitivity of the marginal likelihoods to the choice of prior can be a source of concern, especially if multiple prior models are suitable for modelling one process. Therefore, it is important to check that conclusions based on prior measures are not heavily biased by the choice of prior, and one can do so by modelling with other suitable prior information to assess the sensitivity of the likelihoods to the prior model. Two recent studies investigating the Iron age chronology in Israel by Finkelstein and Piasetzky (2010b,c) show that the date of transition between Iron I and Iron II is sensitive to the number of phases included in the model. This is further discussed in Section 7.3.

The sensitivity of posterior measures to prior information can also be assessed by altering any assumptions that has been built into a Bayesian model. In a paper by Bronk Ramsey et al. (2010b), the authors constructed a radiocarbon based chronology for dynastic Egypt using two sources of prior information: reign lengths from written and archaeological evidence; and a seasonal offset of nineteen radiocarbon years. The outliers within the model were also assessed using outlier analysis (Bronk Ramsey, 2009b). Outlier analysis is discussed in more details in Section 4.3. The authors tested the sensitivity of their analysis to the parameters of the model. The sequence and the reign lengths of the Pharaohs, the uncertainty in the reign lengths and the prior outlier probability were altered; different prior information for the regional seasonal offsets were also applied. An example of sensitivity testing is demonstrated in Section 5.5.

It is apparent that sensitivity testing is important in the construction of robust chronologies. This is because there are many models available and no model is perfect for the scenario. The researcher must evaluate the outputs from the models with different prior assumptions, criticise, and discuss which model is best used to address the research question.

## 4.2 Simulation

Simulation is an approach for assessing the validity of different models. It can be used to determine whether different approaches produce the correct result when presented with known age data. It is not limited to, but is very useful in, assessing radiocarbon information in a chronology. Calibration of radiocarbon determinations is an essential step in constructing a radiocarbon chronology, with or without the use of a formal statistical framework. Calibration improves the precision and accuracy of the radiocarbon dates on the calendar scale. If one assumes that the calibration curve used is indeed reliable for the period in question, then it is possible to test any available modelling approach by generating artificially simulated models using the calibration

curve to simulate radiocarbon dates.

There are two approaches to simulation modelling. One approach allows the researcher to simulate radiocarbon dates for a scenario that mimics what is believed to be going on. Another approach allows the researcher to input very little dating information and tests purely the outputs that one would expect from the prior information alone. This way, any bias that might be caused by any prior (or priors) can be clearly identified and assessed before data is analysed. Both of these methods of simulation modelling are summarised in Bronk Ramsey (2009a) and extensive simulation models can be found in Bayliss et al. (2007).

The former approach can be performed by using simulated radiocarbon dates for a scenario that mimics what is believed to be going on. The simulation process involves the researcher estimating a date on the calendrical time scale for the event (or events) in question. A radiocarbon age is produced with the estimated calendar date. This date is then calibrated, producing the probability distribution for the calibrated date. This procedure would provide errors that are associated with calendar ages from that period. The latter simulation approach is performed by running a model with undated events with the priors constrained, for convergence. Examples are given in Sections 5.6 and 6.4, when all provided was some (fixed) dating information at the start and end of the model.

The outputs of simulation modelling allow the researcher to assess whether or not the project is viable and whether it would give useful results. It will also be able to indicate if any parts of the model are more informative in the simulation than others. Another advantage is that it helps the researcher select samples for radiocarbon dating, for example, multiple samples from a period of the radiocarbon plateau would be costly and might not help reach a precise conclusion.

## 4.3 Hypothesis testing and model selection

Both sensitivity and simulation help to ensure the construction of robust chronologies. However, both of these methods ignore model uncertainty. The models used are selected subjectively from a range of available models, ignoring the uncertainty in the selection process. This could lead to over confident inferences and decisions that might be incorrect. Bayesian methods for hypothesis testing and model selection have been used for outlier analysis in archaeology (Christen, 1994b, 2003; Bronk Ramsey, 2009b). The presence of outliers can have a significant effect on age estimates. Bayesian calculations use the given measured data as "standard" in order to output the marginal or posterior probability functions for the parameters or the data, respectively. Hence it is important to identify the outliers and reduce their impacts on the output. Many statistical packages contain functions for outlier analysis recommended in Christen (1994b).

The factors that affect the reliability of radiocarbon dates are (Bronk Ramsey, 2009b):

- Systematic radiocarbon offsets
- Individual radiocarbon offsets
- Measurement uncertainty
- Uncertainty in context

There are two approaches to dealing with outliers: manual rejection and identification using statistical techniques. The former approach includes identifying samples which might have given anomalous radiocarbon measurements, been contaminated, or have a complex depositional history; the latter approach is essentially hypothesis testing. It involves including all of the data in the analysis and the outliers are identified either by calculating the overlap between the posterior with the likelihood (i.e. the `agreement index`; Bronk Ramsey, 1995) or by weighting them according to how likely they are to be correct. The two approaches to dealing with outliers can also be combined, for example, statistical techniques can be used to identified the outliers,

which are then manually rejected.

### 4.3.1 Bayes factor

One Bayesian approach to hypothesis testing is to represent both the null and alternative hypotheses as parametric probability models and to compute the Bayes factor for one against the other (Raftery, 1996). It evaluates the evidence in favour of a null model (Kass and Raftery, 1995). Bronk Ramsey (1995) and Bronk Ramsey (2009a) employ a similar idea to identify possible outliers from the model.

Data $y$ is assumed to have arisen under model, $M_1$; or model, $M_2$ according to a probability density $p(y|M_1)$ or $p(y|M_2)$. Bayes' theorem states

$$p(M_k|y) = \frac{p(y|M_k)p(M_k)}{p(y|M_1)p(M_1) + p(y|M_2)p(M_2)}$$

where $\{k = 1, 2\}$, so that the posterior odds in favour of model $M_1$ over model $M_2$ is

$$\frac{p(M_1|y)}{p(M_0|y)} = \frac{p(y|M_1)}{p(y|M_0)} \times \frac{p(M_1)}{p(M_0)}$$

or, in words

$$\text{Posterior odds} = \text{Bayes factor} \times \text{Prior odds}$$

(Kass and Raftery, 1995). So the Bayes factor $F$ for a model $M_1$ against the null model $M_0$ given data $y$ is the ratio of the posterior odds to its prior odds (Jeffreys, 1935, 1998; Raftery, 1996; Kass and Raftery, 1995)

$$F = \frac{p(y|M_1)}{p(y|M_0)} \tag{4.1}$$

The distributions of $p(y|M_k)$, where $\{k = 0, 1\}$ are obtained by integrating over the

parameter space (Raftery, 1996; Kass and Raftery, 1995) so that in eq. 4.1

$$F = \frac{\int p(y|\theta_1, M_1)p(\theta_1|M_1)d\theta_1}{\int p(y|\theta_0, M_0)p(\theta_0|M_0)d\theta_0} \tag{4.2}$$

where $\theta_k$ is the parameter of model $M_k$, and $p(\theta_k|M_k)$ is its prior density (Kass and Raftery, 1995).

Bronk Ramsey (1995) made use of this technique as a measure of model consistency. It is termed the `agreement index` and is informative on how well the posterior agrees with the observations (or likelihoods). It is a measure of overlap between the posterior and the likelihood distributions before the prior has been applied. There are three `agreement indices`, which are useful in evaluating model outputs.

A ratio is defined for each likelihood (Bronk Ramsey, 1995, 2009a):

$$F_i = \frac{\int p(y_i|x_i)p_1(x_i|\mathbf{y})dt_i}{\int p(y_i|x_i)p(x_i|y_i)dx_i} \tag{4.3}$$

where $y_i$ and $x_i$ represent the observation and the date parameter, respectively; and the marginal posterior density depends on all measurements is $p_1(x_i|\mathbf{y})$. Using eq. 4.3 the `agreement index` for individual posterior distribution is calculated by (Bronk Ramsey, 1995, 2009a):

$$A_i = 100F_i$$

A second `agreement index` $A_{model}$ is also calculated for the model. It is used to evaluate the model as a whole, accounting for the correlation between parameters, to see if it is likely given the full set of data

$$\begin{aligned} F_{model} &= \frac{\int p(\mathbf{y}|\mathbf{x})p_1(\mathbf{x}|\mathbf{y})d\mathbf{t}}{\int p(\mathbf{y}|\mathbf{x})p_0(\mathbf{x}|\mathbf{y})d\mathbf{t}} \\ A_{model} &= 100F_{model}^{\frac{1}{\sqrt{n}}} \end{aligned}$$

which is dependent on the number of likelihood distributions $n$.

A third `agreement index` $A_{overall}$ is a product of the individual `agreement indices` and can also be used to evaluate the model as a whole:

$$\begin{aligned} F_{overall} &= \prod_{i=1}^{n} A_i \\ A_{overall} &= 100 F_{overall}^{\frac{1}{\sqrt{n}}} \end{aligned}$$

These indices have values of *ca.* 100%, which can sometimes be higher and might fall as low as 60%. The 60% threshold is close to the 5% confidence level of the $\chi^2$ test for simple combinations (Bronk Ramsey, 1995). $A_i$ can be greater than 100 and such index indicates that the date measurement is more likely under the full model with the prior, than under the null model without the prior.

The `agreement indices` are not strictly Bayes factors. They employ the same idea as Bayes factors to compare between different models. The use of Bayes factors is important in assessing model choice and is also used in radiocarbon dating (Nicholls and Jones, 2001). An alternative way to outlier analysis uses Bayesian model averaging (Christen, 1994b, 2003; Bronk Ramsey, 2009b).

### 4.3.2 Bayesian model averaging

Bayesian model averaging is a technique designed to account for the uncertainty in model selection. It incorporates model uncertainty into conclusions about parameters and prediction. Bayesian model averaging approach can be utilised in not only Bayesian techniques, but also in classical methods (Hoeting et al., 1999).

Bayesian model averaging works in not having to choose a single model. It averages over different plausible competing models which have appropriate prior possibilities. The data is then used to evaluate posterior probabilities for the various models. Models with 'low' posterior probabilities may be rejected and a weighted sum for the remaining competing models is taken.

Let $t$ be our quantity of interest, such as an age for a particular event, then its

posterior distribution given data $y$ is (Raftery, 1996; Hoeting et al., 1999)

$$p(t|y) = \sum_{k=1}^{K} p(t|M_k, y)p(M_k|y) \tag{4.4}$$

where $\{M_k, k = 1, \ldots, K\}$ are the models being considered. The posterior for model $M_k$ is given by

$$p(M_k|y) = \frac{p(y|M_k)p(M_k)}{\sum_{i=1}^{K} p(y|M_i)p(M_i)}$$

where

$$p(y|M_k) = \int p(y|\theta_k, M_k)p(\theta_k|M_k)d\theta_k$$

is the integrated likelihood of model $M_k$, $\theta_k$ is the vector of parameters of model $M_k$, $p(\theta_k|M_k)$ is the prior density of $\theta_k$, $p(y|\theta_k, M_k)$ is the likelihood, and $p(M_k)$ is the true model (given that one of the models considered is true). All probabilities are implicitly conditional on the set of all models being considered.

The number of models considered can be very large, hence direct evaluation of eq. 4.4 can be exhausting and impractical. There are two ways to get around this problem: Occam's window and MCMC model composition ($MC^3$). The former consists of selecting and averaging over a much smaller set of models by excluding models that are much less likely than the most likely *a posteriori*, and also optionally excluding models that have more likely models nested within them (Madigan and Raftery, 1994). The $MC^3$ approach is a MCMC algorithm that moves through model space and generates a sample from the posterior distribution of the 'true' model, which is used to approximate eq. 4.4 (Madigan et al., 1995; Hoeting et al., 1999).

#### 4.3.2.1 History

Model combination was first mentioned in a paper studying airline passenger data using forecasting models (Barnard, 1963). Early work related to model averaging includes Roberts (1965), who suggests a distribution which combines the opinion of two

"experts". This distribution, essentially a weighted average of posterior distributions of two models, is similar to model averaging. Leamer (1978, Chapter 4) expanded on this idea and presented the basic idea for Bayesian model averaging. He also pointed out the fundamental idea that Bayesian model averaging accounts for the uncertainty involved selecting the model. Bayesian model averaging has been discussed and recommended by researches and had been summarised thoroughly by Draper (1995) and Hoeting et al. (1999) and in Chatfield (1995) using a simpler example. This approach had been available in principle for a long time and is now routinely feasible, due to the advances in computing technology.

#### 4.3.2.2 Bayesian model averaging in chronology building

Bayesian model averaging is currently used in outlier analysis. Christen (1994b) introduced this method to archaeology for shifts in the radiocarbon time scale, and this method has been extended for shifts in the calendar scale (Bronk Ramsey, 2009b) and also for measurement uncertainty (Bronk Ramsey, 2009b; Scholz and Hoffmann, 2011). In formal outlier analysis, each measurement is given a prior probability of being an outlier (typically 5%, recommended by Christen, 2003; Bronk Ramsey, 2009b) and the samples are further down-weighted if they are inconsistent with the rest of the model. The output from the model is affected by this down-weighting, and a posterior probability for the sample being an outlier is generated. This recent development is a very powerful technique in producing robust chronologies (Bronk Ramsey et al., 2010b; Staff et al., 2010), without the bias of subjective input. By using a prior range to allow the model to average over a range of different values, the model finds the most appropriate posterior for the data. Another use of Bayesian model averaging will be discussed in Section 6.3.

## 4.4 Summary

This chapter discusses the different ways that Bayesian methods can be used to assess the robustness of a chronology. The **sensitivity** of posterior and prior measures to prior information can be assessed by altering the assumptions that have been built into a Bayesian model; **simulation** can be used to assess the validity of different models, and also the absolute dating information; and methods of **hypothesis testing** can be used to identify outliers and remove subjective inputs. However, the steps highlighted in Figure 4.1 are not to be neglected. It is still very important to evaluate data from individual events, consider the sample context, and any information from the measurement process, if the information is available, before the construction of any chronologies. The different methods described in this chapter, although in no particular order, are steps in model revision in Figure 4.1.

In addition to the powerful statistical techniques discussed in this chapter, it also important that the prior models used are applicable and reflect substantial prior archaeological knowledge. There are high demands for robust techniques and recent publications introduced the utilisation of robust prior models for chronology construction. These include designing prior models that, more accurately, reflect prior knowledge, for example, the trapezoidal phase prior for processes with slow transitions (Karlsberg, 2006), and prior models for random deposition processes (Bronk Ramsey, 2008; Blaauw and Christen, 2011). The limitations, development, and evaluation of two of these novel robust methods: the trapezoidal phase prior; and the Poisson process prior, are discussed in Chapters 5–6.

# Part II

# Method development and evaluation

# Chapter 5

# Trapezoidal phase model

Phase prior models are used widely to analyse groups of archaeological data. This relative information used to constrain the data can be informative, to assign relationships to groups of events; or it can be non-informative, removing bias in a group of data (Nicholls and Jones, 2001). Without the use of phase prior models, the data is assumed to be unrelated and independent; and the output from the model will reflect that assumption. For example, the uniform phase prior (Buck et al., 1992) is frequently used to assume that a phase of archaeological events is uniformly distributed between two `boundary` parameters, with the `boundary` parameters as temporal constraints on the phase of events. These temporal constraints often represent the start and end of a process or a phase of archaeological activity, and are often of interest to researchers. Examples of application of the uniform phase prior model can be seen in Blackwell and Buck (2003); Buck and Bard (2007) and Blockley et al. (2004). Recent literature discusses the use of a flexible and robust prior model in the shape of a trapezoid for modelling processes with slow transitions (Housley et al., 1997; Zeidler et al., 1998; Van Strydonck et al., 2004). Application of this model was further discussed in Blackwell and Buck (2003) and Buck and Bard (2007), and implemented in Karlsberg (2006). The trapezoidal phase prior model is separated into three parts: first a gradual increase (introductory period); then a period of constant rate of activity (blooming period); and finally, a gradual decrease (period of decline). It allows a

better and more logical method of estimating the onset and end of non-instantaneous processes with transitional periods and draw inference on how rapidly they occurred.

The limitations of the current trapezoidal phase prior, its development, and evaluation are discussed in this chapter. Most of this chapter is published in Lee and Bronk Ramsey (2012).

## 5.1 Introduction

Consider a single phase of pottery assemblage. A method termed frequency seriation was pioneered by Brainerd (1951) and Robinson (1951), where the authors assume that pottery assemblages gradually become more popular, reach a peak popularity, and then fade away (a phenomenon that diagrammatically produces a shape like a battleship viewed from above; Renfrew and Bahn, 2008, p.127). The temporal constraints of a phase of pottery assemblage that researchers are likely to be interested in are the dates of the start and end of the phase. These dates are particularly problematic to estimate, because it is extremely unlikely that the physical remains of the very first or the very last artefacts are found in the same region. Thus, one cannot deduce from a set of absolute dates, especially radiocarbon dates, alone, which one date represents the earliest or latest age in the period of interest. This is also because absolute date determinations often carry uncertainties associated with the measurements and absolute ages tend to overlap each other on the calendar scale. It is, therefore, impossible to accurately determine the earliest or the latest age in an archaeological phase, even if the very first or the very last samples were obtained. Using a Bayesian framework, inference can be drawn on the earliest and / or the latest dates, with information from the material deposited between them.

Until the introduction of the trapezoidal phase prior, researchers have been estimating the temporal constraints of the pottery assemblage using a uniform phase prior, with the `boundary` parameters representing the date of the start and end of the phase on the calendar scale. However, taking into account Brainerd and Robin-

son's interpretation on ceramic frequency, it is apparent that a prior in the shape of a trapezoid is more appropriate for modelling the occurrence of archaeological types.

Suppose there are $m$ date determinations. Let $x_i : i \in \{1, 2, \ldots, m\}$ be the unknown calendar ages for these events. The trapezoid model of Karlsberg (2006) has four parameters: $\alpha$, $\beta$, $\gamma$, and $\delta$. Let $t_\alpha$, $t_\beta$, $t_\gamma$, and $t_\delta$ denote the calendar date associated with the trapezoid parameters. The trapezoidal prior model is defined mathematically as (Karlsberg, 2006)

$$p_{trap}(x_i|t_\alpha, t_\beta, t_\gamma, t_\delta) = h \begin{cases} 0 & \text{for } t_{x_i} \leq t_\alpha \\ \dfrac{(x_i - t_\alpha)}{(t_\beta - t_\alpha)} & \text{for } t_\alpha < x_i \leq t_\beta \\ 1 & \text{for } t_\beta < x_i \leq t_\gamma \\ \dfrac{t_\delta - x_i}{(t_\delta - t_\gamma)} & \text{for } t_\gamma < x_i \leq t_\delta \\ 0 & \text{for } x_i > t_\delta \end{cases}$$

where $h$ is a constant, with values determined by the parameters

$$h = \frac{2}{t_\alpha + t_\delta - t_\beta - t_\gamma}$$

Another version of the model, the sigmoidal prior model, allows slower transitional changes. It is defined mathematically as (Karlsberg, 2006)

$$p_{sig}(x_i|t_\alpha, t_\beta, t_\gamma, t_\delta) = h \begin{cases} 0 & \text{for } x_i \leq t_\alpha \\ g(t)\dfrac{(x_i - t_\alpha)}{(t_\beta - t_\alpha)} & \text{for } t_\alpha < x_i \leq t_\beta \\ 1 & \text{for } t_\beta < x_i \leq t_\gamma \\ g(t)\dfrac{t_\delta - x_i}{(t_\delta - t_\gamma)} & \text{for } t_\gamma < x_i \leq t_\delta \\ 0 & \text{for } x_i > t_\delta \end{cases}$$

where $g$ is a function of $t$

$$g(t) = \frac{t^2}{t^2 + (1-t)^2}$$

The majority of analyses in this thesis are performed using the trapezoidal prior model. However, the sigmoidal prior model may also be appropriate for modelling phases with slow transitions. Formal model comparison, although not investigated in this thesis, will help determine the most appropriate prior model. The focus of this research is to investigate and to extend the use of these prior models.

Modelling the above archaeological scenario with the trapezoidal phase prior estimates the dates of the very first and the very last use of the pottery assemblage; whereas the `boundary` parameters of a uniform phase prior estimates the onset and the end of significant pottery use. A trapezoidal phase prior also has more degrees of freedom, with more parameters than the uniform prior model, and so it is inherently less constrained.

## 5.2 Alternative parameterisation

Since the assumptions of the parameters of the trapezoidal and uniform phase models are different, it is apparent that an alternative parameterisation of the trapezoid model with two `boundary` parameters ($t_1$ and $t_2$) and two `transition` parameters ($d_1$ and $d_2$), illustrated in Figure 5.1, is more logical. The model is defined in this way because `boundary` parameters are commonly used in existing prior models (Buck et al., 1999; Bronk Ramsey, 2009a), and the trapezoidal `boundary` parameter are comparable with those of the uniform phase prior (this is demonstrated in Section 7.1). Mid-point `boundary` parameters will prove more useful in a contiguous multiple phase scenario (illustrated in Fig. 5.2) and its use is demonstrated in Chapter 7. The two `boundary` parameters with corresponding `transition` parameters make up Karlsberg's trapezoidal phase parameters. The mathematics of the model and the overall prior remains the same despite the change of parameters. The trapezoidal

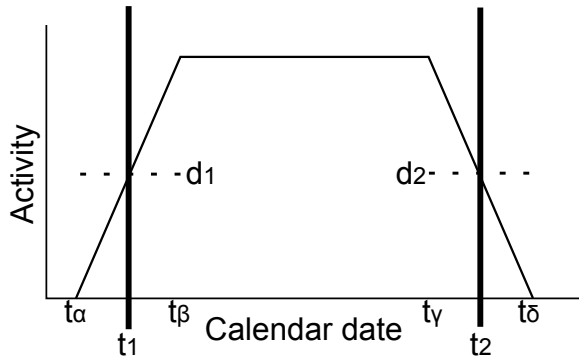


Figure 5.1: Schematic diagram of the current trapezoidal phase model by Karlsberg (2006), where activity relates to phase frequency. The thick vertical lines are the alternative `boundary` parameters, $t_1$ and $t_2$; and the dotted horizontal lines are the `transition` parameters, $d_1$ and $d_2$, proposed in this chapter. $t_\alpha$, $t_\beta$, $t_\gamma$ and $t_\delta$ are Karlsberg's parameters for the model, where $t_\alpha = t_1 - \frac{d_1}{2}$, $t_\beta = t_1 + \frac{d_1}{2}$, $t_\gamma = t_2 - \frac{d_2}{2}$ and $t_\delta = t_2 + \frac{d_2}{2}$.

phase model becomes a uniform phase prior when the length of the `transition` parameters tend towards zero for both of the `boundary` parameters.

## Multiple phases

The trapezoidal phase model can be used singly, to model one group of related events; or it can be used in a multiple phase scenario, to model multiple groups of related events. The different multiple phase relationships include: *overlapping*; *sequential*; and *contiguous* and they have already been discussed in detailed in Section 3.4.2. The overlapping model has already been implemented in Karlsberg (2006) to investigate human reoccupation into North Western Europe after the last ice age. It is also used in Sections 7.2 and 9.1.2.2 to model different phases of related events in this thesis. The implementation of the sequential model is straightforward, constraining the end of an earlier phase before the start of a later phase. The use of the trapezoidal phase model in a contiguous multiple phase scenario has yet to be discussed and implemented. Re-parameterisation of the trapezoidal phase model allows its use in a contiguous phase scenario and this is shown in Figure 5.2. The contiguous model, implemented with the trapezoidal phase model in this way, can be used to analyse archaeological processes with slow transitions and this is demonstrated in Section 7.3.

Inference on the period of transition between adjacent phases can also be drawn.

Sometimes, the simple multiple phase scenarios described above and in Section 3.4.2 are insufficient to reflect prior knowledge. Should this be the case, researchers can assign order to individual trapezoidal phase parameters between different phases. This is the same idea as the `cross referencing` functions in Bronk Ramsey (1995, 2009a), where different phase elements are made inter-linked within a chronological model. The difference between any two parameters can also be calculated if the `transition` parameters do not address the research question. This is a very powerful tool and complexity can be added to models to better reflect archaeological (prior) knowledge. However, it does lead to slower convergence as the different aspects of the model become inter-related.

The use of the trapezoidal phase model in single phase and contiguous phase scenarios are demonstrated in chapters 7 and 9, where the `transition` parameters are used to draw inference on durations of transitional processes.

## 5.3 Calculating the model parameters

Using Bayes' theorem, the overall trapezoidal phase prior is given by

$$p(\mathbf{t}, \mathbf{d}|\mathbf{x}) \propto \prod_{i=1}^{n} p_{Trap}(x_i|\mathbf{t}, \mathbf{d}) p(\mathbf{t}, \mathbf{d}) \tag{5.1}$$

.

The single-component Metropolis-Hastings algorithm is used to implemented the trapezoid. Instead of updating the whole of $t$ (`boundary` parameters), $d$ (`transition` parameters), and $x$ (absolute ages) at once, it is more convenient to update the parameters separately. As a result, an iteration of the single-component Metropolis-Hastings comprises of $k$ updating steps (where $k = n + 4$, and $n$ represents the number of absolute date determinations). A fixed updating order is utilised, though a randomised order is also suitable.

The Metropolis-Hastings algorithm allows an infinite number of proposal distri-

butions, that yield a Markov chain, to converge to a distribution of interest (Gilks et al., 1996) and is discussed in more detail in Section 3.3.1.2. It is used instead of the Gibbs sampler because it is easy and straightforward to construct.

The proposal distribution $q(.|.)$ can have any form and the stationary distribution of the chain will be $\pi(.)$. Once a sample from the stationary distribution has been obtained, all subsequent samples will be from that distribution. Only symmetric proposals are used, as explained in Section 3.3.1.

### `Boundary` parameters update

Each of the `boundary` parameters is updated separately in a single-component algorithm and all of `boundary` parameters are updated in the same way. For this reason, only the update of $t_1$ in a single phase scenario will be described below.

At each iteration, $j$, the next state, $t_1^{j+1}$ is chosen by sampling candidate point $t_1'$ from a proposal distribution. The choice of distribution for the proposal distribution does not have an effect on the posterior distribution. This is because the Markov chain will 'forget' its initial state and will converge to a unique stationary distribution. The proposal distribution will, however, affect the speed of convergence. The closer its shape is to the posterior, the quicker the convergence.

A Gaussian distribution has been chosen as the proposal distribution. This satisfies the constraint of the Metropolis-Hastings algorithm of having equal probability of jumping back to its initial state after the update

$$N(t_1', 25^2) = N(t_1^j, 25^2)$$

A small step update is chosen for a high acceptance rate (Gilks et al., 1996). This value (25) is appropriate for analysing the case studies in Sections 7.1 and 7.2. Higher values (up to 100) are also applicable but convergence is slower in comparison. This step size may need to be lowered for more precisely dated chronologies or raised for

less precisely dated chronologies. The proposal distribution is

$$q(t_1^j|t_1') = N(t_1', 25^2)$$

This is a random walk approach. The choice of the next state is dependent of the previous state. Using a random walk approach allows quicker convergence than using an independent sampler, for example

$$q(t_1^j|t_1') = U(t_L, t_2 - \frac{d_2}{2})$$

where the next state is not dependent on the previous state. If the independence sampler is used for the updating of the trapezoid parameters, the *limits prior* (in Section 5.5) would apply.

The candidate point, $t_1'$, is then accepted with probability

$$p(t_a^j, t_a') = min\left(1, \frac{p(x_i|t_1', d_1, t_2, d_2)p(t_1', d_1, t_2, d_2)q(t_1^j|t_1')}{p(x_i|t_1^j, d_1, t_2, d_2)p(t_1^j, d_1, t_2, d_2)q(t_1'|t_1^j)}\right)$$

Only prior elements contributing to the updating of model parameters are included in the above equation. For example, the *utp* element, which will be defined and discussed below, is only utilised in the update of the start and end `boundary` parameters ($t_1$ and $t_{n+1}$) and not the update of any transitional `boundary` parameters in cases of more than one phases. This is because the prior element does not contribute to the update of the transitional `boundary` parameters and hence is treated as a constant in those cases.

### `Transition` parameters update

The corresponding `transition` parameters for each of the `boundary` parameters are updated using the single-component Metropolis-Hastings algorithm. The sampling

method of random walk is also utilised here for quick convergence

$$q(d_1^j|d_1') = N(d_1', 25^2)$$

The candidate point $d_1'$ in a single phase scenario is then accepted with probability

$$p(d_1^j, d_1') = min\left(1, \frac{p(x_i|t_1, d_1', t_2, d_2)p(t_1, d_1', t_2, d_2)q(d_1^j|d_1')}{p(x_i|t_1, d_1^j, t_2, d_2)p(t_1, d_1^j, t_2, w_2)q(d_1'|d_1^j)}\right)$$

The term $p(y_i|x_i)$ does not contribute to the updating of the trapezoidal phase parameters, hence it is treated as a constant and is not included in the updates.

## 5.4 Calculating the posterior

Using Bayes' theorem, the overall posterior is given by

$$p(\mathbf{x}|\mathbf{y}) \propto p(\mathbf{y}|\mathbf{x})p(\mathbf{x}|\mathbf{t}, \mathbf{d}) \tag{5.2}$$

Again, the single-component Metropolis-Hastings algorithm is used for the update of individual date parameters, $x_i$. A proposal distribution, $q(x_i'|x_i^j)$, is needed to generate the next value, $x_i^{j+1}$. This time, an independence sampler is utilised (for the sake of easier programming) to generate this value. $x_i$ is constrained to lie within the span of the trapezoidal phase in which the parameter belongs (i.e. between $t_1 - \frac{d_1}{2}$ and $t_2 + \frac{d_2}{2}$ in a single phase). This is represented with the proposal

$$q(x_i'|x_i^j) = U(t_1 - \frac{d_1}{2}, t_2 + \frac{d_2}{2})$$

. The candidate point, $x_i'$, is then accepted with probability

$$p(x_i^j, x_i') = min\left(1, \frac{p(y_i|x_i')p(x_i'|t_1, d_1, t_2, d_2)q(x_i^j|x_i')}{p(y_i|x_i^j)p(x_i^j|t_1, d_1, t_2, d_2)q(x_i'|x_i^j)}\right)$$

.

The algorithm can be found in Appendix A.2 and is explained in further detail there.

## 5.5 Model constraints

Let $n$ be the number of phases. In a multiple phase model with contiguous uniform phases, there are $t_1, \ldots, t_{n+1}$ `boundary` parameters. In a model with contiguous trapezoid phases, three are also $t_1, \ldots, t_{n+1}$ `boundary` parameters, with corresponding $d_1, \ldots, d_{n+1}$ `transition` parameters. A schematic diagram of a contiguous multi-phase trapezoid model is shown in Figure 5.2.

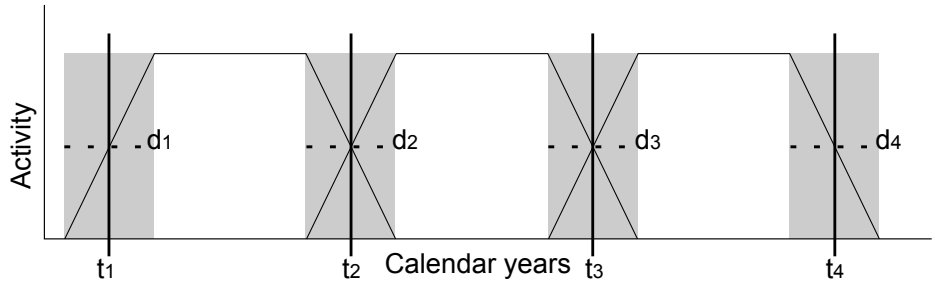


Figure 5.2: Schematic diagram showing the use of the trapezoidal phase model in a contiguous multiple phase scenario, where $n = 3$. The thick vertical lines are the `boundary` parameters and the dotted horizontal lines are their corresponding `transition` parameters. The `transition` parameters can be used to estimate the duration of transition between any two phases, which is highlighted in grey.

The overall time span (`S`) of the trapezoidal phase model

$$\mathtt{S} = t_{n+1} - t_1 + \frac{d_{n+1} + d_1}{2} \tag{5.3}$$

is made up of the total time for the `transition` parameters (`D`; total grey areas in Fig. 5.2) and the total time of the phase tops (`T`; total white areas in Fig. 5.2), where

$$\mathtt{D} = \sum_{i=1}^{n+1} d_i \tag{5.4}$$

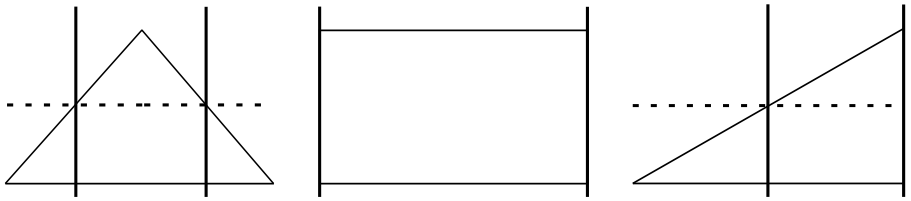


Figure 5.3: Schematic diagrams of the trapezoidal phase model in extreme phase scenarios (Karlsberg, 2006). The vertical lines are the `boundary` parameters and the dotted horizontal lines are the `transition` parameters.

for $i = 1, \ldots, n+1$; and

$$\mathtt{T} = t_{n+1} - t_1 + \frac{d_{n+1} + d_1}{2} - \left( \sum_{i=1}^{n+1} d_i \right) \tag{5.5}$$

The parameters of the simple single phase model are subject to the constraint (Karlsberg, 2006)

$$t_L \leq t_\alpha < t_\beta < t_\gamma < t_\delta \leq t_U \tag{5.6}$$

where $t_L$ and $t_U$ are *termini post quem* and *ante quem*, respectively. So for a contiguous multiple phase model, with the alternative parameterisation suggested in this chapter, this becomes

$$t_L \leq t_1 - \frac{d_1}{2} < t_1 + \frac{d_1}{2} < \ldots < t_{n+1} - \frac{d_{n+1}}{2} < t_{n+1} + \frac{d_{n+1}}{2} \leq t_U \tag{5.7}$$

The calendar years are in the AD time scale, in which years BC are expressed with negative numbers, which is compatible with the internal time-scale in `OxCal`. Hence, all output can be plotted with the `Prior` function in `OxCal`.

The original implementation of the trapezoidal phase prior by Karlsberg was designed to allow the model to vary between the extreme phase scenarios in Figure 5.3. In the absence of absolute dating information, the model parameters have a *constant prior density* (Nicholls and Jones, 2001), i.e.

$$p_{cpd}(\mathbf{t}, \mathbf{d}) \propto 1 \tag{5.8}$$

for all $\mathbf{t}$ and $\mathbf{d}$ satisfying the inequality (5.7). Sum of phase tops (T; eq. 5.5) gives distributions as illustrated in figure 5.4. This weighting is caused by three factors:

- The total time span of the whole model has a bias proportional to S.
- The total time span for the `transition` parameters, of which there are $n+1$, has a bias proportional to $\mathtt{D}^n$.
- The total time span for phase tops, of which there are $n$, has a bias proportional to $\mathtt{T}^{n-1}$.

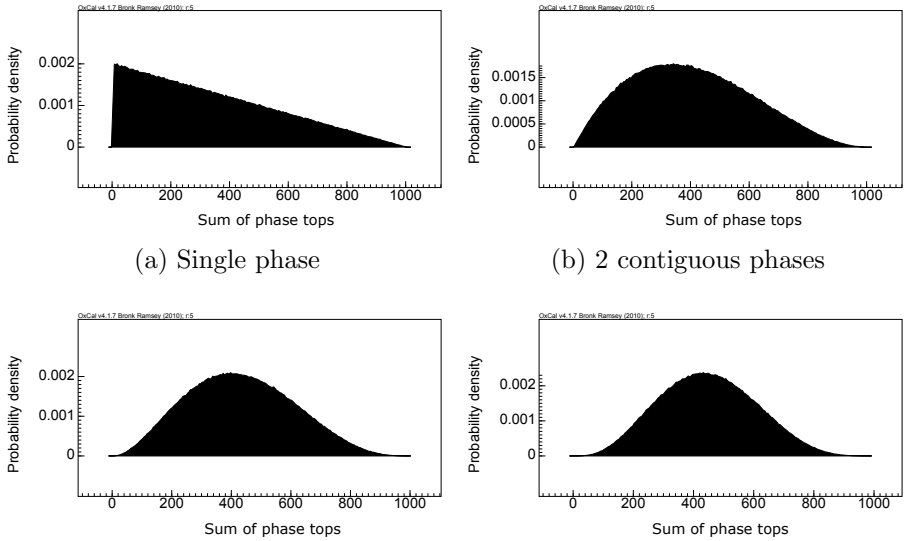


(a) Single phase (b) 2 contiguous phases

(c) 3 contiguous phases (d) 4 contiguous phases

Figure 5.4: Probability distributions of the sum of the phase tops (T) of the trapezoidal phase prior under $p_{cpd}(\mathbf{t},\mathbf{d})$ for up to 4 contiguous phases. The time span (S) of the model is constrained to be 1000.

It is apparent that under $p_{cpd}(\mathbf{t},\mathbf{d})$, the trapezoidal phase model does not reflect substantial prior knowledge. The marginal density for T is $\mathtt{T}^{n-1}\times\mathtt{D}^n\times\mathtt{S}$. Therefore to obtain a uniform prior on T, a prior element

$$p_{utp}(\mathbf{t},\mathbf{d}) \propto \frac{\mathtt{T}^{1-n}}{\mathtt{D}^n \times \mathtt{S}} \tag{5.9}$$

is needed, under which $\mathtt{T}\sim\mathrm{U}(0,\mathtt{S})$ and $\mathtt{D}\sim\mathrm{U}(0,\mathtt{S})$, by definition. This will be called the *utp* element, which stands for *uniform transitions / tops prior* element, since it conditions the total time span for total time span of the `transition` parameters (D) and phase tops (T) to be uniform. The model becomes more robust and better reflects

prior knowledge as expressed in Karlsberg (2006). The overall prior for the trapezoid parameters becomes

$$p(\mathbf{t}, \mathbf{d}) \propto p_{cpd}(\mathbf{t}, \mathbf{d}) \times p_{utp}(\mathbf{t}, \mathbf{d}) \tag{5.10}$$

This prior also applies to overlapping and sequential multiphase scenarios; and to single phase activities (Fig. 5.1). In all of these cases, where $n = 1$, the *utp* element simplifies to

$$p_{utp}(t_1, t_2, d_1, d_2) \propto \frac{1}{(d_1 + d_2) \times (t_2 - t_1 + (d_2 + d_1)/2)}$$

The introduction of a *utp* element is a similar idea to the *uniform span prior* in Nicholls and Jones (2001), which deals with multiple uniform phases.

## Model limits

Karlsberg's trapezoidal phase model is constrained between limits, i.e. *termini post quem* and *ante quem* in inequality (5.6), and the time span (`R`) between the two points is

$$\mathtt{R} = t_U - t_L$$

. The marginal density of the time span of the trapezoid model has a bias towards (`R-S`), which is currently not accounted for. Therefore, a prior for *limits*

$$p(\mathbf{t}, \mathbf{d} | t_L, t_U) \propto (\mathtt{R} - \mathtt{S})^{-1}$$

is needed if the model is surrounded by events, fixed points, and especially if multiple phases are made inter-related, for example $t_\beta$`[n-1]` $< t_\alpha$`[n]` $< t_\delta$`[n-1]`, (notations from Fig. 5.1 and the phases, in which the parameters belong, are indicated in the square brackets). The overall prior for the trapezoid parameter becomes

$$p(\mathbf{t}, \mathbf{d}) \propto p_H(\mathbf{t}, \mathbf{d}) \times p_{UTP}(\mathbf{t}, \mathbf{d}) \times p(\mathbf{t}, \mathbf{d} | t_L, t_U)$$

The *limits* prior would apply to such constraints, with the adjacent events to the model as *termini post quem* and *ante quem*.

## 5.6 Model evaluation

By repeating the experiments illustrated in figure 5.4, constraining the time span (S) of the trapezoidal phase to be 1000, with the addition of the *utp* element; the effect of the prior element can be seen. In the absence of absolute dating information (events), T$\sim$ U(0,S) conditioned by $p_{utp}(\mathbf{t}, \mathbf{d})$, as illustrated in figure 5.5. It is apparent that the trapezoidal phase model is sensitive to the addition of the *utp* element.

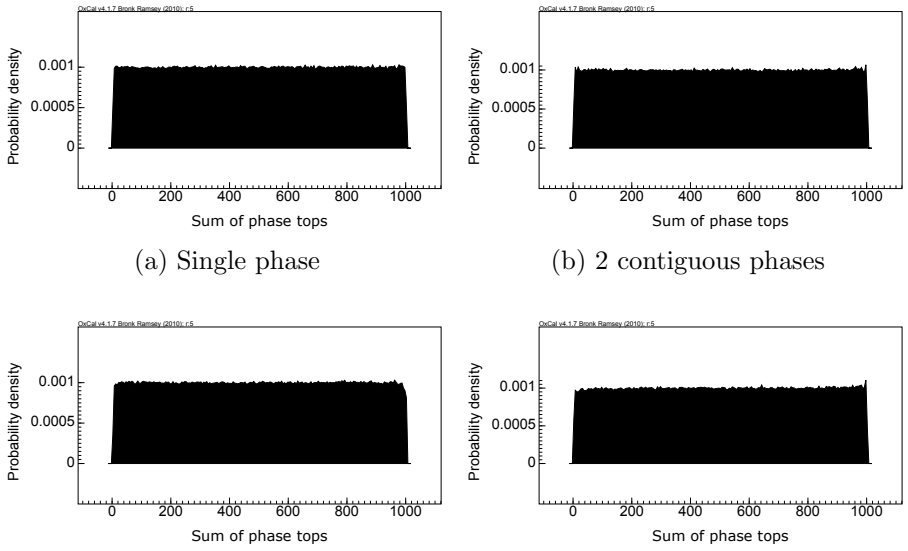


(a) Single phase (b) 2 contiguous phases

(c) 3 contiguous phases (d) 4 contiguous phases

Figure 5.5: Probability distributions of the sum of phase tops (T) under $p_{utp}(\mathbf{t}, \mathbf{d})$ for up to 4 contiguous phases. The time span (S) of the model is constrained to be 1000.

When the trapezoidal phase is constrained by *termini post quem* and *ante quem*, the *limits* prior is needed. Under $p(\mathbf{t}, \mathbf{d})$, the overall `span` of the trapezoidal phase prior becomes uniform and this is shown in Figure 5.6. `T` and `D` stay uniform marginally and are unaffected by the addition of the *limits prior*. The `T/S` and `D/S` ratios are shown instead of `T` and `D`. This is because the `S` is variable in this scenario and `T` and `D` are relative to `S` and not to the limits. Results from the above simulations are still valid because the *limits* prior is 1 in those cases and does not

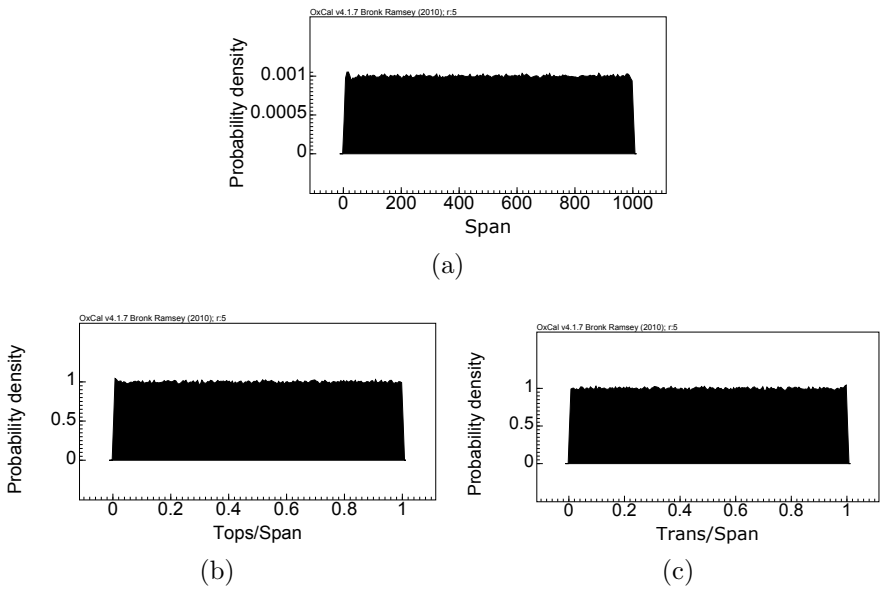


Figure 5.6: Figure showing the effects of the *limits* prior. The lower and upper limits, $t_L$ and $t_U$, are fixed at 0 and 1000 respective, (a) $\texttt{S}\sim\mathrm{U}(t_L, t_U)$ is achieved, marginally. (b) and (c) show that the *utp* element still applies and is unaffected by the addition of the *limits* prior.

contribute to the update.

In order to test the model implementation, two scenarios, both with three contiguous phases (Fig. 5.2), are simulated: a scenario with no events; and another scenario with ten undated events in each of the phases. The time span (`S`) of the model is constrained to be 1000, with $t_1 - \frac{d_1}{2} = 0$ and $t_4 + \frac{d_4}{2} = 1000$. The model outputs are shown in Figures 5.7 and 5.8. The trapezoidal `boundary` and `transition` parameters have the same distributions when modelled with and without undated events. This shows that the underlying assumptions of the trapezoidal model (Fig. 5.7) do not change with the addition of undated event (Fig. 5.8), as one would expect from correct implementation of the MCMC algorithm. This is because the likelihood information is absent. Repeated analyses with different numbers of undated events (e.g. 3 contiguous phases with 0, 1, and 10 undated events respectively) do not yield different results.

In the absence of absolute dating information, the `transition` parameters ($d$)

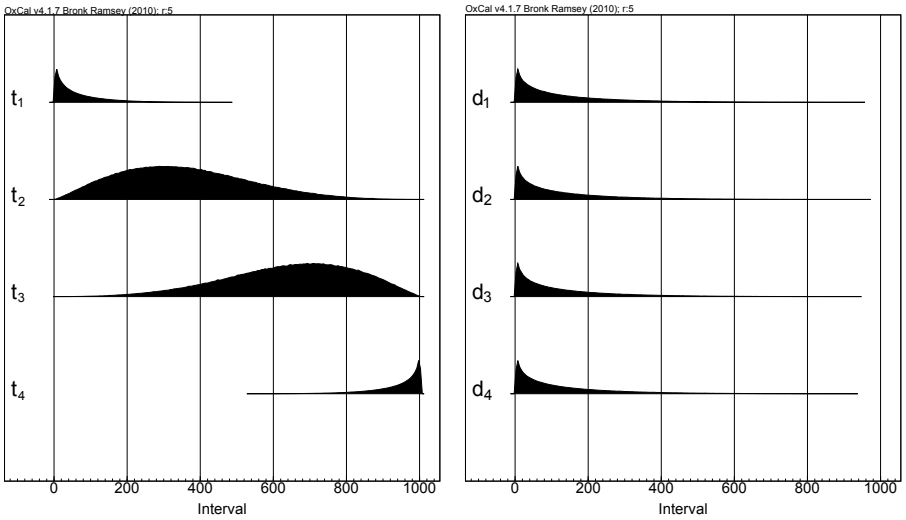


(a) (b)

Figure 5.7: Marginal distributions of the trapezoidal: (a) `boundary` and (b) `transition` parameters under $p_{utp}(\mathbf{t}, \mathbf{d})$ for 3 contiguous phases with no events. The time span (`S`) of the model is constrained to be 1000.

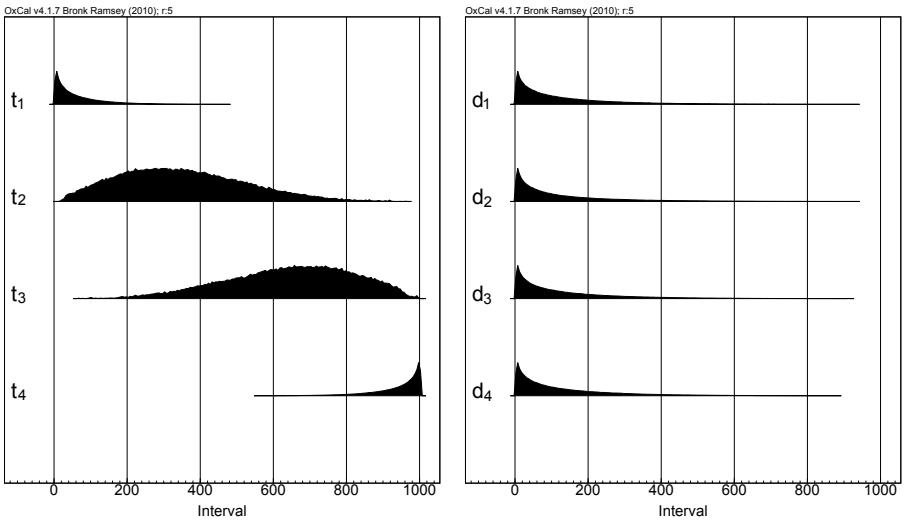


(a) (b)

Figure 5.8: Marginal distributions of the trapezoidal: (a) `boundary` and (b) `transition` parameters under $p_{utp}(\mathbf{t}, \mathbf{d})$ for 3 contiguous phases with 10 undated events. The time span (`S`) of the model is constrained to be 1000. See text for explanation.

might take any values between 0 and D with equal probability

$$p(\mathbf{d}) = \begin{cases} \dfrac{n}{D^n}(D-d)^{n-1} & \text{for } 0 < d < D \\ 0 & \text{otherwise} \end{cases}$$

and for D$\sim$U(0,S), conditioned by $p_{utp}(\mathbf{t}, \mathbf{d})$. The marginal density of any `transition` parameter is represented by the choice

$$p(\mathbf{d}) = \frac{1}{\mathtt{S}} \int_d^{\mathtt{S}} \frac{n}{D^n}(D-d)^{n-1} dD \tag{5.11}$$

This is illustrated in Figures 5.7 and 5.8, as $d \to 0$; $p(\mathbf{d}) \to \infty$. Short `transition` time is favored over long `transition` time. However, $d$ can never be zero and so the marginal distribution, $p(\mathbf{d})$, stays finite. This also means that, in theory, the trapezoidal phase model can never take the forms illustrated in Figure 5.3. It can, however, get very close to those shapes and this is supported by figure 5.5. The trapezoidal phase model without this bias essentially rules out an overall abrupt transition model, which is the assumed scenario in a uniform phase model.

## Simulated case studies using seriation frequencies

In order to observe the effect of the *utp* element on a data set, the frequency of a particular type of artefacts of known dates is simulated. Consider a set of tombstones decorated with a set of similar designs, one is able to record the frequency of tombstones in a particular year or period, for example in Deetz and Dethlefsen (1965) and Dethlefsen and Deetz (1966), where the authors recorded the frequency of tombstones in different designs at 10-year intervals. The frequency of a tombstone type followed the shape of a battleship viewed from above. The simulated frequencies for two designs, A and B, are shown in Table 5.1 in five-year intervals.

| Year (AD) | Frequency of A | Frequency of B |
|---|---|---|
| 1711–15 | 0 | 0 |
| 1716–20 | 0 | 1 |
| 1721–25 | 0 | 1 |
| 1726–30 | 0 | 2 |
| 1731–35 | 3 | 2 |
| 1736–40 | 5 | 1 |
| 1741–45 | 24 | 2 |
| 1746–50 | 23 | 2 |
| 1751–55 | 18 | 5 |
| 1756–60 | 15 | 5 |
| 1761–65 | 2 | 5 |
| 1766–70 | 0 | 4 |
| 1771–75 | 0 | 0 |

Table 5.1: Simulated seriation frequencies of designs A and B, in 5-year intervals.

The population of design A is large, with seriation frequency following the assumptions of Brainerd (1951) and Robinson (1951), that the abundance of the design builds up slowly, reaches a peak, and then decreases. Unlike design A, the population of design B is low, and develops slowly. Its use remained uniform for the first few decades, before becoming more popular for a very short period for time, and then decreases. Both designs are modelled with the trapezoidal phase prior and results are shown in Figures 5.9 and 5.10.

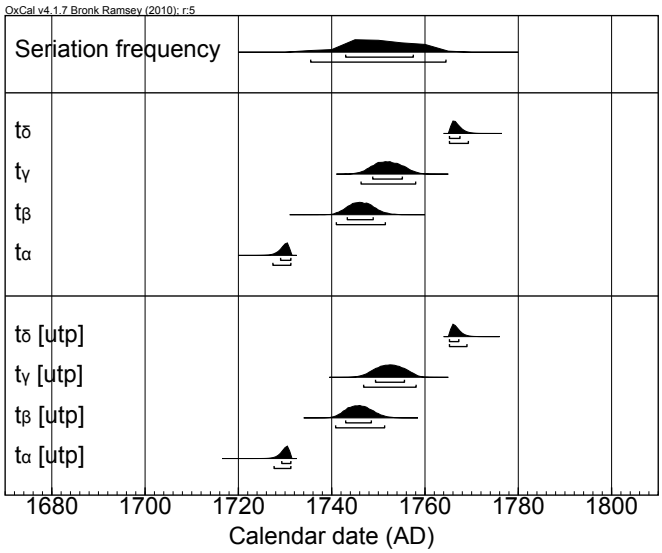


Figure 5.9: Seriation frequency and probability distributions of the trapezoidal phase parameters modelling design A, with and without the *utp* element.

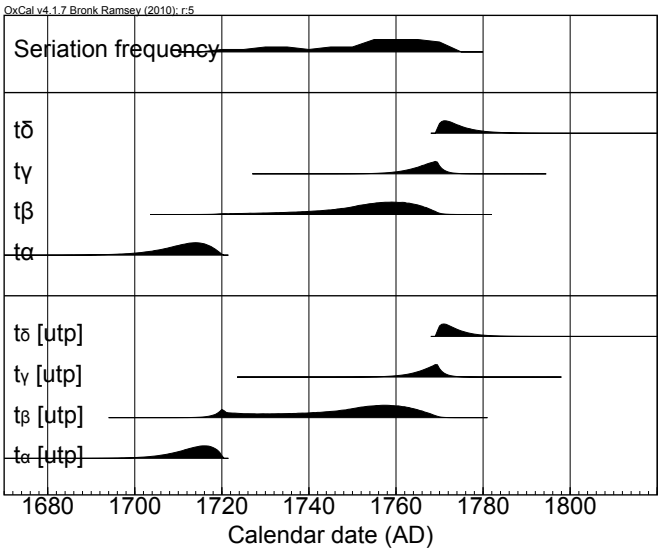


Figure 5.10: Seriation frequency and probability distributions of the trapezoidal phase parameters modelling design B, with and without the *utp* element.

Figures 5.9 and 5.10 show that if the data set is large and the seriation frequency is distinctive, i.e. in the case of design A, the addition of the *utp* element makes no significant difference in the posterior prior measures. However, if the data set is small and the seriation frequency is less distinctive, i.e. in the case of design B, the posterior prior measures are sensitive to the addition of the *utp* element. The purpose of this exercise was to demonstrate the significance of the use of the *utp* element on a data set. It is apparent that the *utp* element allows better estimation of prior measures if the data is scarce, as is often the case in archaeology. The utilisation of the *utp* element is essential in a contiguous phase scenario and this is discussed in Section 7.3.

### Modelling with the sigmoidal phase prior

Both designs A and B are modelled with the sigmoidal phase prior (with the *utp* element) and results are shown in Figures 5.11 and 5.12. The figures show that the sigmoidal prior measures are different from those of the trapezoidal model (Fig. 5.9 and 5.10). This is because their prior assumptions are different.

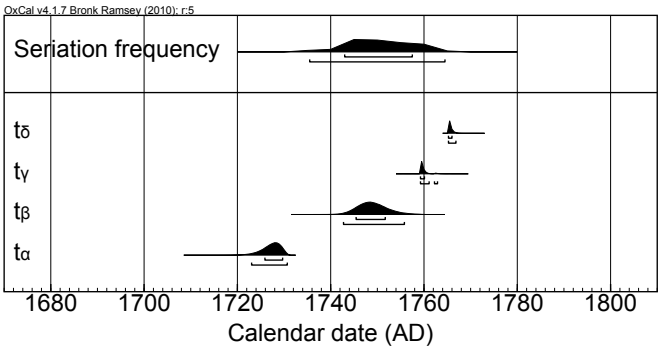


Figure 5.11: Seriation frequency and probability distributions of the sigmoidal phase parameters modelling design A.

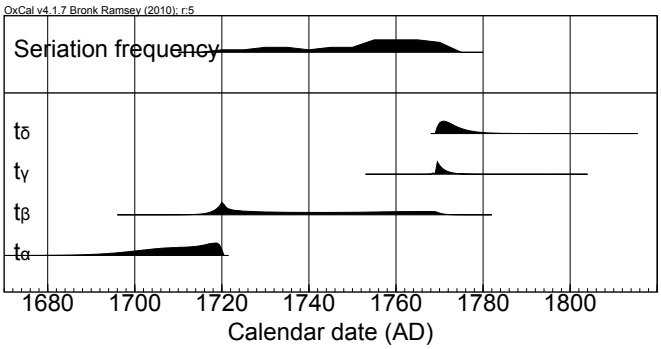


Figure 5.12: Seriation frequency and probability distributions of the sigmoidal phase parameters modelling design B.

It is apparent, from Figures 5.9 and 5.10, that the trapezoidal phase prior measures give a close approximation to the simulated scenarios described in this section. Also, the sigmoidal model prior measures seem too narrow and precise. All of the phase modelling in later chapters of this thesis is performed using the trapezoidal phase prior. The sigmoidal phase prior, although not utilised, may also be suitable in modelling these situations. Although formal model comparison is not the focus of this thesis, it is an avenue that can be explored in future research (Section 10.4).

## 5.7 Summary

Single and multiple phase models have been used extensively in the construction of chronologies. The trapezoidal phase prior is used to model non-abrupt processes since it reflects the nature of the information that goes into the model prior more accurately than the uniform phase prior. This chapter discussed the existing bias in the simple

trapezoidal phase prior (Karlsberg, 2006), which does not reflect substantial prior knowledge and proposed the addition of a non-informative *utp* element to the prior model. Alternative parameterisation was also suggested, which transforms the current abrupt transition (uniform) model to a model that allows for gradual changes. The addition of the *utp* element to the trapezoidal phase prior ensured model flexibility. The `boundary` parameters of the trapezoidal phase prior are comparable to those of the uniform model. This will be discussed in more details in Chapter 7. One use of the trapezoidal phase model is for testing the robustness of models previously run under a uniform phase prior, where there was not good justification for the assumption of rapid phase transitions.

The *utp* element can be thought of as a method of model averaging (previously discussed in Section 4.3.2). The subjectivity of choosing a prior is removed because with the addition of the *utp* element, the model can move freely between different forms and reaches a shape which is most appropriate for the data.

The trapezoid model, together with the *utp* element and the different tests have been implemented independently using the computer language `C++` (see Appendix A). The outputs have been tested against the implementation of the same mathematics in `OxCal`. They give similar results (see Section 7.2). A single-component Metropolis-Hastings algorithm is used to implement the trapezoidal phase model throughout this chapter. All the graphs are plotted in `OxCal` (Bronk Ramsey, 2009a), using the `Prior` function, after two million iterations and using a five-year bin size.

# Chapter 6

# The Poisson process deposition model

Sedimentary sequences provide a wealth of useful information for research into archaeology and palaeoenvironmental studies. Accurate and precise chronologies are needed in order to compare and correlate different stratigraphic records. There are high demands for methods of age-depth relationship construction. Many Bayesian and frequentist methods have been proposed for estimating the expected ages at particular depths and the uncertainties associated with them.

Frequentist methods include linear interpolation, splines, linear regression models (Bennett, 1994; Blaauw, 2010), Bézier curves (Bennett and Fuller, 2002), mixed-effect models (Heegaard et al., 2005), and fuzzy regression (Boreux et al., 1997). Unsurprisingly, the different approaches can give very different results (Bennett, 1994; Bennett and Fuller, 2002), both for the age at a particular depth, and the uncertainty attached to that estimate. It is difficult to determine which relationship is closest to reality.

Radiocarbon determinations form the building blocks of many archaeological chronologies, and it is widely known that calibration is one of the important first steps in accurate (radiocarbon) chronology construction (see Section 3.4.1). Unfortunately, calibration of radiocarbon determinations adds an extra level of complexity as the

resulting distributions are not Gaussian. Many frequentist approaches are unable to account for the irregularity of calibrated radiocarbon ages. Therefore, the uncertainties associated with those ages are often not considered when modelled using frequentist approaches.

Blaauw (2010) acknowledges that a lot of researchers use frequentist approaches for modelling the age-depth relationships of radiocarbon chronologies and wrote the chronology building package `clam`. It uses a Monte Carlo approach to randomly sample points from calibrated age distributions from the entire sequence, which is then modelled using a frequentist method chosen by the researcher.

While some researchers prefer the frequentist approach to age-depth modelling, Bayesian methods are becoming more and more popular. It provides a way of constraining radiocarbon ages by combining them with relative dating, for example stratigraphic information (Buck et al., 1991, 1992). The concept of using Bayesian approaches to model chronological sequences, and an introduction to current deposition models were already discussed in Section 3.4.3. Recent literature discussed the use of more robust techniques for constructing reliable chronologies (Bronk Ramsey, 2008; Haslett and Parnell, 2008; Parnell et al., 2008; Blaauw and Christen, 2011). This chapter focuses on the evaluation of the application of the Bayesian model averaging approach on the Poisson process deposition model described in Bronk Ramsey (2008).

## 6.1 Introduction

Consider a set of $n$ events, $x_i : i \in \{1, \ldots, n\}$, in a sedimentary sequence with corresponding depths, $z_i$. The simplest deposition model uses the ordering of events (Buck et al., 1991) in a chronological record to constrain the posterior ages (eq. 3.9). Although not always recommended, a constant (uniform) deposition rate can also be assumed with given depth information (eq. 3.11). The former is known as the `Sequence` model, and the latter is known as the `U_Sequence` model in the chronology building package `OxCal` (Bronk Ramsey, 1998, 2008). The `Sequence` model assumes

that the deposition is monotonic. It provides little constraint to the data in comparison to the `U_Sequence` model, which constrains the data more rigidly. In most cases, the deposition process is more complicated than either of these models and hence Bronk Ramsey (2008) introduced the Poisson process model, which is also known as the `P_Sequence` model.

As its name suggests, the `P_Sequence` model assumes an underlying Poisson process for modelling a random rate of deposition of events within a chronological sequence. It allows for fluctuations in sedimentation rate between that of the `Sequence` model, and that of the `U_Sequence` model. It provides the a more realistic depiction of events deposition than the `U_Sequence` model. The time of deposition between dated events in a sequence is considered random and is modelled according to the Poisson distribution.

The `P_Sequence` model needs a parameter for step-size, $k$, in the units of depth$^{-1}$. This $k$ value defines the size of the deposition events, hence it defines the variability of accumulation and the rigidity of the model. A high $k$ value assumes smaller steps (fine increments), which constrains the model rigidly (i.e. when $k \to \infty$; the model behaves more like a `U_Sequence` model). Conversely, a low $k$ value assumes larger steps, which gives the model more flexibility (i.e. when $k \to 0$; the model behaves more like a `Sequence` model).

## 6.2 Model specifications

The mathematics of the `P_Sequence` model are published in Bronk Ramsey (2008). The model utilises a Poisson process to model the deposition process. In order to do so, a step-size parameter, $k$ is required. It defines the size of the deposition events. A value of around 100 m$^{-1}$ is suitable for coarse sediments and a value up to 1000 m$^{-1}$ or possibly higher is suitable for fine sediments (as suggested in Bronk Ramsey, 2008). This parameter also exists in the autoregressive gamma process model (`Bacon`; Blaauw and Christen, 2011), where the users are asked to input a value of $K$ to divide

the sequence into $K$ equally spaced sections.

It is difficult to determine an appropriate value for the parameter. Since the determined value has a huge effect on the model output, it is important that a suitable value is used. Bronk Ramsey (2008) suggests a way to estimate this value from direct measurements. In sequences where there are exposed sections or multiple records with stratigraphic marker layers (Fig. 6.1), the variability in distances between the layers can be measured.

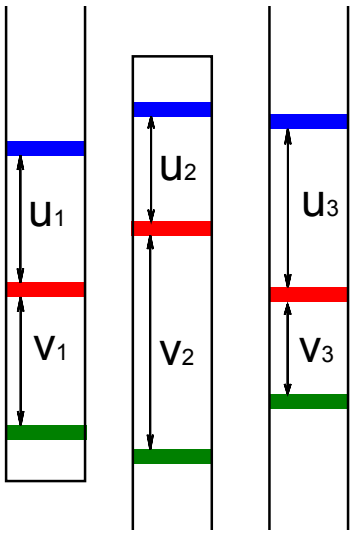


Figure 6.1: Estimating the step-size parameter from stratigraphic markers (the coloured bands). The variability in distances between the layers can be measured and the $k$ parameter estimated using A.20 from Bronk Ramsey (2008).

A varved or ice core sequence, or the presence of tephra layers will provide the necessary information for estimating an appropriate value of $k$. However, known age stratigraphic markers are not always readily available, making the determination of a suitable value for $k$ difficult. A solution to that problem would be to estimate a value for the parameter from the dating information, for example in Blockley et al. (2007) and Blockley et al. (2008b); or use an arbitrary $k$ value that achieves the highest model agreement, for example in Finsinger et al. (2011). Neither of these solutions are satisfactory, since there are dangers of circular reasoning (Bronk Ramsey, 2008), making the results unreliable. In some cases, for example in Mortensen et al. (2011), the choice of $k$ value was obviously arbitrary, with unjustified reasons, resulting in a chronology with unrealistically small uncertainties (Fig. 6.2a). Modelling the same

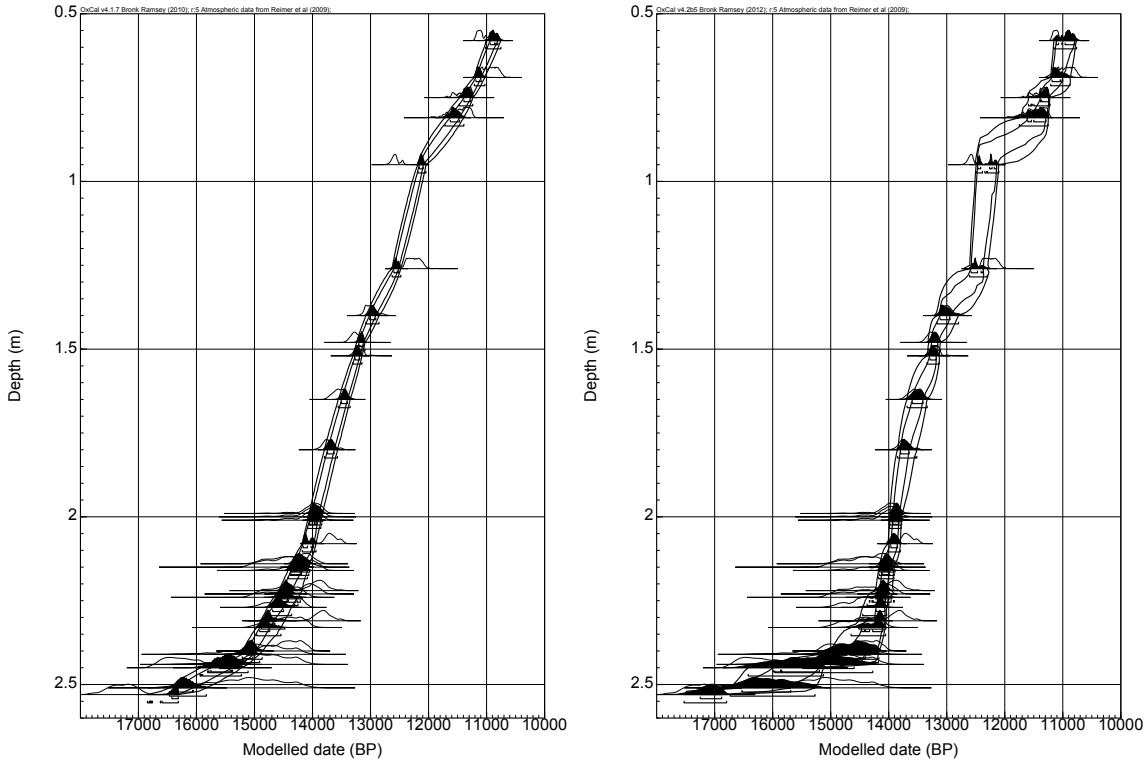


(a) $k = 100$ m$^{-1}$ (b) $k = 10$ m$^{-1}$

Figure 6.2: Radiocarbon chronology from Mortensen et al. (2011), modelled with (a) $k = 100$ m$^{-1}$ and (b) $k = 10$ m$^{-1}$.

chronology with a lower $k$ value results in a chronology that agrees better with the likelihood information.

## 6.3 Prior for the step-size parameter

Bronk Ramsey et al. (2010a) suggest using a model averaging approach to find values for the parameter most consistent with the data. This section discusses and evaluates the utilisation of this method, which has been implemented into the chronology building software, `OxCal`, by Bronk Ramsey. The mathematics remains the same as in Bronk Ramsey (2008), with an extra updating step for the $k$ parameter. A recommendation for a suitable prior is provided at the end of this chapter as a result of this study.

A prior range, instead of a single value, is defined for the $k$ parameter. The parameter becomes a variable and the Bayesian model averaging approach is used by

the analysis to find the suitable values automatically, giving a posterior distribution. The advantage of this method is that the $k$ value, and hence the step-size, is varied in each model run. This means that different values are used in the model instead of one. Using a different $k$ value for each model run makes the model more flexible.

The constraint that applies to this method is

$$p(k) = \begin{cases} 1 & k>0 \\ 0 & \text{otherwise} \end{cases}$$

In `OxCal`, the `CQL` for a Poisson process model, employing the model averaging approach, for a radiocarbon chronology is

```
P_Sequence("name",k,interpolation,magnitude){
    Boundary();
    R_Date(...){z=...;};
    ⋮
    R_Date(...){z=...;};
    }
    Boundary();
};
```

where $k$ defines the parameter, `interpolation` is the number of interpolations per unit depth, and `magnitude` defines the magnitude distribution (and multiplier) of the $k$ parameter. So if

$$\begin{aligned} k &= 10^u \\ u &\sim \mathrm{U}(-2,2) \end{aligned}$$

, the function for the model becomes

```
P_Sequence("",1,0,U(-2,2))
```

for a sequence with no interpolations between events.

The `interpolation` parameter is often neglected when the `P_Sequence` function is employed (e.g. Blockley et al., 2008b). It is useful in estimating the uncertainty between adjacent events. The value of the parameter determines the resolution of

the chronology. This value is defined by the user of the function. A value of 1 would mean that there is 1 interpolated event per unit depth. A higher value would mean smoother lines between events and vice versa. A value of 0 results in a chronology with no interpolation between events. The degree of resolution of the chronology also depends on the density of data. If the events are spaced every 0.5 unit depth, a `interpolation` value of 1 would result in a chronology with no extra interpolation than a chronology with an `interpolation` value of 0.

## 6.4 Model evaluation

This section evaluates the utilisation of the Bayesian model averaging approach in the Poisson process prior for modelling deposition. Various simulations were constructed in order to evaluate this new development, and these are discussed in detail below.

### Simulations using two fixed points

Two fixed points, at 1000 and 0 (BP), are modelled with the Poisson process model, employing the model averaging approach, with the prior range for the $k$ parameter defined as

$$\begin{aligned} k &= 10^u \\ u &\sim U(-1, 2) \end{aligned} \tag{6.1}$$

, i.e. between 0.01–100 events per unit depth (depth$^{-1}$). The results of this simulation are shown in Figure 6.3. Without additional dating information between the fixed points, the posterior distribution for the $k$ parameter is same as its prior distribution. This simulation is repeated with a wider prior range

$$\begin{aligned} k &= 10^u \\ u &\sim U(-4, 4) \end{aligned} \tag{6.2}$$

, i.e. between $10^{-4}$–$10^4$ events depth$^{-1}$. The results of this second simulation (Fig.6.4) show that the posterior deposition model is narrower, with reduced uncertainties.

This is because the prior range for the $k$ parameter had been increased, and the $k$ parameter is allowed to go above $10^2$ depth$^{-1}$, and by allowing higher $k$ values, the model has reduced uncertainties for the posterior distributions. The posterior distribution of the $k$ parameter shows that it is constrained by the density of the data. Since there are only two fixed points in the 10 units of depth in the simulated model, one cannot expect a single deposition unit to be bigger than 10 units of depth. The means that the $k$ parameter cannot be lower than 0.1 depth$^{-1}$ and this is shown in Figure 6.4b.

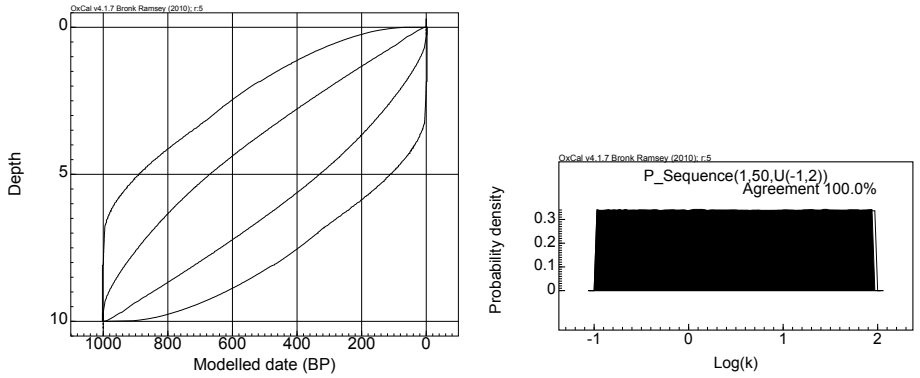


(a) Posterior model (b) Posterior distribution for $k$

Figure 6.3: Modelling two fixed points, at 1000 and 0 BP, with the prior from eq. 6.1 for the $k$ parameter. (a) The posterior age-depth model at 68.2% and 95.4%, and (b) the posterior distribution for the $k$ parameter.

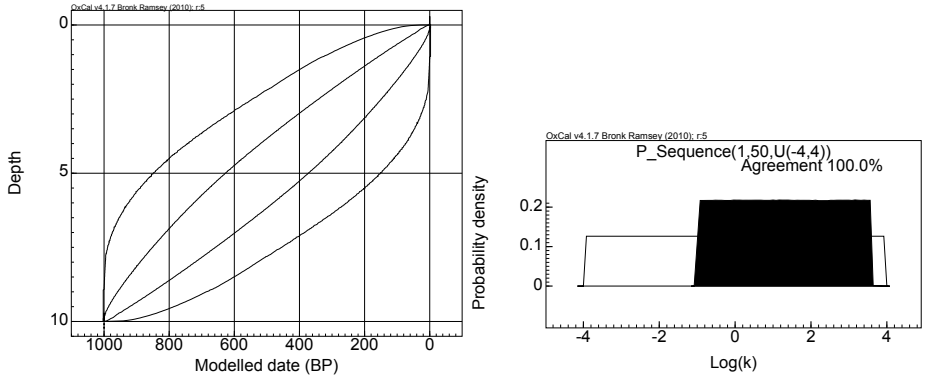


(a) Posterior model (b) Posterior distribution for $k$

Figure 6.4: Modelling two fixed points, at 1000 and 0 BP, with the prior from eq. 6.2 for the $k$ parameter. (a) The posterior age-depth model at 68.2% and 95.4%, and (b) the posterior distribution for the $k$ parameter.

The purpose of this simulation is to test that through the implementation of the addition of the prior range for the $k$ parameter in `OxCal`, the modelling two fixed

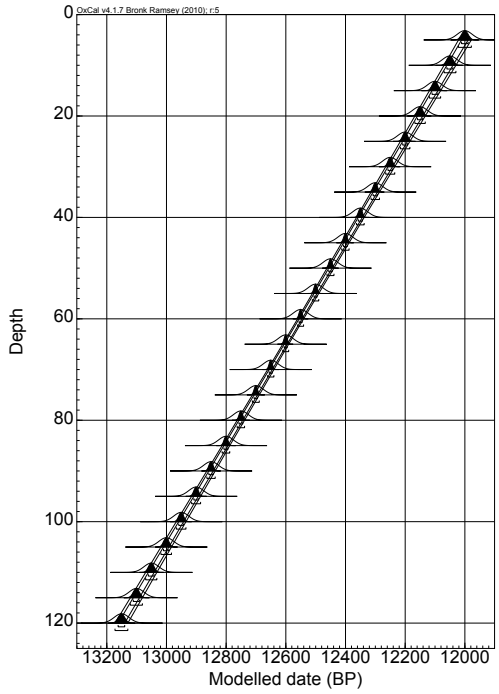


Figure 6.5: A uniform sequence of Gaussian distributions modelled using a prior assuming uniform deposition at 68.2% and 95.4% probability.

points without additional constraints gives a uniform posterior distribution for the $k$ parameter. This is what one would expect because the simulated model does not provide information for modelling $k$, i.e. $p(k|\mathbf{x}, \mathbf{t}, \mathbf{z}) \propto 1$. The $k$ parameter is, however, constrained to the defined prior, and the density of the likelihood information, i.e. the difference in depth between the deposition units.

## Simulations using a sequence of Gaussian distributions

A sequence of Gaussian distributions assuming a uniform rate of deposition is simulated (light grey distributions; Fig. 6.5). The logical choice of prior for this sequence is one that assumes a uniform rate of deposition, i.e. the `U_Sequence` deposition model. Modelling this sequence with `U_Sequence` results in a more refined chronology (dark grey distributions; Fig. 6.5).

The same simulated sequence is modelled using the Poisson process deposition model, using the prior

$$\begin{aligned} k &= 10^u \\ u &\sim U(-1, 3) \end{aligned} \tag{6.3}$$

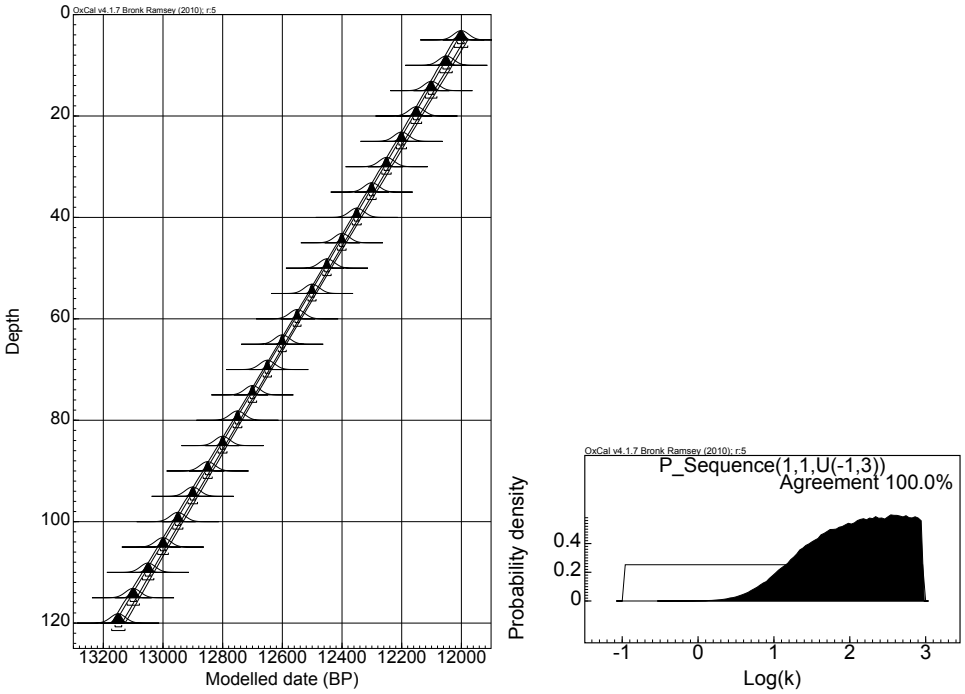


(a) Posterior age-depth model (b) Posterior distribution for $k$

Figure 6.6: A uniform sequence of Gaussian distributions modelled using the Poisson process model, with the prior for the $k$ parameter from eq. 6.1. (a) The posterior age-depth model at 68.2% and 95.4%. (b) The posterior distribution for the $k$ parameter.

in eq. 6.1 for the $k$ parameter. This prior was chosen because the deposition unit is assumed to be no smaller than 0.001 units of depth (or $10^3$ depth$^{-1}$), and no bigger than 5 units of depth (or 0.2 depth$^{-1}$), since that is the size of the gaps between the events. Results are shown in Figure 6.6. The posterior distribution for the $k$ parameter tends towards higher values (Fig. 6.6b), giving the model more rigidity. The resulting posterior age-depth model is thus very close to that of the one modelled assuming a uniform rate of deposition (using `U_Sequence`).

In the third scenario, a uniform sequence of Gaussian distributions with missing data in the middle was simulated. This sequence is modelled using four different priors:

(a) with only the ordering of events defined (`Sequence`);

(b) assuming a Poisson process with a single value of $k$ (`P_Sequence`; with $k = 1$);

(c) assuming a Poisson process with a distribution for $k$ (`P_Sequence`; with eq. 6.1); and

(d) assuming a uniform deposition (`U_Sequence`).

Figure 6.7a shows four posterior chronologies:

(a) the grey distributions (with no interpolation);

(b) the blue chronology;

(c) the red chronology; and

(d) the green chronology.

modelled with the corresponding priors. The posterior age-depth models (Fig. 6.7a) show that defining the order of events in such a uniform sequences provides little constraint for reducing the uncertainties of individual events. The model averaging technique gives a tighter overall (red) chronology, in comparison to the output of the model without the use of model averaging (blue chronology). The red chronology is also very similar to the green chronology, from modelling with a uniform deposition model. The posterior distribution for the $k$ parameter in model (c) is shown in Figure 6.7b, and the interpolated posterior ages at depth at 100 are shown in Figure 6.8.

In a separate simulation, the deposition is assumed to be non-uniform, with offset upper and lower sections. This sequence is modelled with the Poisson process prior with $k$ defined as:

(a) $k = 1$;

(b) $k = 2$;

(c) $k \sim U(10^{-1}, 10^{2})$.

Figure 6.9a shows three posterior interpolated chronologies:

(a) the blue chronology;

(b) the purple chronology; and

(c) the grey chronology.

modelled with the corresponding priors. The posterior age-depth models are shown in Figure 6.9a. The posterior distribution for the $k$ parameter in model (c) is shown in Figure 6.9b, and the interpolated posterior ages at depth at 75 are shown in Figure 6.10.

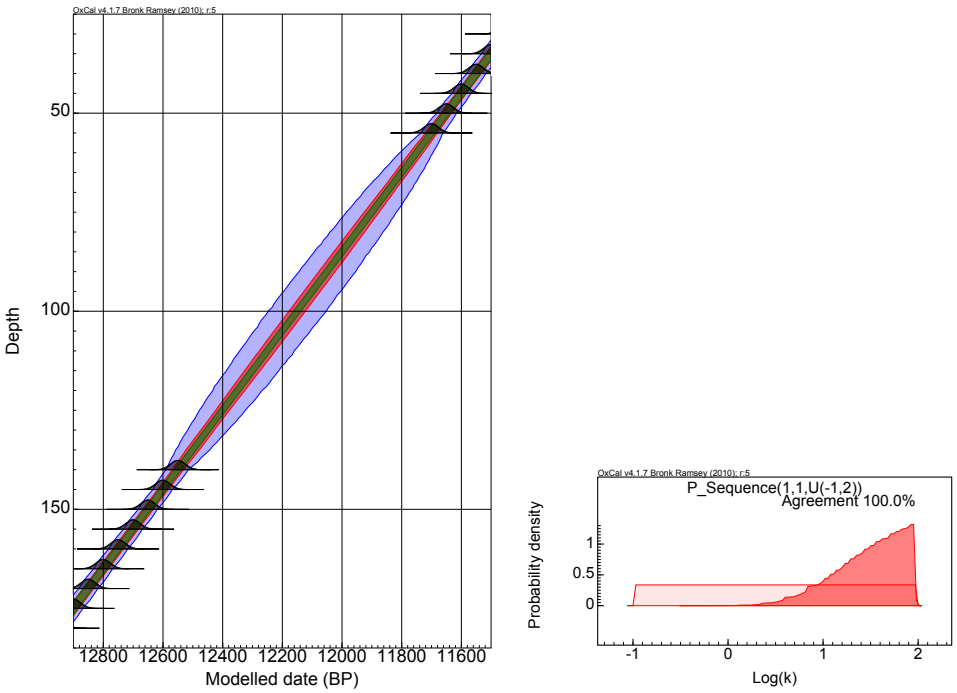


(a) Posterior models (b) Posterior distribution for $k$

Figure 6.7: A uniform sequence of Gaussian distributions (a) modelled using the `U_Sequence` model (grey distributions), the `P_Sequence` model, with $k = 1$ (blue chronology), $k = 2$ (red chronology), and $k \sim \mathrm{U}(10^{-1}, 10^2)$ (green chronology) at 95.4%. (b) Posterior distribution for the $k$ parameter model with $k \sim \mathrm{U}(10^{-1}, 10^2)$. See text for details.

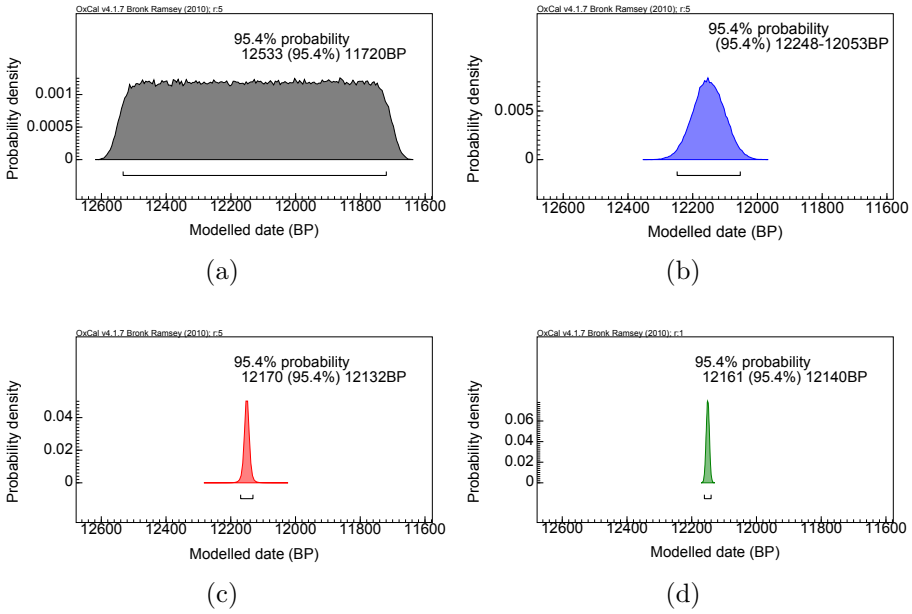


Figure 6.8: Posterior distributions at depth at 100 at 95.4%, modelled with (a) the `Sequence` model; (b) the `P_Sequence` model, with $k = 1$; (c) the `P_Sequence` model with $k \sim U(10^{-1}, 10^2)$; and (d) the `U_Sequence` model.

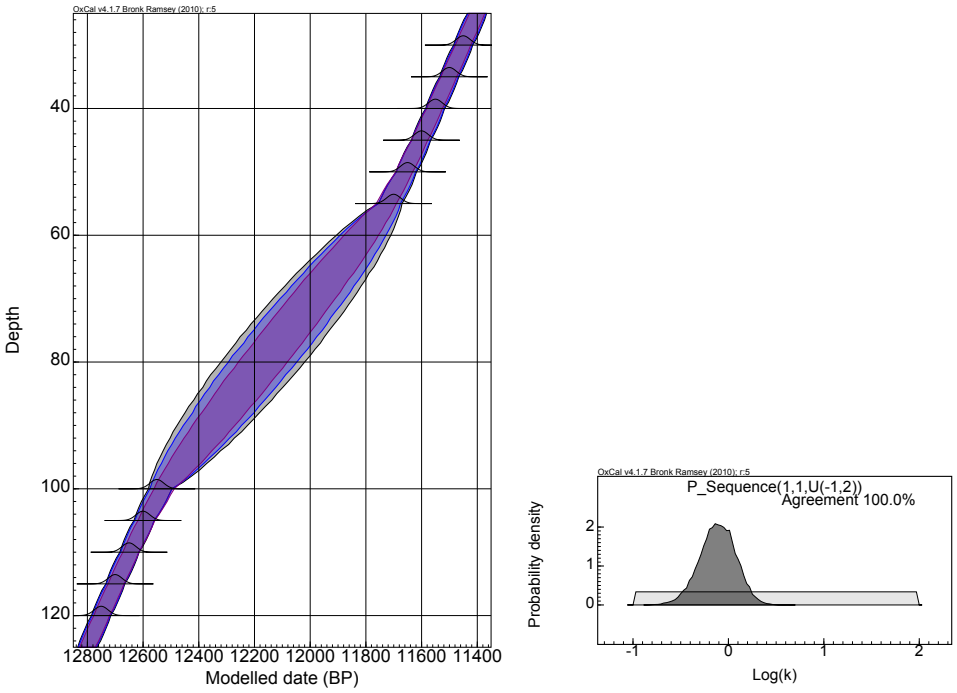


(a) Posterior models (b) Posterior distribution of $k$

Figure 6.9: A non-uniform sequence of Gaussian distributions (a) modelled using the `P_Sequence` model, with $k = 1$ (blue), $k = 2$ (purple), and $k \sim \mathrm{U}(10^{-1}, 10^2)$ (grey) at 95.4%. (b) Posterior distribution for the $k$ parameter in model with $k \sim \mathrm{U}(10^{-1}, 10^2)$. See text for details.

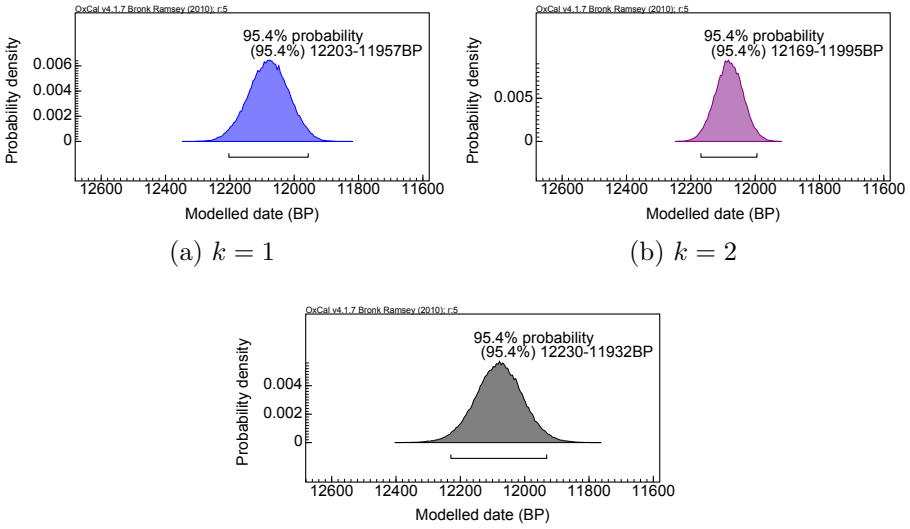


(a) $k = 1$ (b) $k = 2$

(c) $k \sim U(10^{-1}, 10^2)$

Figure 6.10: Posterior distributions at depth at 75 at 95.4%, modelled with the Poisson process prior with (a) $k = 1$; (b) $k = 2$; and (c) eq. 6.1.

The interpolated posterior distributions in Figures 6.8 and 6.10 show that the posterior distributions of the chronologies modelled with the model averaging approach have longer tails (Fig. 6.8c and 6.10c) than those where model averaging was not employed. This suggests that the utilisation of the model averaging approach accounts for more uncertainty and makes the Poisson process deposition model more robust, giving the model more flexibility.

## Simulations using a sequence of radiocarbon determinations

Radiocarbon sequences are simulated using the `R_Simulate` function in `OxCal`, where calendar ages and expected uncertainties are used to calculate a likelihood function. The simulated radiocarbon chronologies with:

(a) no outliers; and

(b) one outlier, (highlighted in purple)

are modelled using the Poisson process model using the model averaging technique. The prior range for the $k$ parameter was defined as eq. 6.1 for deposition using the model averaging technique. The posterior chronologies for these simulations are shown in Figures 6.11 and 6.12. Model (b) was repeated with formal outlier analysis to yield a posterior chronology in Figure 6.13.

These simulations show that the Poisson process deposition model, together with the model averaging approach, can be used to reduce the uncertainties in radiocarbon chronologies. This technique also works together with formal outlier analysis, which is currently available in `OxCal`. The presence of just one outlier has a great effect on the posterior distribution of the $k$ parameter (Fig. 6.12b). This also has an effect on the overall posterior output, increasing the uncertainties in the chronology. However, once the outlier is removed or down-weighted, the resulting posterior distribution for the $k$ parameter (Fig. 6.13) is very similar to that of the simulations without outliers (Fig. 6.11a). The posterior distributions for the $k$ parameters in these simulations are not the same due to the different likelihood distributions from the simulations. This

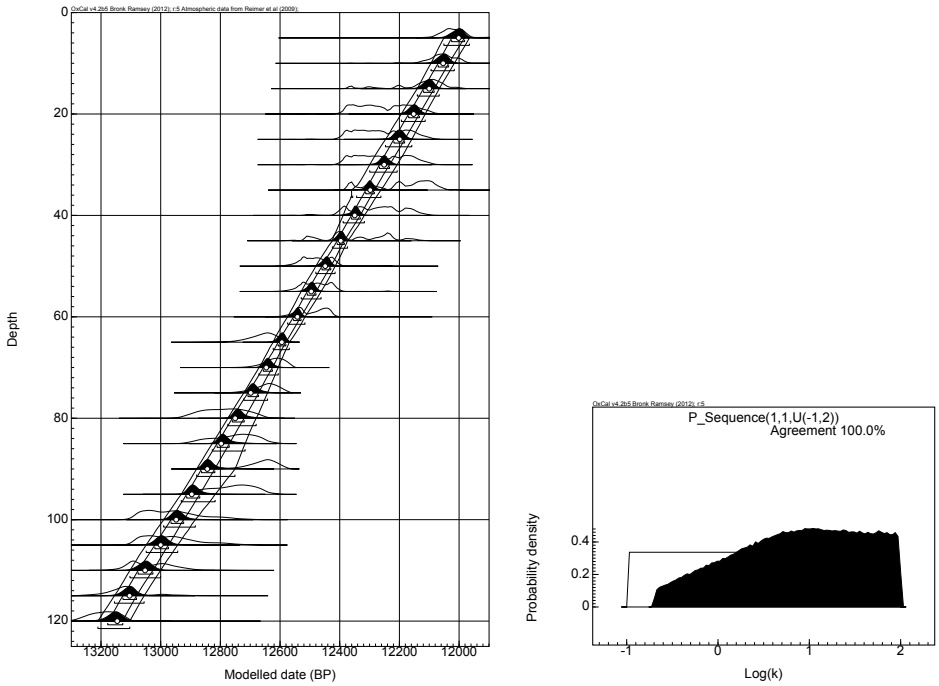


(a) (b)

Figure 6.11: A uniform radiocarbon sequence without outliers (a) modelled with Poisson process, employing the model averaging technique, at 68.2% and 95.4%. The 'true' chronology is shown with white dots. (b) Posterior distribution for the $k$ parameter.

very simple exercise illustrates that the $k$ parameter, and hence the overall posterior chronology, are sensitive to the treatment of outliers.

In all of the above simulations, a uniform rate of deposition was assumed. In a separate simulation, deposition was assumed to be less stable (where the deposition rate is assumed to be non-uniform and varies though the entire sequence). Modelling with the `P_Sequence` model and utilising the model averaging approach gives results in Figure 6.14. The uncertainties in the overall posterior chronology is greater than the other simulations due to less regular sedimentation. This is also the result of a lower $k$ parameter used.

It should be emphasised that when model averaging is employed, a single $k$ value is used and updated in each iteration of the model run. The simulations show that the posterior distribution for $k$ is governed by the density of the likelihood information constrained within a given depth and a given period. This is unsurprising since Bronk Ramsey (2008) proved that $k$ can be estimated using the variability in age and

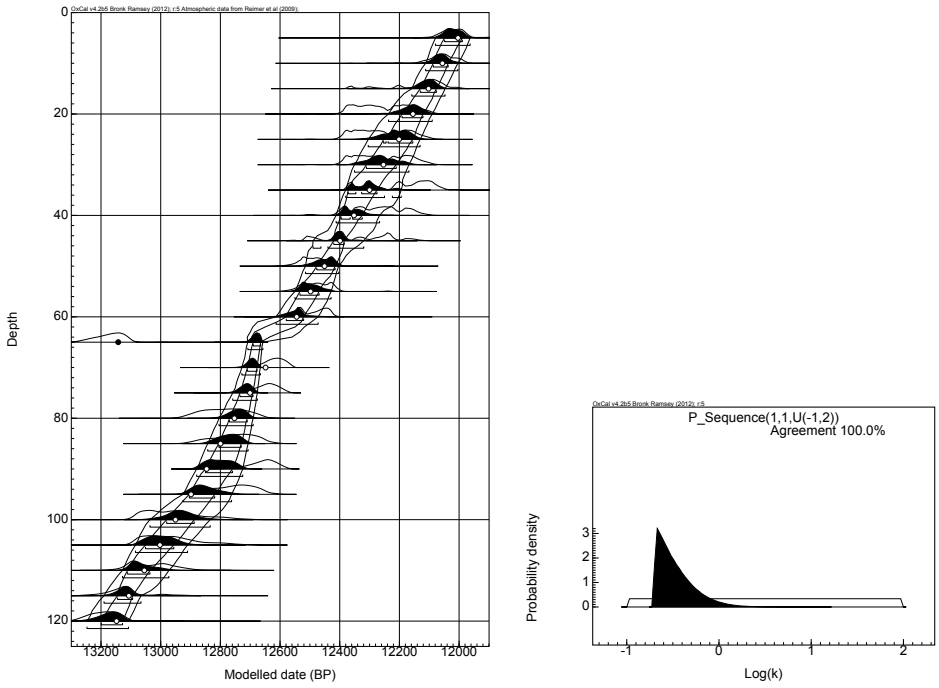


(a) (b)

Figure 6.12: A uniform radiocarbon sequence with one outlier (a) modelled with Poisson process, employing the model averaging technique, at 68.2% and 95.4%. The 'true' chronology are shown with white dots and the outlier is shown with a black dot. (b) Posterior distribution for the $k$ parameter.

depth in sequences.

## 6.5 Summary

There is a high demand for deposition models for sedimentary sequences and a number of models have been made available through various chronology building packages. The Poisson process deposition model (`P_Sequence;` Bronk Ramsey, 2008) is the first robust approach for modelling sedimentary sequences with depth information since it reflects the nature of the information that goes into the model prior more accurately than piece-wise linear, for example, `Bpeat` (Blaauw and Christen, 2005), `BChron` (Haslett and Parnell, 2008); or uniform, for example, `U_Sequence` (Bronk Ramsey, 1998), deposition models. However, the `P_Sequence` model relies on a defined value for step-size (also known as the $k$ parameter). Although Bronk Ramsey (2008) introduced a way of estimating an appropriate value for this parameter, this method relies on the

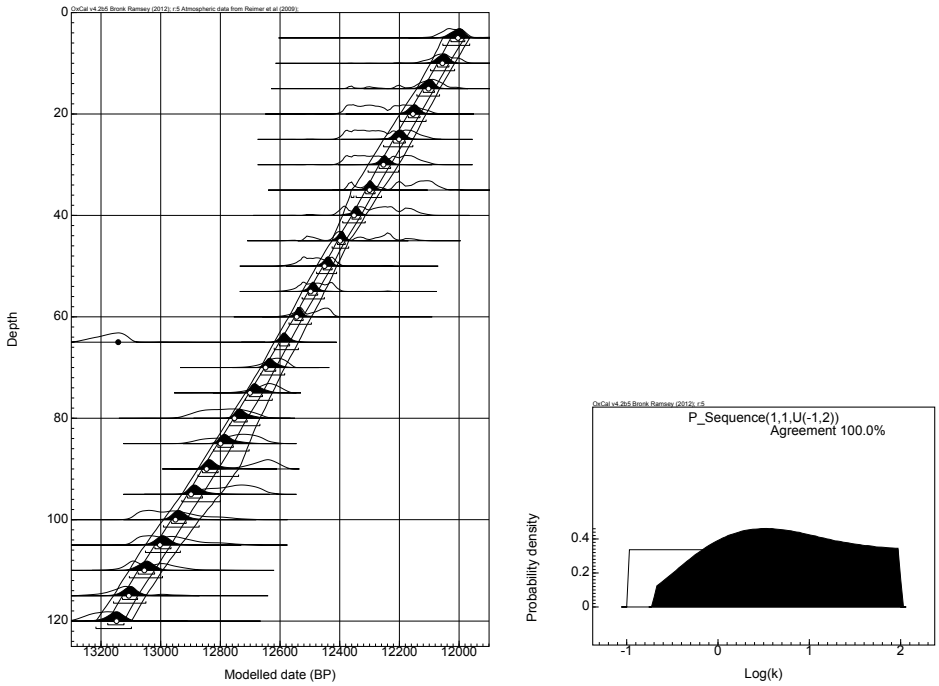


(a) (b)

Figure 6.13: A uniform radiocarbon sequence with one outlier (a) modelled with Poisson process, employing the model averaging technique; and formal outlier analysis, at 68.2% and 95.4%. The 'true' chronology is shown with white dots and the outlier is shown with a black dot. (b) Posterior distribution for the $k$ parameter.

presence of known age stratigraphic markers in the sequence. In sequences without known age markers, the $k$ parameters are often estimated from the dating information, or arbitrarily. This introduces subjectivity in the model selection process, sometimes resulting in circular reasoning, or unrealistic chronologies. This chapter evaluated the use of the Bayesian model averaging approach (previously discussed in Section 4.3.2) in the `P_Sequence` model, removing the subjectivity in model selection by defining a range, instead of a value, for the $k$ parameter and shows that it can accurately model the simulated sequences. The model utilises different parameter values and reaches a posterior distribution which is most appropriate for the data. The model averaging approach in `P_Sequence` is also compatible with the `Outlier` model in `OxCal`, which also utilises model averaging. Below is a suggestion of a prior range for the $k$ parameter suitable for modelling the majority of depositional sequences.

Utilising the Bayesian model averaging approach in the `P_Sequence` model requires the input of a prior range. In theory, the lower the lower limit of the $k$ parameter is,

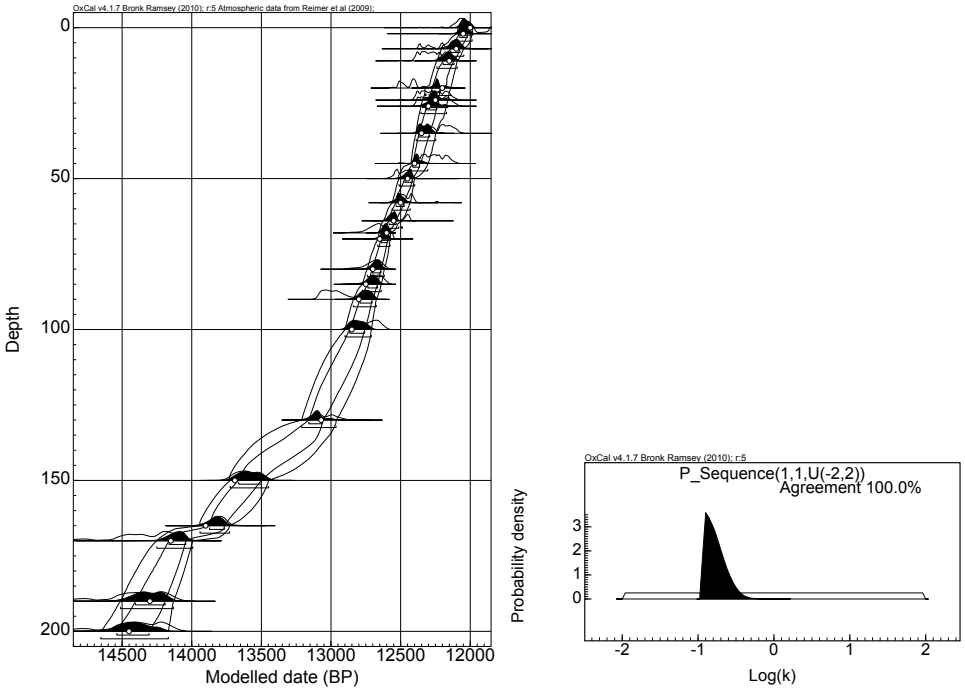


(a) (b)

Figure 6.14: A radiocarbon sequence (a) modelled with Poisson process, employing the model averaging technique; and formal outlier analysis, at 68.2% and 95.4%. The 'true' chronology is shown with white dots. (b) Posterior distribution for the $k$ parameter.

i.e. when $k \to 0$, the closer the posterior chronology is to that of a `Sequence` model; and the higher the higher limit of the $k$ parameter is, i.e. when $k \to \infty$, the closer the posterior chronology is to that of a `U_Sequence` model. However, in practice, the lower limit of the $k$ parameter is irrelevant as it is limited by the density of events within the given depth. The simulations in this chapter were performed without specifying the units in depth. In reality, the depth units of a sequence will affect ones choice of prior range for a model. For example, for a sequence in centimetres, which any of the simulated sequences could be, one might expect a deposition unit to be no bigger than 1 m, and no smaller than 0.01 cm in size. The various simulations in this chapter suggest that an initial prior range of

$$\begin{aligned} k &= 10^u \\ u &\sim U(-2, 2) \end{aligned}$$

is wide enough for a sequence with depths in cm. So for a sequence with depths in

m, this would be

$$\begin{aligned} k &= 10^u \\ u &\sim U(0,4) \end{aligned}$$

. In terms of the `CQL` in `OxCal`, the Poisson process models can be defined as

`P_Sequence("",1,0,U(-2,2)){...};` for a sequence in cm; or

`P_Sequence("",1,0,U(0,4)){...};` for a sequence in m.

The latter function can also be rewritten as

```
P_Sequence("",100,0,U(-2,2)){...};
```

since the `magnitude` parameter is also a multiplier of the $k$ parameter. The lower limit of the prior range can be subsequently adjusted (lowered) if data is sparse within the given depths.

# Part III

# Application of the improved methodologies to archaeological and environmental case studies

# Chapter 7

# Modelling cultural change

Over the years, scholars have been using Bayesian methods to model absolute dates from archaeological finds in order to infer the dates of transitions between different material cultures (e.g. Needham et al., 1997; Bruins et al., 2003; Finkelstein and Piasetzky, 2010b; Mazar, 2011). Phase models are often used to group together, and assign relationship to, archaeological events. Events (or, in most archaeological cases, artefacts) can be related in terms of typology, and / or geographical regions; and a phase prior can be used to model activity in terms of their rate of usage, deposition, or production. The most commonly used model is the uniform phase prior (Buck et al., 1992), which assumes a uniform distribution of material within two temporal constraints. These constraints are also the `boundary` parameters of the model (discussed in Section 3.4.2) and are useful for modelling the onset and end of significant activity of a group of events. A recent development by Karlsberg (2006) introduced a trapezoid prior for modelling non-instantaneous processes. It is a more realistic prior for modelling cultural change because phase transitions can take time.

Chapter 5 already discussed the reparameterisation and the addition of a *utp* element to the trapezoidal phase prior model. Reparameterisation allows the modelling of contiguous (or abutting) phases and draws inference on the duration of transition between two phases. The model becomes more robust with the addition of a *utp* element, and better reflects prior knowledge. This chapter presents three case stud-

ies: firstly, an Early Bronze Age Irish bowl data set is used to examine the effects of the modifications from Chapter 5; secondly, the use of the trapezoidal phase prior is extended to model a multiple phase scenario addressing British Bronze Age metalwork and compare two independent implementations of the model; and thirdly, the trapezoidal phase prior is used to address the Iron Age chronology in Israel.

The case studies in this, and the following chapters, are modelled following the framework suggested in Bayliss (2009) and discussed in Chapter 4. Part of this chapter is published in Lee and Bronk Ramsey (2012).

## 7.1 The Early Bronze Age Irish bowl tradition

The Early Bronze Age Irish pottery is made up of a number of recognised cultural and stylistic groups. Irish bowl pottery is one of the traditions that is found in clearly defined contexts of comparable type (in this case, graves). They occur singly or in small numbers, are associated with materials which are suitable for dating, and are usually complete when found (Brindley, 2007, p.11). The bowl tradition is known primarily through its funeral customs. The graves of Early Bronze Age Ireland often include a vessel, sometimes more than one. Burials accompanied by bowls are found at passage tombs, court tombs and in the mounds of the Linkardstown Burial group (Brindley, 2007, p.51). Bowls are also found in rare and poorly preserved Bronze Age settlement sites. However, the assemblage of sherds of bowl pottery from such contexts is often mixed with sherds of beaker pottery (of an earlier assemblage). Therefore, the temporal relationship between the two cannot be shown on the basis of the excavated context (Brindley, 2007, p.52).

Bayliss and O'Sullivan (forthcoming) use a uniform phase prior to estimate the temporal constraints of the bowl pottery and associated burial tradition after reassessing the reliability of each radiocarbon date. The authors mention that the trapezoidal phase model would be more appropriate for modelling the occurrence of archaeological types due to the classic "battleship" shape of seriation frequency graphs (discussed

in Chapter 5).

### 7.1.1 Modelling

The temporal constraints of interest are the start and end of the bowl usage. In this section, the Early Bronze Age Irish bowl data set is analysed using the uniform phase prior, the simple trapezoidal phase prior (Karlsberg, 2006), and the modified trapezoidal phase prior, with the new parameters and *utp* element, to draw inference on the temporal constraints. The differences in the outputs are also discussed.

Seventy-two radiocarbon determinations were reported in a catalogue produced by Brindley (2007, Chapter 4) and the full dataset can be found in Appendix B.2. Five of these measurements were duplicates used to cross check the reproducibility using both conventional and AMS techniques. The conventional measurements (GrN-14616, GrN-11352, GrN-12958, GrN-9323 and GrN-11901) are reported as being too old for reasons unknown, and will be excluded in this analysis. Another three duplicate dates are used in a testing program for carbonate from unburnt bone. The carbonate results from these samples (GrA-13331, GrA-13332 and GrA-13330) appear reliable, but carbonate in unburnt bone is likely to take up contamination (Brindley, 2007). Thus, these samples are also excluded from this analysis. A further eleven dates (GrN-11363, UB-3987, UB-3988, UB-3989, GrN-12958, UB-3985, UB-3986, GrA-24152, GrA-24193, GrN-11450 and GrA-24154) are removed from this analysis due to contamination or mis-association. Three more measurements (GrN-15491, GrN-15492 and GrN-15493) were excluded from Brindley's analysis due to possible dietary offset, but are included in our analysis as these measurements do not appear to be anomalous when compared with the remainder. A total of fifty-three dates are therefore included in the models in this section.

#### 7.1.1.1 Modelling with a uniform phase prior

Figure 7.1 and Table 7.1 summarise the results from modelling the Early Bronze Age Irish bowl data set with a uniform phase prior, at 68.2% and 95.4% probability.

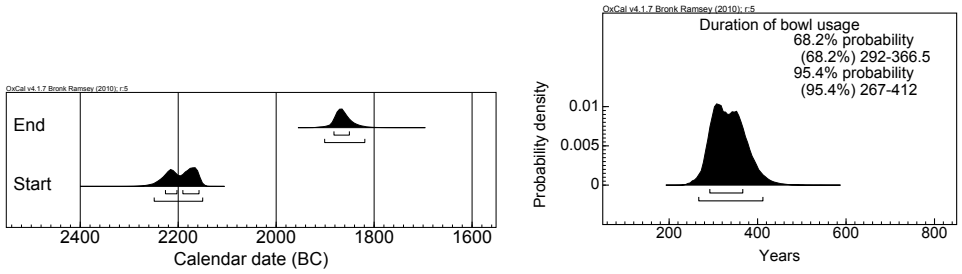


(a) (b)

Figure 7.1: Uniform prior estimates of the: (a) start and end, and (b) duration of the Irish bowl tradition, at 68.2% and 95.4% probability.

The model parameters give prior estimates of the start and end of significant phase activity.

| | Modelled date (cal BC) | |
|---|---|---|
| | 68.2% | 95.4% |
| Start | 2227–2158 | 2250–2151 |
| End | 1883–1851 | 1902–1820 |

Table 7.1: Uniform prior estimates of the start and end of the Irish Bowl tradition, at 68.2% and 95.4% probability.The calendar limits are set the same for this and the following figures.

#### 7.1.1.2 Modelling with a simple trapezoidal phase prior

Figure 7.2 and Table 7.2 summarise the results from modelling the Early Bronze Age Irish bowl data set with a simple trapezoidal phase prior (Karlsberg, 2006), at 68.2% and 95.4% probability. The model parameters give prior estimates of the start ($t_\alpha$), the start of peak popularity ($t_\beta$), the start of decline ($t_\gamma$), and the end ($t_\delta$) of phase activity.

| | Modelled date (cal BC) | |
|---|---|---|
| | 68.2% | 95.4% |
| $t_\alpha$ | 2314–2219 | 2362–2168 |
| $t_\beta$ | 2152–2010 | 2204–1943 |
| $t_\gamma$ | 2022–1897 | 2096–1858 |
| $t_\delta$ | 1863–1787 | 1881–1720 |

Table 7.2: Trapezoidal prior (Karlsberg, 2006) estimates of the Irish Bowl tradition, at 68.2% and 95.4% probability.

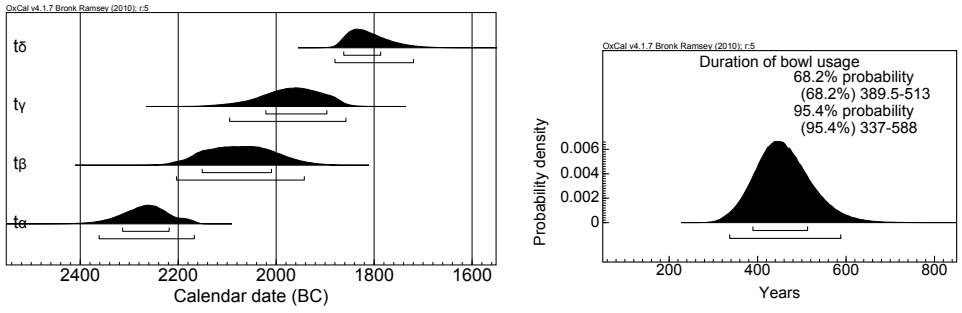


(a) (b)

Figure 7.2: Trapezoidal prior (Karlsberg, 2006) estimates of the Irish bowl tradition: (a) model parameters and (b) time span of the model, at 68.2% and 95.4% probability.

#### 7.1.1.3 Modelling with the modified trapezoid phase prior

Chapter 5 introduced new parameters and the addition of a *utp* element to Karlsberg's trapezoidal phase prior model, and the modified prior (Fig. 5.1) is used here to model the Irish bowl data set. Figures 7.3 and 7.4 and Table 7.3 summarise the results, at 68.2% and 95.4% probability. The model parameter give prior estimates of the start ($t_\alpha$), the start of peak popularity ($t_\beta$), the start of decline ($t_\gamma$), and the end ($t_\delta$) of phase activity. The new `boundary` parameters give prior estimates of the start ($t_1$) and end ($t_2$) of significant phase activity; and the transition parameters give prior estimates of the duration of phase transitions, which are essentially the differences between $t_\alpha$ and $t_\beta$ ($d_1$), and between $t_\gamma$ and $t_\delta$ ($d_2$).

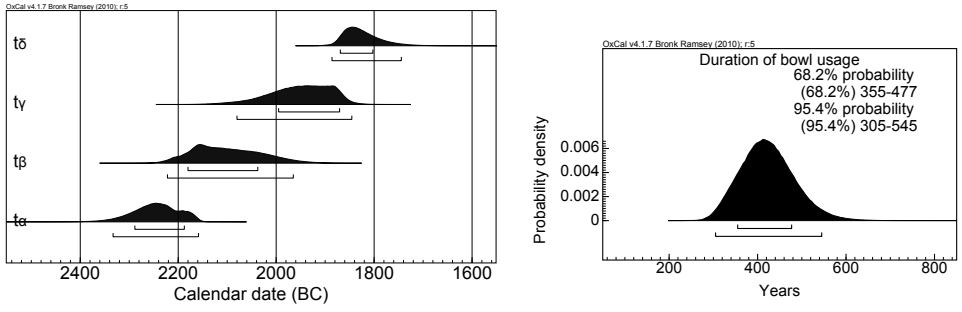


(a) (b)

Figure 7.3: Trapezoidal prior estimates of the Irish bowl tradition: (a) model parameters and (b) time span of the model, conditioned by the *utp* element (eq. 5.10), at 68.2% and 95.4% probability.

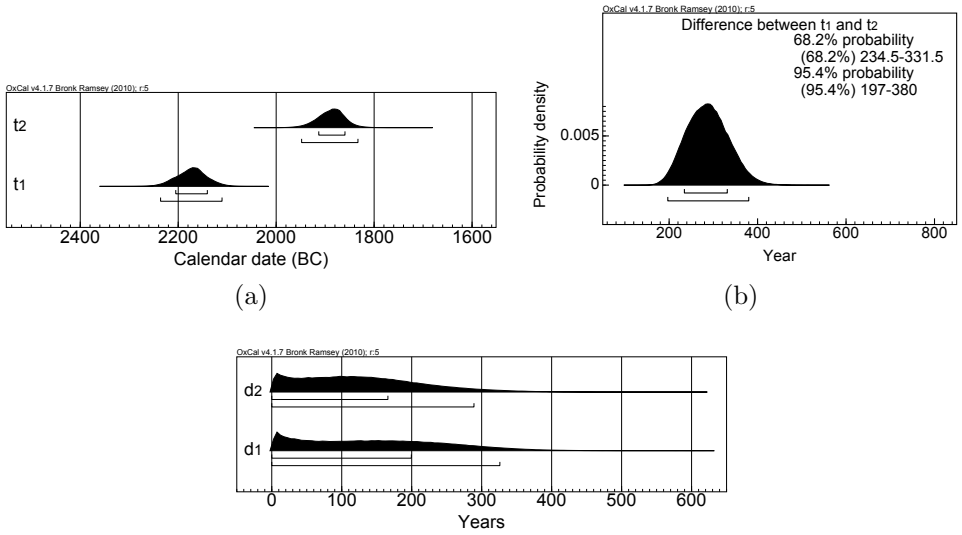


Figure 7.4: Trapezoidal prior estimates of the Irish bowl tradition: (a) `boundary` parameters; (b) the difference between the `boundary` parameters ($t_2 - t_1$) and (c) `transition` parameters, conditioned by the *utp* element (eq. 5.10), at 68.2% and 95.4% probability.

| | Modelled date (cal BC) | | | Modelled date (cal BC) | | | Years | |
|---|---|---|---|---|---|---|---|---|
| | 68.2% | 95.4% | | 68.2% | 95.4% | | 68.2% | 95.4% |
| $t_\alpha$ | 2289–2188 | 2334–2159 | $t_1$ | 2206–2141 | 2237–2111 | $d_1$ | 0–199.5 | 0–326 |
| $t_\beta$ | 2181–2038 | 2223–1966 | | | | | | |
| $t_\gamma$ | 1996–1871 | 2081–1846 | $t_2$ | 1914–1860 | 1949–1834 | $d_2$ | 0–166 | 0–289 |
| $t_\delta$ | 1870–1803 | 1887–1745 | | | | | | |

Table 7.3: Trapezoidal prior estimates of the Irish Bowl tradition, at 68.2% and 95.4% probability.

The new `boundary` parameters of the trapezoidal phase model give comparable prior estimates to those of the uniform phase model. The difference between said parameters is also more comparable to that modelled using the uniform phase prior, but is slightly shorter as one would expect. The utilisation of the *utp* element has reduced the duration of bowl usage (Fig. 7.2b and 7.3b) by 34.5–36 and 32–43 years, 68.2% and 95.4% probability, respectively.

### 7.1.2 Discussion

The trapezoidal phase prior is more appropriate than the uniform phase prior for modelling the start and end of the Irish bowl pottery usage, and associated burial

tradition. This is because, *a priori*, the change in artefact types is a non-instantaneous process and using the trapezoidal phase model better reflects the nature of the information that goes into the prior.

Two modifications of the trapezoidal phase prior were proposed in Chapter 5: alternative parameterisation; and the addition of a non-informative prior element, the *utp*. Reparameterisation does not alter the underlying mathematics of the model but gives prior estimates comparable to those of the uniform phase model parameters. It also means that the trapezoidal phase model can be used in contiguous phase scenarios (see next section). Interestingly, the new `boundary` estimates from the trapezoidal phase prior (Fig. 7.4a) are comparable to those of the uniform phase prior (Fig. 7.1a). They overlap significantly (80%). The probability density functions are shifted slightly in some cases because different underlying usage rates were assumed in both models. The addition of the *utp* is essential in removing the bias, which exists in the simple trapezoidal phase prior model. The utilisation of the *utp* element has reduced the duration of the Irish bowl usage, as one would expect due to the shortening of the `transition` parameters.

The trapezoidal phase prior is useful for situations where the phase activity follows the pattern of a gradual increase, then a period of constant activity, and finally a gradual decrease, and also in cases where a more robust prior than that provided by the uniform phase prior is needed. It is appropriate for modelling many forms of material culture, such as pottery (as here), and types of metalwork (see next section).

## 7.2 British Bronze Age metalwork

The British Bronze Age is separated into major periods (also known as stages). Within the stages, there are sub-divisions. The sub-divisions within the major periods of British Bronze Age that are discussed in this section have been relatively dated to be in the order of: Acton and Taunton; Penard; Wilburton; Blackmoor; and Ewart Park (O'Connor, 1980).

Needham et al. (1997) obtained radiocarbon measurements from organic materials in immediate physical contact with various types of bronze objects in an attempt to derive an independent chronology of British Bronze Age metalwork. The authors combined absolute dates from the organic materials with relative information using a Bayesian framework. Thirty-eight dates were put into five phases based on the artefact types: Acton and Taunton; Penard; Wilburton; Blackmoor; and Ewart Park (appendix B.1). Two separate Bayesian models were constructed using the uniform phase prior: Model A, which assumes independent overlapping phases; and Model B, which assumes contiguous phases. Needham et al. (1997) concluded that the independent British Bronze Age chronology supports the relative chronology of O'Connor (1980).

### 7.2.1 Modelling

In this section, the Needham et al. analyses are repeated using the modified trapezoidal phase model (Fig. 5.1), with the new parameters and the additional *utp* element (discussed in Chapter 5). Two separate models are constructed: Model A, which assumes independent overlapping phases; and Model B, which assumes contiguous phases. Karlsberg's parameters of the trapezoidal prior model are also used to draw inference on the start ($t_\alpha$), the start of peak popularity ($t_\beta$), the start of decline ($t_\gamma$), and end of phases ($t_\delta$). The differences in outputs from the trapezoid phase prior and the uniform phase prior are also discussed.

#### 7.2.1.1 Model A: *Overlapping phases*

Model A includes five independent overlapping trapezoid phases: Acton and Taunton; Penard; Wilburton; Blackmoor; and Ewart Park. This model assumes no ordering relationship between the five phases (Fig. 7.5a). Results of this model are summarised in Figure 7.5b. The letters in square brackets next to the model parameters indicate the phases in which they belong, where AT = Acton & Taunton,; P = Penard; W = Wilburton; B = Blackmoor; and EP = Ewart Park.

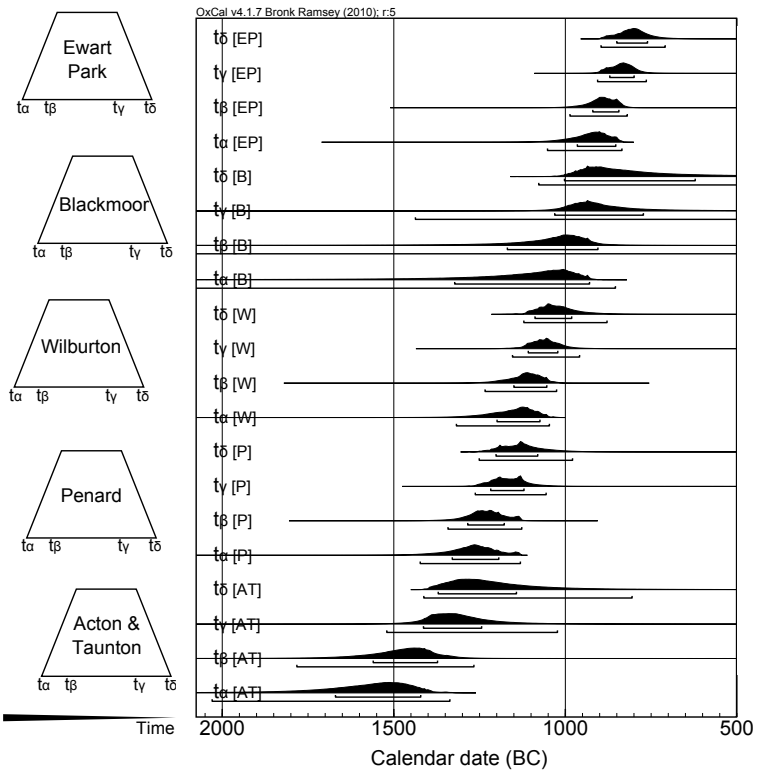


(a) (b)

Figure 7.5: Model A: (a) model schematic; and (b) trapezoidal prior estimates for the Bronze Age metalwork assemblages, at 68.2% and 95.4% probability.

The degree of overlap between the rise and decline of phases are also investigated by calculating differences between the last two parameters of an earlier phase ($t_\gamma$ and $t_\delta$) and the first two parameters of a later phase ($t_\alpha$ and $t_\beta$). For example, in order to draw inference on the degree of overlap between the decline of Acton and Taunton and the rise of Penard, the marginal distributions representing the start and end of the rise of Penard ($t_\alpha$ and $t_\beta$) are subtracted from the start and end of the decline of

Acton and Taunton ($t_\gamma$ and $t_\delta$), respectively. This is done by importing these posterior distributions into `OxCal` using the `Prior` command, and the differences between the parameters are calculated using the `Difference` command for the adjacent phases. Differences between the parameters in Wilburton and Ewart Park are also calculated due to the imprecision of the Blackmoor phase. The results are summarised in Figure 7.6. Tables 7.4 and 7.5 summarise the overlap and gaps, respectively, in years between distributions.

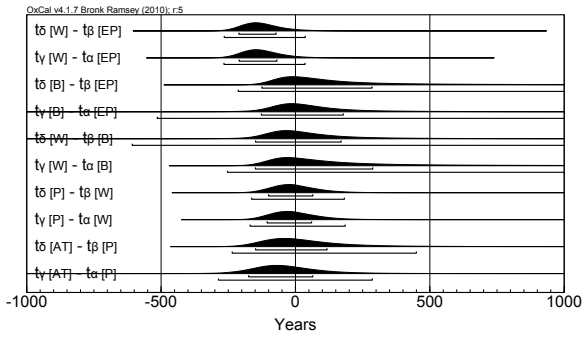


Figure 7.6: Estimates for the overlap between the rise and decline of adjacent phases; negative values here indicate a gap between the specified parameters, and positive values an overlap. Figure generated based on Model A.

| Phase | | Overlap (years) between | | | |
|---|---|---|---|---|---|
| [A] | [B] | $t_\gamma$ [A] and $t_\alpha$ [B] | | $t_\delta$ [A] and $t_\beta$ [B] | |
| | | 68.2% | 95.4% | 68.2% | 95.4% |
| Acton & Taunton | Penard | 65 | 286 | 118 | 450 |
| Penard | Wilburton | 60 | 185 | 65 | 182 |
| Wilburton | Blackmoor | 288 | 4591 | 170 | 2067 |
| Blackmoor | Ewart Park | 178 | 1862 | 285 | 3751 |
| Wilburton | Ewart Park | 0 | 36 | 0 | 37 |

Table 7.4: Estimates of overlap in years between the Bronze Age metalwork assemblages, at 68.2% and 95.4% probability. figure generated based on Model A.

| Phase | | Gap (years) between | | | |
|---|---|---|---|---|---|
| [A] | [B] | $t_\gamma$ [A] and $t_\alpha$ [B] | | $t_\delta$ [A] and $t_\beta$ [B] | |
| | | 68.2% | 95.4% | 68.2% | 95.4% |
| Acton & Taunton | Penard | 174 | 286 | 148 | 235 |
| Penard | Wilburton | 105 | 169 | 100 | 163 |
| Wilburton | Blackmoor | 149 | 153 | 148 | 607 |
| Blackmoor | Ewart Park | 127 | 514 | 125 | 213 |
| Wilburton | Ewart Park | 209–69 | 266 | 210–72 | 265 |

Table 7.5: Estimates of gaps in years between the Bronze Age metalwork assemblages, at 68.2% and 95.4% probability. Figure generated based on Model A.

Results from this model suggest that the order of the Bronze Age sub-divisions follows: Acton and Taunton; Penard; Wilburton; and Ewart Park, with a possible gap between the Wilburton and Ewart phases. The Blackmoor phase has very imprecise estimates due to the presence of only three radiocarbon determinations in the phase. However, there appears to be a gap between the Wilburton and Ewart Park phases. It is, therefore, possible that materials from the Blackmoor phase is chronologically intermediate between Wilburton and Ewart Park. This conclusion supports the relative chronology of O'Connor (1980) and also the analysis of Needham et al. (1997).

#### 7.2.1.2 Model B: *Contiguous phases*

Model B includes five contiguous trapezoid phases: Acton and Taunton; Penard; Wilburton; Intermediate (characterised by the Blackmoor phase); and Ewart Park. This model assumes that the decline of an earlier phase overlaps exactly with the rise of a later, adjacent phase, sharing the same `boundary` and `transition` parameters (Fig. 7.7a). The results of this model are summarised in Figure 7.7b and Table 7.6. The letters in square brackets next to the model parameters indicate the phases in which they belong, where AT = Acton & Taunton, P = Penard, W = Wilburton, I = Intermediate and EP = Ewart Park.

Both models (A and B) supports the relative chronology of O'Connor (1980), that the sub-divisions of British Bronze Age follow the order of Acton and Taunton, Penard, Wilburton, Intermediate (characterised by Blackmoor), and Ewart Park. The extra constraints in this model give a tighter overall posterior chronology than the chronology given by Model A. The precision of the Intermediate phase has, as expected, improved significantly. The new trapezoidal parameters give prior estimates of the middle of the transitions (`boundary` parameters) between phases and the duration of each transition (`transition` parameters) (Fig. 7.8 and tab. 7.6).

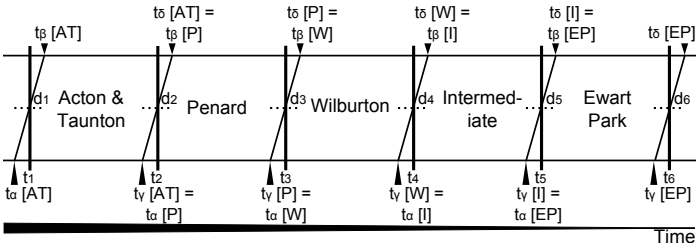


(a)

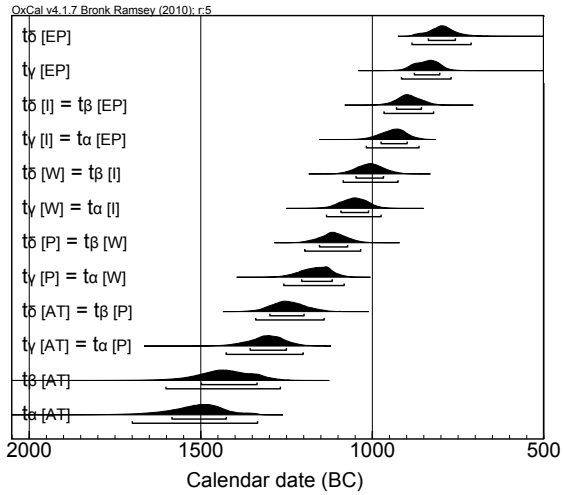


(b)

Figure 7.7: Model B: (a) model schematic, where Karlsberg's parameters are used to draw inference on the start and end of each phase ($t_\alpha$ and $t_\delta$) and the new parameters are used to draw inference on the middle of the transitions between phases (vertical lines; $t_1 \ldots t_6$) and their durations (horizontal dotted lines; $d_1 \ldots d_6$). (b) trapezoidal prior estimates for the Bronze Age metalwork assemblages, at 68.2% and 95.4% probability.

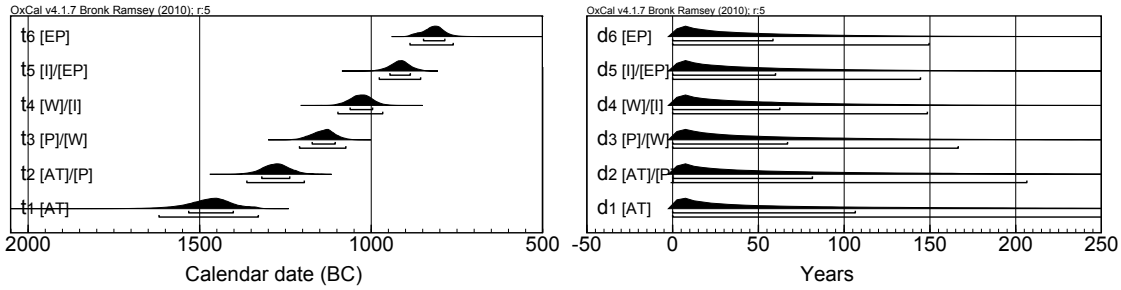


(a) Middle of Transitions (b) Duration of transitions

Figure 7.8: Trapezoidal prior estimates for the: (a) `boundary` parameters and (b) `transition` parameters for the Bronze Age metalwork assemblages, at 68.2% and 95.4% probability.

| | Modelled date (cal BC) | | | Modelled date (cal BC) | | | Years | |
|---|---|---|---|---|---|---|---|---|
| | 68.2% | 95.4% | | 68.2% | 95.4% | | 68.2% | 95.4% |
| $t_\alpha$ [AT] | 1585–1426 | 1700–1335 | $t_1$ | 1533–1403 | 1619–1330 | $d_1$ | 0–106.5 | 0–305.5 |
| $t_\beta$ [AT] | 1499–1337 | 1602–1269 | | | | | | |
| $t_\gamma$ [AT] $= t_\alpha$ [P] | 1357–1251 | 1427–1202 | $t_2$ | 1320–1238 | 1363–1196 | $d_2$ | 0–81.5 | 0–206.5 |
| $t_\delta$ [AT] $= t_\beta$ [P] | 1299–1200 | 1341–1141 | | | | | | |
| $t_\gamma$ [P] $= t_\alpha$ [W] | 1207–1118 | 1259–1083 | $t_3$ | 1173–1106 | 1210–1075 | $d_3$ | 0–67 | 0–166.5 |
| $t_\delta$ [P] $= t_\beta$ [W] | 1155–1073 | 1198–1035 | | | | | | |
| $t_\gamma$ [W] $= t_\alpha$ [I] | 1092–1012 | 1134–975 | $t_4$ | 1062–997 | 1098–967 | $d_4$ | 0–62.5 | 0–148.5 |
| $t_\delta$ [W] $= t_\beta$ [I] | 1048–968 | 1086–926 | | | | | | |
| $t_\gamma$ [I] $= t_\alpha$ [EP] | 975–899 | 1018–865 | $t_5$ | 946–887 | 977–857 | $d_5$ | 0–60 | 0–144.5 |
| $t_\delta$ [I] $= t_\beta$ [EP] | 930–858 | 967–822 | | | | | | |
| $t_\gamma$ [EP] | 878–804 | 916–771 | $t_6$ | 848–786 | 888–762 | $d_6$ | 0–58.5 | 0–149.5 |
| $t_\delta$ [EP] | 837–759 | 885–713 | | | | | | |

Table 7.6: Trapezoidal prior estimates of the Bronze Age metalwork assemblages, at 68.2% and 95.4% probability.

Modelling with contiguous uniform phases gives results in Figure 7.9 and Table 7.7. The trapezoidal `boundary` parameters give estimates remarkably similar to those of the uniform phase prior, only differing in the start of the earliest phase.

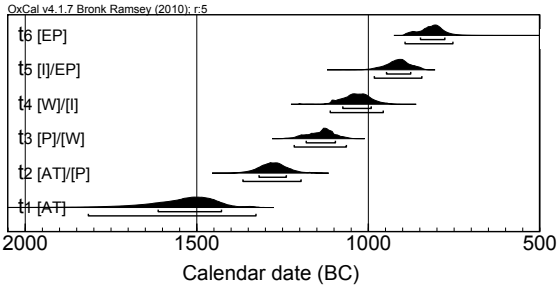


Figure 7.9: Uniform prior estimates of the Bronze Age metalwork assemblages, at 68.2% and 95.4% probability.

| | Modelled date (cal BC) | |
|---|---|---|
| | 68.2% | 95.4% |
| $t_1$ | 1613–1429 | 1817–1328 |
| $t_2$ | 1319–1240 | 1366–1197 |
| $t_3$ | 1182–1097 | 1217–1065 |
| $t_4$ | 1075–992 | 1112–957 |
| $t_5$ | 948–877 | 983–845 |
| $t_6$ | 849–778 | 894–754 |

Table 7.7: Uniform prior estimates of the transitions between the Bronze Age metalwork assemblages, at 68.2% and 95.4% probability.

#### 7.2.1.3 Modelling with `OxCal`

The trapezoidal and uniform phase prior models described so far in this chapter (and also in Chapter 5) have been implemented using the computer language `C++`. The implementation can be found in appendix A. The posterior distributions of the prior estimates of the models have been plotted using the `Prior` command in `OxCal`. Following the above tests in this chapter and in Chapter 5, the trapezoidal phase model functions were also implemented in `OxCal [v4.2 beta]` by Bronk Ramsey. The trapezoidal phase model can be implemented in `OxCal` using the `CQL`:

```
Sequence(){
    Boundary(){
        Transition();
        Start();
        End();
    };
    Phase(){
        R_Date(...);
        ⋮
        R_Date(...);
    };
    Boundary(){
        Transition();
        Start();
        End();
    };
};
```

where the addition of the `Transition();` command turns a uniform (abrupt) `boundary` parameter to a transitional trapezoidal `boundary` parameter. The `Start();` and `End();` commands are optional. They give the Karlsberg parameters. Modelling the Bronze Age metalwork data with contiguous trapezoidal phases in `OxCal` gives results in Figure 7.10 and Table 7.8.

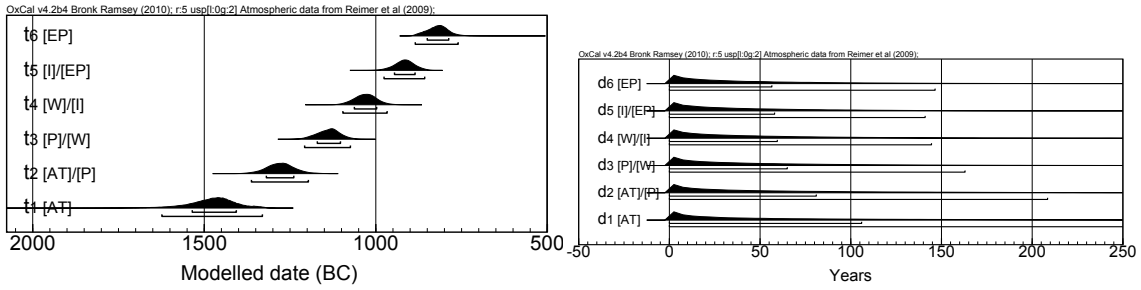


(a) Middle of Transitions (b) Duration of transitions

Figure 7.10: Trapezoidal prior estimates of the: (a) `boundary` parameters and (b) `transition` parameters for the Bronze Age metalwork assemblages, at 68.2% and 95.4% probability, implemented in `OxCal`.

| | Modelled date (cal BC) | | | Years | |
|---|---|---|---|---|---|
| | 68.2% | 95.4% | | 68.2% | 95.4% |
| $t_1$ | 1536–1407 | 1624–1331 | $d_1$ | 0–106 | 0–307 |
| $t_2$ | 1320–1240 | 1363–1197 | $d_2$ | 0–81 | 0–209 |
| $t_3$ | 1171–1104 | 1208–1075 | $d_3$ | 0–65 | 0–163 |
| $t_4$ | 1063–998 | 1097–968 | $d_4$ | 0–60 | 0–145 |
| $t_5$ | 946–886 | 977–858 | $d_5$ | 0–58 | 0–141 |
| $t_6$ | 851–788 | 886–761 | $d_6$ | 0-57 | 0–147 |

Table 7.8: Trapezoidal prior estimates of the Bronze Age metalwork assemblages, at 68.2% and 95.4% probability, implemented in `OxCal`.

Results from the two independent implementations in Figures 7.8 and 7.10 are different due to the differences in the underlying algorithms. The differences in the 68.2% and 95.4% probability ranges are very subtle and are very likely to be due to sampling chance and the number of iterations for the model runs. Two million iterations are defined for both implementations, however, in `OxCal` this defines the number of (passed) iterations (with accepted results) and not the total number of iterations. Since the results do not differ significantly, subsequent trapezoidal models in this thesis from this point forward will be implemented using `OxCal` to take advantage of the different functions available.

#### 7.2.1.4 Model limits

Another non-informative prior element which deals with model limits was also discussed in Chapter 5. The *limits* prior only applies when the model has limits, i.e. *termini post quem* and *ante quem*. Nicholls and Jones (2001) recommend using a prior like this to remove a bias towards wider date ranges. The *limits* prior has also been implemented into `OxCal [v4.2 beta]`. It can be activated by using the `CQL`:

```
Options(){ UniformSpanLimits=1; };
```

but the more complex form of the *limits* prior, which deals with with the overall span of a sub-phase (Bronk Ramsey, 2009a), is included as a default, i.e. when this command is not utilised. Setting this option to zero will switch off the *limits* prior altogether.

Application of the *limits* prior yields results in Figure 7.11 and Table 7.9. The prior does not appear to have a significant effect on this data set. The date range for the middle of the start of the Acton and Taunton phase has been brought forward by a decade. The agreement indices for using and not using the *limits* prior are $A_{model} = 125.6\%$ and $A_{model} = 125.2\%$, respectively. They do not differ significantly. This is because this data set does not contain massively deviating wide date ranges.

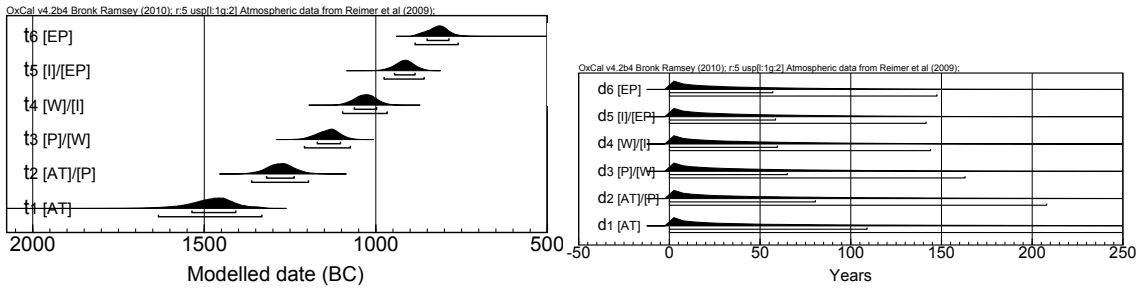


(a) Middle of Transitions (b) Duration of transitions

Figure 7.11: Prior estimates of the: (a) trapezoid `boundaries` and (b) `transitions` for the Bronze Age phases, at 68.2% and 95.4% probability, implemented in `OxCal` with the *limits* prior.

| | Modelled date (cal BC) | | | Years | |
|---|---|---|---|---|---|
| | 68.2% | 95.4% | | 68.2% | 95.4% |
| $t_1$ | 1537–1409 | 1634–1333 | $d_1$ | 0–109 | 0–313 |
| $t_2$ | 1319–1239 | 1363–1197 | $d_2$ | 0–81 | 0–208 |
| $t_3$ | 1171–1104 | 1209–1075 | $d_3$ | 0–65 | 0–163 |
| $t_4$ | 1063–998 | 1097–968 | $d_4$ | 0–60 | 0–144 |
| $t_5$ | 946–886 | 977–860 | $d_5$ | 0–59 | 0–142 |
| $t_6$ | 851–788 | 886–761 | $d_6$ | 0-57 | 0–148 |

Table 7.9: Trapezoidal prior estimates of the: (a) `boundary` and (b) `transition` parameters for the Bronze Age metalwork assemblages, at 68.2% and 95.4% probability, implemented in `OxCal` with the *limits* prior.

### 7.2.2 Discussion

This section utilised the modified trapezoidal phase prior (see Chapter 5) to draw inference on the temporal constraints on British Bronze Age metalwork culture. The trapezoidal phase prior is more appropriate than the uniform phase prior for modelling this data set since it allows more gradual phase transitions. It is assumed that it better reflects prior knowledge because the materials were found in different geographical regions and transitions between the regions cannot be instantaneous since ideas take time to travel.

The two modifications proposed in Chapter 5: alternative parameterisation; and the addition of a non-informative prior element, the *utp*, were important in modelling the British Bronze age transition. The contiguous trapezoidal phase model assumes that the decline of an earlier phase overlaps exactly with the rise of a later, adjacent phase, sharing the same `boundary` and `transition` parameters. The results in this section support the relative chronology of O'Connor (1980) and also the analysis of Needham et al. (1997). The trapezoidal phase prior gives similar `boundary` estimates to those of the uniform phase prior when used in a contiguous phase scenario. This is an important finding as it confirms that the more robust trapezoidal phase model supports the analysis from the simpler, more rigid, uniform phase model. The `transition` parameters give information on the duration of transitions between adjacent phases (Fig. 7.8b). This information was previously not available with a uniform phase prior because phase transitions were considered as abrupt events and not slow

processes. This is valuable archaeological information which is sometimes available but missed when modelled with an abrupt prior (see next section). The presence of the *utp* element is important in this multiple phase case study because there is insufficient information to determine the abruptness of the transitions between different assemblages. Next section discusses, in more detail, the significance of the *utp* element in a contiguous trapezoidal phase scenario.

The *limits* prior was recommended by Nicholls and Jones (2001) to remove a bias towards wider date ranges. Results from Section 7.2.1.4 show that the *limits* prior does not have a significant effect on the British Bronze Age metalwork data set. This is because it does not contain deviating wide date ranges. It would, however, make a difference if the data set contains outlying constraints (Nicholls and Jones, 2001). This also means that it formal outlier analysis is employed, for example the `Outlier_Model` available in `OxCal`, to account for the outlying dates in a data set, the *limits* prior is unlikely to make a difference to the trapezoidal prior measures.

This section also shows that modelling with two different implementations of the same mathematical functions gave similar results that do not differ significantly. The subtle differences are small enough to be due to sampling chance.

## 7.3 Iron Age chronology in Israel

The Iron Age in the Levant is also known as the Israelite period, when the land of Canaan was dominated by a Hebrew speaking community, forming a new local culture. Canaan corresponds to modern day Israel and Palestine. This period marks the fall of regional empires, and the rise and fall of the Kingdoms of Israel and Judah. Much of this period is described in the Hebrew Bible.

Typical of Biblical archaeology, the Iron Age chronology in the Levant has been a hotly debated issue. Scholars have been trying to establish a chronology for the period between the collapse of the Egypto-Canaanite system in the twelfth century BCE (1140/1130 BCE) and the Assyrian conquests in the eighth century BCE (between 732 and 701 BCE) (Mazar, 2005; Finkelstein and Piasetzky, 2010b). These are dates anchored in historical sources and give us a period of around 450 years of uncertain chronology.

Establishing a consensus on the Iron Age chronology has far reaching implications on relative chronologies in other regions around the Mediterranean (e.g. Coldstream, 2003), Israelite history, historiography, and biblical history.

### 7.3.1 The debate

Two main chronologies have been proposed: the 'high chronology' (also known as the 'conventional chronology'); and the 'low chronology'. Both of these are discussed in more detail below. The chronologies are based on data from pottery typologies, stratigraphic analyses, and attempted correlation to biblical sources across different sites. Many scholars accept the historical accuracy of the biblical account (e.g. Albright, 1956); conversely, a group of scholars cast doubts on its historicity (e.g. Garbini and Bowden, 1988; Davies, 1995; Finkelstein, 1996; Thompson, 2000).

There are two phases of Philistine pottery which are relevant to the debate: The local Mycenaean IIIC, or Philistine monochrome pottery, and the bichrome pottery. The monochrome pottery is characteristic of the Iron I period, while the bichrome

pottery is indicative of the Iron II period. The main focus of the debate centres around the transition between the Iron I and Iron II periods. The 'high chronology' places the Iron I to Iron II transition in the first half of the 10th century BCE; and the 'low chronology', which shifts the chronology to a later date, places this transition between first half of the 10th century BCE to ca. 920 BCE (or later, in earlier publications by Finkelstein).

#### 7.3.1.1 The 'high chronology'

The Philistines settled in Canaan ca. 1175 BCE after the battle between the Egyptians and the Mediterranean Sea Peoples during the reign of Ramses III. This date is recorded in detailed Egyptian inscriptions that are linked to many historical and astronomical events (Balter, 2000). This Philistine occupancy is reported as being broken by King David through the expansion of the Israelite empire in biblical sources. This accession date of David, ca. 1000 BCE from biblical sources, is taken to mark the end of Philistine material culture and hence represents the transition between Iron I to Iron II.

The 'high chronology' follows the biblical account on Israelite history. After his accession, King David started reconstructing a great United Monarchy. Below outlines the Biblical narrative of the important events that happened during the reign of King David and his son, Solomon, and before the destruction of the United Monarchy by the Egyptian Pharaoh Sheshonq I (biblical Shishak).

> "So all the elders of Israel came to the king to Hebron; and king David made a covenant with them in Hebron before the LORD; and they anointed David king over Israel."
>
> **—2 Samuel 5:3 (JPS)**

> "In Hebron he reigned over Judah seven years and six months; and in Jerusalem he reigned thirty and three years over all Israel and Judah."
>
> **—2 Samuel 5:5 (JPS)**

For the Jews, it was King David who made Jerusalem their holy city, when he summoned the ark of the covenant. His son, Solomon, who later became king, stabilised the United Monarchy. He took part in the construction of monumental buildings in administrative centres of his state (e.g. Dever, 1997; Stager, 2003; Yadin, 1970).

> "And this is the account of the levy which king Solomon raised; to build the house of the LORD, and his own house, and Millo, and the wall of Jerusalem, and Hazor, and Megiddo, and Gezer."
>
> **—1 Kings 9:15 (JPS)**

King Solomon was a wise man and ruled over a glamorous, rich and prosperous state (**1 Kings 10 (JPS)**) for forty years.

> "And the time that Solomon reigned in Jerusalem over all Israel was forty years. And Solomon slept with his fathers, and was buried in the city of David his father; and Rehoboam his son reigned in his stead."
>
> **—1 Kings 11:42–43 (JPS)**

The United Monarchy blossomed until the invasion by the Egyptian Pharaoh Sheshonq I to Palestine ca 925 BCE, according to both Egyptian inscription at Karnak and the Hebrew bible.

> "And it came to pass in the fifth year of king Rehoboam, that Shishak king of Egypt came up against Jerusalem"
>
> **—1 Kings 14:25 (JPS)**

The late Iron I (monochrome) pottery assemblage is found at the destruction layers of Megiddo stratum VIA, Tel Qasile stratum X, Tel Masos stratum II, and parallel strata at other sites. The Iron IIA (bichrome) pottery assemblage is found at the destruction layers of Megiddo strata VA-IVB, Taanach period IIB, Yokneam stratum XIV, Beth Shean stratum S1, Lachish stratum V, Arad stratum XII, and parallel strata at other sites. These destruction layers have been associated with the conquests of King David (Mazar, 2005).

In the early 1990s, Wightman (1990) and Jamieson-Drake (1991) cast doubts on the archaeology of the conventional paradigm. They questioned the concept of the United Monarchy of Israel and suggested 'lowering' the chronology.

#### 7.3.1.2 The 'low chronology'

Finkelstein (1996) put forward a specific 'low chronology' which moves the overall chronology later by 50–80 years. This shifts the dates of the Iron Age I assemblages from the late 11th century to the 10th century BCE and also shifts the dates of traditional 10th century assemblages to the 9th century BCE. This is widely known as the 'low chronology' for the Iron Age of Israel. Finkelstein's reason for that was because monochrome pottery has not been found in the 12th Dynasty Egyptians strongholds in a couple of sites in the south, especially Lachish stratum VI and Tel Sera stratum IX. This suggestion has since been rejected because it creates unsolvable problems in correlating the archaeology of Philistia with that of Cyprus (e.g. Dothan and Zukerman, 2004; Mazar, 2005).

Finkelstein (2005) put forward two more arguments: (1) the ashler blocks excavated in the foundations of Palace 1723 at Megiddo strata VA-IVB, which were associated with the conquests of King David (Mazar, 2005), carry the same masons' marks (Lamon and Shipton, 1939) as the ones found in the palace of the Omride Dynasty at Samaria (Reisner et al., 1924) and (2) the destruction layer at Jezreel, which was dated to 9th century BCE, yielded an identical pottery assemblage to the one found in Megiddo VA-IVB (Zimhoni, 1997).

The low chronology shifts the destruction layer that was originally attributed to the conquests of King David to a later period. It implies that the United Monarchy never existed, and that the state of King David and Solomon was overstated in the bible. Finkelstein (1996) and Finkelstein and Piasetzky (2011) believe that the Palace compounds belong to the Omride Dynasty in the days of King Ahab (873–852 BCE), which was understated in the bible.

The low chronology has since been a subject of controversy. There are disagree-

ments between scholars regarding which destruction layers at different sites are attributed to Pharaoh Sheshonq I (Bruins et al., 2003; Mazar, 1999; Finkelstein, 2005). Other arguments against the low chronology point out that the same pottery found at the destruction layer at Jezreel and Megiddo strata VA-IVB was also found below the royal enclosure at Jezreel, dating to the 10th century BCE (Zimhoni, 1997). This suggests that the pottery assemblage of concern (Iron IIA) has a long duration and should be dated to 10th century to 9th century BCE. The same is observed at Hazar, Tel Rehov, and other sites (Mazar, 2005).

#### 7.3.1.3 The modified conventional chronology

Realising the long duration of the Iron IIA period, Mazar (2005) proposed a 'modified conventional chronology'. This places the transition of Iron I and Iron II to ca. 980 BCE and the end of the Iron IIA period to ca. 840/30 BCE. In the 450 years of uncertain chronology, this chronology allows three major pottery periods: Iron IB, Iron IIA and Iron IIB, each lasting about 150 years. This is supported by Herzog and Singer-Avitz (2004, 2006).

The above chronologies have all been dated relatively. To continue the debate, scholars have turned to absolute dating using radiocarbon in attempts to try and establish a consensus for the Iron Age chronology in Israel.

### 7.3.2 Dating

During the late 1990s, scholars saw the potential of radiocarbon dating in helping to solve the Iron Age chronological debate. Many different sites were investigated over the past decade: Tel Dor (Gilboa and Sharon, 2001, 2003; Sharon, 2001), Tel Beth Shean and Tel Rehov (Mazar and Carmi, 2001; Bruins et al., 2003), Tel Hadar and Megiddo (Sharon et al., 2007). Hundreds of samples were measured, sometimes more than once, and inter-laboratory comparison was also performed to double check that different dating methods in different laboratories did not bias results (Boaretto et al., 2005). Despite tens of thousands of pounds spent on dating, scholars still

cannot reach a consensus for the Iron Age chronology in Israel. This is because the radiocarbon calibration curve for this period is very unhelpful. Oscillations in the calibration curve mean that calibration yields very imprecise dates. A radiocarbon date in this period rarely gives a calibrated range (95.4% probability) of less than a century. Unfortunately, this chronological debate centres around 100 years between 10th century and 9th century BCE.

To illustrate the limitations of the radiocarbon calibration curve for this period, the `R_Simulate` function in `OxCal` was used to simulate some important events in the Iron Age period. The events listed in Table 7.10 are simulated independently four times, using the biblical dates from the conventional chronology. Random sampling in the function means that it is unlikely to yield the same radiocarbon results in multiple simulations. An expected uncertainty of 25 is chosen for radiocarbon dates in that period, since most radiocarbon dates for this period have $1\sigma$ uncertainty of around 25. The simulated radiocarbon results are shown in Figure 7.12 and Table 7.10.

| Events | Biblical dates (BCE) | Expected uncertainties | Simulated radiocarbon dates (BP) for Figure: | | | |
|---|---|---|---|---|---|---|
| | | | 7.12a | 7.12b | 7.12c | 7.12d |
| Philistine settled in Canaan | 1175 | 25 | 2978 | 2965 | 2935 | 2990 |
| Egypto-Canaanite system collapse | 1140/30 | 25 | 2946 | 2965 | 2923 | 2962 |
| Accession of King David | 1000 | 25 | 2826 | 2897 | 2869 | 2795 |
| Shoshenq I's campaign | 925 | 25 | 2781 | 2795 | 2816 | 2735 |
| King Ahab's reign | 873-852 | 25 | 2691 | 2737 | 2633 | 2756 |
| Hazael's campaign | 835 | 25 | 2728 | 2741 | 2673 | 2711 |
| Assyrian conquest | 732 | 25 | 2423 | 2464 | 2470 | 2452 |

Table 7.10: Results of the simulated radiocarbon dates of the events relevant to the Iron Age chronological debate.

Figure 7.12 shows very clearly that, although the same calendar date was used in the simulations, the radiocarbon results can be very different especially in the controversial events in the debate: accession of King David; Shoshenq I's campaign and King Ahab's reign. This is due to the oscillations in the calibration curve. In one simulation (Fig. 7.12d), King Ahab's reign precedes Pharaoh Shoshenq I and Hazael's campaign in radiocarbon years BP. The likelihood for the three events also

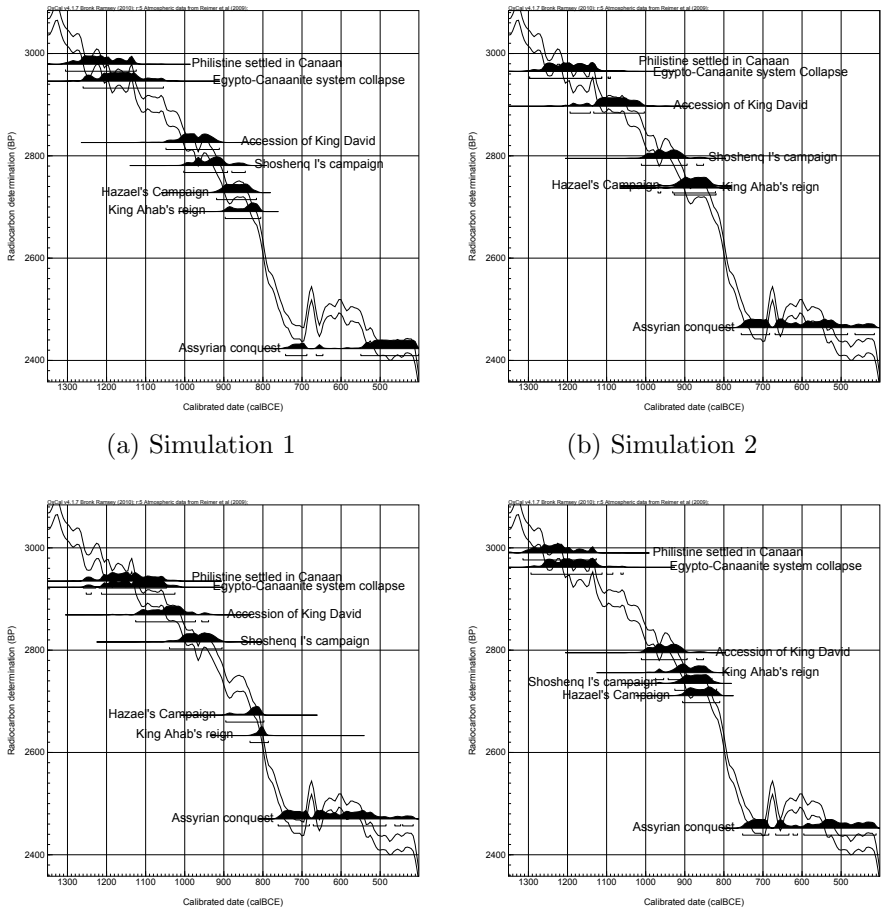


(a) Simulation 1




(b) Simulation 2




(c) Simulation 3




(d) Simulation 4

Figure 7.12: Results of the simulated radiocarbon dates of the events relevant to the Iron Age chronological debate, plotted against IntCal09 (Reimer et al., 2009).

overlap significantly in the calendar scale, making them indistinguishable from each other.

The most controversial event in this period is the accession of King David. Simulated radiocarbon ages of the biblical date (1000 BCE) attributed to King David's accession have a range of at least a century, and different simulations provide dates which cover two centuries (1194–853 BCE, with 95.4% probability) on the calendar scale. The same applies to radiocarbon dates attributed to Shoshenq I's campaign; their 95.4% probability ranges cover 1040–819 BCE on the calendar scale. Scholars are unable to distinguish the events from one another using radiocarbon dating alone.

### 7.3.3 Modelling

As demonstrated in Section 2.3, Bayesian modelling can help improve precision and accuracy of radiocarbon dates. Bronk Ramsey (2005) suggested using this method to address the Iron Age chronological debate. Since then, scholars have been using this approach to analyse multiple measurements on samples from different periods to try and recover the underlying chronology. Duplicate radiocarbon determinations from the same sample, or samples from the same stratum, were often combined (using the `R_Combine` function in `OxCal`) to produce a weighted average to improve on the precision of the calibrated date of the sample before modelling with a Bayesian framework. This method is valid for single sample or sample groups from the same stratum spanning less than a year.

Relative information is combined with the absolute dates to draw inference on the date of transition between Iron I and Iron II. Radiocarbon dates are attributed to individual Iron Age phases and grouped together using the uniform phase prior (Buck et al., 1992) (e.g. Sharon et al., 2005; Bruins et al., 2005; Mazar and Bronk Ramsey, 2008; Finkelstein and Piasetzky, 2010b, 2011).

The attribution of a stratum from a site to a particular Iron Age period forms the bases of the Iron Age chronological models. It is an important piece of prior information since inference on the controversial transitional dates is drawn using the marginal distributions based on this relative information. However, the attribution of strata to either the end of Iron I or early Iron IIA is not always consistent. Definitions of what is "Late Iron I" and what is "Early Iron IIA" are based on relative sequences of stratigraphic horizons which include pottery assemblages. There is a great deal of continuity in the ceramic typology between these two periods but there are also a lot of differences. An example is from Tel Rehov, the transition from Iron IB to Iron IIA is well defined from stratum VII to VI and must have occurred in a limited time frame (Mazar, pers. comm.). At a separate site, Khirbet Qeiyafa is defined by the excavators, Garfinkel and Ganor (2008), as belonging to the beginning of Iron IIA while Singer-Avitz (2010) defines the same assemblage as belonging to

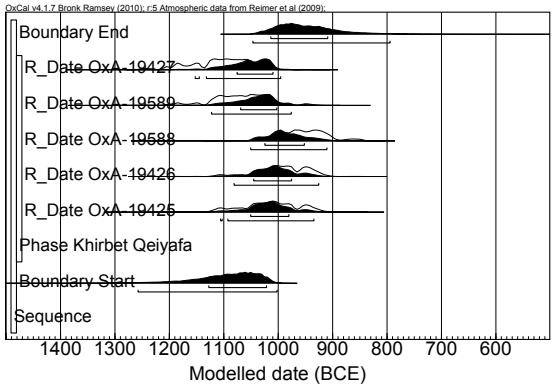


Figure 7.13: Uniform prior estimates of the Khirbet Qeiyafa dates.

the end of Iron I. Modelling the Khirbet Qeiyafa dates can lead to two conclusions, supporting either side of the debate. This is demonstrated very clearly in Finkelstein and Piasetzky (2010a). By attributing the site to Late Iron I, the model supports the low chronology (`end boundary`; Fig. 7.13); conversely, by attributing the site to Early Iron IIA, the model supports the high chronology (`start boundary`; Fig. 7.13) at 68.2% probability. Despite the fludity in the definitions of "Late Iron I" and "Early Iron II" pottery assemblages, scholars have built comprehensive age-models to support both sides of the debate.

#### 7.3.3.1 The Mazar and Bronk Ramsey model

Mazar and Bronk Ramsey (2008) performed a comprehensive analysis on the date of Iron I and Iron II transition using the radiocarbon dates from different sites. The authors used a combination of weighted averages and Bayesian methods.

The authors built multi-phase models, which assume that the change from Iron I to Iron II is synchronous across the region. Radiocarbon dates from different strata were grouped into three phases: Iron I, late Iron I or Iron II. In one model, the Iron I phase is constrained to be before the Iron II phase contiguously. In a separate model, the same constraints were used, with an added late Iron I phase. The late Iron I phase is constrained to overlap the Iron I phase and they share the same contiguous (or transition) `boundary` parameter (Fig. 7.14).

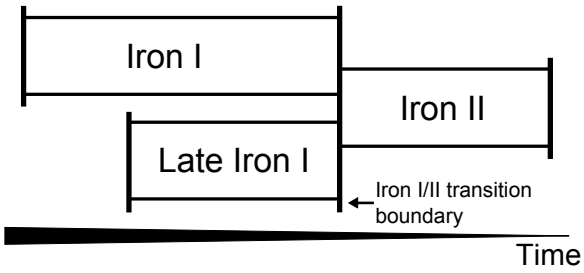


Figure 7.14: Model schematic from Mazar and Bronk Ramsey (2008) for Iron I and Iron II transition.

Another multiple phase model was built using a single site, Megiddo. This is because synchronous change across the sites is a strong assumption and would bias the results, since the calibrated likelihoods for this period overlap significantly. The resulting marginal distribution, which is used to represent the date of transition, is relied heavily upon the choice of prior information (discussed in Section 4.1). The results from the three models place the Iron I and Iron II transition in the middle of the 10th century BCE, which supports the modified conventional chronology.

#### 7.3.3.2 The Finkelstein and Piasetzky model

Finkelstein and Piasetzky also built a comprehensive age model using a Bayesian framework to draw conclusions on the date of Iron I and Iron II transition using all of the radiocarbon ages available for that period. The authors published results of two models: Finkelstein and Piasetzky (2010b) analysed the radiocarbon ages using seven sequential uniform phases (Figure 7.15); and Finkelstein and Piasetzky (2010c) modelled only Late Iron I and the Early Iron IIA of those seven phases. The first model places the Iron I to Iron II transition in 960–899 BCE, which supports the results of the Mazar and Bronk Ramsey (2008) model; the second model places the transition in 915–898 BCE, which is similar to that in the Boaretto et al. (2005) paper and supports the low chronology.

Both studies by Finkelstein and Piasetzky used the same Bayesian framework. The authors used the complete data set for the first model with seven sequential phases but only used the radiocarbon ages belonging to phases Late Iron I and Early Iron IIA for the second model. Phases Late Bronze II, Early Iron I, Middle Iron

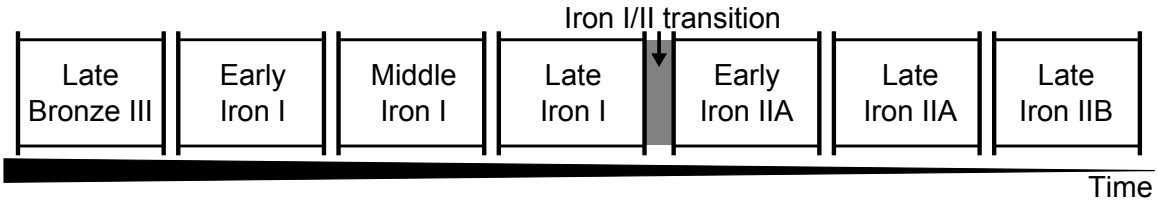


Figure 7.15: Model schematic from Finkelstein and Piasetzky (2010b) showing seven sequential phases for the Iron Age chronology. The grey area denotes the transition between Iron I and Iron II. The study by Finkelstein and Piasetzky (2010c) included only the Late Iron I and the Early Iron IIA phases.

I, Late Iron IIA and Late Iron IIB were not included and thus the corresponding radiocarbon ages belonging in these five phases were omitted. The date of Iron I and Iron II transition is therefore more constrained in the first model than it is in the second model. Results from both studies show that this transition date, analysed using this framework, is sensitive to the number of phases, and thus the number of radiocarbon dates, included in the model.

It is worth emphasising the assumptions built into both the Mazar and Bronk Ramsey (2008) and Finkelstein and Piasetzky (2010b,c) models. Mazar and Bronk Ramsey (2008) assume that transition between Iron I and Iron II was synchronous across sites. Finkelstein and Piasetzky (2010b,c) also assume synchronicity across the sites and that there was a hiatus between the end of Iron I and the start of Iron II, with the hiatus being the transitional period. Both models use the uniform phase prior (Buck et al., 1992), assuming that the temporal constraints of each of the Iron Age phases are abrupt events.

Is the abrupt uniform phase prior the correct prior for modelling the Iron Age transition? Does it appropriately and sufficiently represent the underlying assumptions? The uniform phase prior is the correct prior to use if archaeological evidence indicate abrupt events, for example destruction layers, which are observed in some of the Iron Age sites across the Levant. A destruction layer in archaeology is a stratum which shows evidence of destruction. This can include evidence of a wide spread fire, volcanic eruptions, earthquakes, burial of valuables, and abrupt site abandonment. An example of correct modelling of a destruction layer is demonstrated in Mazar

and Bronk Ramsey (2008), where the authors questioned the sensitivity of using the uniform phase prior to model dates from across the region and did a single site investigation using information from Megiddo. This is the correct prior to use because occupation of the site terminated abruptly, as suggested by the destruction layer. The Iron Age transition across the region can be non-abrupt, since it is largely based on pottery assemblages. Modelling non-abrupt transitions with an abrupt model gives estimates of the mid-points of transitions, as discussed in Section 7.2.1.2.

### 7.3.4 A new Bayesian model

The work in this section has been performed in collaboration with Professor Amihai Mazar from the Institute of Archaeology at the Hebrew University of Jerusalem. Mazar has also kindly provided twenty-three new radiocarbon ages obtained since the Finkelstein and Piasetzky (2010b,c) publications, eight of which are unpublished averages provided by Dr. Elisabetta Boaretto from the Weizmann Institute of Science at Rehovot. The complete data set can be found in appendix B.3. The Iron Age pottery phases have been separated into five phases in the order of: Iron IA; Iron IB; Early Iron IIA; Late Iron IIA; and Iron IIB. The attribution of strata from different sites to individual Iron Age periods were made according to Mazar's expert opinion on Iron Age archaeology. Only measurements from short-lived plant materials are used in the model runs to ensure that the age of the sample represents the age of the stratum it is found in.

The complete data set contains 533 radiocarbon determinations from mostly plant material, with 80 from charcoals. The samples had been prepared and measured in four different laboratories: Groningen; Oxford; Rehovot; and Tucson. Some of the samples measured in Tucson had been prepared in Rehovot. Boaretto et al. (2005) carried out a comprehensive inter-laboratory comparison and concluded that samples prepared from Tucson and Rehovot produce comparable radiocarbon determinations. As a result of this comparison, many determinations are duplicates from either the same sample or samples from the same stratum, and are considered to be the same

age. Thus, samples with the same laboratory numbers are combined to produce a weighted average before modelling.

Modelling is performed employing a Bayesian framework using the calibration and chronology building software `OxCal`. The contiguous trapezoidal prior model (Figure 7.16) is used to draw inference on the time of transition between Iron I and Iron II in Israel, where the decline of an earlier phase overlaps exactly with the rise of a later, adjacent, phase, sharing the same transitional `boundary` parameter. The trapezoidal phase prior used here is conditioned by the *utp* element to better reflect prior assumptions. The reasons for using a trapezoidal model instead of a uniform model are:

- pottery assemblages gradually become more popular, reach a peak popularity, and then fade away. Pottery production and usage are non-instantaneous processes (Brainerd, 1951; Robinson, 1951);
- the trapezoidal phase prior also takes into account the geographical spread of the pottery; and
- the different pottery phases can be overlapped, indicating transitional periods.

The trapezoidal phase prior can be seen as combining the efforts and ideas of both Mazar and Bronk Ramsey (2008) and Finkelstein and Piasetzky (2010b,c): the Late Iron I phase is contiguous to the Early Iron IIA phase and that there is a transitional period between the phases. The overlap between successive phases are considered, meaning that problems arising from uncertain attributions are also dealt with.

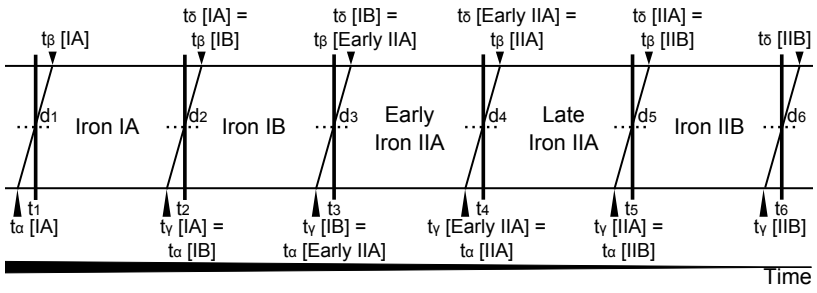


Figure 7.16: Model schematic for the new Iron Age chronology.

The overall framework of the models consists of the application of the function `R_Combine` to produce a weighted average of duplicate radiocarbon determinations of the same sample or of samples from the same stratum. In general, samples with the

same laboratory numbers before the decimal points are considered to be determinations of samples of the same age. Formal outlier analysis is utilised to account for outliers in the radiocarbon scale (`type r`) and the calendar scale (`type t`). `Type r` analyses are employed when producing weighted averages of radiocarbon determinations and `type t` analyses are employed to account for possible outlying calibrated ages. The `CQL` for the outlier models are:

```
Outlier_Model("RScaled",T(5),U(0,4),"r");
Outlier_Model("General",T(5),U(0,4),"t");
```

Both outlier models are specified to allow the possible shifts in the specified scale to be drawn from a long tailed student $t$ distribution. The outliers can be in the scale of anywhere between $10^0$ and $10^4$ years. These are the models recommended by Bronk Ramsey (2009b) for general purposes when the scale of the possible offsets is unknown. When employed, the overall model is not affected by the odd extreme outlier. Each measurement is assigned a prior probability of 5% of being an outlier. An example `CQL` listing for an `R_Combine` date is:

```
R_Combine("RT-4501"){
     Outlier("General",0.05);
     R_Date("RT-4501.3",2790,40){ Outlier("RScaled",0.05); };
     R_Date("RT-4501.4",2764,50){ Outlier("RScaled",0.05); };
     R_Date("RT-4501.5",2767,40){ Outlier("RScaled",0.05); };
};
```

For the trapezoidal model, an additional constraint of a hundred years is added for the transition time between Iron IB and Early IIA within the model ($d_3$; Fig. 7.16). This is because at sites like Tel Rehov, the transition from Iron IB to Iron IIA is well defined, and a horizon of a hundred years or more for this transition is considered too wide (Mazar, pers. comm.). All other transition times between phases ($d_2, d_4$ and $d_5$; Fig. 7.16) are also constrained. The reason for that is because transition times between the different Iron Age periods are considered short, as suggested by

both archaeological evidence and the less-than-a-century difference between the conventional and low chronologies. Limiting the `transition` parameters also provides a domain from which a starting point for the `transition` parameters can be generated (see Section 3.3.1), thus it helps the model run smoothly. The model would not start running at all due to the closely spaced events and complicated constraints if the transition times are not limited. The end `transitions` ($d_1$ and $d_6$) are left unconstrained to allow maximum flexibility to the ends of the model.

The trapezoidal parameters give prior estimates of the start ($t_\alpha$), the start of peak phase activity ($t_\beta$), the start of decline ($t_\gamma$), and the end ($t_\delta$) of each of the Iron Age phases. The full data set of short-lived plant materials is included in the model. In terms of the `type r` outlier analysis applied to duplicated dates during combination, only four of the 350 radiocarbon dates were found to yield $\geq$95% probability of being outlying (and no further date $\geq$90%), whilst 278 of the 350 dates were given a posterior probability of $\leq$5% of being outliers (as compared to the abitrary 5% prior probability applied). With the `type t` outlier analysis applied to both the 103 uncombined and 94 weighted averages of the radiocarbon dates, only one of the latter were found to yield $\geq$95% probability of being outlying (and one further date $\geq$90%), whilst 96 of the former 103, and 73 of the 94 latter radicoarbon dates were given a posterior probability of $\leq$5% of being outliers. Such findings support the validity of the individual radiocarbon determinations themselves (Staff et al., 2010).

Figures 7.17 and 7.18 and Table 7.11 summarise the Iron Age chronology for the five ceramic phases and the transitions between them, where the phases are abbreviated as IA = Iron IA; IB = Iron IB; E IIA = Early Iron IIA; L IIA = Late Iron IIA; and IIB = Iron IIB.

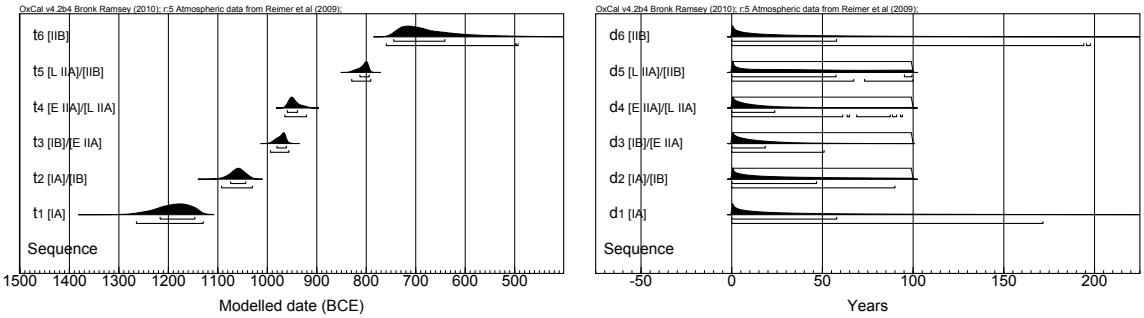


(a) Middle of Transitions (b) Duration of transitions

Figure 7.18: Trapezoidal prior estimates of the: (a) `boundary` and (b) `transition` parameters for the Iron Age phases, at 68.2% and 95.4% probability.

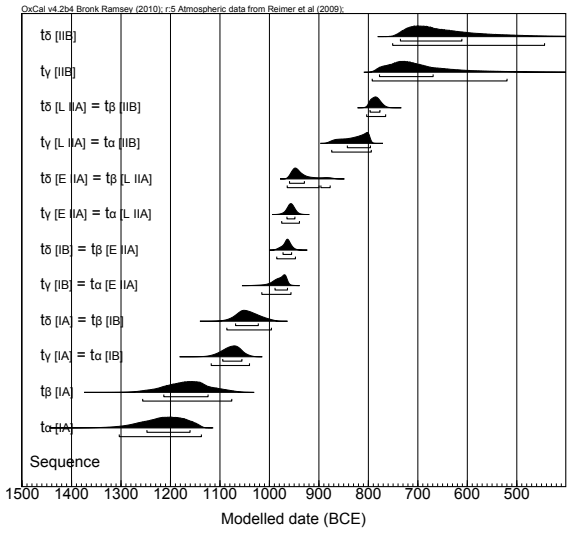


Figure 7.17: Trapezoidal prior estimates for the Iron Age chronology, at 68.2% and 95.4% probability.

#### 7.3.4.1 The beginning of the Iron Age

The beginning of the Iron Age (Iron IA) in the Levant is characterised by the initial Philistine settlement (monochrome ware), the beginning of settlement in the hill country, and the continuity of Canaanite and Egyptian centres at certain lowland sites such as MegiddoVIIA, Lachish VI, and Beth-Shean VI (Mazar, 2011). My Bayesian model, at 95.4% probability, places the start of the Iron Age in the range 1304–1138 BCE ($t_{\alpha\ [\mathrm{IA}]}$; Fig. 7.17). This agrees with the conventional chronology, which dates the Philistine settlement to 1175 BCE and rejects Finkelstein and Piasetzky's 'low chronology', which dates the Iron Age to after 1130 BCE. Adding the Late Bronze

III phase to the left of the model, with no additional constraints on the `transition` parameter, constrains this age to the range 1275–1138 BCE, at 95.4% probability. This suggests that the modelled date for the beginning of the Iron Age is robust.

#### 7.3.4.2 The transition between Iron I and II

My Bayesian model, at 95.4% probability, places the start of the Early Iron IIA phase in the range 1016–957 BCE; and the end of the Iron IB phase in the range 986–948 BCE ($t_{\alpha\ [\text{E IIA}]}$ and $t_{\delta\ [\text{IB}]}$; Fig. 7.17, respectively). The middle of the transition is estimated to lie in the range 994–957 ($t_3$; Fig. 7.18a) and the duration of this transition is estimated to be between 0 and 51 years ($d_3$; Fig. 7.18b). These results agree well with the conventional chronology and with Mazar's 'modified conventional chronology'; but negate all other theories, including Finkelstein and Piasetzky's 'low chronology', which places this transition in the range 960–899 BCE; Herzog and Singer-Avitz's proposal of mid tenth century; and Boaretto et al. and Sharon et al.'s proposal of 900 BCE. It is also interesting to see that limiting this transition time to less than a century did not affect the posterior output. However, it is worth reminding ourselves at this point that the `transition` parameters, $d_2$, $d_4$ and $d_5$, are constrained to be less than a hundred and these have limited their posterior outputs (see discussion above).

#### 7.3.4.3 The transition between Early to Late Iron IIA

At 95.4% probability, the start of the Late Iron II phase is placed in the range 976–940 BCE ($t_{\alpha\ [\text{L IIA}]}$; Fig. 7.17); and the end of the Early Iron IIA phase is placed in the range 965–900 BCE and 896–878 BCE ($t_{\delta\ [\text{E IIA}]}$ at 88.3% and 7.1% probability; Fig. 7.17, respectively). The middle of this transition is estimated to lie in the range 965–921 BCE ($t_4$; Fig. 7.18a) and the duration of this transition is estimated to be between 0 and 94 years ($d_4$; Fig. 7.18b). These results reject Finkelstein and Piasetzky's 'low chronology', which places this transition in the range 900–865 BCE.

#### 7.3.4.4 The end of Iron IIA

At 95.4% probability, the start of the Iron IIB phase is placed in the range 875–795 BCE; and the end of the Iron IIA phase is placed in the range 804–766 BCE ($t_{\alpha\ [\mathrm{IIB}]}$ and $t_{\delta\ [\mathrm{L\ IIA}]}$; Fig. 7.17, respectively). The middle of the transition is estimated to lie in the range 830–791 BCE ($t_5$; Fig. 7.18a) and the duration of this transition is estimated to be between 0 and 67 (73.7% probability), and 73–100 (21.7% probability) years ($d_5$; Fig. 7.18b). The main problem for dating this transition is that the radiocarbon dates in the Late Iron IIA phase land on an oscillation of the calibration curve between ca. 910–830 BCE. This means that interpreting results of this transition is not so straightforward. The broad posterior distribution for the end of start of Iron IIB (which is equated to the end of the peak ($t_\gamma$) of Iron IIA in this analysis) could be a reflection of reality or an artefact of calibration. This is also the cause of having uncertain transition time for this period.

A separate model with 200 year constraints for phase transitions show that the results (Fig. 7.19 and 7.20) are very similar to those of the previous model. This shows the model is not too sensitive to a constraint of 100 years for phase transitions.

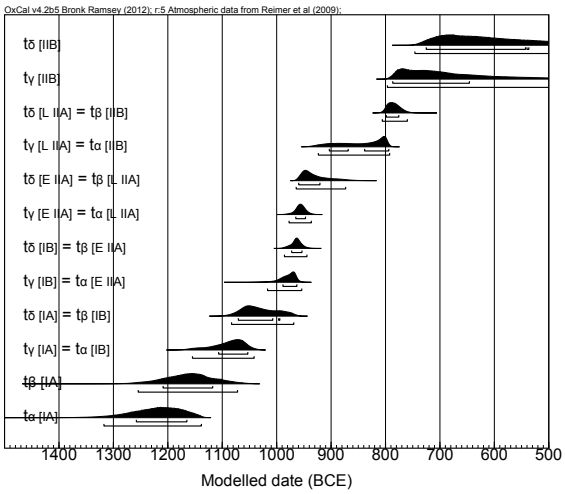


Figure 7.19: Trapezoidal prior estimates for the Iron Age chronology, at 68.2% and 95.4% probability, with a 200 year constraint for phase transitions.

Unfortunately, these results are unable to distinguish between the thirty years of Mazar's 'modified conventional chronology', of the date of transition as 830 BCE; and Finkelstein and Piasetzky's 'low chronology', of 800 BCE. The limited amount of

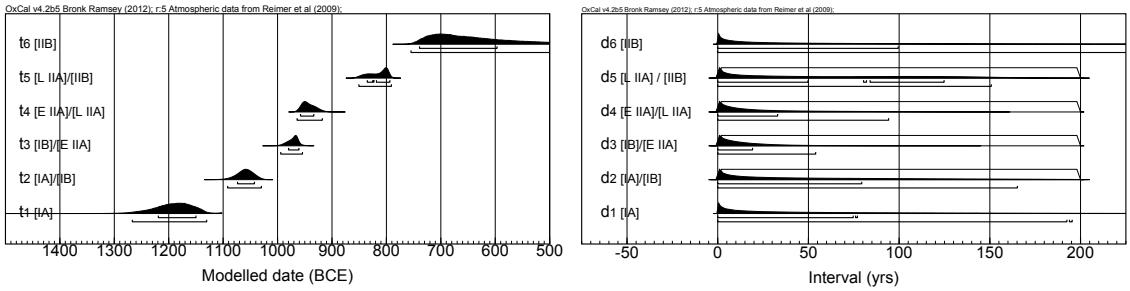


(a) Middle of Transitions (b) Duration of transitions

Figure 7.20: Trapezoidal prior estimates of the: (a) `boundary` and (b) `transition` parameters for the Iron Age phases, at 68.2% and 95.4% probability, with a 200 year constraint for phase transitions.

data in the Iron IIB phase provides little constraint to the end of the Iron IIA period. If more data becomes available for the Iron IIB phase, the end of the Iron IIA period will be be more constrained and may provide more informative estimates of the start and end of the Iron IIB and the IIA phases, respectively.

In order to investigate whether the broad distribution is caused by the oscillation of the calibration in that period, radiocarbon dates (using the `R_Simulate` function in `OxCal`) for the duration of the Early Iron IIA phase (between 980 and 900 BCE) and the Late Iron IIA phase (between 950 and 830 BCE), were simulated with $1\sigma$ uncertainty of 25 years. These date ranges are chosen to fit the 'modified conventional chronology', and to demonstrate what effect they have on the posterior age ranges for the transitional period, between the two sub-phases within Iron IIA, when the end of the earlier phase and the start of the later phase falls on the oscillation between 910–830 BCE on the radiocarbon calibration curve. No additional information regarding the frequency of pottery distribution has been included. Results are shown in Figure 7.21.

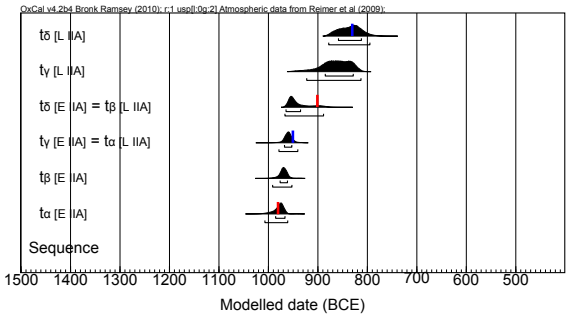

Figure 7.21: Trapezoidal prior estimates of a simulated chronology of Iron IIA, at 68.2% and 95.4% probability. The simulated start and end of the Early and Late phases are indicated by the red and blue vertical bars, respectively.

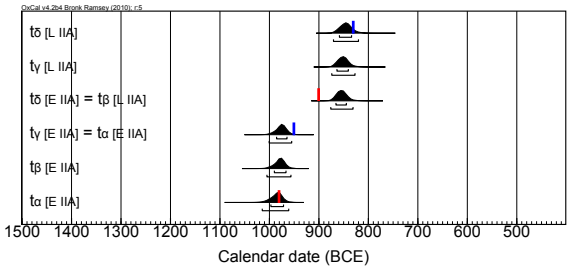


Figure 7.22: Trapezoidal prior estimates of a simulated chronology of Iron IIA, without the use of the *utp* element, at 68.2% and 95.4% probability. The simulated start and end of the Early and Late phases are indicated by the red and blue vertical bars, respectively.

The simulation illustrates that, the contiguous trapezoid model, with the *utp* element, can accurately estimate the inner Iron II chronology at 95.4% probability (Fig. 7.21). It, together with the model results (Fig. 7.17), suggest that there is a possibility that the Late Iron IIA finished after 830 BCE. The broad distribution for $t_\gamma$ of the Late IIA phase is likely to have been caused by the oscillation of the radiocarbon curve for that period. This suggests that the marginal distributions, $t_\gamma$ and $t_\delta$, cannot be used to precisely estimate the end of the Late IIA phase. Without the *utp* element, i.e. Karlsberg's model, the contiguous trapezoid model does not accurately estimate the inner Iron II chronology (Fig. 7.22).

A model with only two phases, Iron IB and Early Iron IIA was also constructed to test for model sensitivity, since the models of different sizes from Finkelstein and Piasetzky (2010b) and Finkelstein and Piasetzky (2010c) yielded conflicting outputs. A contiguous trapezoidal framework is used in this two phase model, with the `transition` parameter between Iron IB and Early Iron IIA unconstrained to give maximum model flexibility. Results are shown in Figures 7.23 and 7.24. They show that the trapezoidal phase model is a robust approach to modelling the Iron Age transition. This is because the trapezoidal prior estimates for the middle of the transition in this model yield almost identical results to that of a larger model (above). The model is not sensitive to the number of phases, and hence the number of radio-

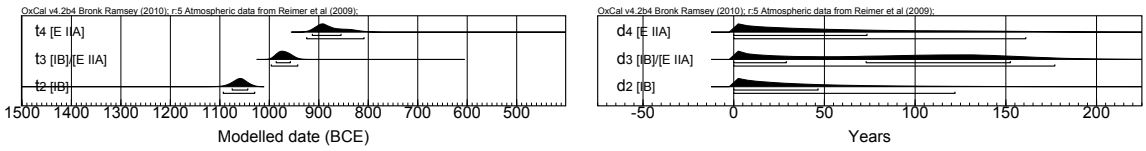


(a) Middle of Transitions (b) Duration of transitions

Figure 7.24: Trapezoidal prior estimates of the: (a) `boundary` and (b) `transition` parameters for the Iron I/II transition, at 68.2% and 95.4% probability.

carbon determinations included. The `transition` parameter between the two phases was not constained, thus the model parameters estimating the start and end of the phases are different to that of the bigger model.

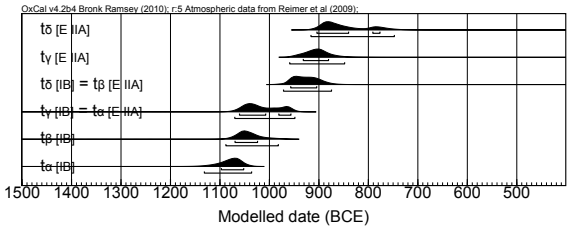


Figure 7.23: Trapezoidal prior estimates of the Iron I/II transition, at 68.2% and 95.4% probability.

### 7.3.5 Discussion

Before concluding, it is worth the mention that the comprehensive Bayesian model built in this section on the Iron Age chronology takes into account information on pottery assemblages, as well as the geographical spread of the data. It draws inference on the start and end of each of the Iron Age phases across the region. The quoted date ranges above are not restricted to single sites. Where abrupt transitions, i.e. destruction layers, are observed at individual sites, an abrupt (uniform) phase prior should be used to model those events. This section provided an alternative, and better, approach to modelling transitional processes, where phases, and indeed the radiocarbon dates, are found to overlap. The trapezoidal phase model also takes into account the abundance, or frequency, of ceramic styles over time.

Since prior measures are drawn from the prior distributions over the parameters, they are sensitive to the prior (Vanpaemel, 2010). This means that the prior estimates

here, and those of Mazar and Bronk Ramsey and Finkelstein and Piasetzky, are sensitive to the modelling framework, and the prior models used. However, unlike the Finkelstein and Piasetzky models, where the prior estimates are sensitive to the number of phases, hence radiocarbon determinations, used; the results presented here are not sensitive to the same factors. Results from a model with only two phases support those from a larger model. The trapezoidal prior estimates for the middle of the transitions (Fig. 7.24a) yielded almost identical results to those of a larger model (Fig. 7.18a). The contiguous trapezoidal phase prior is a more robust framework for this case study, since the same parameters in Finkelstein and Piasetzky's studies yielded different results.

The *utp* element of the trapezoid phase prior is used throughout this section. The effect of the *utp* element on the Iron Age chronology is shown in the simulated chronology in Figure 7.21. Without the use of this prior element, i.e. Karlsberg's trapezoidal phase prior, the model has a bias towards a shorter period of maximum phase activity (between $t_\beta$ and $t_\gamma$) for the pottery assemblage in Late Iron IIA (Fig. 7.22). It also gives a less accurate estimation of the end of the Early Iron IIA phase. Since no additional information has been incorporated into the model regarding the frequency of dates within the modelled period, the addition of the *utp* better reflects prior knowledge and makes the trapezoid model more robust. It therefore gives more reliable results. Without the *utp* element, the trapezoid phase cannot be used in a contiguous multi-phase scenario because it is not flexible enough to accurately estimate the transitional period between two adjacent phases.

The Bayesian model results in this section are summarised in Table 7.11. It confirms Mazar's 'modified conventional chronology' but rejects Finkelstein and Piasetzky's 'low chronology' on the start of the Iron Age and the most controversial age of transition between Iron I and Iron II. The end of the Iron IIA phase and its inner chronology are problematic to model and to draw conclusions on as demonstrated in the simulation. The oscillation in the radiocarbon calibration curve between 910–830 BCE results in an uncertain estimation of the ages associated with the decline of the

Late Iron IIA phase. More data in the Iron IIB period will help constrain the Iron IIA to IIB transition and may provide estimates which can distinguish between the 'low' and 'modified conventional' chronology, which is not possible at present with the available data. The simulation, together with the model results, suggest that the end of the Iron IIA period finished later than the date suggested by Mazar. However, it is not implausible to suggest that the decline of the Iron IIA phase began ca. 830 BCE and ended ca. 800 BCE, as supported by the model results. This study suggests that, at 95.4% probability, it is likely that the start of the Iron Age I/II transition – the beginning of King David's reign – fell before 1000 BCE. As well as having implications on Israelite and biblical history, these results will also have implications on the Iron Age cultural processes in the Levant, Cyprus, and Greece (Sharon et al., 2007). This latter point however, is beyond the scope of this thesis and is not discussed here.

| | Modelled date (BCE) | | | Modelled date (BCE) | | | Years | |
|---|---|---|---|---|---|---|---|---|
| | 68.2% | 95.4% | | 68.2% | 95.4% | | 68.2% | 95.4% |
| $t_{\alpha\ [\mathrm{IA}]}$ | 1248–1161 | 1304–1138 | $t_1$ | 1217–1147 | 1265–1130 | $d_1$ | 0–58 | 0–172 |
| $t_{\beta\ [\mathrm{IA}]}$ | 1214–1125 | 1257–1077 | | | | | | |
| $t_{\gamma\ [\mathrm{IA}]} = t_{\alpha\ [\mathrm{IB}]}$ | 1095–1056 | 1118–1041 | $t_2$ | 1075–1044 | 1093–1031 | $d_2$ | 0–47 | 0-90 |
| $t_{\delta\ [\mathrm{IA}]} = t_{\beta\ [\mathrm{IB}]}$ | 1069–1023 | 1087–996 | | | | | | |
| $t_{\gamma\ [\mathrm{IB}]} = t_{\alpha\ [\mathrm{E\ IIA}]}$ | 989–964 | 1016–957 | $t_3$ | 981–962 | 994–957 | $d_3$ | 0–19 | 0–51 |
| $t_{\delta\ [\mathrm{IB}]} = t_{\beta\ [\mathrm{E\ IIA}]}$ | 973–956 | 986–948 | | | | | | |
| $t_{\gamma\ [\mathrm{E\ IIA}]} = t_{\alpha\ [\mathrm{L\ IIA}]}$ | 965–949 | 976–940 | $t_4$ | 960–940 | 965–921 | $d_4$ | 0–24 | 0–94 |
| $t_{\delta\ [\mathrm{E\ IIA}]} = t_{\beta\ [\mathrm{L\ IIA}]}$ | 960–930 | 965–878 | | | | | | |
| $t_{\gamma\ [\mathrm{L\ IIA}]} = t_{\alpha\ [\mathrm{IIB}]}$ | 843–796 | 875–795 | $t_5$ | 813–795 | 830–791 | $d_5$ | 0–99 | 0–100 |
| $t_{\delta\ [\mathrm{L\ IIA}]} = t_{\beta\ [\mathrm{IIB}]}$ | 797–777 | 804–766 | | | | | | |
| $t_{\gamma\ [\mathrm{IIB}]}$ | 778–670 | 793–520 | $t_6$ | 745–642 | 760–494 | $d_6$ | 0–58 | 0–198 |
| $t_{\delta\ [\mathrm{IIB}]}$ | 736–670 | 751–444 | | | | | | |

Table 7.11: Trapezoidal prior estimates of the Iron Age chronology, at 68.2% and 95.4% probability.

# Chapter 8

# Modelling sedimentary sequences

Bayesian analysis is a well-established tool for combining information with absolute dates to improve the precision and accuracy of archaeological and palaeoenvironmental chronologies. The last chapter demonstrated a framework which includes use of robust phase models to constrain and draw inference on transitional events. Another kind of prior knowledge, which can be incorporated into palaeochronology construction, includes sequential information. Sequential or deposition models can be used to estimate the age of a particular event given the order. Additional information such as known age gaps or depth will enhance the precision even further (e.g. Blockley et al., 2008b; Dee, 2009; Bronk Ramsey et al., 2010b; Staff et al., 2011).

There are many age-depth modelling programs freely available to researchers (e.g. Buck et al., 1999; Bronk Ramsey, 2009a; Blaauw and Christen, 2011). A recent development by Bronk Ramsey (2008) introduced a Poisson process (`P_Sequence`) prior for modelling random deposition. It relies on the use of a model parameter for step-size ($k$) to define the increment in the model runs, which can be estimated using the variability in distances between the known age layers. Therefore, it is most suitable in modelling primarily sequences with more than three known age points, for example, in annually laminated sequences or sequences with stratigraphic marker layers (refer to Fig. 6.1), so that the $k$ parameter can be estimated. In non-annually laminated sequences with no stratigraphic marker layers, $k$ would have to be estimated using

other means, such as the dating information, instead. Sometimes, model agreement with the data is also used to justify the use of a particular $k$ value (e.g. Mortensen et al., 2011). Neither of these methods are satisfactory since there are dangers of circular reasoning (as discussed in Goring et al., 2012). Chapter 6 evaluated the addition of a prior range for modelling the $k$ parameter in the `P_Sequence` model, and recommended suitable a prior range of $\text{Log}(k) \sim \text{U}(-2, 2)$ and $\text{Log}(k) \sim \text{U}(0, 4)$, for modelling sequences in depth units of centimetre and metre, respectively. This chapter presents two case studies, firstly through the estimation of a very important tephra horizon in the eastern Mediterranean region, the two `P_Sequence` approaches (with and without the model averaging prior range) are discussed; secondly, an archaeological sequence in the Grotte des Pigeons cave in Morocco is modelled using the model averaging approach to shed new light on the timing of different periods of cave use. The research in this chapter forms part of the research constructed in the Response of Humans to Abrupt Environmental Transitions (RESET) project.

## 8.1 Tracking environmental change and isochronous markers

Understanding palaeoclimate, and the mechanisms behind abrupt environmental shifts, adds significant value to our understanding of future climate change, and how different species respond to climate change. It is apparent that this process is heavily dependent on reliable chronological information. Bayesian modelling plays a big role in enhancing the precision and accuracy of chronologies. In this section, the age of a widespread tephra horizon in eastern Mediterranean records is evaluated using available chronological and stratigraphic information in a Bayesian framework using the `P_Sequence` model. The implications of the new modelled age has on our understanding of eastern Mediterranean climate, in relation to global climate around that time period are also discussed.

Tephra from the Cape Riva (also known as Y-2) eruption of the island of Santorini

is a widespread tephra and presents an important link between different marine and terrestrial environmental records across the eastern Mediterranean region. It is found in deep-sea sediments from the Black Sea (Kwiecien et al., 2008), Aegean Sea and the Marmara Sea (Çağatay et al., 2000; Wulf et al., 2002; Aksu et al., 2008); in eastern Mediterranean deep-sea sediments near western Cyprus (Wulf et al., 2002); and in various terrestrial peat records in Greece (Seymour et al., 2004; Margari et al., 2007; Müller et al., 2011). The Y-2 tephra (at 7.61 m) is of particular interest in the Tenaghi Philippon record because it is found adjacent to an abrupt increase in tree pollen (at 7.75 m). This environmental event has been assumed to be synchronous with the Greenland interstadial (GI-2) event observed from the Greenland ice-core (NGRIP) record (Andersen et al., 2006; Müller et al., 2011). Obtaining an accurate age for this tephra is important because it is frequently used to date and correlate different marine and terrestrial chronologies (e.g. Çağatay et al., 2000; Kwiecien et al., 2008). It can also be used to precisely track abrupt climate changes in regional records (Hardiman, pers. comm.).

### 8.1.1 Dating

Tephras can be directly dated using $^{40}Ar/^{39}Ar$ or indirectly dated using radiocarbon, usually of charred organic material found in the same context. They can also be dated relatively using annual laminations if they were found in varved sequences.

Recent developments in $^{40}Ar/^{39}Ar$ dating has been shown to provide accurate and precise ages of young mafic volcanic rocks, with $1\sigma$ uncertainties ranging from 0.5–2% (Lanphere, 2000). Dating using the $^{40}Ar/^{39}Ar$ technique relies on the presence of K-rich minerals (sanidine or anorthoclase) in the form of either phenocrysts (Singer and Pringle, 1996) or bulk crystals (Lanphere, 2000); or of radiogenic argon bearing glass shards. These materials are usually found in alkali-rich young tephras, and in coarse-grained, crystal-bearing proximal deposits. Hence, the applicability of the $^{40}Ar/^{39}Ar$ technique is limited (Blockley et al., 2008c). Unfortunatey, the Y-2 tephra does not contain sanidine crystals for $^{40}Ar/^{39}Ar$ dating, nor has it yet been found in laminated

sequences. Instead, radiocarbon has been used previously to date the tephra.

The Y-2 tephra has several proposed radiocarbon ages from both marine and terrestrial environments. Interpolation between two radiocarbon dates in the marine record from Edremit Bay provided a calibrated age of 21,620 cal BP (Aksu et al., 2008) and in another marine record from the Black Sea provided a radiocarbon determination of 19,770 BP (Kwiecien et al., 2008). Reservoir correction was applied to the former age and the latter age was derived from the radiocarbon scale. Both ages were given without uncertainty. Charred trees from the lower part of the terrestrial pumice flow have provided radiocarbon determinations of 18,050±340, 18,165±210, and 18,880±230 BP (Pichler and Friedrich, 1976). This is supported by Eriksen et al. (1990), who dated charcoal from small trees and branches covered by ignimbrites and provided a radiocarbon determination of 18,150±200 BP. Seymour et al. (2004) also provided radiocarbon determinations of 18,527±145 BP and 18,244±143 BP below the Y-2 tephra layer as part of a tephrochronological record. In addition to the available radiocarbon dates, the Y-2 tephra is found in two terrestrial radiocarbon dated palaeoclimatic records from Lesvos Island (Margari et al., 2009) and Tenaghi Philippon (Müller et al., 2011), Greece.

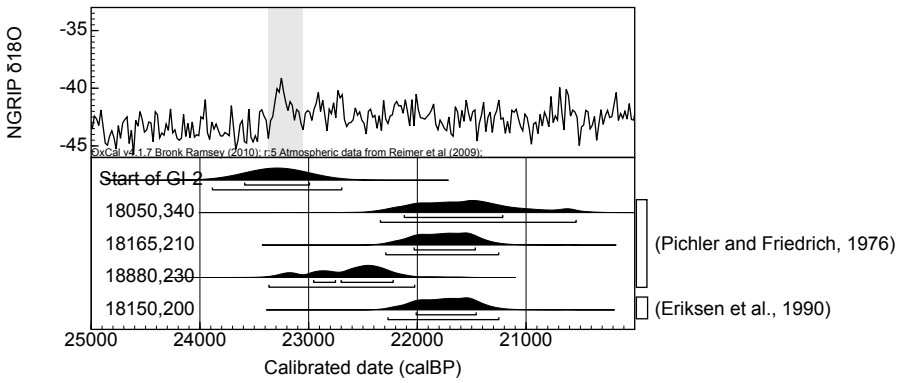


Figure 8.1: Published radiocarbon determinations of the Y-2 tephra. The GI-2 event is highlighted in grey.

There is substantial overlap between the 95.4% calibrated age ranges for the radiocarbon determinations (Fig. 8.1), with a possible outlying age of 18,880±230 BP (23,365–22,025 cal BP at 95.4% probability) from Pichler and Friedrich (1976), which

appears to be up to a thousand calendar years older in comparison to all the other radiocarbon dates. However, if this is the correct age, it would imply that there is a 95.4% probability that the abrupt increase in tree pollen in the Tenaghi Philippon peat record (Müller et al., 2011) occurred between 266 years before, and 1578 years after the GI-2 event in the NGRIP record (Andersen et al., 2006; Blockley et al., 2012). This is calculated by subtracting the Greenland Ice core chronology (GICC05) age of the start of the GI-2 event (23290±298 cal BP; Blockley et al., 2012) from the calibrated age of the radiocarbon determination 18,880±230 BP (Pichler and Friedrich, 1976). If the other younger ages are correct, the Y-2 tephra is well dated and places the environmental event in Tenaghi Philippon between 828 and 2305 years (95.4% probability) after the GI-2 event from the NGRIP record. This is calculated by subtracting the GICC05 age of the GI-2 event from the calibrated combined radiocarbon determinations of the younger ages. It is therefore important to test that the age of the Y-2 tephra is robust given its stratigraphic position as a key marker of the abrupt environmental change in terrestrial archives (Margari et al., 2009; Müller et al., 2011), while retaining accuracy and precision, and this is attempted below using the radiocarbon chronologies from the Megali Limni (ML) basin on Lesvos Island (Margari et al., 2007, 2009) and Tenaghi Philippon (Müller et al., 2011), together with the radiocarbon determinations below the Y-2 tephra layer from the Philippi peat basin in Macedonia (Seymour et al., 2004), Greece.

### 8.1.2 Modelling

A Bayesian framework is employed here to estimate the precise age of the Y-2 tephra. Previous applications of Bayesian techniques in modelling tephra ages can be found in Blockley et al. (2008a,c), where the authors used a mixture of phase and age-depth models to test the robustness, and to enhance the precision and accuracy, of published tephra ages.

Bulk sediments and plant macrofossils form the majority of radiocarbon samples for the two records from the ML basin on Lesvos Island: the ML00 sequence (8.15 m

in length); and the ML01 sequence (10.97 m in length) (Margari et al., 2009). The former sequence consists of fifteen radiocarbon determinations, and the latter sequence consists of nine radiocarbon determinations. Three of these dates are too old (>43000 $^{14}$C yr BP) and are excluded from the analyses. The Y-2 tephra is found in the ML01 sequence at depth 1.81 m and is not included in the ML00 sequence. The Tenaghi Philippon record (14.52 m in length) consists of twenty radiocarbon determinations from bulk sediments, wood and carbonates from shells (Müller et al., 2011). The reliability of radiocarbon determinations from these samples was previous discussed in Section 2.1.5. The Y-2 tephra is found at depth 7.61 m in the Tenaghi Philippon sequences. The complete data set can be found in appendix B.4. In addition to the two chronologies, radiocarbon determinations on bulk sediments underneath the Y-2 tephra layer are also available from the Philippi peat basin in Macedonia (Seymour et al., 2004). Another widespread tephra, the Campanian Ignimbrite (CI), is also found in all sequences.

The CI (also known as Y-5) eruption is the largest known eruption of the last 100,000 years (Barberi et al., 1978). This eruption has been located in the Campi Flegrei region of southern Italy, which is close to the present day Bay of Naples. The ash horizon of this event is widespread and is recognised in cores across the eastern Mediterranean (Pyle et al., 2006). An extensive study of the age of this tephra yielded a high precision $^{40}$Ar/$^{39}$Ar age of 39,280±110 BP (de Vivo et al., 2001) and this is the age recommended by Pyle et al. (2006) as the accepted geological age of this eruption. It is in good agreement with another $^{40}$Ar/$^{39}$Ar age of this tephra (41,100±2,100 BP; Ton-That et al., 2001). The age of the Y-5 tephra can be integrated on its own and / or as a tie-point (point of equal age), into the above sequences to enhance the precision of the overall chronologies.

Age-depth models are constructed for records from Lesvos Island and Tenaghi Philippon using the `P_Sequence` model, for estimating the age of the Y-2 tephra, because it provides the most realistic depiction of sedimentation for this case study, with the complexity (randomness) of the underlying sediment deposition modelled

according to a Poisson process. The sequences are modelled firstly, with the function described in Bronk Ramsey (2008), which employs a single value for the $k$ parameter; and then with a prior range for model averaging. The differences in the posterior outputs are also discussed. Formal outlier analysis is not employed for this case study due to the good agreement between the radiocarbon likelihoods and the posterior model outputs (as determined in `OxCal` by agreement indices, $A$, of >60%; Bronk Ramsey, 1995).

#### 8.1.2.1 The Lesvos models

Two sequences from ML basin, ML00 and ML01, are available from Lesvos Island. The former sequence covers only a portion of the latter, longer record, but in much greater resolution. Margari et al. (2009) constructed a composite age-depth model using radiocarbon dates from both sequences. The authors used the correlation based on pollen biostratigraphy, the position of the Y-5 tephra horizon and calibrated radiocarbon ages to modify and adjust the depth scale of ML00 sequence to that of the ML01 sequence. Correlation using independent stratigraphic markers is recommended (Blockley et al., 2012). However, using common features on proxy records to align different sequences is a widely used process known as tuning, but it is not recommended (Blockley et al., 2012; Blaauw, 2012). Tuning might be more acceptable in this scenario, where the two records originated from the same basin, than investigations of synchroneity across a region. However, environmental signals can be different even in the same basin (for example, in Turner et al., 1993). Using (calibrated or non-calibrated) radiocarbon ages as tie-points to construct a composite age-depth model presents dangers of circular reasoning. Hence, the composite age-depth sequence will not be employed here.

The age of the Y-2 tephra is particularly problematic to model because it is found at the very top edge of the ML01 sequence, which is not only low in resolution, but also has evidence which suggests the presence of a hiatus between the radiocarbon dates in close proximity to the tephra, stratigraphically. Evidence includes a radiocarbon

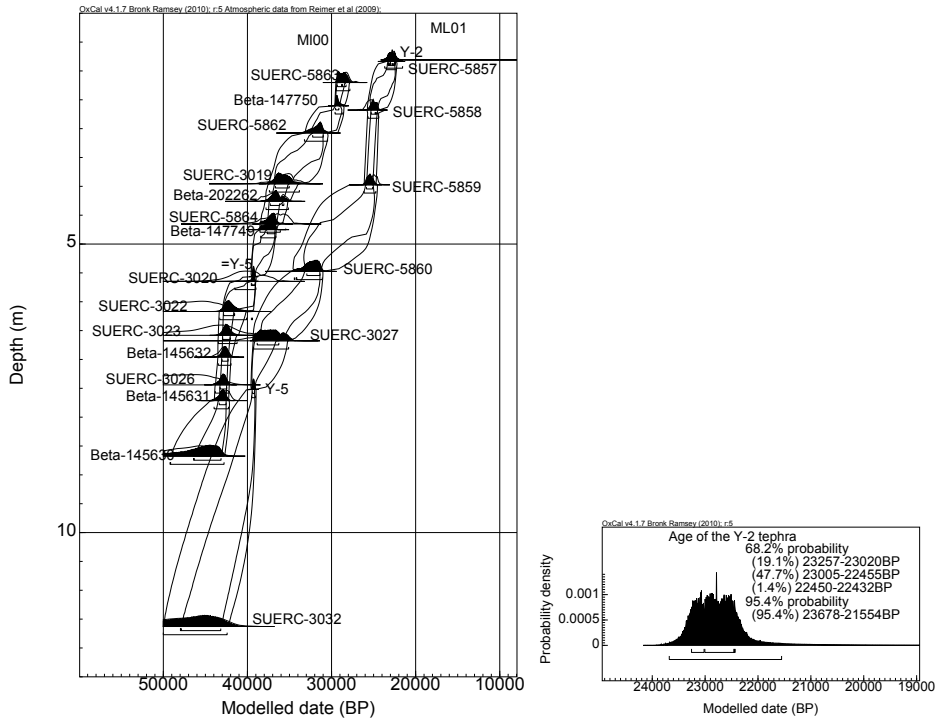


(a) (b)

Figure 8.2: Posterior Poisson process deposition models at Lesvos Island with $k = 1$ $m^{-1}$ (a) for ML00 (left) and ML01 (right) and (b) the modelled age for the Y-2 tephra, at 68.2% and 95.4% probability.

determination (SUERC–1287) of 1,538±28 BP at 0.65 m, an erosional surface at 1.29, and also a significant transition to primarily inorganic sediments at 1.5 m (Margari et al., 2009). For these reasons, the radiocarbon determination, SUERC-1287, will be excluded from the analyses. The rest of the ML01 sequence is still reliable for modelling the age of the Y-2 tephra because it is found at 1.81 m, which is below the erosion surface and the significant transition to inorganic sediments.

The posterior outputs for the model with arbitrary values of $k = 1$ $m^{-1}$, i.e. 1 depositional event per m, are shown in Figure 8.2 and suggest that the age of the Y-2 tephra is in the range of 23,678–21,554 cal BP, at 95.4% probability. $k = 1$ $m^{-1}$ was chosen because the the ML01 sequence was sparsely dated. Although ML00 is also modelled, the sequence does not contribute to the modelling of the ML01 sequence, and thus does not contribute to the modelling of the age of the Y-2 tephra. Convergence of the age of the tephra is poor (as determined in `OxCal` by the convergence integral, $C$, of 0.9%; Bronk Ramsey, 1995) after over 50 million

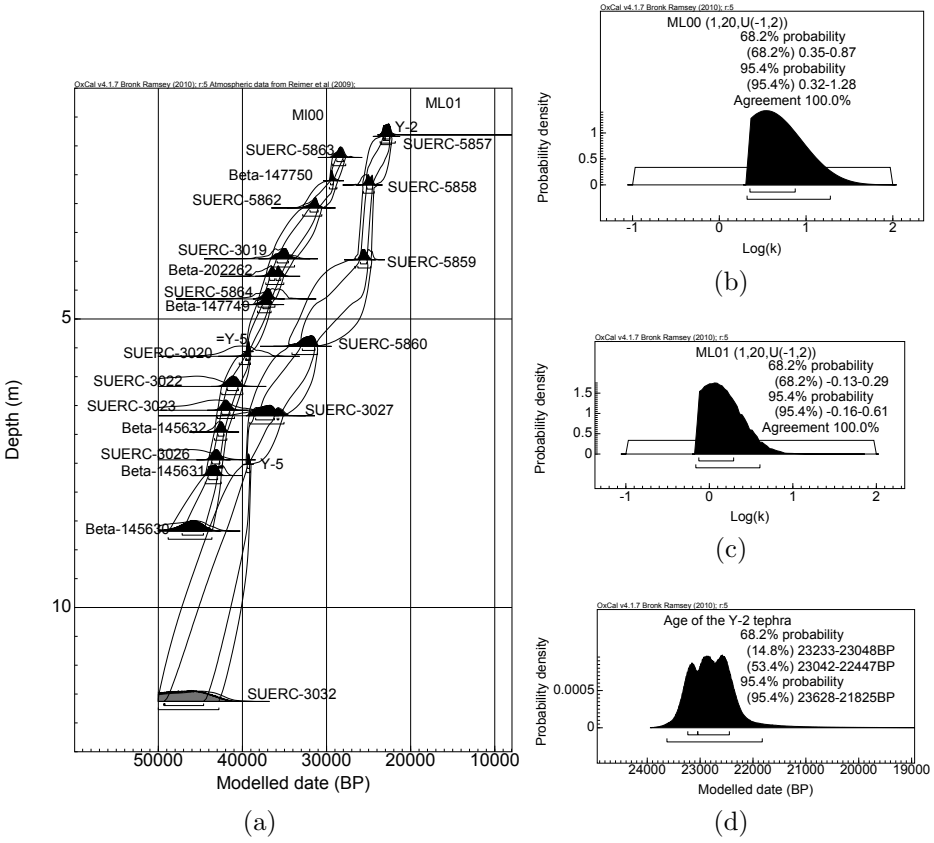


Figure 8.3: Posterior Poisson process deposition models at Lesvos Island with $\text{Log}(k) \sim U(-1, 2)$ (a) for ML00 (left) and ML01 (right), posterior distributions for the $k$ parameter for (b) ML00 and (c) ML01, and (d) the modelled age for the Y-2 tephra, at 68.2% and 95.4% probability.

iterations. This suggests that the model is unstable. However, repeated model runs yield similar age ranges, suggesting that it is likely that this is the best posterior age estimate for the Y-2 tephra from this analysis.

The second `P_Sequence` model was initially run with a prior range of $\text{Log}(k) \sim U(0, 4)$, i.e. between 1 to 10,000 events per m. Results show that a prior range of $\text{Log}(k) \sim U(-1, 2)$ is a better range for the ML01 sequence and so it is used in the final analysis. The posterior deposition models are shown in Figure 8.3. The modelled age of the Y-2 tephra is in the range 23,636–21,833 years BP, at 95.4% probability. It is in good agreement with the modelled age from the previous model. Convergence for the posterior age of the Y-2 tephra ($C = 62.2\%$) has improved greatly (by $\sim 70$ fold) from the previous model after 300 million iterations. Repeated model runs yield similar age ranges but varying convergence integrals. This is not unexpected since

the Y-2 tephra lies at the edge of a sequence, with only information on its depth. This also makes the modelled age of the Y-2 tephra impossible to validate using this analysis alone. As with the first analysis, the ML00 sequence is also modelled but does not contribute to the modelling of the ML01 sequence. Figures 8.3b and 8.3c show the posterior distributions for the modelled $k$ values for the individual ML sequences and confirm that the arbitrary values of $k = 1$ m$^{-1}$ chosen for the previous model are suitable for modelling both the ML sequences. The modelled $k$ values for the ML00 sequences are higher than those of the ML01 sequence because ML00 is dated to a higher resolution and the sedimentation rate is relatively more consistent than that of the entire ML01 sequence.

#### 8.1.2.2 The Tenaghi Philippon models

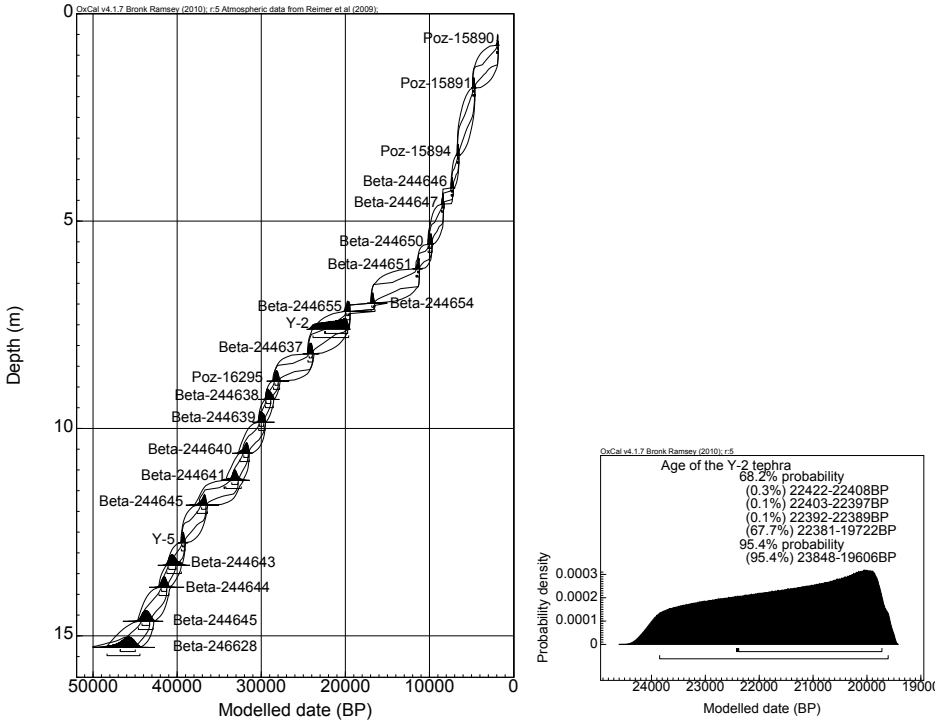


(a) (b)

Figure 8.4: Posterior Poisson process deposition model for the Tenaghi Philippon sequence with $k = 2$ m$^{-1}$. (a) The radiocarbon chronology, and (b) the modelled age for the Y-2 tephra, given at 68.2% and 95.4% probability ranges.

The Y-2 tephra is positioned in the middle of the Tenaghi Philippon sequence, which means that it is better constrained than it is in the ML01 sequence from Lesvos

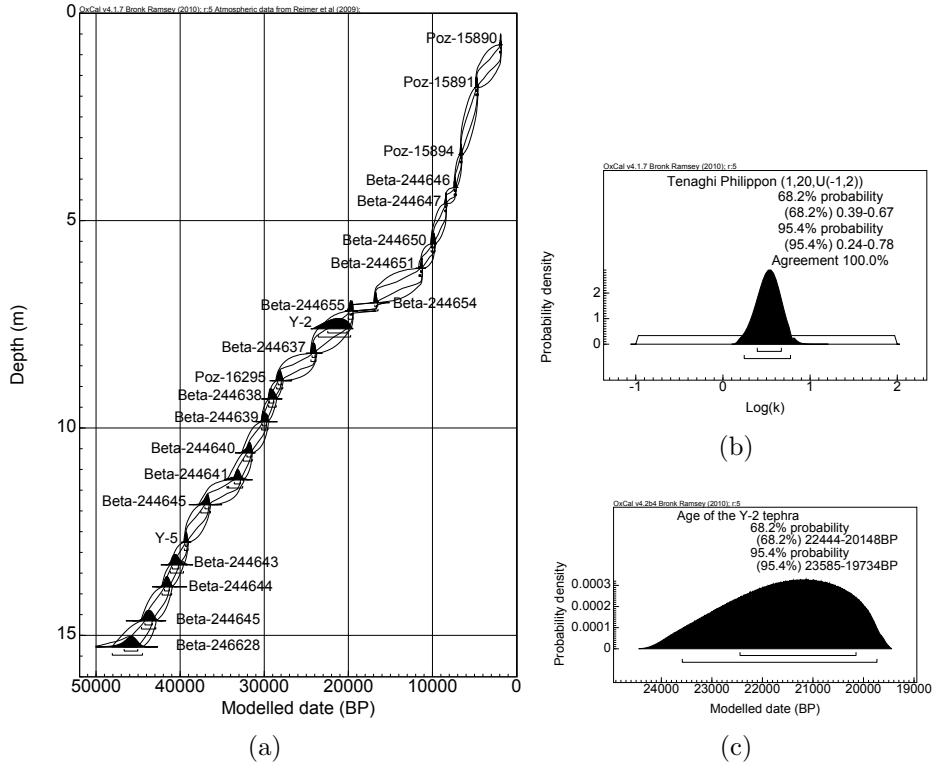


(a) (b) (c)

Figure 8.5: Posterior Poisson process deposition model for the Tenaghi Philippon sequence with Log$k \sim$ U$(-1, 2)$. (a) The radiocarbon chronology, (b) posterior distribution for the $k$ parameter, and (c) the modelled age for the Y-2 tephra, at 68.2% and 95.4% probability.

Island. Similar to the Lesvos Island model, two models were constructed using either a single value or a prior for $k$. The posterior outputs for the model with an arbitrary value of $k = 2$ m$^{-1}$, i.e. 2 depositional events per m, are shown in Figure 8.4 and suggest that the age of the Y-2 tephra is in the range of 23,848–19,606 cal BP, at 95.4% probability. Convergence for this model is satisfactory, with $C > 99\%$ for all posterior ages.

The second `P_Sequence` model was run with a prior for step-size parameter, where Log$(k) \sim$ U$(-1, 2)$. The posterior outputs are shown in Figure 8.5. The modelled age of the Y-2 tephra is in the range 23,585–19,734 cal BP. This model gives a sightly more precise tephra age than the previous model without the use of a prior for the $k$ parameter. The modelled distribution for the $k$ parameter is shown in Figure 8.5b. It confirms that the arbitrary value of $k = 2$ m$^{-1}$ chosen for the previous model is suitable for modelling this sequence.

All of the modelled ages for the Y-2 tephra are consistent, with a more precise output from the ML01 sequence from Lesvos Island. In both of the above cases, the arbitrary values chosen for the $k$ parameters are suitable for the individual models. However, results from Figures 8.3b, 8.3c, and 8.5b suggest that values higher or lower than those of the chosen ones, but within the posterior ranges, are also suitable for the individual sequences and would give reliable chronologies. A higher $k$ value would give a more precise age-depth model; conversely, a lower $k$ value would give a more uncertain age-depth model and consequently resulting in a less precise age for the Y-2 tephra. The difference in uncertainty can be as big as a thousand years. One cannot distinguish between these different ages alone by looking at the agreement indices of the different models because they are all >60%, which means that the models are in good agreement with the data (Bronk Ramsey, 1995). By employing the model averaging approach in the `P_Sequence` model, i.e. using a prior range instead of a single value for the $k$ parameter, the model samples a range of $k$ values and becomes more robust. It removes the subjectivity involved in model selection, i.e. choosing the most appropriate single value for the $k$ parameter.

#### 8.1.2.3 Cross-linking different records

Tephra dispersal is considered as an abrupt event in terms of the uncertainty associated with absolute age measurements and so the same tephra horizons found in different sequences can be cross-linked to further enhance the precision of chronologies. This method is employed here to further enhance the precision of the modelled age of the Y-2 tephra.

A first attempt at producing a more precise age for the Y-2 tephra can be performed by using the ML01 and Tenaghi Philippon sequences. The ML00 sequence is not used since it does not contribute to the modelling of the age of the Y-2 tephra. Results of this model (Fig. 8.6) suggest that the age of the Y-2 tephra is in the range of 23,518–21,488 cal BP, at 95.4% probability, which is consistent with the age from previous models. However, since the modelled age overlaps with the age from the

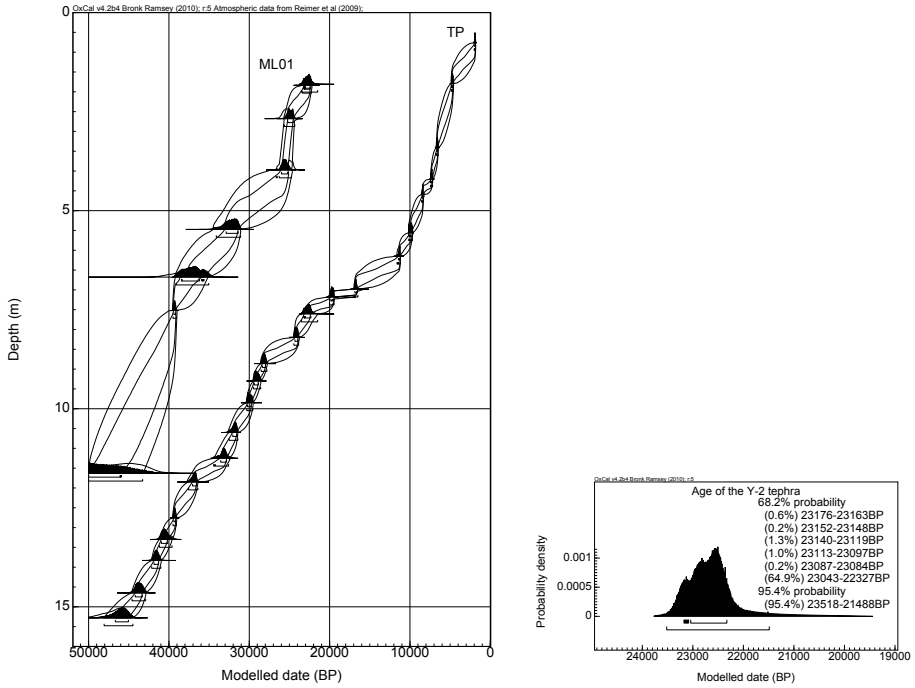


(a) (b)

Figure 8.6: Posterior Poisson process deposition models for (a) the ML01 (left) and the Tenaghi Philippon (TP; right) sequences with $\text{Log}(k) \sim \text{U}(-1, 2)$ and (b) the modelled age for the Y-2 tephra, given at 68.2% and 95.4% probability ranges.

Lesvos Island models more precisely, it is apparent that the posterior age of the Y-2 tephra is heavily biased by its position in the ML01 sequence from Lesvos Island. Convergence for the posterior age of the Y-2 tephra is low ($C = 1.8\%$) after 4 million iterations. Repeated, longer, model runs do not improve convergence but yield similar age ranges.

To further test the reliability of the age of the Y-2 tephra, recent high-precision AMS ages by Seymour et al. (2004) are also incorporated into the model using an exponential distribution as prior information. The exponential `Tau_Boundary` is applied to the radiocarbon dates, as materials just underlying the tephra (Seymour et al., 2004, Fig. 3) are most likely to be buried just before the eruption, but with a gradually decreasing probability of being from material deposited substantially earlier than the eruption. This approach had been previously used by Blockley et al. (2008c) to precisely estimate the age of the Neapolitan Yellow Tuff (NYT), with the `Boundary` parameter as a measure of the abrupt event. This model yields a 95.4% probability

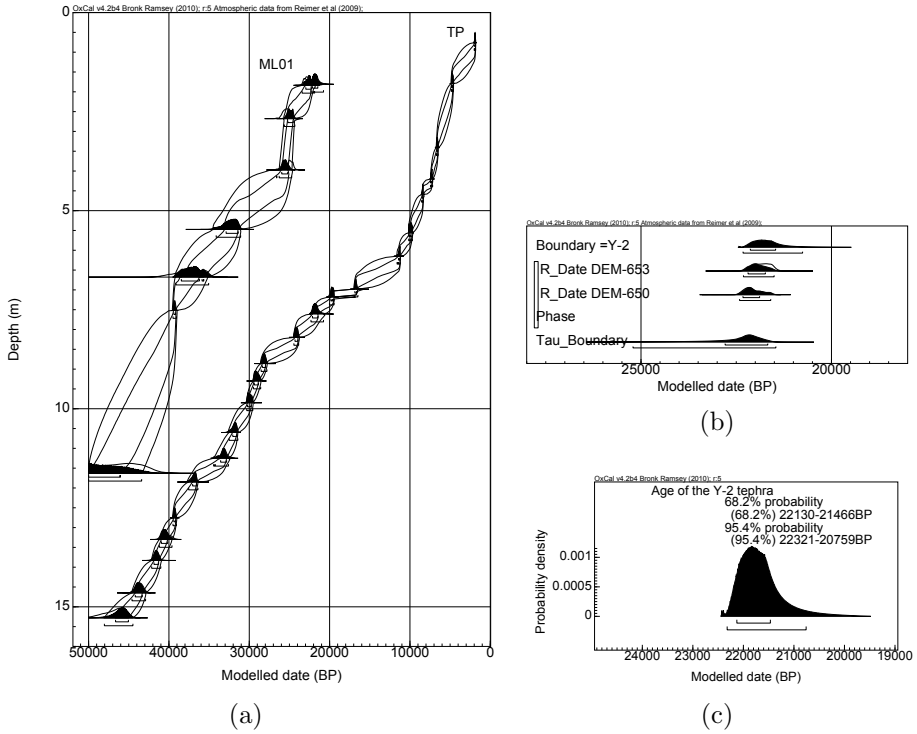


Figure 8.7: Posterior Poisson process deposition models for (a) the ML01 (left), and the Tenaghi Philippon (TP; right) sequences with $\text{Log}(k) \sim \text{U}(-1, 2)$, (b) exponential model with data from Seymour et al. (2004), and (c) the modelled age for the Y-2 tephra, given at 68.2% and 95.4% ranges.

age range for the Y-2 tephra of 22,321–20,759 cal BP. This age range, although broad, is in good agreement with some of the radiocarbon ages on terrestrial plant material buried by ash and for this tephra within their error ranges (Pichler and Friedrich, 1976; Eriksen et al., 1990). The convergence of this model has improved from the previous model ($C = 90.5\%$) after 4 million iterations. Repeated, longer, model runs do not improve convergence but yield similar age ranges.

It is unfortunate that the Y-2 tephra is positioned at the edge of the ML01 sequence, providing little constraint on its age. This is also the reason for having low convergence ($C < 95\%$). While it is still possible that the age of the Y-2 tephra to be as old as 23,518 cal BP (95.4% probability), it would imply that the dates from material buried by the eruption are incorrect and this possibility is unlikely. Charred plant materials covered in ignimbrite (Eriksen et al., 1990) suggest that the sample was killed and charred by the volcanic event, which means that their radiocarbon determinations represent the time of the eruption; or that the plant materials were

killed before the charring, which means that their radiocarbon determinations represent time before the eruption. It is therefore unlikely that the age of the Y-2 tephra be 23,518 cal BP. Results from this section proposes that, on currently available dating evidence, the 95.4% probability model age range for the Y-2 tephra (22,321–20,759 cal BP) is the best calendar age estimate for the eruption. With this modelled age, the age different of the three relevent events (increase in tree pollen, GI-2 in NGRIP, and Y-2) can be calculated and the results are shown in Figure 8.8.

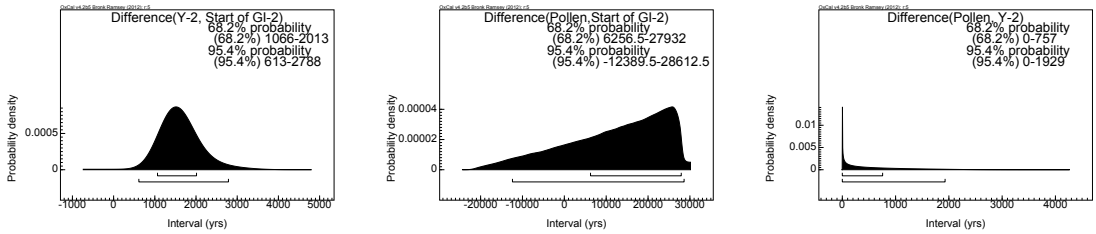


Figure 8.8: Time lag between the GI-2 event, increase in tree pollen and the modelled age of the Y-2 tephra.

### 8.1.3 Discussion

The Poisson process model have proved useful in modelling sequences where high precision chronological resolution is required. The model averaging approach, i.e. prior range for the step-size parameter, $k$, has made a significant contribution to the modelling of the age of the Y-2 tephra in this section. It removes the subjectivity in model selection, improves model convergence (in the ML01 sequence), as well as making the model applicable and easier to use in sequences that are not annually laminated, in this case, peat sequences.

In terms of tracking climate change, having an age of 22,321–20,759 cal BP for the Y-2 tephra would imply that the increase in pollen observed from Tenaghi Philippon occurred after the GI-2 event of the NGRIP record, with a possible 613–2788 year gap (95.4% probability). A more accurate way of quantifying this time difference would be to obtain quantitative estimates of the timing of events between archives by calculating probabilities of events within moving time windows of varying widths (e.g. Bennett and Fuller, 2002; Blaauw et al., 2007, 2010; Blaauw, 2012). This, un-

fortunately, has not been possible for this analysis because the raw pollen data is not available.

The conclusion of asynchroneity of environmental events between the Tenaghi Philippon and the NGRIP records contradicts Müller et al. (2011), that "all interstadials at Tenaghi Philippon can be linked with Greenland interstadials". The authors came to that conclusion based on the radiocarbon chronology, which was constructed using mean calibrated ages in a piece-wise linear interpolation manner, and calibration of the radiocarbon determinations was performed using the calibration curve provided by Weninger and Jöris (2008). Since Müller et al.'s publication, a more updated and precise version of the international consensus calibration curve, IntCal09 (Reimer et al., 2009), has become available. It, together with Bayesian modelling, provide a more precise and accurate chronology than can be provided with tuning and / or a piece-wise linear age-depth model with the means of calibrated ages alone. The analyses described in this section take into account the uncertainty associated with each radiocarbon determination, and also the deposition process of non-dated events. They are therefore able to provide a more accurate age estimate for the Y-2 tephra.

Asynchroneity between records from Greenland and the eastern Mediterranean is not so surprising since the environmental proxies used in the two records are different. The NGRIP record was constructed using $\delta$18O values and the Tenaghi Philippon record was constructed with pollen diagrams. $\delta$18O value is a measure of oxygen isotope ($^{18}O : {}^{16}O$) ratio relative to that of a laboratory standard, and it is a reflection of global temperature. Fractionation of oxygen isotopes occurs during evaporation of water from the sea surface. The lighter water molecule ($H_2^{16}O$) is drawn into the atmosphere in preference to the heavier molecule ($H_2^{18}O$). Glacial ice obtains this temperature dependent signal from the moisture-bearing winds which nourish the polar glaciers (Lowe and Walker, 1997, p.150). Pollen diagrams, on the other hand, show changes in pollen content, which may be interpreted as indicating temporal changes in vegetation cover in the area adjacent to the site (Lowe and Walker, 1997,

p.165). Since atmospheric isotope mixing is a more rapid *global* process than changes in *regional* vegetation, one can expect asynchroneity between the two. There could be a possible time lag in vegetational response to climate change. It is even possible that they are two independent events.

Using the rest of the radiocarbon chronology, Müller et al. (2011) argued that the North African humid period faciliated the successful dispersal of anatomically modern humans (AMH) from Africa. The initial AMH movement into Europe was dated to a weighted mean of 48,200 ± 1900 years BP. Although contradicting synchroneity, the last dated event in the Tenaghi Philippon sequence is in close proximity to another increase in tree pollen, which is modelled to be 48,032–44,486 cal BP. This suggests that it is likely that the natural environments were favourable for AMH to migrate directly into Europe already at that time.

Obtaining a robust age for the Y-2 tephra is a starting point in testing the leads and lags of eastern Mediterranean and the NGRIP records. Further work is currently being carried out by Hardiman and colleagues on improving the chronologies and pollen stratigraphy from different eastern Mediterranean sites in order to better constrain the progression of climate change and to draw conclusion on the influence of environmental changes on the migration of AMH Africa into Europe.

## 8.2 Chronology of the Grotte des Pigeons cave in north-east Morocco

The Grotte des Pigeons cave site is located close to the village of Taforalt in north-east Morocco. It is a very important archaeological site as it contains a long, continuous sequence of Middle and Epipalaeolithic occupation evidence (Barton et al., 2007; Bouzouggar et al., 2008). The Epipalaeolithic in the Meghreb (regions in north-west Africa comprising northern parts of Morocco, Algeria, and Tunia) is also referred to as the Iberomaurusian (Barton et al., 2007). The archaeological sequence at Grotte des Pigeons is very distinctive and is separated into two major units: the 'grey series' and the 'yellow series'. The major sedimentary boundary separating the two series is associated with a potential change in subsistence patterns (Taylor et al., 2011). Similar sedimentary patterns, where grey midden deposits overlay a lighter deposit are also observed at Ifri n'Ammar and Rhafas, which are cave sites in close proximity to Taforalt (Barton, pers. comm.).

The grey series at Grotte des Pigeons cave lies above the yellow series. It is a 4 m thick sequence of grey deposits containing a large amount of ash and charcoal - an indication that fires were regularly lit inside the cave and frequently causing roof fall (Barton et al., 2007). It also contains burnt materials including artefacts, lithics, cut-marked animal bones, and a large amount of land snail shells, which are evidence of intensive use of the cave (Barton et al., 2007; Bouzouggar et al., 2008; Taylor et al., 2011). A number of human burials were also recovered from this series towards the back of the cave (Humphrey et al., 2012).

The underlying yellow series contains fine-grained and very well stratified sandy, silty, and sometimes stony deposits (Barton et al., 2007; Bouzouggar et al., 2008). Similar culturally to the grey series, it also contains lithics, charcoals, and cut-marked animal bones, suggesting intermittent human occupation (Barton et al., 2007; Taylor et al., 2011). No human bones have been found in this series (Humphrey et al. 2012; Barton, pers. comm.), suggesting that burials in the cave started after the transition

between the yellow and the grey series.

The sedimentary boundary at Grotte des Pigeons is thus associated with the appearance of a large scale cemetery (Humphrey et al., 2012), and increase of molluscs (Taylor et al., 2011). Obtaining a precise and accurate chronology for the cave site will contribute to our understanding of the timing of such changes and whether these can be correlated with the high frequency, abrupt climatic oscillations observed in the Greenland ice core core records (Andersen et al., 2006) and proxy records from the Alboran Seas (Moreno et al., 2002; Jullien et al., 2007).

The possible impact of rapid climatic change on human occupation has already been discussed in Barton et al. (2007). Heinrich events, in particular, are assumed to have had an indirect impact on population density. They represent periodic collapses of ice sheets from the Laurentide, Greenland, Icelandic, Fennoscandian, and British regions (e.g. MacAyeal, 1993; Bond et al., 1997; Scourse et al., 2000; Hemming, 2004; Nygård et al., 2004), causing dramatic marine and terrestrial temperature reductions and increased aridity througout the Northern hemisphere (e.g. Rohling et al., 2003; Hemming, 2004; Standford et al., 2011). The former is recored in marine sediment cores recovered from the Ice Rafted Debris (IRD) belt in the North Atlantic (e.g. Heinrich, 1988; Bond et al., 1992; Hemming, 2004; Standford et al., 2011), and the latter is recored in pollen records (Fletcher and Sánchez Goñi, 2008), and the input of Saharan dust in the Alboran Sea cores (Moreno et al., 2002) and in the North Atlantic (Jullien et al., 2007).

### 8.2.1 Modelling

The work in this section has been performed in collaboration with Professor Nick Barton, from the University of Oxford; and Dr. Simon Collcutt, who worked on the stratigraphy for the Grotte des Pigeons sequence. Barton kindly provided 38 new radiocarbon determinations since the Barton et al. (2007) and Bouzouggar et al. (2008) publications, and Collcutt kindly provided the depth of individual samples. The complete data set contains 55 radiocarbon determinations on cut-marked bones,

charcoals, and ostrich egg shells and can be found in appendix B.5. Three radiocarbon determinations from ostrich egg shells were omitted from the analysis because they were considered unreliable due to possible carbonate exchange with materials of a different age. A Bayesian framework was employed to model the chronology of Grotte des Pigeons at Taforalt. The sequence of radiocarbon determinations was from samples taken from the same section in the cave, no more than several decimetres apart horizontally. All samples have spot heights and can be confidently identified to stratigraphic unit. Thus, prior information on depth (in metres) is available. The entire sequence from Grotte des Pigeons runs from 0.22–5.77 m.

Some samples were taken from sediment blocks of 10–15 cm thickness. A Poisson process deposition model (`P_Sequence`; discussed in Chapter 6) was used because it provides a realistic depiction of sedimentation for cave sites, with the complexity (randomness) of the underlying sedimentation deposition modelled according to a Poisson process. The sequence is divided in places where hiatuses are observed. The `P_Sequence` model is chosen over the `Sequence` model because the posterior distributions from the former have longer tails, hence robust estimates can be obtained. The determinations without spot heights, which can only be constrained within sediment blocks were modelled with a `Sequence` model, where they are constrained with `boundary` parameters. These `boundary` parameters are then imported into the bigger `P_Sequence` model according to their depths, using the `cross-referencing` function in `OxCal`.

Since the sediments are not annually laminated and do not provide means of estimating an appropriate value for the step-size parameter ($k$), the model averaging approach (discussed in Chapter 6), was used to enhance the precision and accuracy of the chronology. The sequence were modelled firstly with a prior range of

$$\text{Log}(k) \sim \text{U}(0, 4)$$

i.e. between 1 to 10,000 events per metre, for the step-size parameter. After initial

model runs, it was found that a range of $\text{Log}(k) \sim \text{U}(1, 2)$ was wide enough for this chronology. A `boundary` parameter has been used to represent the major sedimentary boundary between the yellow and grey series in order to: (1) draw inference on the age of the major change in sedimentation; and (2) tell the model that there is a likely change in the rate of sedimentation. The function `R_Combine` is applied to produce a weighted average of duplicate radiocarbon determinations of the same sample (3 samples have duplicate measurements).

Formal outlier analysis was also utilised to account for outliers in the radiocarbon scale (`type r`) and the calendar scale (`type t`). `Type r` analyses were employed when producing a weighted average of radiocarbon determinations and `type t` analyses were employed to account for possible outlying calibrated ages. The `CQL` for the outlier functions used are:

```
Outlier_Model("RScaled",T(5),U(0,4),"r");
Outlier_Model("General",T(5),U(0,4),"t");
```

Both outlier models are specified to allow the possible shifts in the specified scale to be drawn from a long tailed student $t$ distribution. The outliers can be in the scale of anywhere between $10^0$ and $10^4$ years. These are the models recommended by Bronk Ramsey (2009b) for general purposes when the scale of the possible offsets is unknown. When employed, the overall model is not affected by the odd extreme outlier. Each measurement is assigned a prior probability of 5% of being an outlier.

A first attempt at producing a robust and precise chronology for the Grotte des Pigeons sequence was performed with one `P_Sequence` function for samples with spot heights and one `Sequence` function for samples less accurately located to sediments blocks no thicker than 15 cm. Using one `P_Sequence` function means that the $k$ parameter is assumed to be consistent for the entire chronology for each model run. In terms of the `type r` outlier analysis applied to duplicated radiocarbon determinations during combination, none of the dates were found to yield $\geq$ 90% probability of being outlying, whilst 6 of the 6 dates were given a posterior probability of $\leq$ 5% of being outliers (as compared to the arbitrary 5% prior probability applied). In terms

of the `type t` outlier analysis applied to both the 46 uncombined and 3 weighted averages of the radiocarbon determinations, only 1 of the former was found to yield $\geq$ 95% probability of being outlying (and no further date $\geq$ 90%), whilst 30 of the former 46, and 3 of the latter 3 radiocarbon determinations were given a posterior probability of $\leq$ 5% of being outliers. Such findings support the validity of the individual radiocarbon determinations themselves (Staff et al., 2011).

The results of this model are summarised in Figure 8.9, with the yellow series in blue and the grey series in green. The model suggests that the transition between the yellow and grey series occurred in the range of 15134–14839 cal BP (95.4% probability; Fig. 8.9d). This modelled age is very precise, giving a 95.4% posterior range with precision of $<$ 300 years. However, although the sediment was described as "fine-grained", and this is supported by the high step-size parameter value, suggesting a deposition unit (event) per 4.68–6.45 cm (95.4% probability), it is evident that the types of deposition material were different between the yellow and grey series, giving rise to their different colours. Modelling with a consistent step-size parameter for the entire sequence for each model run might enforce too much constraint on the chronology, making it too rigid and hence the results unreliable.

#### 8.2.1.1 A high precision radiocarbon chronology for the Grotte des Pigeons cave

In order to enhance the accuracy of the radiocarbon chronology at Grotte des Pigeons cave, a second model run was performed with four `P_Sequence` and one `Sequence` functions. Three `P_Sequence` functions were used to model the samples with spot heights in the yellow series, and one `P_Sequence` function was used to model the samples with spot heights in the grey series. The yellow series was modelled with three separate functions, instead of one continuous function, because of the two possible hiatuses observed from Figure 8.9a, between OxA-16271 (at 4.96 m) and OxA-16273 (at 4.9 m), and between OxA-16267 (at 4.16 m) and OxA-22788 (at 4.12 m), although no stratigraphical indications were reported. The yellow and grey series were modelled

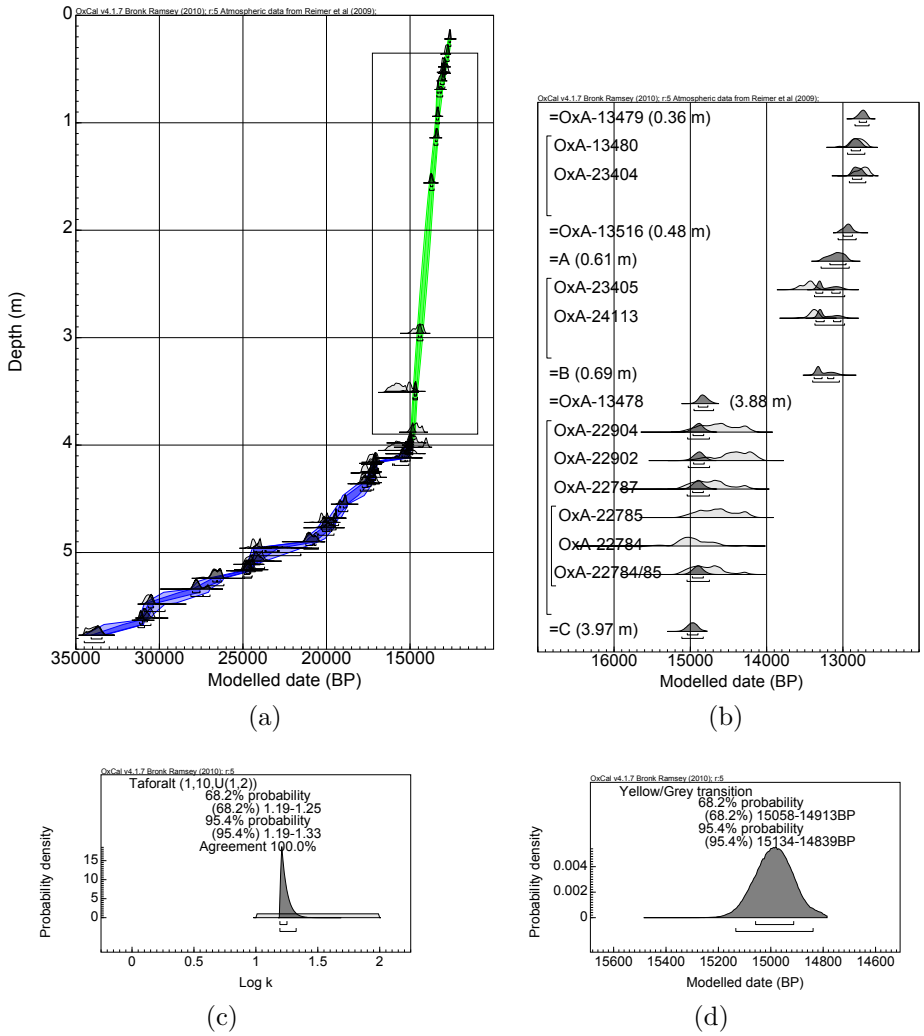


Figure 8.9: Posterior chronology of Grotte des Pigeons cave at Taforalt, modelled with (a) one `P_Sequence` function for samples with spot heights. The boxed area contains (b) `Sequence` function for samples from sediment blocks, given at 68.2% and 95.4% ranges. The chronology for the yellow series is in blue and the grey series in green. Constraints (depths) for the sediment blocks are specified in the brackets. (c) The step-size parameter for the `P_Sequence` model, and (d) the modelled age of the yellow / grey series transition `boundary`.

with separate functions because it is obvious that different sediments make up the yellow and grey series, and that the dating resolution of the series are different. The `Sequence` function, again, was used to model samples from sediment blocks. Using four `P_Sequence` functions meant that the step-size parameter was assumed to be consistent for the grey series, and that three different step-size parameters were assumed to be consistent for each section of the yellow series. An initial model run suggested that the grey series required a prior range of $\text{Log}(k) \sim \text{U}(0, 2)$ for the step-size parameter instead of the range, $\text{Log}(k) \sim \text{U}(1, 2)$, used for the yellow series.

In terms of the `type r` outlier analysis applied to duplicated radiocarbon determinations during combination, none of the dates were found to yield $\geq 90\%$ probability of being outlying, whilst 6 of the 6 dates were given a posterior probability of $\leq 5\%$ of being outliers. In terms of the `type t` outlier analysis applied to both the 46 uncombined and 3 weighted averages of the radiocarbon determinations, only 1 of the former was found to yield $\geq 95\%$ probability of being outlying (and no further dates $\geq 90\%$), whilst 30 of the former 46, and 3 of the latter 3 radiocarbon determinations were given a posterior probability of $\leq 5\%$ of being outliers.

The results of this model are summarised in Figures 8.10 and 8.11, with the yellow series in blue and the grey series in green. The step-size parameters for the separate `P_Sequence` models suggest that the grain sizes of the yellow and grey deposits are indeed different, with coarser grains (lower step-size parameter) in the grey series, and finer grains (higher step-size parameter) in the yellow series. The dating resolution of the two units also had an impact on the posterior distributions of the step-size parameters. This implies that modelling the two units with separate functions was more appropriate and therefore giving more reliable results than modelling with one function for the entire cave sequence. Modelling with one function resulted in a chronology which was perhaps too rigid for the grey series.

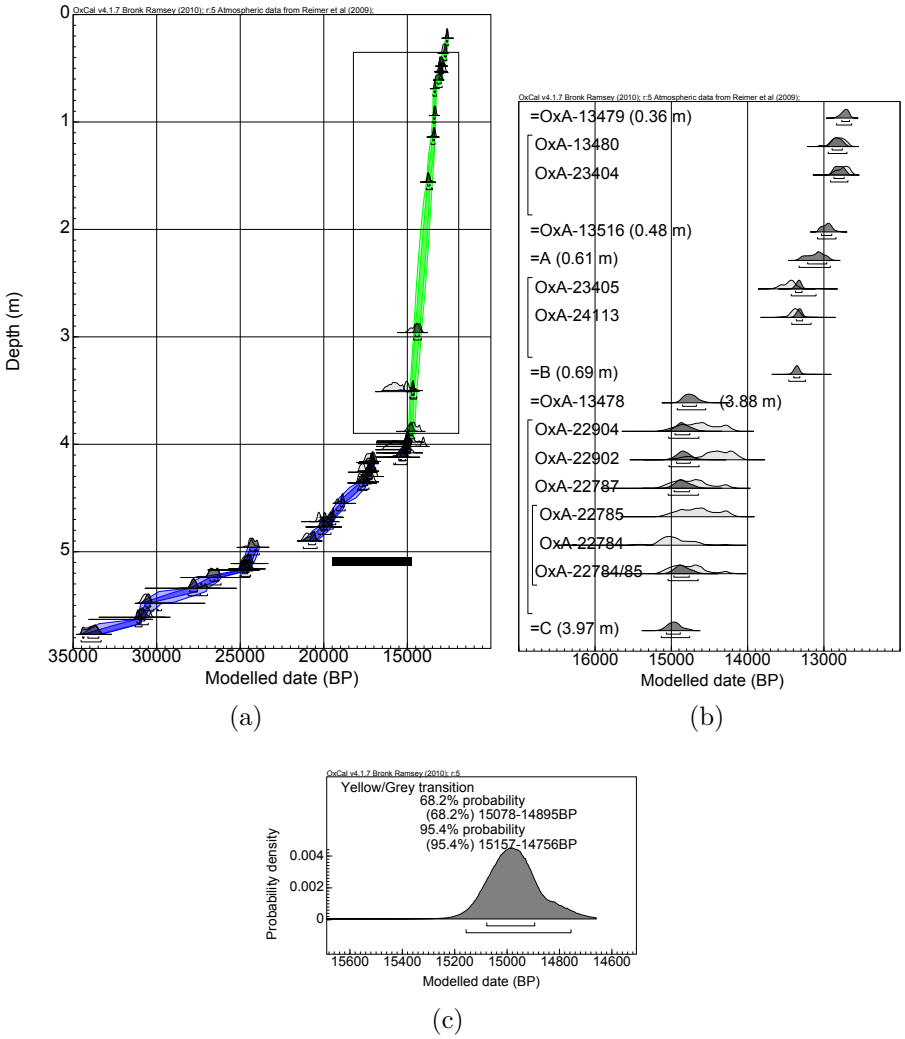


Figure 8.10: Posterior chronology of Grotte des Pigeons cave at Taforalt, modelled with (a) three `P_Sequence` functions for samples with spot heights, the black box marks the entire duration of H1 event (∼19,000–14,600 cal BP; Standford et al., 2011). The boxed area contains (b) `Sequence` function for samples from sediment blocks, given at 68.2% and 95.4% probability ranges. The chronology for the yellow series is in blue and the grey series in green. Constraints (depths) for the sediment blocks are specified in the brackets. (c) The modelled age of the yellow / grey series transition `boundary`.

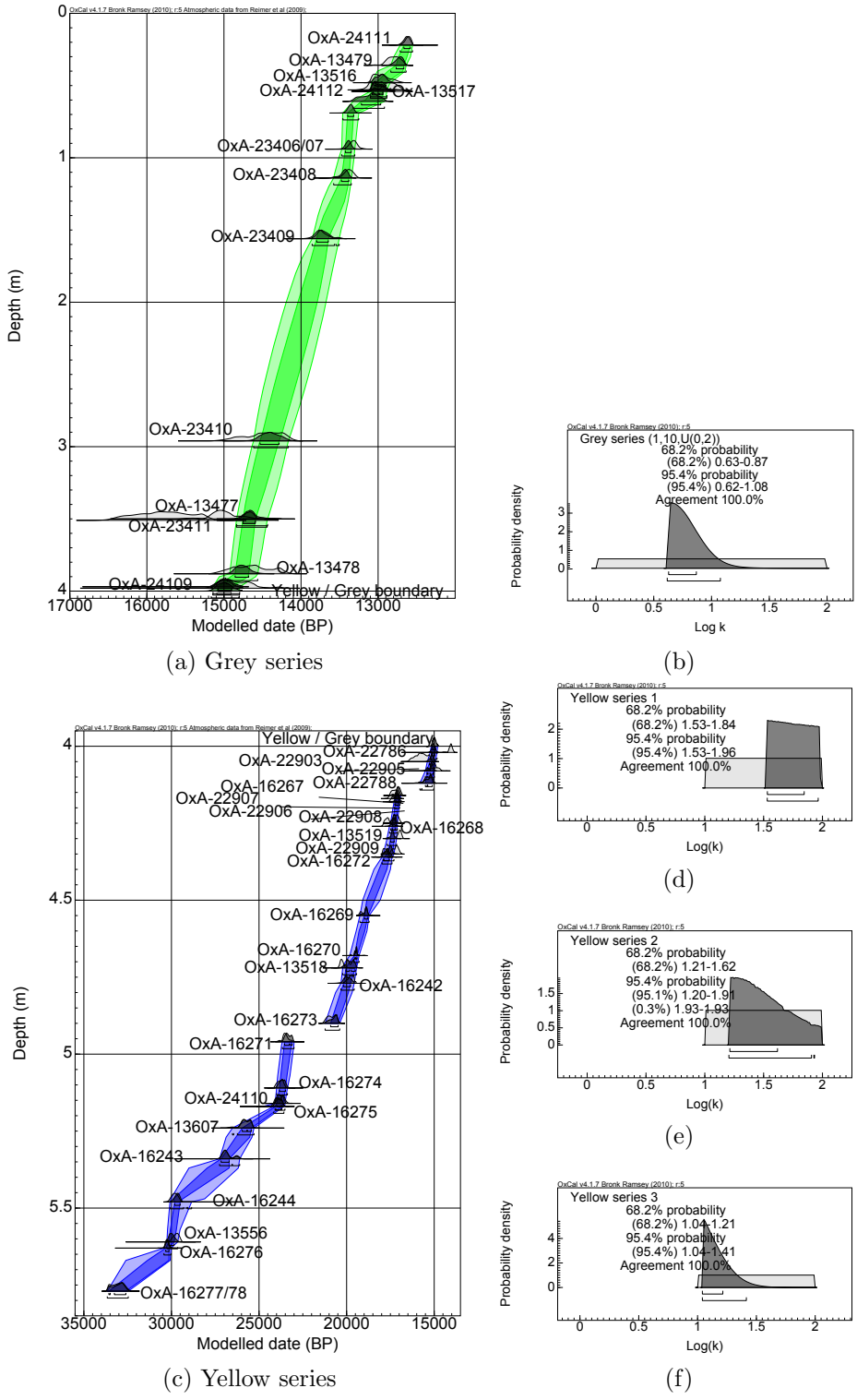


(a) Grey series (b)

(c) Yellow series (d) (e) (f)

Figure 8.11: Posterior chronology of Grotte des Pigeons cave at Taforalt, modelled with (a) one `P_Sequence` function, with (b) step-size parameter for the grey series; and (c) two `P_Sequence` functions, with (c), (e), & (f) step-size for the yellow series, given at 68.2% and 95.4% probability ranges.

### Change in sedimentation

The Grotte des Pigeons cave sequence is separated into two major units: the yellow and grey series. This distinctive change in sedimentation occurred at the depth of 4 m in the dated sequence described in this section. The model suggests that this transition occurred in the range of 15157–14756 cal BP (95.4% probability; Fig. 8.10c). This modelled age is less precise than the previous model, giving a 95.4% posterior range with precision of ∼400 years. It is, however, considered more reliable for the reasons discussed above.

The change in sedimentation coincided with the use of large scale cemeteries (Humphrey et al., 2012) and the increase of molluscs – suggesting a possible diet source (Taylor et al., 2011). This dramatic change observed between the yellow and grey series could be explained by possible feasting, including the use of fire inside the cave, which could perhaps also be linked with the change in funerary practices, or it could be completely unrelated and caused by other factors. It is also interesting to note that the modelled age for the change in sedimentation overlapped with the end of the last phase (3) of Heinrich event (H) 1 (∼16,700–14,600 cal BP; Standford et al., 2011). Figure 8.12 shows the time difference between H1 phase 3 and the modelled age of the yellow/grey boundary. The modelled age of the top of the Y2 sequence (sample OxA-16267 at 4.16 m) lies in the range of 17,219–16,898 (95.4% probability), and overlaps with the middle phase (2) of H1 (∼17,500–16,700 cal BP; Standford et al., 2011).

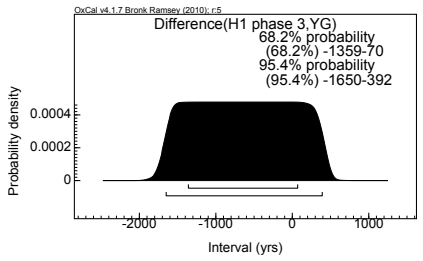


Figure 8.12: Difference in age between H1 phase 3 and Yellow / Grey transition, where negative values indicate overlap and positive values indicate a lag.

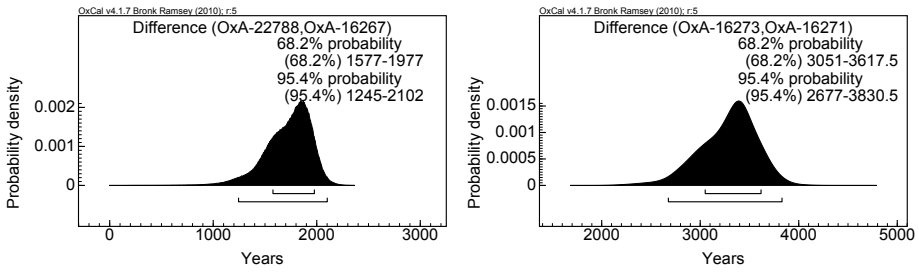


(a) (b)

Figure 8.13: Duration of the 'gaps' in the yellow series.

**'Gaps' in the yellow series**

The presence of hiatuses meant that the yellow series was modelled using multiple `P_Seuqence` functions. Coincidentally, the hiatus between samples OxA-16267 (at 4.16 m) and OxA-22788 (at 4.12 m) also represent the cultural boundary between two types of backed bladelet industries (Hogue, pers. comm.). By calculating the difference between the posterior of the samples, one could obtain the time for the transition between the two lithic industries. Figure 8.13a suggests that the transition between the two lithic cultures took between 1245 and 2102 years (95.4% probability). However, whether this is a 'true' cultural gap, or a temporally mixed interval is unknown. The hiatus lower down the sequence occurs between samples OxA-16273 (at 4.9 m) and OxA-16271 (at 4.96 m). Figure 8.13b shows that the 'gap' between these two samples has a 95.4% probability of being betweem 2593 and 3786.5 years.

## 8.2.2 Discussion

The Poisson process model has proved useful in a number of research areas where high precision chronology resolution is required. The new model averaging approach, i.e. prior for the step-size parameter, has made a large contribution to enhancing the precision and accuracy of the chronology of Grotte des Pigeons cave at Taforalt. The use of a Bayesian model averaging approach removes the subjectivity in model selection, making it possible to model sequences that are not annually laminated.

The Iberomaurusian lithic evidence suggests that the Grotte des Pigeons cave was

occupied during H1. A modelled age of 15,157–14,756 cal BP (95.4% probability) for the transition between yellow and grey series overlapped with the end of the last phase of H1 (∼16,700–14,600 cal BP). This phase represents the termination of H1 cooling and represented perhaps by continental drying. There could have been a correlation between the end of H1, and the change in cave use at that time, resulting in the abrupt change in sedimentation. However, it is unrealistic to suggest that climate is the sole reason for the abrupt change. There is, at present, no evidence to suggest a change in use of the cave occurred for the period of the grey series, from an intermittent shelter to that of an ancestral cemetery with more sedentary occupation nearby.

The Bayesian framework presented in this section provides a basis for constructing high precision chronologies at such sites. Having high precision chronologies is essential to our understanding of the timing of cultural and / or sedimentary changes in archaeological and environmental sequences. The investigation of further sites in the Maghreb, showing similar grey midden deposits overlaying lighter deposits, may provide cumulative evidence in support of whether such changes took place across a wider area of the Maghreb and whether these could be linked to external forcing factors that brought about an abrupt cultural change. Equally, one may be able to throw further light on the changes that brought about the end of the Middle Palaeolithic and were followed by the reoccupation of this region by people with an epipalaeolithic way of life.

# Chapter 9

# Modelling asynchronous / transitional events within sequences

Bayesian methods are widely used to improve the precision and accuracy of chronologies. There are two main categories of prior models, which are suitable for analysing archaeological and palaeoenvironmental data. They allow us to explicitly include phase and stratigraphical information in chronology construction. As well as enhancing the precision and accuracy of chronological information, phase models allow us to assign and estimate the temporal constraints of a groups of related events; and deposition models can be used to estimate ages between known ages.

In the last chapter, abrupt environmental changes between different regions were discussed, focusing on robustly estimating the age of a tephra in close stratigraphic proximity to a rise in tree pollen in the eastern Mediterranean, and comparing that to the GI-2 event observed in the NGRIP record. Robust chronological information can be used test the leads and lags of regional, as well as continental, environmental change. In this chapter, a case study in the investigation on the timing of the decline of elm tree pollen during the mid-Holocene is presented, where stratigraphic information are used to assess and enhance individual site chronologies, phase priors are utilised

in order to better evaluate this phenomenon across the different sites in the British Isles.

## 9.1 The mid-Holocene elm decline in the British Isles

The decline of elm tree is a very distinctive horizon in Holocene pollen records of north-west Europe. The decline in elm pollen frequencies during that period was sharp (to less than one-third of their former frequencies) and sometimes permanent (Parker et al., 2002). This decline event has received a lot of attention over the past 60 years and extensive scientific study has generated a large number of literature on the timing, mechanisms, origin, and extent (e.g. Garbett, 1981; Delcourt, 1987; Brasier, 1990; Brown, 1997). Some believe that the decline was synchronous across northern and north-west Europe (Smith and Pilcher, 1973; Huntley and Birks, 1983). Others believe that the phenomenon of the decline was asynchronous (Turner et al., 1993). Some sites have more than one episodes of decline. A recent review by Parker et al. (2002) concluded that the decline was asynchronous across the British Isles and took place over centuries. The mid-Holocene elm decline is the most extensively dated horizon in north-west European pollen diagrams (Parker et al., 2002).

### 9.1.1 Dating

Before absolute scientific dating methods were introduced, a zonation system was applied to common features in peat sequences (Sernander, 1908) and pollen diagrams (Godwin, 1940a,b) as a means of relative dating. The decline in elm pollen was used as a boundary (pollen zone VIIa/VIIb in Godwin's system) to separate the Atlantic (warm and moist period) from the Sub-Boreal (cool and dry period) in European pollen records (Parker et al., 2002). This also means that records were sometimes aligned and cross-dated based on their pollen stratigraphy alone (von Post, 1946).

The introduction of radiocarbon dating enabled the validation of the relative pollen stratigraphy from different sites with independent chronologies.

The elm decline phenomenon had been extensively dated since the 1960's using the radiocarbon method on peat samples and absolute chronologies are available for over 100 sites in the British Isles. The limitations of dating peat samples have already been discussed in Section 2.1.5. Some chronologies contain multiple dates and a single date for the decline horizon, and some contain dates spanning the horizon and interpolation is needed to obtain the date of the decline (Baillie, 1991). Parker et al. (2002) constructed an extensive study to investigate the timing (hence synchrony) and mechanism of the elm decline in the British Isles. The authors first used a summed probability distribution of calibrated ages to provide a summary of a group of distributions:

> The combined probability distribution appears uni-modal, indicating a single uniform phase of events, within the errors of the technique. The sum probability for the combined sum spans the calibrated range of 6347–5281 cal BP ($2\sigma$), a period of 1066 years.

Indeed, a summed distribution may provide a summary of a group of distributions, especially when many ($> 100$) dates are available, and that if the uncertainties of the dates are much smaller than the time span of the period (i.e. phase) modelled (Millard, 2009). Although the elm decline phenomenon satisfies these constraints, the resulting summed probability cannot be used to reliably provide quantitative estimates with archaeological meaning (Millard, 2009). Parker et al. (2002) also used Bayesian methods to model radiocarbon dates from the decline horizon with a uniform phase prior. Interpolated ages were not included in their study. Inference was drawn on the start and end dates, duration, and conclusions were made on the possible mechanism of the decline. The rate of the start and end of the phenomenon were also investigated using the 68.2% probability estimates of uniform `boundary` parameters:

> The start of the elm decline event lies between 6343 and 6307 cal BP ($1\sigma$), a period of 36 years, indicating that the onset was rapid. The end of the event lies between 5290 and 5420 cal BP ($1\sigma$), a period of 130 years.

Unfortunately, the `boundary` estimates of the uniform phase prior have been wrongly interpreted by Parker et al. (2002). The 68.2% range suggests that the true date of the event (the start or the end date in this case) has a 68.2% probability of falling within that range. It does not, however, give an indication on the rate of the event. The uncertainties associated with the uniform phase `boundary` estimates are dependent on the uncertainties associated with the radiocarbon determinations, hence the calibrated date ranges, and the number of dates in the phase (e.g. Millard, 2009). Nevertheless, Parker et al. (2002) believe that the start and end of the decline period were not instantaneous across the British Isles and can be quantified with time span for `transitions`. Based on this hypothesis, the British Isles elm decline phenomenon can be more appropriately and accurately modelled with a trapezoidal phase prior (discussed in Chapter 5) and this is implemented in this chapter.

### 9.1.2 Modelling

Before the modelling is discussed, a few definitions need to be clarified. In this chapter, the elm decline is defined as the point where pollen frequency for *Ulmus* was less than one-third of its former frequency (Parker et al., 2002), or where the position (and/or depth) of the decline horizon is stated in the literature. This means that the temporal constraints, applied and modelled using Bayesian methods (`phases`), represent the start and end dates of the decline across a geographical region. The sampling density of pollen has an effect on the age determination of the elm decline (Liu et al., 2012), however, due to the limitations of the data set used in this study, this point is not explored here.

A modelling framework similar to that of Bennett and Fuller (2002) is employed. Bennett and Fuller (2002) constructed age-depth models using classical methods to obtain an interpolated radiocarbon age of the hemlock decline in North America, before using a summed probability distribution of calibrated ages to draw inference on the date of decline. This two stage approach is employed here, where individual sites are modelled to determine the date of the elm decline horizon before the modelling of

the elm decline phenomenon across the British Isles. It is a more practical approach than a single nested model incorporating data from over 100 sites. Bayesian methods are used in this section to draw inference on the dates of the decline period. The calibration and chronology building software `OxCal` (Bronk Ramsey, 2009a) is used. Deposition models are constructed to assess the reliability of the absolute chronologies, and to accurately determine the age of the date of the elm decline for sites with multiple dates spanning the decline. Interpolation (`P_Sequence`) is carried out for sites with a radiocarbon dated chronology but no single age determination for the decline horizon. The trapezoidal phase model parameters are then used to draw inference on the dates of the elm decline in the British Isles, using the posterior ages from the deposition models and calibrated dates as likelihood information in Bayes' theorem (eq. 3.1 in Chapter 3).

The complete data set contains radiocarbon determinations from 125 sites across the British Isles, and is available in appendix B.6. Most of the available radiocarbon determinations were from bulk peat samples, with a minority from plant macrofossils. Some sites provide a single radiocarbon age for the elm decline horizon, some provide multiple radiocarbon ages with a specified age for the decline horizon, and some provide ages spanning the horizon. Some sites are dated more than once. Low resolution sites will contribute little to obtaining a precise estimate, nevertheless, they will help constrain the date of the decline event.

A total of six radiocarbon ages from six sites, and 134 chronologies from 119 sites are available for modelling. Four sites are rejected before modelling: Morden Bog, because of the sediment being rootlet peat (Harkness, 1981); Thrang Moss, because the date has been previously cited as suspect (Parker et al., 2002; Smith and Pilcher, 1973); An Druim, because of possible hard-water errors due to the site being near outcrops of Durness limestone (Harkness, 1981); and Loch Salen, because of possible inwash of organic debris to lacustrine depositional environment (Harkness, 1981). If the radiocarbon chronologies have associated depth information, deposition models are constructed using the Poisson process model (`P_Sequence`; Bronk Ramsey, 2008).

Since peat chronologies do not provide means of estimating an appropriate value for the step-size parameter ($k$), the model averaging approach (discussed in Chapter 6), is used to enhance the precision and accuracy of the age of the elm decline from each site. The sequences are modelled firstly with a prior range for step-size

$$\text{Log}(k) \sim \text{U}(-2, 2)$$

i.e. between 0.01 to 100 events per centimetre. After initial model runs, the prior ranges for the step-size parameter for each model are adjusted accordingly. Individual prior ranges for each model, and their posterior distributions can be found in appendix B.6. In chronologies where depths are not provided, and in chronologies where modelling with the `P_Sequence` model causes non convergence, deposition models are constructed based on the ordering of the samples alone (`Sequence`; Bronk Ramsey, 1995). For one site, North Gill 5B, only part of the sequence has associated depths with the radiocarbon determinations, so both `Sequence` and `P_Sequence` functions were used to model the chronology. Individual modelled chronologies for each site can be found in appendix B.6.

Formal outlier analysis was employed to account for outliers in the calendar scale (`type t`) when constructing deposition models and phase models. The `CQL` for the outlier function used is:

```
Outlier_Model("General",T(5),U(0,4),"t");
```

The outlier model is specified to allow the possible shifts in the specified scale to be drawn from a long tailed student $t$ distribution. the outliers can be in the scale of anywhere between $10^0$ and $10^4$ years. this is the model recommended by Bronk Ramsey (2009b) for general purposes when the scale of the possible offsets is unknown. When employed, the overall model is not affected by the odd extreme outlier. Each measurement is assigned a prior probability of 5% of being an outlier. Individual outlying dates in deposition models, together with their posterior probability of being an outlier, are highlighted in appendix B.6.

One chronology, North Gill 1A, from England was rejected because four of the six dates, which make up the chronology, are found to yield ≥99% probability of being outlying, suggesting that the whole chronology is unreliable. Two posterior ages for the elm decline horizon from the North Gill sites, 6 and 8, appear to be younger than the rest of the ages of the elm decline horizon in the data set. They are, however, included in the phase model because the chronologies of the sites, although only containing three radiocarbon determinations each, do not suggest that any of the determinations in the model were outlying. In some cases, the depositions models are able to enhance the precision of the posterior ages of the elm decline horizon, some examples include Abbotsway, North Gill 5B, Ballyscullion, and Fallahogy. Unfortunately, this does not apply to the majority of the site because the chronologies were often sparsely dated around the elm decline horizon. A total of 135 posterior and calibrated ages for the elm decline are incorporated into a trapezoidal phase model.

The trapezoidal phase model parameters are used to draw inference on dates of the elm decline based on the hypothesis that the decline was asynchronous across the British Isles (Turner et al., 1993; Parker et al., 2002), and also because the trapezoidal phase prior takes into account the geographical spread of the data. The trapezoid phase prior model parameters represent: the date of the start of the decline ($t_\alpha$); the date when the number of sites showing decline in elm pollen peaked ($t_\beta$); the date when the number of sites showing decline in elm pollen began to drop ($t_\gamma$); and the date of the end of the decline ($t_\delta$). Two models are implemented: a single trapezoid phase prior is used to model the ages from all the sites across the British Isles; and four overlapping trapezoid phases are used to model the decline in England, Ireland, Scotland, and Wales. Although not implemented here, it would also be interesting to divide the phases according to upland/lowland. The differences (e.g. delay) between different regions are also investigated. Formal outlier analysis was utilised in phase modelling to account for possible outlying dates of the elm decline horizon (in the calendar scale), which themselves might not be outlying within their individual site chronologies, for example North Gill sites 6 and 8, as mentioned above. The same

CQL as the one employed for the deposition models is used here.

#### 9.1.2.1 Model A: *Single phase*

Model A includes a single trapezoid phase modelling elm decline across the British Isles. 3 of the 135 posterior ages for elm decline (including North Gill sites 6 and 8) were found to yield 100% (and no further date $\geq 90\%$) probability of being outlying, whilst 122 of the 135 dates were given a posterior probability of $\leq 5\%$ of being outliers (as compared to the arbitrary 5% prior probability applied). This supports the validity of the individual radiocarbon determinations themselves (Staff et al., 2010). Results of this model are summarised in Figure 9.1 and table 9.1. The `transition` parameters (Fig. 9.1d) suggest that there was a clear time difference between $t_\alpha$ and $t_\beta$, and between $t_\gamma$ and $t_\delta$, with the modes of the distributions deviating from zero. This supports the hypothesis that the elm decline period can be more appropriately modelled with a trapezoid phase prior. The elm decline across the British Isles is estimated to have covered a period of between 1020.5 and 1465 years at 95.4% range (Fig. 9.1b).

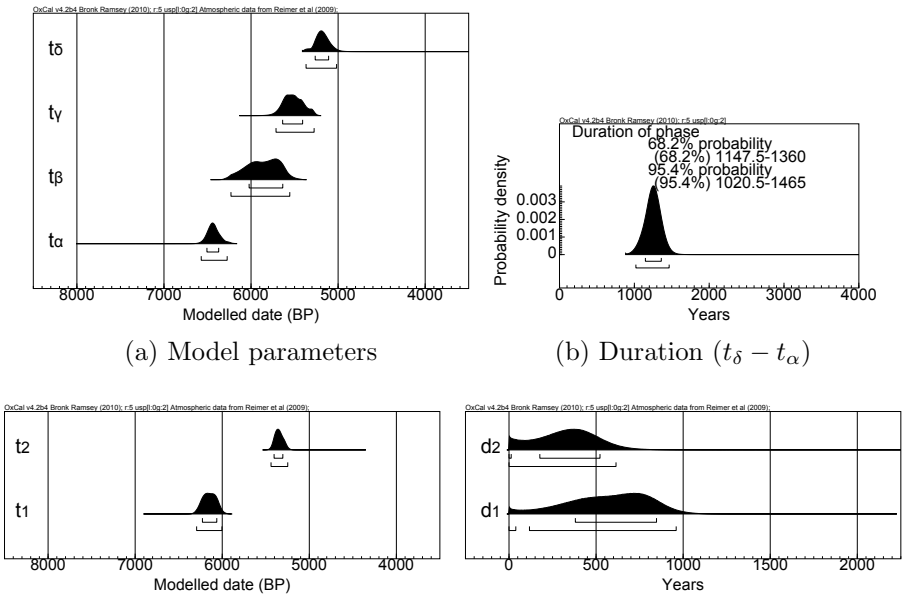


(a) Model parameters (b) Duration ($t_\delta - t_\alpha$)

(c) `Boundary` parameters (d) `Transition` parameters

Figure 9.1: Trapezoidal prior estimates of elm decline across the British Isles, at 68.2% and 95.4% probability.

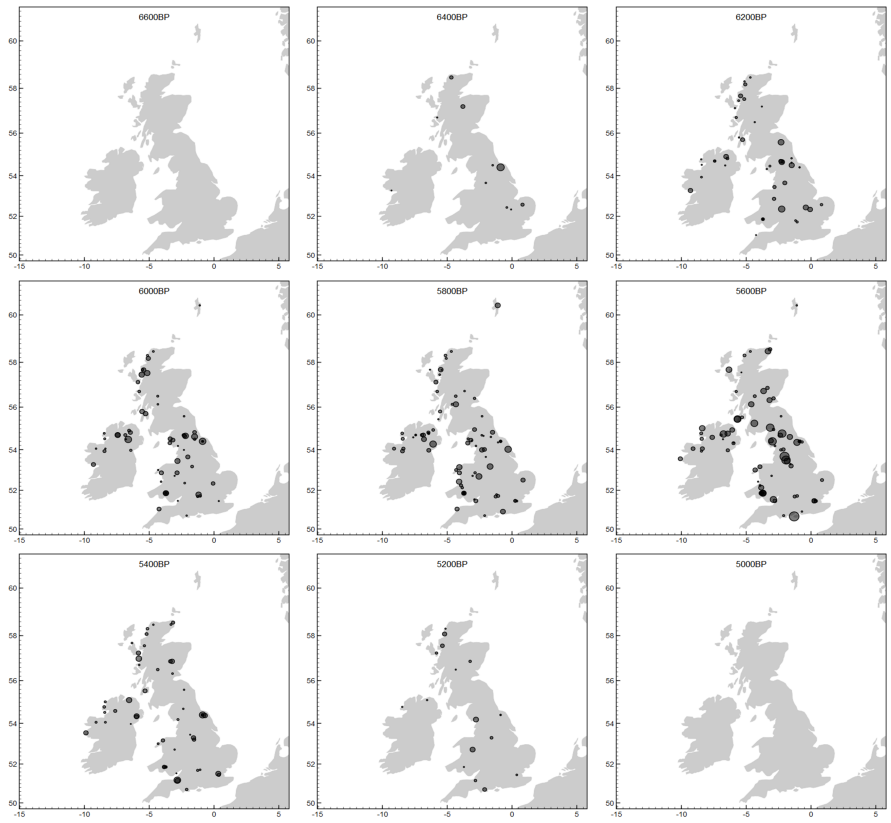


Figure 9.2: Maps of elm decline across the British Isles at different dates, modelled using a single trapezoidal phase.

| | Modelled date (cal BP) | | | Modelled date (cal BP) | | | Years | |
|---|---|---|---|---|---|---|---|---|
| | 68.2% | 95.4% | | 68.2% | 95.4% | | 68.2% | 95.4% |
| $t_\alpha$ | 6507–6372 | 6572–6274 | $t_1$ | 6228–6066 | 6292–6003 | $d_1$ | 381–847 | 0–960 |
| $t_\beta$ | 6022–5636 | 6231–5555 | | | | | | |
| $t_\gamma$ | 5637–5408 | 5713–5276 | $t_2$ | 5405–5304 | 5440–5248 | $d_2$ | 0–523 | 0–615 |
| $t_\delta$ | 5263–5109 | 5368–5018 | | | | | | |

Table 9.1: Trapezoidal estimates of elm decline across the British Isles, at 68.2% and 95.4% probability.

Figure 9.2 shows the spread of elm decline between 6600 and 5000 BP every 200 years, where the size of the circles represent the posterior probability at the year stated. Decline of elm trees was first recorded in England and Scotland, before Ireland and Wales. The end of the decline, constrained by a single trapezoidal phase prior, appears to have finished at about the same time in all four regions.

#### 9.1.2.2 Model B: *Four independent phases*

Model B includes four independent overlapping trapezoid phases: England; Ireland; Scotland; and Wales. This model assumes no ordering relationship between the four phases. The dates for the elm decline from the four regions are as follows:

### England

2 of the 55 posterior ages for elm decline from the deposition models from the English sites (North Gill 6 and 8) were found to yield 100% (and no further dates $\geq$ 90%), whilst 50 of the 55 dates were given a posterior probability of $\leq$5% of being outliers. The results for England are summarised in Figure 9.3 and table 9.2. The elm decline across England is estimated to have covered a period of between 926.5 and 1510 years at 95.4% range (Fig. 9.3b).

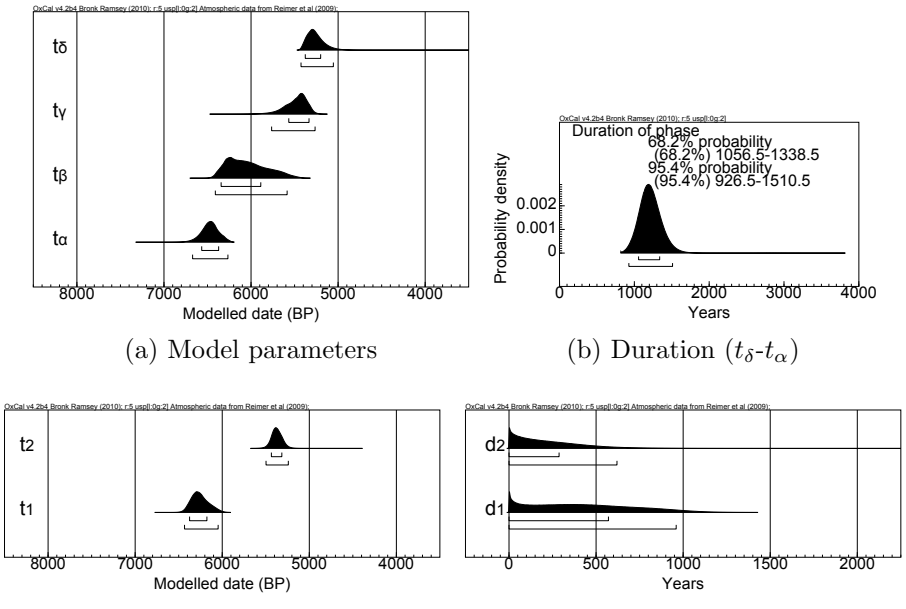


(a) Model parameters

(b) Duration ($t_\delta$-$t_\alpha$)

(c) `Boundary` parameters

(d) `Transition` parameters

Figure 9.3: Trapezoidal prior estimates of elm decine across England, at 68.2% and 95.4% probability.

| | Modelled date (cal BP) | | | Modelled date (cal BP) | | | Years | |
|---|---|---|---|---|---|---|---|---|
| | 68.2% | 95.4% | | 68.2% | 95.4% | | 68.2% | 95.4% |
| $t_\alpha$ | 6567–6372 | 6671–6266 | $t_1$ | 6375–6176 | 6433–6047 | $d_1$ | 0–571 | 0–960 |
| $t_\beta$ | 6344–5888 | 6410–5586 | | | | | | |
| $t_\gamma$ | 5567–5334 | 5764–5265 | $t_2$ | 5436–5316 | 5497–5241 | $d_2$ | 0–288 | 0–620 |
| $t_\delta$ | 5377–5201 | 5426–5055 | | | | | | |

Table 9.2: Trapezoidal prior estimates of elm decline across England, at 68.2% and 95.4% probability.

### Ireland

None of the 27 posterior ages for elm decline from the deposition models from the Irish sites were found to yield $\geq 95\%$ (and no further dates $\geq 90\%$), whilst 26 of the 27 dates were given a posterior probability of $\leq 5\%$ of being outliers. The results for Ireland are summarised in Figure 9.4 and table 9.3. The elm decline across Ireland is estimated to have covered a period of between 665 and 1475 years at 95.4% range (Fig. 9.4b).

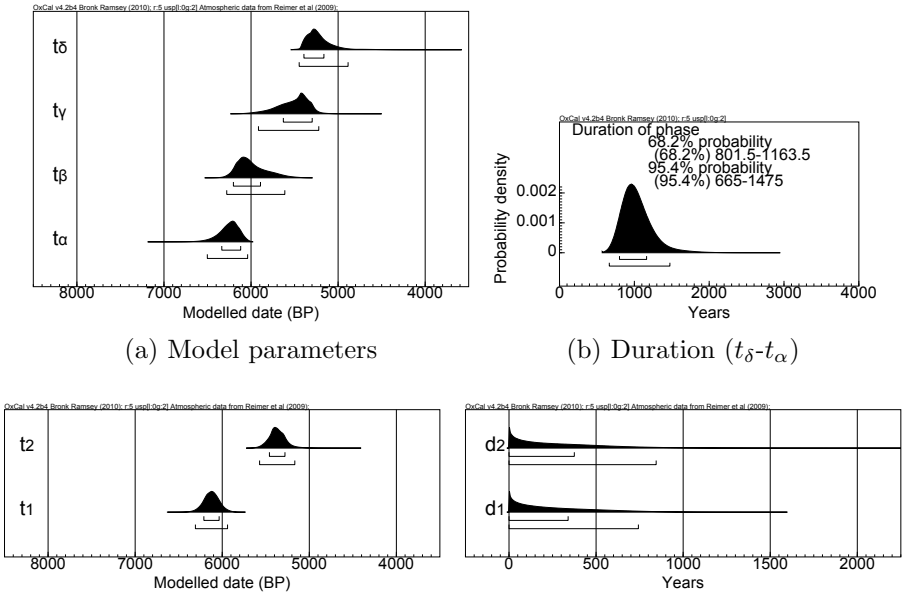


(a) Model parameters (b) Duration ($t_\delta$-$t_\alpha$)

(c) `Boundary` parameters (d) `Transition` parameters

Figure 9.4: Trapezoidal estimates of elm decine across Ireland, at 68.2% and 95.4% probability.

| | Modelled date (cal BP) | | | Modelled date (cal BP) | | | Years | |
|---|---|---|---|---|---|---|---|---|
| | 68.2% | 95.4% | | 68.2% | 95.4% | | 68.2% | 95.4% |
| $t_\alpha$ | 6336–6119 | 6502–6039 | $t_1$ | 6211–6036 | 6308–5939 | $d_1$ | 0–340 | 0–743 |
| $t_\beta$ | 6203–5892 | 6279–5612 | | | | | | |
| $t_\gamma$ | 5629–5298 | 5915–5222 | $t_2$ | 5459–5279 | 5570–5164 | $d_2$ | 0–375 | 0–845 |
| $t_\delta$ | 5393–5163 | 5447–4886 | | | | | | |

Table 9.3: Trapezoidal prior estimates of elm decline across Ireland, at 68.2% and 95.4% probability.

### Scotland

None of the 33 posterior ages for elm decline from the deposition models from the Scottish sites were found to yield $\geq 95\%$ (and no further dates $\geq 90\%$), whilst 30 of the 33 dates were given a posterior probability of $\leq 5\%$ of being outliers. The results for Scotland are summarised in Figure 9.5 and table 9.4. The elm decline across Scotland is estimated to have covered a period of between 1059.5 and 2306 years at 95.4% range (Fig. 9.5b).

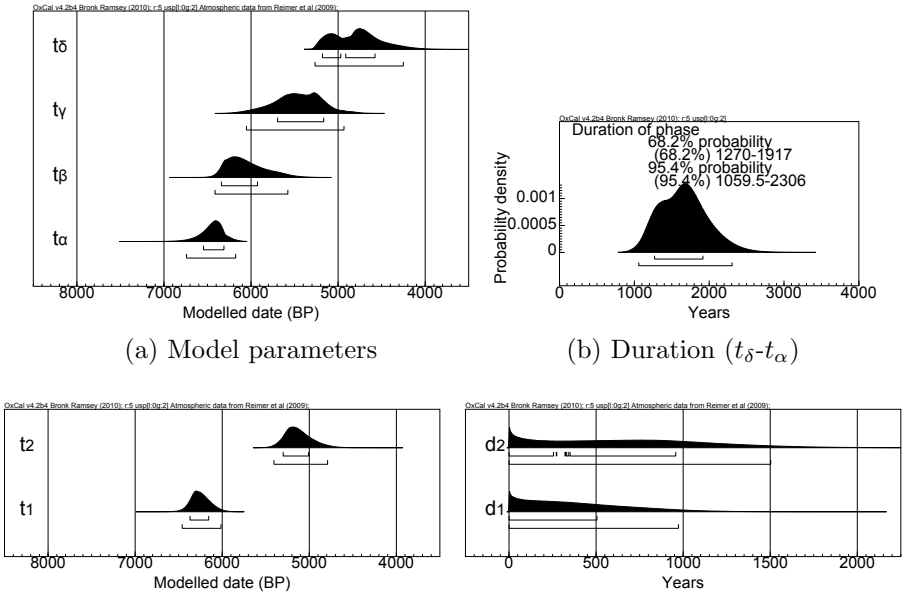


(a) Model parameters (b) Duration ($t_\delta$-$t_\alpha$)

(c) `Boundary` parameters (d) `Transition` parameters

Figure 9.5: Trapezoidal prior estimates of elm decine across Scotland, at 68.2% and 95.4% probability.

| | Modelled date (cal BP) | | | Modelled date (cal BP) | | | Years | |
|---|---|---|---|---|---|---|---|---|
| | 68.2% | 95.4% | | 68.2% | 95.4% | | 68.2% | 95.4% |
| $t_\alpha$ | 6547–6311 | 6741–6176 | $t_1$ | 6370–6155 | 6460–6015 | $d_1$ | 0–505 | 0–973 |
| $t_\beta$ | 6340–5926 | 6414–5577 | | | | | | |
| $t_\gamma$ | 5696–5165 | 6053–4933 | $t_2$ | 5300–5009 | 5406–4790 | $d_2$ | 0–958 | 0–1503 |
| $t_\delta$ | 5180–4576 | 5265–4251 | | | | | | |

Table 9.4: Trapezoidal prior estimates of elm decline across Scotland, at 68.2% and 95.4% probability.

### Wales

None of the 20 posterior ages for elm decline from the deposition models from the Welsh sites were found to yield $\geq 95\%$ (and no further dates $\geq 90\%$), whilst 18 of

the 20 dates were given a posterior probability of ≤5% of being outliers. The results for Wales are summarised in Figure 9.6 and table 9.5. The elm decline across Wales is estimated to have covered a period of between 488 and 1431 years at 95.4% range (Fig. 9.5b).

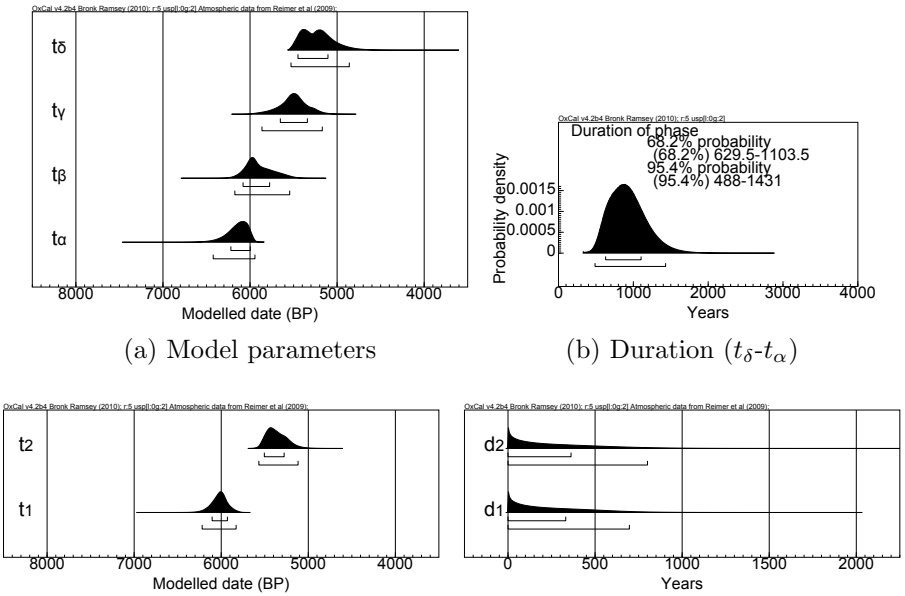


(a) Model parameters (b) Duration ($t_\delta$-$t_\alpha$)

(c) `Boundary` parameters (d) `Transition` parameters

Figure 9.6: Trapezoidal prior estimates of elm decine across Wales, at 68.2% and 95.4% probability.

| | Modelled date (cal BP) | | | Modelled date (cal BP) | | | Years | |
|---|---|---|---|---|---|---|---|---|
| | 68.2% | 95.4% | | 68.2% | 95.4% | | 68.2% | 95.4% |
| $t_\alpha$ | 6220–5998 | 6423–5944 | $t_1$ | 6105–5929 | 6219–5819 | $d_1$ | 0–331 | 0–697 |
| $t_\beta$ | 6080–5775 | 6175–5545 | | | | | | |
| $t_\gamma$ | 5652–5342 | 5863–5170 | $t_2$ | 5505–5278 | 5568–5118 | $d_2$ | 0–362 | 0–801 |
| $t_\delta$ | 5450–5105 | 5530–4860 | | | | | | |

Table 9.5: Trapezoidal prior estimates of elm decline across Wales, at 68.2% and 95.4% probability.

Order matrices are used to investigate the order of the start and end dates of elm decline between the different regions. For each iteration, the relative order of the start parameters ($t_\alpha$), and the relative order of the end parameters ($t_\delta$) between the different regions are determined. This is a similar approach used by Blackwell and Buck (2003) and Buck and Bard (2007) on investigating human reoccupation of north-west Europe and megafauna extinction, respectively. The order matrix is employed using the following `CQL` in `OxCal`:

```
Order(){
     Date("=Start England");
     Date("=Start Ireland");
     Date("=Start Scotland");
     Date("=Start Wales");
};
```

to determine the relative order for the start parameters; and

```
Order(){
     Date("=End England");
     Date("=End Ireland");
     Date("=End Scotland");
     Date("=End Wales");
};
```

to determine the relative order for the end parameters, where the trapezoidal parameters for the `"Start"` ($t_\alpha$) and the `"End"` ($t_\delta$) of the elm decline from each of the overlapping phases are `cross-referenced` to the `Order()` command. Results of the order matrices are summarised in table 9.6.

| | | $t_2$ | | | |
|---|---|---|---|---|---|
| | | [E] | [I] | [S] | [W] |
| $t_1$ | [E] | 0 | 0.93 | 0.15 | 0.98 |
| | [I] | 0.07 | 0 | 0.03 | 0.79 |
| | [S] | 0.85 | 0.97 | 0 | 0.99 |
| | [W] | 0.02 | 0.21 | 0.01 | 0 |

(a) Start ($t_\alpha$) of elm decline

| | | $t_2$ | | | |
|---|---|---|---|---|---|
| | | [E] | [I] | [S] | [W] |
| $t_1$ | [E] | 0 | 0.31 | 0.87 | 0.18 |
| | [I] | 0.69 | 0 | 0.94 | 0.28 |
| | [S] | 0.13 | 0.06 | 0 | 0.04 |
| | [W] | 0.82 | 0.72 | 0.96 | 0 |

(b) End ($t_\delta$) of elm decline

Table 9.6: Order matrices summarising the relative order of (a) the start ($t_\alpha$), and (b) the end ($t_\delta$) of elm decline between different regions. The probabilities of $t_1 < t_2$ after over 10 millions model runs are shown.

Results from the order matrices suggest that elm decline in England and Scotland started earlier than elm decline in Ireland and Wales; and elm decline in Scotland ended later than in other regions (in $> 85\%$ of the model runs).

Figure 9.7 shows the spread of elm decline between 6600 BP and 4400 BP every 200 years, where the size of the circles represent the posterior probability at the

year stated; circles in blue represent ages from England, yellow represent Ireland, red represent Scotland, and green represent Wales. Similar to Figure 9.2, decline of elm trees was first recorded in England and Scotland, before Ireland and Wales. The decline was last recorded in Scotland. Figure 9.8 shows the same results in 20 year intervals between 6380 BP and 6220 BP every 20 years. This figure was generated to give a clearer, higher resolution, visual representation of the direction of the spread of the elm decline. It indicates that the decline started in the east before moving west across the British Isles.

Figures 9.2, 9.7, and 9.8 are produced using the new `plot on map` function in `OxCal v4.2beta`.

### 9.1.3 Discussion

The mid-Holocene elm decline phenomenon is the most extensively dated horizon in Northwest European pollen diagrams. This chapter presents a Bayesian modelling framework which is not only applicable to this case study, but also applicable for the evaluation of asynchronous events in environmental records. Deposition models were initially employed to assess the reliability of the absolute chronologies, and to accurately determine the age of the date of the elm decline horizon for different sites. The `P_Sequence` model was applied to chronologies where depth information is available, and a simple `Sequence` model was applied to chronologies where only the ordering of the samples is available. Although age-depth modelling in this case study was not able to improve the precision on the majority of the dates of the decline horizon, nonetheless, it was a means to validate the reliability of the dates within the sparsely dated chronologies. The posterior ages for the decline horizon were incorporated into a trapezoid phase model as *likelihood* information to draw inference on the start and end of the elm decline.

Mathematical details of the different models utilised in this case study, together with their recent modifications, had already been discussed in chapters 5 and 6. The prior for the step-size parameter in the `P_Sequence` model removes the subjectivity in

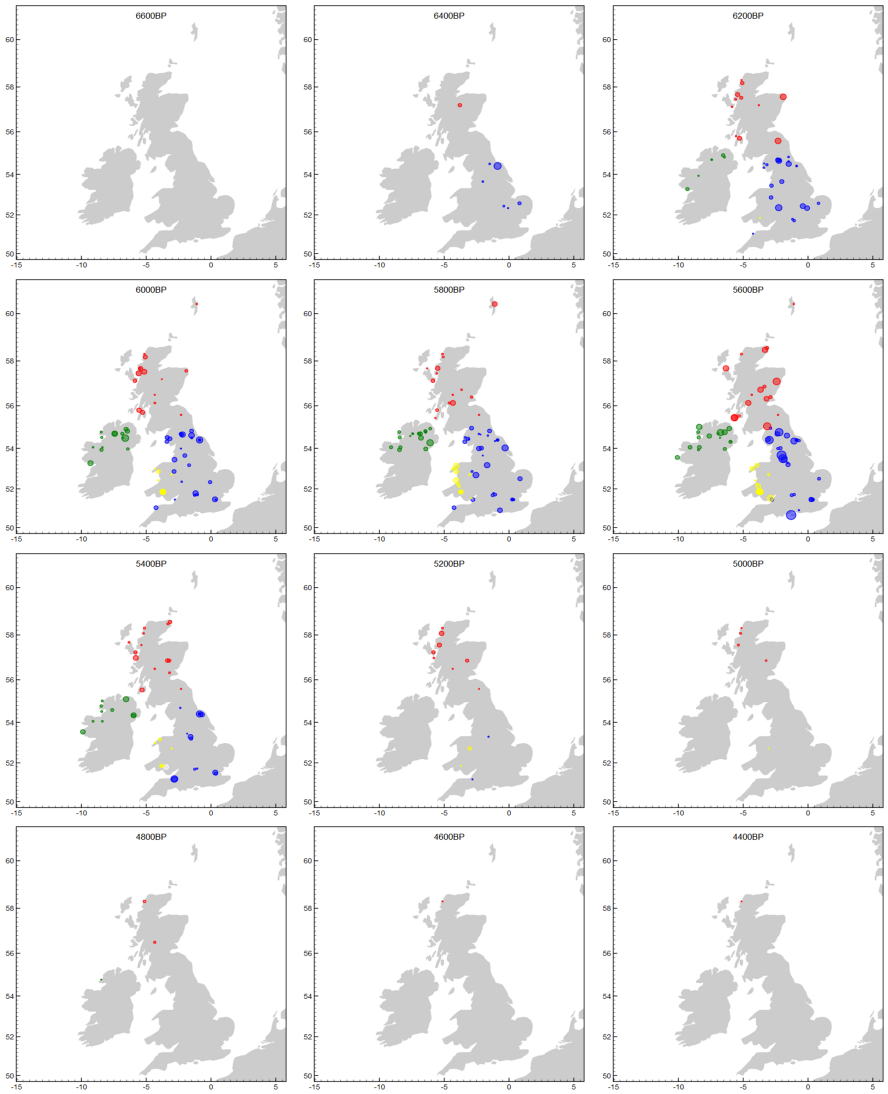


Figure 9.7: Maps showing the progression of elm decline across the British Isles every 200 years, modelled using four overlapping trapezoid phases. The colours represent the different regions: blue = England; green=Ireland; red = Scotland; and yellow = Wales.

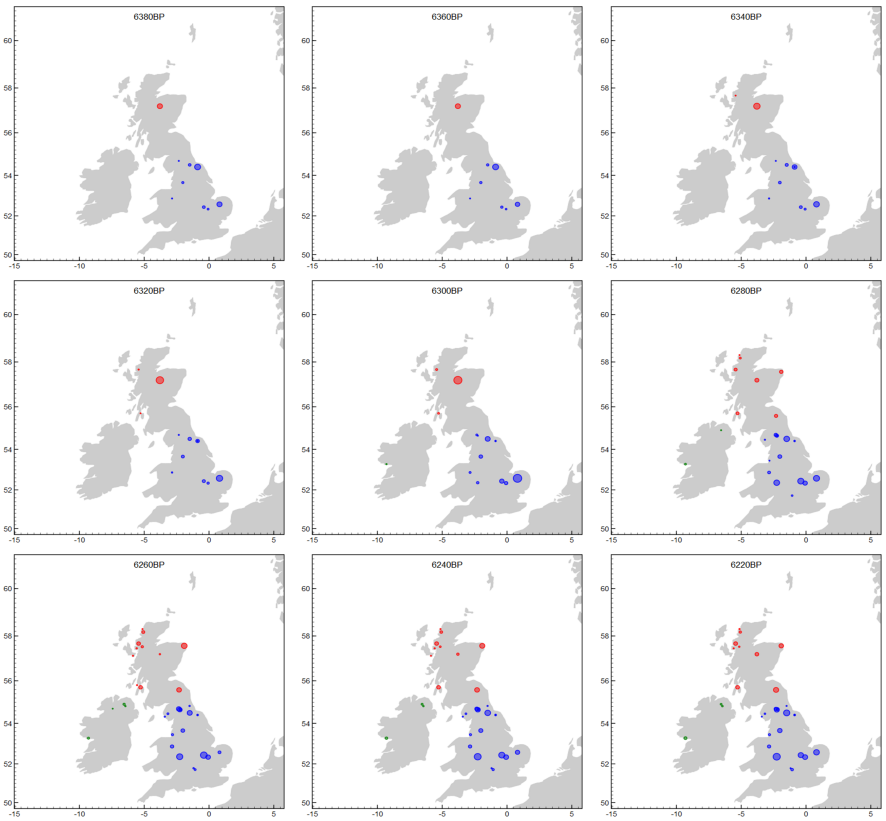


Figure 9.8: Maps of elm decline across the British Isles every 20 years, modelled using four overlapping trapezoid phases. The colours represent the different regions: blue = England; green=Ireland; red = Scotland; and yellow = Wales.

model selection and makes it more accessible to chronologies which are not annually laminated, in this case, peat deposits. The trapezoid phase prior is also a more appropriate model and this is supported by the marginal distributions of the `transition` parameters of the single phase model for across the British Isles, with their modes deviating from zero. The `transition` parameters will also reflect on how rapidly the phenomenon affected the different regions.

The findings presented in this chapter show that elm decline in England and Scotland started before elm decline in Ireland and Wales, and elm decline in Scotland ended later than all of the other regions. This contradicts Parker et al. (2002), who concluded that there is no significant difference in the timing of the elm decline between the four countries. The authors reached that conclusion based on calibrated dates alone, without any additional modelling of the regional data. Additional phase modelling allows inference to be drawn on unknown dates of temporal constraints, i.e. the start and end of regional elm decline, instead of drawing conclusions based on calibrated dates of known events, which are the dates of the depth of the samples. Modelling also took into account of possible outlying dates in the data set.

In terms of the mechanism for elm decline, several hypothesis had been put foward for Europe and they include: climate change (Fægri, 1944; Nilsson, 1948); human activity (Troels-Smith, 1960; Garbett, 1981; Delcourt, 1987); disease (Girling and Greig, 1985; Brasier, 1990); and soil change (Smith, 1961; Sturludottir and Turner, 1985). A recent publication by Parker et al. (2002) concluded the phenomenon was a result of the complex interrelationship between these factors, with emphasis on the disease process. Pathogenic attacks on elm trees involve elm bark beetles, in the genus *Scolytus*, as vectors for the fungus which causes the disease. Presence of *Scolytus* beetles were found at the Hampstead Heath site in England, at 15 cm below the elm decline horizon (Girling and Greig, 1985); and at two sites, Red Moss and St Fergus Moss, in Scotland (Clark and Edwards, 2004). At Red Moss, the earliest layer in which the beetles were found was 120 cm below the elm decline horizon and disappeared after the elm decline horizon. At St Fergus Moss, the beetles were found

at the decline horizon. These findings neither prove nor disproves the role of the elm bark beetle in the disease mechanism for the elm decline, but do suggest that elm trees and *Scolytus* beetles co-existed for a period as long as 3000 years, with the beetles disappearing before or at the time of the elm decline at all three sites. Plotted posterior ages on maps show that the decline was first recorded in England and Scotland, followed by Ireland and Wales. This suggests that if disease was the primary decline mechanism caused by contamination, it originated from England and Scotland, within the British Isles. However, the resolution of the radiocarbon determination is low, and the majority of determinations were from peat samples, which are themselves problematic to date. In the future, short-lived samples could be used to more accurately date individual site chronologies (Parker et al., 2002), followed by utilising the Bayesian framework presented in this chapter to enhance the precision of the date of the decline horizon. Inference can also be drawn on how long the phenomenon took to populate each phase / region using the `transition` parameter of the trapezoid phase prior. More detailed spatial-temporal analysis can also be performed using details on the geographic coordinates, i.e. longitude, latitude, and altitude, of individual sites, instead of grouping them into generic regions.

# Part IV

# Conclusion

# Chapter 10

# Summary and recommendations

It is important that the methods used in chronology building are robust and reflect substantial prior knowledge. The overall objective of this thesis was to test, further develop, and evaluate recent novel (robust) Bayesian techniques used in chronology construction. This work focuses on two recently developed models: the trapezoidal phase model (Karlsberg, 2006; Lee and Bronk Ramsey, 2012); and the Poisson process deposition model (Bronk Ramsey, 2008), for the construction of archaeological and palaeoenvironmental chronologies. The application of the two modified methods to different case studies and the results of which were already discussed in Chapters 7–9. This chapter focuses on the results of the evaluation of the two models.

## 10.1 Trapezoidal model

The trapezoidal phase model was originally designed to better reflect the prior knowledge in non-abrupt processes. It is separated into three parts: first a gradual increase (introductory period); then a period of constant rate of activity (blooming period); and finally a gradual decrease (period of decline). It is a more flexible model than the commonly used uniform phase model for the construction of robust chronologies. Upon investigation, it was found that a simple trapezoidal phase model described in Karlsberg (2006) has a bias towards the extreme prior shapes (Chapter 5). The addi-

tion of a non-informative, *uniform transitions/tops prior* (*utp*) element was proposed to overcome said bias, giving equal weight to a range of prior shapes. With the *utp* element, the trapezoidal phase prior better reflects prior beliefs.

It was also apparent that the assumptions of the parameters of the trapezoidal and uniform phase models are different. Hence, an alternative parameterisation was also proposed in Chapter 5. Karlsberg's trapezoid has four parameters: $t_\alpha$; $t_\beta$; $t_\gamma$, and $t_\delta$, which make up the four corners of the trapezoid on the calendar scale. The new parameters proposed in this thesis also has four parameters: two `boundary` parameters, which are comparable to the `boundary` parameters in the uniform model; and two corresponding `transition` parameters. The `boundary` parameters, together with their `transition` parameters make up Karlsberg's parameters. The overall mathematics remain the same. Re-parameterisation means that the use of the trapezoidal phase model can be extended to a contiguous phase scenario, where the rise of a later phase overlaps exactly with the decline of an earlier phase, sharing the same transitional `boundary` parameter. Karlsberg's parameters are nevertheless more appropriate for drawing inference on the start and end of a trapezoidal phase and thus were also used in Chapters 7 and 9.

The modified trapezoidal phase model provided an alternative, and better, approach to modelling non-abrupt, transitional processes. It has made significant contributions to our understanding of the time of transitions between adjacent phases in the Iron age chronology in Israel, and of how rapid the rise and the decline of a historical phase were (Chapters 7 and 9). The *utp* element is an essential component of a multiple phase contiguous model to ensure model flexibility for estimating the transitional period between two adjacent phases (Section 7.3).

## 10.2 Poisson process deposition model

The Poisson process deposition model considers the deposition process as being random. It is the first one of its kind to more realistically model the deposition process

without the use of a prior for sediment accumulation rate. It is a more robust deposition model than those published before it. It relies on a given parameter for step-size ($k$), which gives the number of accumulation events per unit depth. Bronk Ramsey (2008) provided a way of estimating an appropriate $k$ value from direct measurements from sequences with three or more known age points from primarily sequences which are annually laminated. Should that be unavailable, users of the model would have to resort to estimating $k$ from the dating information itself (for example, in Blockley et al., 2007, 2008b) or use an arbitrary value that gives the highest model agreement (for example, in Finsinger et al., 2011); neither methods are satisfactory since there are dangers of circular reasoning (Bronk Ramsey, 2008).

Bronk Ramsey et al. (2010a) suggested the use of a model averaging approach to allow the model to find the values of $k$ that are most consistent with the data. This involved a small addition of a prior into the Poisson process model. A prior distribution for $k$ is defined instead of a single value, allowing the model to choose the parameter from across a range. This also means that the $k$ parameter for step-size is now modelled and a posterior distribution is generated. This was implemented in `OxCal` by Bronk Ramsey. The model was evaluated and suitable prior distributions for deposition models in different depth units were suggested in Chapter 6.

This addition has widened the application of the Poisson process model to include peat and cave sequences (Chapters 8 and 9; also in Appendix B.6), which are not annually laminated and sometimes do not contain known age markers, such as tephra horizons. It also makes the model more robust by allowing for different $k$ values within each model run. It is a more realistic model because the step-size (related to the grain size of the sediment) cannot be assumed to be constant throughout the sequence.

## 10.3 Robust chronology construction

A reliable chronological model is essential in contributing to our understanding of time in archaeological and historical records. This thesis has assessed the limitations, proposed mathematical solutions, and evaluated two novel robust prior models (Chapters 5 and 6). The proposed changes have also widened the applications of the models to different scenarios.

It should be stressed that using robust prior models alone is not enough to ensure a reliable chronology. Other statistical measures discussed in Chapter 4 and all of the steps in Figure 4.1 (page 40) carry equal weight in chronology building. It is very important to make sure that the statistical models used are appropriate and reflect substantial prior knowledge, since they can greatly affect the posterior output; however, other steps in chronology building are also important and are discussed in detail in Chapters 7–9.

## 10.4 Future work

Future work for individual case studies were suggested in their corresponding chapters (7–9). In terms of statistical input, this thesis, and also the work of Nicholls and Jones (2001) have emphasised the importance of thorough evaluation of prior information incorporated into a model.

At present, when the *utp* element is utilised in the trapezoidal phase model, a bias still exists for each of the sub-phases within the model, with each of the white and grey segments in figure 5.2 (page 61) as an individual sub-phase. This is clearly illustrated in the simulations shown in figures 5.7b and 5.8b (page 67). This is because the model, in a contiguous multiple phase scenario, is considered as a whole. However, there might be situations where the removal of that bias be useful, making the individual sub-phases uniformly distributed within constraints, whilst keeping the onset and the decline of adjacent phases overlapped. An additional prior element would be needed to overcome the bias in equation 5.11 (page 5.11). It would also be interesting to

see how this addition would affect the posterior outputs, and whether the resulting marginal distributions for the `transition` parameters would better reflect the time taken for transition between adjacent phases.

One of the areas of research that was not addressed, but is important, is the choice of phase models, especially between the use of the trapezoidal and the sigmoidal models. This might be a situation where the Bayes factor would be useful in comparing two competing prior models. Details of the Bayes factor were discussed in chapter 4.

The different Bayesian frameworks presented in this thesis can be adapted to address different archaeological and palaeoenvironmental questions, and it is hoped that this thesis will stimulate much further work in these fields.

# Bibliography

Aksu, A. E., Jenner, G., Hiscott, R. N. and Isler, E. B. (2008). Occurrence, stratigraphy and geochemistry of Late Quaternary tephra layers in the Aegean Sea and the Marmara Sea, *Marine Geology* **252**(3-4): 174–192.

Albright, W. (1956). *The archaeology of Palestine*, Vol. 199, Taylor & Francis.

Andersen, K. K., Svensson, A., Johnsen, S. J., Rasmussen, S. O., Bigler, M., Röthlisberger, R., Ruth, U., Siggaard-Andersen, M.-L., Steffensen, J. P., Dahl-Jensen, D., Vinther, B. M. and Causen, H. B. (2006). The Greenland ice core chronology 2005, 15-42 ka. Part 1: constructing the time scale, *Quaternary Science Reviews* **25**(23-24): 3246–3257.

Anderson, D. E. (1996). *Abrupt Holocene climatic change recorded in terrestrial peat sequences from Wester Ross, Scotland*, PhD thesis, University of Oxford.

Arnold, J. R. and Libby, W. F. (1949). Age determinations by radiocarbon content: Checks with samples of known age, *Science* **110**(2869): 678–680.

Atherden, M. A. (1976a). Late Quaternary vegetational history of the North York Moors. III. Fen bogs, *Journal of Biogeography* **3**(2): 115–124.

Atherden, M. A. (1976b). The impact of late prehistoric cultures on the vegetation of the North York Moors, *Transactions of the Institute of British Geographers* **1**(3): 284–300.

Baillie, M. (1991). Suck-in and smear: two related chronological problems for the 90s, *Journal of theoretical archaeology* **2**: 12–16.

Balter, M. (2000). The Two Tels: Armageddon For Biblical Archaeology?, *Science* **287**(5450): 31.

Barberi, F., Innocenti, F., Lirer, L., Munno, R., Pescatore, T. S. and Santacroce, R. (1978). The Campanian Ignimbrite: a major prehistoric eruption in the Neapolitan area (Italy), *Bulletin of Volcanology* **41**(1): 10–31.

Barnard, G. A. (1963). New methods of quality control, *Journal of the Royal Statistical Society. Series A (General)* **126**(2): 255–258.

Bartley, D. D. and Chambers, C. (1992). A pollen diagram, radiocarbon ages and evidence of agriculture on Extwistle Moor, Lancashire, *New phytologist* **121**(2): 311–320.

Bartley, D. D., Chambers, C. and Hart-Jones, B. (1976). The vegetational history of parts of south and east Durham, *New Phytologist* **77**(2): 437–468.

Bartley, D. D., Jones, I. P. and Smith, R. T. (1990). Studies in the Flandrian Vegetational History of the Craven District of Yorkshire: The Lowlands, *The Journal of Ecology* **78**(3): 611–632.

Barton, R. N. E., Bouzouggar, A., Bronk Ramsey, C., Collcutt, S. N., Higham, T. F. G., Humphrey, L. T., Parfitt, S. A., Rhodes, E. J., Schwenninger, J.-L., Stringer, C., Turner, E. and Ward, S. (2007). Abrupt climate change and chronology of the Upper Palaeolithic in northern and eastern Morocco, *Rethinking the human revolution: New behavioural & biological perspectives on the origins and dispersal of modern humans*, Research Monographs of the Macdonald Institute, Cambridge, pp. 177–186.

Bayes, M. and Price, M. (1763). An Essay towards solving a Problem in the Doctrine of Chances. By the late Rev. Mr. Bayes, FRS communicated by Mr. Price, in a letter to John Canton, AMFRS, *Philosophical Transactions* **53**: 370–418.

Bayliss, A. (2009). Rolling out revolution: using radiocarbon dating in archaeology, *Radiocarbon* **51**(1): 123–147.

Bayliss, A., Bronk Ramsey, C., van der Plicht, J. and Whittle, A. (2007). Bradshaw and Bayes: towards a timetable for the Neolithic, *Cambridge Archaeological Journal* **17**(1): 1–28.

Bayliss, A. and O'Sullivan, M. (forthcoming). Interpreting chronologies for the Mound of the Hostages, Tara and its contemporary Irish contexts.

Beales, P. W. (1980). The late Devensian and Flandrian vegetational history of Crose Mere, Shropshire, *New Phytologist* **85**(1): 133–161.

Beckett, S. C. (1981). Pollen diagrams from Holderness, north Humberside, *Journal of Biogeography* **8**(3): 177–198.

Beckett, S. C. and Hibbert, F. A. (1979). Vegetational change and the influence of prehistoric man in the Somerset Levels, *New Phytologist* **83**(2): 577–600.

Bennett, K. D. (1988). Holocene pollen stratigraphy of central East Anglia, England, and comparison of pollen zones across the British Isles, *New phytologist* **109**(2): 237–253.

Bennett, K. D. (1994). Confidence intervals for age estimates and deposition times in late-Quaternary sediment sequences, *The Holocene* **4**(4): 337.

Bennett, K. D., Boreham, S., Sharp, M. J. and Switsur, V. R. (1992). Holocene history of environment, vegetation and human settlement on Catta Ness, Lunnasting, Shetland, *Journal of Ecology* **80**(2): 241–273.

Bennett, K. D. and Fuller, J. L. (2002). Determining the age of the mid-Holocene *Tsuga canadensis* (hemlock) decline, eastern North America, *The Holocene* **12**(4): 421.

Bernoulli, J. (1713). *Ars conjectandi, opus posthumum. Accedit Tractatus de seriebus infinitis, et epistola Gallic scripta de ludo pil reticularis*, Basel: Thurneysen Brothers.

Bernoulli, J. (2006). *The art of conjecturing, together with Letter to a friend on sets in court tennis*, Johns Hopkins University Press. Transated by Sylla, E.D.

Birks, H. H. (1972). Studies in the Vegetational History of Scotland. III. A Radiocarbon-Dated Pollen Diagram from Loch Maree, Ross and Cromarty, *New Phytologist* **71**(4): 731–754.

Blaauw, M. (2010). Methods and code for 'classical' age-modelling of radiocarbon sequences, *Quaternary Geochronology* **5**(5): 512–518.

Blaauw, M. (2012). Out of tune: the dangers of aligning proxy archives, *Quaternary Science Reviews* **36**: 38–49.

Blaauw, M. and Christen, J. A. (2005). Radiocarbon peat chronologies and environmental change, *Journal of the Royal Statistical Society: Series C (Applied Statistics)* **54**(4): 805–816.

Blaauw, M. and Christen, J. A. (2011). Flexible paleoclimate age-depth models using an autoregressive Gamma process, *Bayesian Analysis* **6**(3): 457–474.

Blaauw, M., Christen, J. A., Mauquoy, D., van der Plicht, J. and Bennett, K. D. (2007). Testing the timing of radiocarbon-dated events between proxy archives, *The Holocene* **17**(2): 283–288.

Blaauw, M., van der Plicht, J. and van Geel, B. (2004). Radiocarbon dating of bulk peat samples from raised bogs: non-existence of a previously reported 'reservoir effect'?, *Quaternary Science Reviews* **23**(14-15): 1537–1542.

Blaauw, M., Wohlfarth, B., Christen, J. A., Ampel, L., Veres, D., Hughen, K. A., Preusser, F. and Svensson, A. (2010). Were last glacial climate events simultane-

ous between Greenland and France? A quantitative comparison using non-tuned chronologies, *Journal of Quaternary Science* **25**(3): 387–394.

Blackwell, P. G. and Buck, C. E. (2003). The Late Glacial human reoccupation of north-western Europe: new approaches to space-time modelling, *Antiquity* **77**(296): 232–240.

Blockley, S. P. E., Blaauw, M., Bronk Ramsey, C. and van der Plicht, J. (2007). Building and testing age models for radiocarbon dates in Lateglacial and Early Holocene sediments, *Quaternary Science Reviews* **26**(15-16): 1915–1926.

Blockley, S. P. E., Bronk Ramsey, C. and Higham, T. F. G. (2008a). The Middle to Upper Paleolithic transition: dating, stratigraphy, and isochronous markers, *Journal of Human Evolution* **55**(5): 764–771.

Blockley, S. P. E., Bronk Ramsey, C., Lane, C. S. and Lotter, A. F. (2008b). Improved age modelling approaches as exemplified by the revised chronology for the Central European varved lake Soppensee, *Quaternary Science Reviews* **27**(1-2): 61–71.

Blockley, S. P. E., Bronk Ramsey, C. and Pyle, D. M. (2008c). Improved age modelling and high-precision age estimates of late Quaternary tephras, for accurate palaeoclimate reconstruction, *Journal of Volcanology and Geothermal Research* **177**(1): 251–262.

Blockley, S. P. E., Lane, C. S., Hardiman, M., Rasmussen, S. O., Seierstad, I. K., Steffensen, J. P., Svensson, A., Lotter, A. F., Turney, C. S., Bronk Ramsey, C. and members, I. (2012). Synchronisation of palaeoenvironmental records over the last 60,000 years, and an extended INTIMATE event stratigraphy to 48,000 b2k, *Quaternary Science Reviews* **36**: 2–10.

Blockley, S. P. E., Lowe, J. J., Walker, M. J. C., Asioli, A., Trincardi, F., Coope, G. R. and Donahue, R. E. (2004). Bayesian analysis of radiocarbon chronologies: examples from the European Late-glacial, *Journal of Quaternary Science* **19**(2): 159–175.

Boaretto, E. (2006). Radiocarbon dates, *in* E. Finkelstein, D. Ussishkin and B. Halpem (eds), *Megiddo IV: The 1998–2002 seasons*, Tel Aviv: Emery and Chaire Yass Publications in Archaeology, Institute of Archaeology, Tel Aviv University, pp. 550–557.

Boaretto, E., Jull, A. J., Gilboa, A. and Sharon, I. (2005). Dating the iron age i/ii transition in israel: first intercomparison results, *Radiocarbon* **47**(1): 39–55.

Bond, G., Heinrich, H., Broecker, W., Labeyrie, L., McManus, J., Andrews, J., Huon, S., Jantschik, R., Clasen, S., Simet, C., Tedesco, K., Klas, M., Bonani, G. and Ivy, S. (1992). Evidence for massive discharges of icebergs into the North Atlantic ocean during the last glacial period, **360**(6401): 245–249.

Bond, G., Showers, W., Cheseby, M., Lotti, R., Almasi, P., Demenocal, P., Priore, P., Cullen, H., Hajdas, I. and Bonani, G. (1997). A pervasive millennial-scale cycle in North Atlantic Holocene and glacial climates, *Science* **278**(5341): 1257.

Boreux, J. J., Pesti, G., Duckstein, L. and Nicolas, J. (1997). Age model estimation in paleoclimatic research: fuzzy regression and radiocarbon uncertainties, *Palaeogeography, Palaeoclimatology, Palaeoecology* **128**(1-4): 29–37.

Bouzouggar, A., Barton, R. N. E., Blockley, S., Bronk Ramsey, C., Collcutt, S. N., Gale, R., Higham, T. F. G., Humphrey, L. T., Parfitt, S., Turner, E. and Ward, s. (2008). Reevaluating the age of the Iberomaurusian in Morocco, *African Archaeological Review* **25**(1): 3–19.

Box, G. E. P. and Draper, N. R. (1987). *Empirical model-building and response surfaces*, New York. Chilchester. Wiley.

Boyd, W. E. and Dickson, J. H. (1987). A post-glacial pollen sequence from Loch a'Mhuilinn, North Arran: a record of vegetation history with special reference to the history of endemic Sorbus species, *New phytologist* **107**(1): 221–244.

Brainerd, G. W. (1951). The place of chronological ordering in archaeological analysis, *American Antiquity* **16**(4): 301–313.

Brannon, N. F., Williams, B. B. and Wilkinson, J. L. (1990). The salvage excavation of Bronze Age cists, Straid townland, county Londonderry, *Ulster journal of archaeology* **53**: 29–39.

Brasier, C. M. (1990). China and the origins of Dutch elm disease: an appraisal, *Plant Pathology* **39**(1): 5–16.

Brauer, A., Endres, C. and Negendank, J. F. W. (1999). Lateglacial calendar year chronology based on annually laminated sediments from Lake Meerfelder Maar, Germany, *Quaternary International* **61**(1): 17–25.

Brindley, A. L. (2007). *The dating of food vessels and urns in Ireland*, Bronze Age Studies; 7, Galway: Department of Archaeology, National University of Ireland, 2007.

Brock, F., Lee, S., Housley, R. A. and Bronk Ramsey, C. (2011). Variation in the radiocarbon age of different fractions of peat: A case study from Ahrenshöft, northern Germany, *Quaternary Geochronology* **6**(6): 550–555.

Bronk Ramsey, C. (1995). Radiocarbon calibration and analysis of stratigraphy: the OxCal program, *Radiocarbon* **37**(2): 425–430.

Bronk Ramsey, C. (1998). Probability and dating, *Radiocarbon* **40**(1): 461–474.

Bronk Ramsey, C. (2001). Development of the radiocarbon calibration program, *Radiocarbon* **43**(2A): 355–363.

Bronk Ramsey, C. (2005). Improving the resolution of radiocarbon dating by statistical analysis, *in* T. E. Levy and T. Higham (eds), *The Bible and Radiocarbon Dating: Archaeology, Text and Science*, Equinox Publishing Ltd. London, pp. 57–64.

Bronk Ramsey, C. (2008). Deposition models for chronological records, *Quaternary Science Reviews* **27**: 42–60.

Bronk Ramsey, C. (2009a). Bayesian analysis of radiocarbon dates, *Radiocarbon* **51**(1): 337–360.

Bronk Ramsey, C. (2009b). Dealing with outliers and offsets in radiocarbon dating, *Radiocarbon* **51**(3): 1023–1045.

Bronk Ramsey, C., Dee, M., Lee, S., Nakagawa, T. and Staff, R. A. (2010a). Developments in the calibration and modelling of radiocarbon dates, *Radiocarbon* **52**(2-3): 953–961.

Bronk Ramsey, C., Dee, M. W., Rowland, J. M., Higham, T. F. G., Harris, S. A., Brock, F., Quiles, A., Wild, E. M., Marcus, E. S. and Shortland, A. J. (2010b). Radiocarbon-based chronology for Dynastic Egypt, *Science* **328**(5985): 1554–1557.

Bronk Ramsey, C., van der Plicht, J. and Weninger, B. (2001). "wiggle matching" radiocarbon dates, *Radiocarbon* **43**(2A): 381–390.

Brown, A. G. (1988). The palaeoecology of *Alnus* (alder) and the Postglacial history of floodplain vegetation. Pollen percentage and influx data from the West Midlands, United Kingdom, *New phytologist* **110**(3): 425–436.

Brown, T. (1997). Clearances and clearings: deforestation in Mesolithic / Neolithic Britain, *Oxford Journal of Archaeology* **16**(2): 133–146.

Bruins, H. J., van der Plicht, J. and Mazar, A. (2003). $^{14}$C dates from Tel Rehov: Iron-Age chronology, pharaohs, and Hebrew kings, *Science* **300**(5617): 315.

Bruins, H. J., van der Plicht, J., Mazar, A., Bronk Ramsey, C. and Manning, S. W. (2005). The Groningen radiocarbon series from Tel Rehov: OxCal Bayesian computations for the Iron IB–IIA boundary and Iron IIA destruction events, *in* T. E. Levy and T. Higham (eds), *The Bible and Radiocarbon Dating: Archaeology, Text and Science*, Equinox Publishing Ltd. London, pp. 271–93.

Buck, C. E. and Bard, E. (2007). A calendar chronology for Pleistocene mammoth and horse extinction in North America based on Bayesian radiocarbon calibration, *Quaternary Science Reviews* **26**(17-18): 2031–2035.

Buck, C. E. and Christen, J. A. (1998). A novel approach to selecting samples for radiocarbon dating, *Journal of archaeological science* **25**(4): 303–310.

Buck, C. E., Christen, J. A. and James, G. N. (1999). BCal: an on-line Bayesian radiocarbon calibration tool, *Internet Archaeology* **7**.

Buck, C. E., Kenworthy, J. B., Litton, C. D. and Smith, A. F. M. (1991). Combining archaeological and radiocarbon information: a Bayesian approach to calibration, *Antiquity* **65**(249): 808–21.

Buck, C. E., Litton, C. D. and Scott, E. M. (1994). Making the most of radiocarbon dating: some statistical considerations, *Antiquity* **68**: 252–252.

Buck, C. E., Litton, C. D. and Smith, A. F. M. (1992). Calibration of radiocarbon results pertaining to related archaeological events, *Journal of Archaeological Science* **19**(5): 497–512.

Çağatay, M., Görür, N., Algan, O., Eastoe, C., Tchapalyga, A., Ongan, D., Kuhn, T. and Kuş cu, I. (2000). Late Glacial–Holocene palaeoceanography of the Sea of Marmara: timing of connections with the Mediterranean and the Black Seas, *Marine Geology* **167**(3): 191–206.

Carmi, I. and Ussishkin, D. (2004). $^{14}$C dates, *The Renewed Archaeological Excavations at Lachish (1973–1994)*, Vol. 5 (Monograph Series of the Institute of Archaeology of Tel Aviv University 22), Tel Aviv, pp. 2508–2513.

Chambers, F. M. (1982). Environmental history of Cefn Gwernffrwd, near Rhandirmwyn, mid-Wales, *New Phytologist* **92**(4): 607–615.

Chambers, F. M. (1983). Three radiocarbon-dated pollen diagrams from upland peats north-west of Merthyr Tydfil, South Wales, *The Journal of Ecology* **71**(2): 475–487.

Chambers, F. M. and Price, S. M. (1985). Palaeoecology of *Alnus* (alder): early post-glacial rise in a valley mire, north-west Wales, *New phytologist* **101**(2): 333–344.

Chatfield, C. (1995). Model uncertainty, data mining and statistical inference, *Journal of the Royal Statistical Society. Series A. Statistics in society* **158**(3): 419–466.

Christen, J. A. (1994a). *Bayesian interpretation of radiocarbon results*, PhD thesis, University of Nottingham.

Christen, J. A. (1994b). Summarizing a set of radiocarbon determinations: a robust approach, *Applied Statistics* **43**(3): 489–503.

Christen, J. A. (2003). Bwigg: an Internet facility for Bayesian radiocarbon wiggle-matching, *Internet Archaeology* **13**.

Christen, J. A. and Litton, C. D. (1995). A Bayesian approach to wiggle-matching, *Journal of archaeological science* **22**(6): 719–725.

Clark, J. and Godwin, H. (1962). The Neolithic in the Cambridgeshire fens, *Antiquity* **36**(141): 10–23.

Clark, S. H. E. and Edwards, K. J. (2004). Elm bark beetle in Holocene peat deposits and the northwest European elm decline, *Journal of Quaternary Science* **19**(6): 525–528.

Coldstream, N. (2003). Some Aegean reactions to the chronological debate in the southern Levant, *Tel Aviv: Journal of the Institute of Archaeology of Tel Aviv University* **2003**(2): 247–258.

Cook, G. T., Dugmore, A. J. and Shore, J. S. (1998). The influence of pretreatment on humic acid yield and $^{14}$C age of *Carex* peat, *Radiocarbon* **40**(1): 21–27.

Davies, P. (1995). *In search of 'ancient Israel'*, Vol. 148, T&T Clark.

Day, S. P. (1991). Post-glacial vegetational history of the Oxford region, *New phytologist* **119**(3): 445–470.

de Vivo, B., Rolandi, G., Gans, P. B., Calvert, A., Bohrson, W. A., Spera, F. J. and Belkin, H. E. (2001). New constraints on the pyroclastic eruptive history of the Campanian volcanic Plain (Italy), *Mineralogy and Petrology* **73**(1): 47–65.

Dee, M. W. (2009). *A high-precision radiocarbon chronolgy for ancient Egypt using Bayesian statistical modelling*, PhD thesis, University of Oxford.

Deetz, J. and Dethlefsen, E. (1965). The doppler effect and archaeology: a consideration of the spatial aspects of seriation, *Southwestern Journal of Anthropology* **21**(3): 196–206.

Delcourt, H. R. (1987). The impact of prehistoric agriculture and land occupation on natural vegetation, *Trends in Ecology & Evolution* **2**(2): 39–44.

Dethlefsen, E. and Deetz, J. (1966). Death's heads, cherubs, and willow trees: experimental archaeology in colonial cemeteries, *American Antiquity* **31**(4): 502–510.

Dever, W. (1997). Archaeology and the Age of Solomon: A case study in archaeology and historiography, *in* L. Handy (ed.), *The Age of Solomon: Scholarship at the Turn of the Millennium*, Leiden: Brill, pp. 217–51.

Devoy, R. J. N. (1979). Flandrian sea level changes and vegetational history of the lower Thames estuary, *Philosophical Transactions of the Royal Society of London. Series B, Biological Sciences* **285**(1010): 355–407.

Dodson, J. R. and Bradshaw, R. H. W. (1987). A history of vegetation and fire, 6,600 BP to present, County Sligo, Western Ireland, *Boreas* **16**(2): 113–123.

Donaldson, A. M. and Turner, J. (1977). A pollen diagram from Hallowell Moss, near Durham City, UK, *Journal of Biogeography* **4**(1): 25–33.

Dothan, T. and Zukerman, A. (2004). A preliminary study of the Mycenaean IIIC: pottery assemblages from Tel Miqne-Ekron and Ashdod, *Bulletin of the American Schools of Oriental Research* (333): 1–54.

Draper, D. (1995). Assessment and propagation of model uncertainty, *Journal of the Royal Statistical Society. Series B (Methodological)* **57**(1): 45–97.

Dresser, Q. (1985). University College Cardiff radiocarbon dates I, *Radiocarbon* **27**(2B): 338–385.

Dugmore, A. J., Cook, G. T., Shore, J. S., Newton, A. J., Edwards, K. J. and Larsen, G. (1995). Radiocarbon dating tephra layers in Britain and Iceland, *Radiocarbon* **37**(2): 379–388.

Edwards, K. J. and McIntosh, C. J. (1988). Improving the detection rate of cereal-type pollen grains from *Ulmus* decline and earlier deposits from Scotland, *Pollen et spores* **30**(2): 179–188.

Eriksen, U., Friedrich, W. L., Buchardt, B., Tauber, H. and Thomson, M. S. (1990). The Stronghyle Caldera: Geological, palaeontological and stable isotope evidence from radiocarbon dated stromatolites from Santorini, *Thera and the Aegean world III*, Vol. 2, pp. 139–150.

Fægri, K. (1944). On the introduction of agriculture in western Norway, *Geologiska Föreningen i Stockholm Förhandlingar* **66**(3): 449–462.

Faure, G. (1986). *Principles of isotope geology*, 2nd edn, John Wiley & Sons, Inc., New York.

Finkelstein, I. (1996). The archaeology of the United Monarchy: an alternative view, *Levant* **28**(1): 177–187.

Finkelstein, I. (2005). A low chronology update: archaeology, history and Bible, *in* T. E. Levy and T. Higham (eds), *The Bible and Radiocarbon Dating: Archaeology, Text and Science*, Equinox Publishing Ltd. London, pp. 31–42.

Finkelstein, I. and Piasetzky, E. (2010a). Khirbet Qeiyafa: Absolute Chronology, *Tel Aviv: Journal of the Institute of Archaeology of Tel Aviv University* **37**(1): 84–88.

Finkelstein, I. and Piasetzky, E. (2010b). Radiocarbon dating the Iron Age in the Levant: a Bayesian model for six ceramic phases and six transitions, *Antiquity* **84**(324): 374–85.

Finkelstein, I. and Piasetzky, E. (2010c). The Iron I/IIA transition in the Levant: a reply to Mazar and Bronk Ramsey and a new perspective, *Radiocarbon* **52**(4): 1667–80.

Finkelstein, I. and Piasetzky, E. (2011). The Iron Age chronology debate: Is the gap narrowing?, *Near Eastern Archaeology* **74**(1): 50–54.

Finsinger, W., Lane, C. S., van Den Brand, G. J., Wagner-Cremer, F., Blockley, S. P. E. and Lotter, A. F. (2011). The lateglacial Quercus expansion in the southern European Alps: rapid vegetation response to a late Allerød climate warming?, *Journal of Quaternary Science* **26**: 694–702.

Fletcher, W. J. and Sánchez Goñi, M. F. (2008). Orbital-and sub-orbital-scale climate impacts on vegetation of the western Mediterranean basin over the last 48,000 yr, *Quaternary Research* **70**(3): 451–464.

Fossitt, J. A. (1994). Late-glacial and Holocene vegetation history of western Donegal, Ireland, *Biology and Environment: Proceedings of the Royal Irish Academy* **94B**(1): 1–31.

Garbett, G. (1981). The elm decline: the depletion of a resource, *New Phytologist* **88**(3): 573–585.

Garbini, G. and Bowden, J. S. (1988). *History and ideology in ancient Israel*, Crossroad. London.

Garfinkel, Y. and Ganor, S. (2008). Khirbet Qeiyafa: Sha'arayimn, *Journal of Hebrew Scriptures* **8**(22).

German, S. and German, D. (1984). Stochastic relaxation, Gibbs distribution, and the Bayesian restoration of images, *IEEE Transactions on Pattern Analysis and Machine Intelligence* **6**(9): 721–741.

Gilbertson, D. D., Hawkins, A. B., Mills, C. M., Harkness, D. D. and Hunt, C. O. (1990). The Late Devensian and Holocene of industrial Severnside and the Vale of Gordano: stratigraphy, radiocarbon dating and palaeoecology, *Proceedings of the Ussher Society* **7**: 279–284.

Gilboa, A. and Sharon, I. (2001). Early Iron Age radiometric dates from Tel Dor: preliminary implications for Phoenicia and beyond, *Radiocarbon* **43**(3): 1343–1351.

Gilboa, A. and Sharon, I. (2003). An archaeological contribution to the Early Iron Age chronological debate: alternative chronologies for Phoenicia and their effects on the Levant, Cyprus, and Greece, *Bulletin of the American Schools of Oriental Research* (332): 7–80.

Gilks, W. R., Richardson, S. and Spiegelhalter, D. J. (1996). Introducing Markov chain Monte Carlo, *in* W. R. Gilks, S. Richardson and D. J. Spiegelhalter (eds), *Markov chain Monte Carlo in practice*, Chapman & Hall, London, pp. 1–19.

Girling, M. and Greig, J. (1985). A first fossil record for *Scolytus scolytus* (F.) (Elm Bark Beetle): its occurrence in elm decline deposits from London and the implications for Neolithic elm disease, *Journal of archaeological science* **12**(5): 347–351.

Godwin, H. (1940a). Pollen analysis and forest history of England and Wales, *New Phytologist* **39**(4): 370–400.

Godwin, H. (1940b). Studies in the Post-Glacial History of British Vegetation. III. Fenland Pollen Diagrams. IV. Post-Glacial Changes in Relative Land-and Sea-Level in the English Fenland, *Philosophical Transactions of the Royal Society of London. Series B, Biological Sciences* **230**(570): 239–303.

Godwin, H. (1962). Half-life of radiocarbon, *Nature* **195**: 984.

Godwin, H., Walker, D. and Willis, E. H. (1957). Radiocarbon dating and post-glacial vegetational history: Scaleby Moss, *Proceedings of the Royal Society of London. Series B-Biological Sciences* **147**(928): 352–366.

Godwin, H. and Willis, E. (1961). Cambridge University natural radiocarbon measurements III, *Radiocarbon* **3**: 60–76.

Godwin, H. and Willis, E. H. (1959). Cambridge University natural radiocarbon measurements I, *American Journal of Radiocarbon Supplement* **1**: 63–75.

Godwin, H., Willis, E. H. and Switsur, V. R. (1965). Cambridge University natural radiocarbon measurements V, *Radiocarbon* **7**: 206–212.

Goring, S., Williams, J. W., Blois, J. L., Jackson, S. T., Paciorek, C. J., Booth, R. K., Marlon, J. R., Blaauw, M. and Christen, J. A. (2012). Deposition times in the northeastern United States during the Holocene: establishing valid priors for Bayesian age models, *Quaternary Science Reviews* **48**: 54–60.

Grimm, E. C., Jacobson, G. L., Watts, W. A., Hansen, B. C. S. and Maasch, K. A. (1993). A 50,000-year record of climate oscillations from Florida and its temporal correlation with the Heinrich events, *Science* **261**(5118): 198–200.

Harkness, D. D. (1981). Scottish Universities Research and Reactor Centre radiocarbon measurements IV., *Radiocarbon* **23**(2): 252–304.

Harkness, D. D. and Wilson, H. W. (1973). Scottish Universities Research and Reactor Centre radiocarbon measurements I, *Radiocarbon* **15**(3): 554–565.

Harkness, D. D. and Wilson, H. W. (1974). Scottish Universities Research and Reactor Centre radiocarbon measurements II, *Radiocarbon* **16**(2): 238–251.

Harkness, D. D. and Wilson, H. W. (1979). Scottish Universities Research and Reactor Centre radiocarbon measurements III, *Radiocarbon* **21**(2): 203–256.

Haslett, J. and Parnell, A. C. (2008). A simple monotone process with application to radiocarbon-dated depth chronologies, *Journal of the Royal Statistical Society: Series C (Applied Statistics)* **57**(4): 399–418.

Hastings, W. K. (1970). Monte Carlo sampling methods using Markov chains and their applications, *Biometrika* **57**(1): 97–109.

Hedges, R. E. M., Housley, R. A., Bronk Ramsey, C. and van Klinken, G. J. (1990). Radiocarbon dates from the Oxford AMS system: Archaeometry datelist 11, *Archaeometry* **32**(2): 211–237.

Hedges, R. E. M., Housley, R. A., Bronk Ramsey, C. and van Klinken, G. J. (1994). Radiocarbon dates from the Oxford AMS system: Archaeometry datelist 18, *Archaeometry* **36**(2): 337–374.

Heegaard, E., Birks, H. J. B. and Telford, R. J. (2005). Relationships between calibrated ages and depth in stratigraphical sequences: an estimation procedure by mixed-effect regression, *The Holocene* **15**(4): 612–618.

Heinrich, H. (1988). Origin and consequences of cyclic ice rafting in the Northeast Atlantic Ocean during the past 130,000 years, *Quaternary Research* **29**(2): 142–152.

Hemming, S. (2004). Heinrich events: Massive late Pleistocene detritus layers of the North Atlantic and their global climate imprint, *Reviews of Geophysics* **42**(1): RG1005.

Herzog, Z. and Singer-Avitz, L. (2004). Redefining the centre: the emergence of state in Judah, *Tel Aviv: Journal of the Institute of Archaeology of Tel Aviv University* **2004**(2): 209–244.

Herzog, Z. and Singer-Avitz, L. (2006). Sub-dividing the Iron Age IIA in northern Israel: a suggested solution to the chronological debate, *Tel Aviv: Journal of the Institute of Archaeology of Tel Aviv University* **2006**(2): 163–195.

Heyworth, A., Kidson, C. and Wilks, P. (1985). Late-glacial and Holocene sediments at Clarach Bay, near Aberystwyth, *The Journal of Ecology* **73**(2): 459–480.

Hibbert, F. A. and Switsur, V. R. (1976). Radiocarbon dating of Flandrian pollen zones in Wales and northern England, *New Phytologist* **77**(3): 793–807.

Hibbert, F. A., Switsur, V. R. and West, R. G. (1971). Radiocarbon dating of Flandrian pollen zones at Red Moss, Lancashire, *Proceedings of the Royal Society of London. Series B. Biological Sciences* **177**(1047): 161–176.

Hirons, K. R. and Edwards, K. J. (1986). Events at and around the first and second *Ulmus* declines: palaeoecological investigations in Co. Tyrone, Northern Ireland, *New phytologist* **104**(1): 131–153.

Hoeting, J. A., Madigan, D., Raftery, A. E. and Volinsky, C. T. (1999). Bayesian model averaging: A tutorial, *Statistical science* **14**(4): 382–401.

Housley, R. A., Gamble, C. S., Street, M. and Pettitt, P. (1997). Radiocarbon evidence for the lateglacial human recolonisation of northern europe, *Proceedings of the Prehistoric Society* **63**: 25–54.

Hua, Q., McDonald, J., Redwood, D. Drysdale, R., Lee, S., Fallon, S. and Hellstrom, J. (in press). Robust chronological reconstruction for young speleothems using radiocarbon, *Quaternary Geochronology* .

Humphrey, L., Bello, S., Turner, E., Bouzouggar, A. and Barton, R. N. E. (2012). Iberomaurusian funerary behaviour: Evidence from Grotte des Pigeons, Taforalt, Morocco, *Journal of Human Evolution* **62**: 261–273.

Huntley, B. (1981). The past and present vegetation of the Caenlochan National Nature Reserve, Scotland. II. Palaeoecological investigations, *New Phytologist* **87**(1): 189–222.

Huntley, B. and Birks, H. J. B. (1983). *An atlas of past and present pollen maps of Europe: 0-13, 000 years ago*, Cambridge: Cambridge University Press.

Innes, J. B. (1994). Palaeoecological survey, *in* R. W. Cowell and J. B. Innes (eds), *The wetlands of Merseyside*, Lancaster University Archaeological Unit, pp. 139–151.

Jamieson-Drake, D. W. (1991). *Scribes and schools in monarchic Judah: a socio-archeological approach*, Vol. 109, Sheffield Academic Press.

Jeffreys, H. (1935). Some tests of significance, treated by the theory of probability, *Proceedings of the Cambridge Philosophical Society*, Vol. 31, Cambridge Univ Press, pp. 203–222.

Jeffreys, H. (1998). *Theory of probability*, Oxford University Press, USA.

Johnson, R. H., Tallis, J. H. and Wilson, P. (1990). The Seal Edge Coombes, North Derbyshire — a study of their erosional and depositional history, *Journal of Quaternary Science* **5**(1): 83–94.

Jullien, E., Grousset, F., Malaizé, B., Duprat, J., Sanchez-Goni, M. F., Eynaud, F., Charlier, K., Schneider, R., Bory, A., Bout, V. and Flores, J. A. (2007). Low-latitude "dusty events" vs. high-latitude "icy Heinrich events", *Quaternary Research* **68**(3): 379–386.

Karlsberg, A. J. (2006). *Flexible Bayesian methods for archaeological dating*, PhD thesis, University of Sheffield.

Kass, R. E. and Raftery, A. E. (1995). Bayes factors, *Journal of the american statistical association* **90**(430): 773–795.

Kigoshi, K., Aizawa, H. and Suzuki, N. (1973). Gakushuin natural radiocarbon measurements VII, *Radiocarbon* **11**(2): 295–326.

Kitagawa, H. and van der Plicht, J. (1998). A 40,000-year varve chronology from Lake Suigetsu, Japan: extension of the $^{14}$C calibration curve, *Radiocarbon* **40**(1): 505–515.

Kitagawa, H. and van der Plicht, J. (2000). Atmospheric radiocarbon calibration beyond 11,900 cal BP from Lake Suigetsu laminated sediments, *Radiocarbon* **42**(3): 369–380.

Kwiecien, O., Arz, H. W., Lamy, F., Wulf, S., Bahr, A., Röhl, U. and Haug, G. (2008). Estimated reservoir ages of the Black Sea since the last glacial, *Radiocarbon* **50**(1): 99–118.

Lamon, R. S. and Shipton, G. M. (1939). *Megiddo: Seasons of 1925-34 (strata IV)*, University of Chicago Press.

Langou, J. (2009). Translation and modern interpretation of Laplace's Théorie Analytique des Probabilités, pages 505-512, 516-520.

Lanphere, M. (2000). Comparison of conventional K-Ar and $^{40}Ar/^{39}Ar$ dating of young mafic volcanic rocks, *Quaternary Research* **53**(3): 294–301.

Laplace, P. S. (1812). *Théorie analytique des probabilités*, Courcier.

Leamer, E. E. (1978). *Specification searches: ad hoc inference with nonexperimental data*, John Wiley & Sons, New York.

Lee, S. and Bronk Ramsey, C. (2012). Development and application of the trapezoidal model for archaeological chronologies, *Radiocarbon* **54**(1): 107–122.

Libby, W. F. (1955). *Radiocarbon dating*, Vol. 175, University of Chicago Press Chicago.

Libby, W. F., Anderson, E. C. and Arnold, J. R. (1949). Age determination by radiocarbon content: world-wide assay of natural radiocarbon, *Science* **109**(2827): 227.

Litton, C. D. and Buck, C. E. (1996). An archaeological example: radiocarbon dating, *in* W. Gilks, S. Richardson and D. Spiegelhalter (eds), *Markov chain Monte Carlo in practice*, Chapman & Hall/CRC.

Liu, Y., Brewer, S., Booth, R. K., Minckley, T. A. and Jackson, S. T. (2012). Temporal density of pollen sampling affects age determination of the mid-holocene hemlock (*Tsuga*) decline, *Quaternary Science Reviews* **45**: 54–59.

Lowe, D. J. (2011). Tephrochronology and its application: A review, *Quaternary Geochronology* **6**: 107–153.

Lowe, D. J. and Hunt, J. B. (2001). A summary of terminology used in tephra-related studies, *in* E. T. Jevigné and J.-P. Raynal (eds), *Tephras: Chronology, Archaeology*, CDERAD éditeur, Goudet. Les Dossiers de l'Archéo-Logis 1, pp. 17–22.

Lowe, J. J. and Walker, M. J. C. (1997). *Reconstructing Quaternary Environments*, Longman Harlow, UK.

MacAyeal, D. R. (1993). Binge/purge oscillations of the Laurentide ice sheet as a cause of the North Atlantic's Heinrich events, *Paleoceanography* **8**(6): 775–784.

Madigan, D. and Raftery, A. E. (1994). Model selection and accounting for model uncertainty in graphical models using Occam's window, *Journal of the American Statistical Association* **89**(428): 1535–1546.

Madigan, D., York, J. and Allard, D. (1995). Bayesian graphical models for discrete data, *International Statistical Review* **63**(2): 215–232.

Manning, C. (1987). A cist grave at Newtownbalregan, *Journal of the County Louth Archaeological and Historical Society* **21**(3): 274–278.

Margari, V., Gibbard, P. L., Bryant, C. L. and Tzedakis, P. C. (2009). Character of vegetational and environmental changes in southern Europe during the last glacial period; evidence from Lesvos Island, Greece, *Quaternary Science Reviews* **28**(13-14): 1317–1339.

Margari, V., Pyle, D. M., Bryant, C. and Gibbard, P. L. (2007). Mediterranean tephra stratigraphy revisited: results from a long terrestrial sequence on Lesvos Island, Greece, *Journal of volcanology and geothermal research* **163**(1-4): 34–54.

Mazar, A. (1999). The 1997-1998 Excavations at Tel Rehov: Preliminary Report, *Israel Exploration Journal* **49**: 1–52.

Mazar, A. (2005). The debate over the chronology of the Iron Age in the Southern Levant, *in* T. E. Levy and T. Higham (eds), *The Bible and Radiocarbon Dating: Archaeology, Text and Science*, Equinox Publishing Ltd. London, pp. 15–30.

Mazar, A. (2011). The Iron Age chronology debate: Is the gap narrowing? Another viewpoint, *Near Eastern Archaeology* **74**(2): 105–111.

Mazar, A. and Bronk Ramsey, C. (2008). $^{14}$C dates and the Iron Age chronology of Israel: a response, *Radiocarbon* **50**(2): 159–180.

Mazar, A. and Carmi, I. (2001). Radiocarbon dates from Iron Age strata at Tel Beth Shean and Tel Rehov, *Radiocarbon* **43**(3): 1333–1342.

McAulay, I. R. and Watts, W. A. (1961). Dublin radiocarbon dates I, *Radiocarbon* **3**(1): 26–38.

McGeehin, J., Burr, G. S., Jull, A. J. T., Reines, D., Gosse, J., Davis, P. T., Muhs, D. and Southon, J. R. (2001). Stepped-combustion $^{14}$C dating of sediment: A comparison with established techniques, *Radiocarbon* **43**(2A): 255–262.

Metropolis, N., Rosenbluth, A. W., Rosenbluth, M. N., Teller, A. H. and Teller, E. (1953). Equation of state calculations by fast computing machines, *The journal of chemical physics* **21**(6): 1087–1092.

Millard, A. (2009). What does it mean to sum the probabilities of dates? Poster #P-42 at 20th International Radiocarbon conference 2009.

Mitchell, G. F. (1950). Studies in Irish Quaternary Deposits: No. 7, *Proceedings of the Royal Irish Academy. Section B: Biological, Geological, and Chemical Science* **53**: 111–206.

Mitchell, G. F. (1954-1956). Post-boreal pollen-diagrams from Irish raised-bogs (Studies in Irish Quaternary deposits: no. 11), *Proceedings of the Royal Irish Academy. Section B: Biological, Geological, and Chemical Science* **57**: 185–251.

Moar, N. T. (1969). A radiocarbon-dated pollen diagram from north-west Scotland, *New Phytologist* **68**(1): 209–214.

Molloy, K. and O'Connell, M. (1987). The nature of the vegetational changes at about 5000 BP with particular reference to the elm decline: fresh evidence from Connemara, western Ireland, *New phytologist* **107**(1): 203–220.

Moore, F. (1984). A Bronze Age burial at Killinane, near Bagenalstown, Co. Carlow, *Old Kilkenny Review* **3**: 64–8.

Moreno, A., Cacho, I., Canals, M., Prins, M. A., Sánchez-Goni, M. F., Grimalt, J. O. and Weltje, G. J. (2002). Saharan dust transport and high-latitude glacial climatic variability: the Alboran Sea record, *Quaternary Research* **58**(3): 318–328.

Mortensen, M. F., Birks, H. H., Christensen, C., Holm, J., Noe-Nygaard, N., Odgaard, B. V., Olsen, J. and Rasmussen, K. L. (2011). Lateglacial vegetation development in Denmark-New evidence based on macrofossils and pollen from Slotseng, a small-scale site in southern Jutland, *Quaternary Science Reviews* **30**: 2534–2550.

Mount, C. and Buckley, L. (1997). Adolf Mahr's excavations of an Early Bronze Age cemetery at Keenoge, County Meath, *Proceedings of the Royal Irish Academy. Section C: Archaeology, Celtic Studies, History, Linguistics, Literature* **97C**(1): 1–68.

Mount, C., Buckley, L. and Lynch, P. (1998). Five Early Bronze Age cemeteries at Brownstown, Graney West, Oldtown and Ploopluck, County Kildare, and Strawhall, County Carlow, *Proceedings of the Royal Irish Academy. Section C: Archaeology, Celtic Studies, History, Linguistics, Literature* **98C**(2): 25–99.

Müller, U. C., Pross, J., Tzedakis, P. C., Gamble, C., Kotthoff, U., Schmiedl, G., Wulf, S. and Christanis, K. (2011). The role of climate in the spread of modern humans into Europe, *Quaternary Science Reviews* **30**: 273–279.

Naylor, J. C. and Smith, A. F. M. (1988). An archaelogical inference problem, *Journal of the American Statistical Association* **83**(403): 588–595.

Needham, S., Bronk Ramsey, C., Coombs, D., Cartwright, C. and Pettitt, P. (1997). An independent chronology for British Bronze Age metalwork: the results of the Oxford Radiocarbon Accelerator Programme, *Archaeological journal* **154**: 55–107.

Nicholls, G. and Jones, M. (2001). Radiocarbon dating with temporal order constraints, *Journal of the Royal Statistical Society: Series C (Applied Statistics)* **50**(4): 503–521.

Nilsson, M., Klarqvist, M., Bohlin, E. and Possnert, G. (2001). Variation in $^{14}$C age of macrofossils and different fractions of minute peat samples dated by AMS, *The Holocene* **11**(5): 579.

Nilsson, T. (1948). On the application of the Scanian Post-Glacial zone system to Danish pollen diagrams, *Det Kongelige Danske videnskabernes selskab. Biologiske Skrifter* **V**: 1–53.

Nygård, A., Sejrup, H. P., Haflidason, H., Cecchi, M. and Ottesen, D. (2004). Deglaciation history of the southwestern Fennoscandian Ice Sheet between 15 and 13 $^{14}$C ka BP, *Boreas* **33**(1): 1–17.

Ó Ríordáin, B. and Waddell, J. (1993). *The funerary bowls and vases of the Irish Bronze Age*, Galway University Press.

O'Connell, M. (1990). Origins of Irish lowland blanket bog, *Ecology and conservation of Irish peatlands* **49**(71): 259–79.

O'Connell, M., Mitchell, F. J. G., Readman, P. W., Doherty, T. J. and Murray, D. A. (1987). Palaeoecological investigations towards the reconstruction of the post-

glacial environment at Lough Doo, County Mayo, Ireland, *Journal of Quaternary Science* **2**(2): 149–164.

O'Connor, B. (1980). *Cross-channel relations in the Later Bronze Age*, Vol. 91 of *International Series 91*, British Archaeological Report.

O'Sullivan, M., Herity, M. and Mattenberger, U. (2005). *Duma na nGiall*, Wordwell.

O'Sullivan, P. E. (1976). Pollen analysis and radiocarbon dating of a core from Loch Pityoulish, Eastern Highlands of Scotland, *Journal of Biogeography* **3**(3): 293–302.

Parker, A. G. (1995). *Late Quaternary Environmental Change in the Upper Thames Basin, Central Southern England*, PhD thesis, University of Oxford.

Parker, A. G., Goudie, A. S., Anderson, D. E., Robinson, M. A. and Bonsall, C. (2002). A review of the mid-Holocene elm decline in the British Isles, *Progress in physical geography* **26**(1): 1–45.

Parnell, A. C., Haslett, J., Allen, J. R. M., Buck, C. E. and Huntley, B. (2008). A flexible approach to assessing synchroneity of past events using Bayesian reconstructions of sedimentation history, *Quaternary Science Reviews* **27**(19-20): 1872–1885.

Pearson, G. W. (1979). Belfast radiocarbon dates IX, *Radiocarbon* **21**(2): 274–290.

Pearson, G. W. and Pilcher, J. R. (1975). Belfast radiocarbon dates VIII, *Radiocarbon* **17**(2): 226–238.

Peglar, S. (1979). A radiocarbon-dated pollen diagram from Loch of Winless, Caithness, north-east Scotland, *New Phytologist* **82**(1): 245–263.

Peglar, S. and Waller, M. (1994). The Ouse channel, Haddenham, *in* M. Waller (ed.), *The Fenland Project,No. 9: Flandrian environmental change in Fenand*, East Anglian Archaeology Report Number 70, Cambridgeshire Archaeological Committee, pp. 47–84.

Pennington, W. and Lishman, J. P. (1984). The post-glacial sediments of Blelham Tarn: geochemistry and palaeoecology, *Archiv feur Hydrobiologie. Supplementband Monographishce* **69**(1): l–54.

Pennington, W., Tutin, T. G., Haworth, E. Y., Bonny, A. P. and Lishman, J. P. (1972). Lake sediments in northern Scotland, *Philosophical Transactions of the Royal Society of London. Series B, Biological Sciences* **264**(861): 191–294.

Pichler, H. and Friedrich, W. (1976). Radiocarbon dates of Santorini volcanics, *Nature* **262**: 373–374.

Pilcher, J. R. (1969). Archaeology, palaeoecology and $^{14}$C dating of the Beaghmore stone circle site, *Ulster Journal of Archaeology* **32**: 73–91.

Pilcher, J. R. (1973). Pollen analysis and radiocarbon dating of a peat on Slieve Gallion, Co. Tyrone, N. Ireland, *New Phytologist* **72**(3): 681–689.

Pilcher, J. R. and Larmour, R. (1982). Late-glacial and post-glacial vegetational history of the Meenadoan Nature Reserve, County Tyrone, **82B**: 277–295.

Pilcher, J. R., Smith, A. G., Pearson, G. W. and Crowder, A. (1971). Land clearance in the Irish Neolithic: new evidence and interpretation, *Science* **172**(3983): 560–562.

Pyle, D. M., Ricketts, G. D., Margari, V., van Andel, T. H., Sinitsyn, A. A., Praslov, N. D. and Lisitsyn, S. (2006). Wide dispersal and deposition of distal tephra during the Pleistocene 'Campanian Ignimbrite/Y5' eruption, Italy, *Quaternary Science Reviews* **25**(21-22): 2713–2728.

Raftery, A. E. (1996). Hypothesis testing and model selection, *in* W. R. Gilks, S. Richaedson and D. J. Spiegelhalter (eds), *Markov chain Monte Carlo in practice*, Chapman & Hall, London, pp. 163–188.

Reimer, P. J., Baillie, M. G. L., Bard, E., Bayliss, A., Beck, J. W., Blackwell, P. G., Bronk Ramsey, C., Buck, C. E., Burr, G. S., Edwards, R. L., Friedrich, M., M.,

G. P., Guilderson, T. P., Hajdas, I., Heaton, T. J., Hogg, A. G., Hughen, K. A., Kaiser, K. F., Kromer, B., McCormac, F. G., Manning, S. W., Reimer, R. W., Richards, D. A., Southon, J. R., Talamo, S., Turney, C. S. M., van der Plicht, J. and Weyhenmeyer, C. E. (2009). IntCal09 and Marine09 radiocarbon age calibration curves, 0–50,000 years cal BP, *Radiocarbon* **51**(4): 1111–1150.

Reisner, G. A., Fisher, C. S. and Lyon, D. G. (1924). *Harvard excavations at Samaria*, Harvard University Press.

Renfrew, C. and Bahn, P. G. (2008). *Archaeology: theories, methods and practice*, 5th edn, Thames and Hudson.

Ríordáin, B., Brindley, A. L. and Donnabháin, B. (1997). A Bronze Age cemetery mound at Grange, Co. Roscommon, *The Journal of Irish Archaeology* **8**: 43–72.

Roberts, H. V. (1965). Probabilistic prediction, *Journal of the American Statistical Association* **60**(309): 50–62.

Robinson, D. (1987). Investigations into the Aukhorn peat mounds, Keiss, Caithness: pollen, plant macrofossil and charcoal analyses, *New phytologist* **106**(1): 185–200.

Robinson, D. E. and Dickson, J. H. (1988). Vegetational history and land use: a radiocarbon-dated pollen diagram from Machrie Moor, Arran, Scotland, *New phytologist* **109**(2): 223–235.

Robinson, W. S. (1951). A method for chronologically ordering archaeological deposits, *American antiquity* **16**(4): 293–301.

Rohling, E., Mayewski, P. and Challenor, P. (2003). On the timing and mechanism of millennial-scale climate variability during the last glacial cycle, *Climate Dynamics* **20**(2): 257–267.

Rowell, T. K. and Turner, J. (1985). Litho-, humic-and pollen stratigraphy at Quick Moss, Northumberland, *The Journal of Ecology* **73**(1): 11–25.

Scaife, R. G. (1987a). A review of later Quaternary plant microfossil and macrofossil research in Southern England; with special reference to environmental archaeological evidence, *in* H. C. M. Keeey (ed.), *Environmental Archaeology: a regional review*, Vol. 2, Historic Buildings and Monuments Commission for England, Occasional Paper No. 1, pp. 125–179.

Scaife, R. G. (1987b). Pollen analysis, *in* N. D. Balaam, B. Levitan and V. Straker (eds), *Studies in the palaeoeconomy and environment in South West England*, British Archaeological Reports, British Series 181, pp. 223–232.

Scholz, D. and Hoffmann, D. L. (2011). StalAge — An algorithm designed for construction of speleothem age models, *Quaternary Geochronology* **6**(3–4).

Scourse, J. D., Hall, I. R., McCave, I. N., Young, J. R. and Sugdon, C. (2000). The origin of Heinrich layers: evidence from H2 for European precursor events, *Earth and Planetary Science Letters* **182**(2): 187–195.

Sernander, R. (1908). On the evidences of postglacial changes of climate furnished by the peat-mosses of Northern Europe, *Geologiska Foereningan i Stockholm. Foerhandlingar* **30**(7): 465–473.

Seymour, K. S., Christanis, K., Bouzinos, A., Papazisimou, S., Papatheodorou, G., Moran, E. and Dénès, G. (2004). Tephrostratigraphy and tephrochronology in the Philippi peat basin, Macedonia, Northern Hellas (Greece), *Quaternary International* **121**(1): 53–65.

Sharon, I. (2001). "Transition dating"; a heuristic mathematical approach to the collation of radiocarbon dates from stratified sequences, *Radiocarbon* **43**(2A): 345–354.

Sharon, I., Gilboa, A., Boaretto, E. and Jull, A. J. T. (2005). The Early Iron Age Dating Project: introduction, methodology, progress report and an update on the Tel Dor radiometric dates, *in* T. E. Levy and T. Higham (eds), *The Bible and Ra-*

*diocarbon Dating: Archaeology, Text and Science*, Equinox Publishing Ltd. London, pp. 65–92.

Sharon, I., Gilboa, A., Jull, A. J. and Boaretto, E. (2007). Report on the first stage of the Iron Age dating project in Israel: supporting a low chronology, *Radiocarbon* **49**(1): 1–46.

Shore, J. S., Bartley, D. D. and Harkness, D. D. (1995). Problems encountered with the $^{14}$C dating of peat, *Quaternary Science Reviews* **14**(4): 373–383.

Simmons, I. G. and Innes, J. B. (1988). Late Quaternary vegetational history of the North York Moors. X. Investigations on East Bilsdale Moor, *Journal of Biogeography* **15**(2): 299–324.

Sims, R. E. (1973). The anthropogenic factor in East Anglian vegetational history: an approach using A. P. F. techniques, *in* H. J. B. Birks and R. G. West (eds), *Quaternary Plant Ecology*, Oxford: Blackwell Scientific Publications, pp. 223–236.

Singer-Avitz, L. (2010). The Relative Chronology of Khirbet Qeiyafa, *Tel Aviv: Journal of the Institute of Archaeology of Tel Aviv University* **37**(1): 79–83.

Singer, B. S. and Pringle, M. S. (1996). Age and duration of the Matuyama-Brunhes geomagnetic polarity reversal from incremental heating analyses of lavas, *Earth and Planetary Science Letters* **139**(1-2): 47–61.

Smith, A. G. (1961). The Atlantic / Sub-Boreal transition, *Proceedings of the Linnean Society of London* **172**(1): 38–49.

Smith, A. G. and Cloutman, E. W. (1988). Reconstruction of Holocene vegetation history in three dimensions at Waun-Fignen-Felen, an upland site in South Wales, *Philosophical Transactions of the Royal Society of London. Series B, Biological Sciences* **322**(1209): 159–219.

Smith, A. G. and Goddard, I. C. (1991). A 12,500 year record of vegetational history at Sluggan Bog, Co. Antrim, N. Ireland (incorporating a pollen zone scheme for the non-specialist), *New Phytologist* **118**(1): 167–187.

Smith, A. G. and Morgan, L. A. (1989). A succession to ombrotrophic bog in the Gwent Levels, and its demise: a Welsh parallel to the peats of the Somerset Levels, *New Phytologist* **112**(1): 145–167.

Smith, A. G., Pearson, G. W. and Pilcher, J. R. (1970). Belfast radiocarbon dates II, *Radiocarbon* **12**(1): 291–297.

Smith, A. G., Pearson, G. W. and Pilcher, J. R. (1971a). Belfast radiocarbon dates III, *Radiocarbon* **13**(1): 103–125.

Smith, A. G., Pearson, G. W. and Pilcher, J. R. (1971b). Belfast radiocarbon dates IV, *Radiocarbon* **13**(2): 450–467.

Smith, A. G., Pearson, G. W. and Pilcher, J. R. (1973). Belfast radiocarbon dates V, *Radiocarbon* **15**(1): 212–228.

Smith, A. G. and Pilcher, J. R. (1973). Radiocarbon dates and vegetational history of the British Isles, *New Phytologist* **72**(4): 903–914.

Smith, A. G. and Willis, E. H. (1961/1962). Radiocarbon dating of the Fallahogy Landnam phase, *Ulster journal of archaeology* **24/25**: 16–24.

Staff, R. A., Bronk Ramsey, C., Bryant, C. L., Brock, F., Payne, R. L., Schlolaut, G., Marshall, M. H., Brauer, A., Lamb, H. F., Tarasov, P., Yokoyama, E., Haraguchi, T., Gotanda, K., Yonenobu, H., Nakagawa, T. and Suigetsu 2006 Project Members (2011). New $^{14}$C Determinations from Lake Suigetsu, Japan: 12,000 to 0 cal BP, *Radiocarbon* **53**(3): 511–528.

Staff, R. A., Bronk Ramsey, C., Nakagawa, T. and Suigetsu 2006 Project Members (2010). A re-analysis of the Lake Suigetsu terrestrial radiocarbon calibration

dataset, *Nuclear Instruments and Methods in Physics Research Section B: Beam Interactions with Materials and Atoms* **268**(7-8): 960–965.

Stager, L. E. (2003). The patrimonial kingdom of Solomon, *in* W. Dever and S. Gitin (eds), *Symbiosis, symbolism, and the power of the past–Canaan, ancient Israel, and their neighbors from the Late Bronze Age through Roman Palaestina*, Winona Lake, IN: Eisenbrauns, pp. 63–74.

Standford, J. D., Rohling, E. J., Bacon, S., Roberts, A. P., Grousset, F. E. and Bolshaw, M. (2011). A new concept for the paleoceanographic evolution of Heinrich event 1 in the North Atlantic, *Quaternary Science Reviews* **30**(9–10): 1047–1066.

Steiger, R. H. and Jäger, E. (1977). Subcommission on geochronology: convention on the use of decay constants in geo-and cosmochronology, *Earth and planetary science letters* **36**(3): 359–362.

Stewart, D. A., Walker, A. and Dickson, J. H. (1984). Pollen diagrams from Dubh Lochan, near Loch Lomond, *New phytologist* **98**(3): 531–549.

Stigler, S. M. (1986). Laplace's 1774 memoir on inverse probability, *Statistical Science* **1**(3): 359–363.

Stuiver, M. (1971). Evidence for the variation of atmospheric $^{14}$C content in the Late Quaternary, *in* K. Turekian (ed.), *The Late Cenozoic Glacial Ages*, New Haven: Yale University Press, pp. 57–70.

Stuiver, M. and Braziunas, T. F. (1993). Modeling atmospheric $^{14}$C influences and $^{14}$C ages of marine samples to 10 000 BC, *Radiocarbon* **35**(1): 137–189.

Sturludottir, S. A. and Turner, J. (1985). The elm decline at Pawlaw Mire: an anthropogenic interpretation, *New phytologist* **99**(2): 323–329.

Switsur, V. R. (1981). Cambridge University natural radiocarbon measurements XV, *Radiocarbon* **23**(1): 81–93.

Switsur, V. R., Hall, M. A. and West, R. G. (1970). University of Cambridge natural radiocarbon measurements IX, *Radiocarbon* **12**(2): 590–598.

Switsur, V. R. and West, R. G. (1973). University of Cambridge natural radiocarbon measurements XII, *Radiocarbon* **15**(3): 534–544.

Tallis, J. H. and Switsur, V. R. (1990). Forest and Moorland in the South Pennine Uplands in the Mid-Flandrian Period: II. The Hillslope Forests, *The Journal of Ecology* **78**(4): 857–883.

Taylor, D. M., Griffiths, H. I., Pedley, H. M. and Prince, I. (1994). Radiocarbon-dated Holocene pollen and ostracod sequences from barrage tufa-dammed fluvial systems in the White Peak, Derbyshire, UK, *The Holocene* **4**(4): 356–364.

Taylor, V., Barton, R. N. E., Bell, M., Bouzouggar, A., Collcutt, S., Black, S. and Hogue, J. T. (2011). The Epipalaeolithic (Iberomaurusian) at Grotte des Pigeons (Taforalt), Morocco: A preliminary study of the land Mollusca, *Quaternary International* **244**: 5–14.

Thompson, T. (2000). *Early history of the Israelite people: from the written & archaeological sources*, Vol. 4, Brill.

Tipping, R. (1994). Williamsons Moss: Palynological evidence for the Mesolithic-Neolithic transition in Cumbria, *in* J. Boardman and J. Walden (eds), *The Quaternary of Cumbria; Field Guide*, Oxford: Quaternary Research Association, pp. 104–127.

Tipping, R. (1995a). Holocene evolution of a lowland Scottish landscape: Kirkpatrick Fleming. Part I, peat-and pollen-stratigraphic evidence for raised moss development and climatic change, *The Holocene* **5**(1): 69–81.

Tipping, R. (1995b). Holocene evolution of a lowland Scottish landscape: Kirkpatrick Fleming. Part II, regional vegetation and land-use change, *The Holocene* **5**(1): 83–96.

Tipping, R. (1995c). Holocene landscape change at Carn Dubh, near Pitlochry, Perthshire, Scotland, *Journal of Quaternary Science* **10**(1): 59–75.

Tipping, R., Edmonds, M. and Sheridan, A. (1993). Palaeoenvironmental investigations directly associated with a neolithic axe 'quarry' on Beinn Lawers, near Killin, Perthshire, Scotland, *New phytologist* **123**(3): 585–597.

Ton-That, T., Singer, B. and Paterne, M. (2001). $^{40}Ar/^{39}Ar$ dating of latest Pleistocene (41 ka) marine tephra in the Mediterranean Sea: implications for global climate records, *Earth and Planetary Science Letters* **184**(3-4): 645–658.

Troels-Smith, J. (1960). *Ivy, mistletoe and elm climate indicators-fodder plants: a contribution to the interpretation of the pollen zone border VII-VIII*, Vol. Series IV 4, København: Reitzels Forlag.

Turner, J. (1965). A contribution to the history of forest clearance, *Proceedings of the Royal Society of London. Series B, Biological Sciences* **161**(984): 343–354.

Turner, J., Hewetson, V. P., Hibbert, F. A., Lowry, K. H. and Chambers, C. (1973). The history of the vegetation and flora of Widdybank Fell and the Cow Green reservoir basin, Upper Teesdale, *Philosophical Transactions of the Royal Society of London. Series B, Biological Sciences* **265**(870): 327–408.

Turner, J., Innes, J. B. and Simmons, I. G. (1993). Spatial diversity in the mid-Flandrian vegetation history of North Gill, North Yorkshire, *New phytologist* **123**(3): 599–647.

van den Bogaard, P. (1995). $^{40}Ar/^{39}Ar$ ages of sanidine phenocrysts from Laacher See Tephra (12,900 yr BP): Chronostratigraphic and petrological significance, *Earth and Planetary Science Letters* **133**(1-2): 163–174.

Van Strydonck, M., De Moor, A. and Benazeth, D. (2004). $^{14}C$ dating compared to art historical dating of Roman and Coptic textiles from Egypt, *Radiocarbon* **46**(1): 231–244.

Vanpaemel, W. (2010). Prior sensitivity in theory testing: An apologia for the Bayes factor, *Journal of Mathematical Psychology* **54**(6): 491–498.

von Post, L. (1946). The prospect for pollen analysis in the study of the earth's climatic history, *New Phytologist* **45**(2): 193–217.

Waddell, J. (1990). *The Bronze Age Burials of Ireland*, Galway University Press.

Walker, M. J. C. (2005). *Quaternary dating methods*, John Wiley & Sons, England.

Walker, R. (1978). Diatom and pollen studies of a sediment profile from Melynllyn, a mountain tarn in Snowdonia, North Wales, *New Phytologist* **81**(3): 791–804.

Waller, M. P. (1993). Flandrian vegetational history of south-eastern England. Pollen data from Pannel Bridge, East Sussex, *New phytologist* **124**(2): 345–369.

Waller, M. P., Long, A. J. and Schofield, J. E. (2006). Interpretation of radiocarbon dates from the upper surface of late-Holocene peat layers in coastal lowlands, *The Holocene* **16**(1): 51–61.

Ward, G. K. and Wilson, S. R. (1978). Procedures for comparing and combining radiocarbon age determinations: a critique, *Archaeometry* **20**(1): 19–31.

Weinstock, B. (1969). Carbon monoxide: residence time in the atmosphere, *Science* **166**(3902): 224–225.

Weninger, B. and Jöris, O. (2008). A $^{14}$C age calibration curve for the last 60 ka: the Greenland-Hulu U/Th timescale and its impact on understanding the Middle to Upper Paleolithic transition in Western Eurasia, *Journal of Human Evolution* **55**(5): 772–781.

Whittington, G., Edwards, K. J. and Cundill, P. R. (1991). Palaeoecological investigations of multiple elm declines at a site in north Fife, Scotland, *Journal of biogeography* **18**(1): 71–87.

Wiggins, K., Higgins, V. and Power, C. (2000). A rescue excavation on Rathlin Island, County Antrim, *Ulster Journal of Archaeology* **59**: 47–70.

Wightman, G. J. (1990). The myth of Solomon, *Bulletin of the American Schools of Oriental Research* pp. 5–22.

Williams, B. B. (1987). A Bronze Age burial at Shanco, Co. Fermanagh, *Ulster Journal of Archaeology* **50**: 134–136.

Williams, C. T. and Switsur, V. R. (1985). *Mesolithic exploitation patterns in the Central Pennines: a palynological study of Soyland Moor*, British Archaeological Reports. British Series 139.

Williams, J. B. (1989). Examination of freshwater peat pretreatment methodology, *Radiocarbon* **31**(3): 269–275.

Williams, R. G. and Johnson, A. S. (1976). Birmingham University radiocarbon dates X, *Radiocarbon* **18**(3): 249–267.

Wohlfarth, B. and Possnert, G. (2000). AMS radiocarbon measurements from the Swedish varved clays, *Radiocarbon* **42**(3): 323–333.

Wulf, S., Kraml, M., Kuhn, T., Schwarz, M., Inthorn, M., Keller, J., Kuscu, I. and Halbach, P. (2002). Marine tephra from the Cape Riva eruption (22 ka) of Santorini in the Sea of Marmara, *Marine geology* **183**(1): 131–141.

Yadin, Y. (1970). Megiddo of the Kings of Israel, *The Biblical Archaeologist* **33**(3): 66–96.

Zeidler, J. A., Buck, C. E. and Litton, C. D. (1998). Integration of archaeological phase information and radiocarbon results from the Jama River Valley, Ecuador: a Bayesian approach, *Latin American Antiquity* **9**: 160–179.

Zimhoni, O. (1997). *Studies in the Iron age pottery of Israel: typological, archaeological, and chronological aspects*, Tel Aviv University, Institute of Archaeology.

# Appendix A

# Computer program listings

Programs for radiocarbon calibration (Section 3.4.1), and for obtaining the trapezoidal prior measures for the case studies (Sections 7.1, 7.2, and Chapter 9) are listed below. Annotations can be found throughout the listings after a doubleslash (`//`) which is the `C++` command that tells the compiler to ignore everything that follows, until the end of the line. Programs for investigating trapezoidal model constraints (chapter 5); for modelling with the uniform and the sigmoidal phase priors, and for calculating the histograms for prior measures were also written but they are not listed here. This is because the listings for investigating model constraints, the uniform, and the sigmoidal model are very similar to that of the trapezoidal phase prior, and annotations (after `//`) are added to section A.2 where the code is different; and the tabulated frequencies from the latter program are exactly the same as those obtained from Microsoft® Office Excel® 2007 with the same bin sizes. The purpose of writing a separate program for calculating the frequencies of a histogram was to speed up the process. Using Microsoft Office Excel to analyse a data set of 2 million takes a long time. The bins and their corresponding frequencies are imported into `OxCal` as `.prior` files and are plotted there.

A lot of time was invested in the work described in this appendix due to the lack of previous programming experience. The function for calculating the trapezoidal phase prior listed below was adapted from Karlsberg (2006), since the mathematics

of the prior is the same. The computing language C++ was chosen for fast computing time.

The trapezoidal phase model has also been implemented independently in OxCal by Bronk Ramsey in order to make use of the different OxCal functions, for example outlier analysis, in different case studies. Results from OxCal for a simple trapezoidal phase model are the same as the results from the implementation in this appendix.

## A.1 Radiocarbon calibration

The code for radiocarbon calibration is very straightforward. It uses equation (3.5) from section 3.4.1. An animated version of radiocarbon calibration can be seen on Dr. Maarten Blaauw's website: http://chrono.qub.ac.uk/blaauw/. The program listed in this section gives the same likelihood distributions as OxCal.

The outputs of this program have two columns, one for bins and one for bin frequencies. They can be used by the program below for modelling with trapezoidal phases directly without additional alterations.

### Main program

```
// an example for calibrating 3 radiocarbon determinations
#include "calibrate.h"
int main(){
  calibrate("OxA-5186",2840,40);
  calibrate("OxA-5185",2770,50);
  calibrate("OxA-5184",2830,65);
  return 0;
}
```

### Headers

```
double calibrate(const char*filename,unsigned long DATE,double UNCERTAINTY);
```

### Functions

```
#include <cmath>
#include <iostream>
#include <fstream>
#include <vector>
#include "calibrate.h"

double calibrate(const char*filename,unsigned long DATE,double UNCERTAINTY){
// opens calibration curve file for input
  std::ifstream curve("curve\\IntCal09.txt");
// instantiating std::vector for curve data
```

```
  std::vector<double>vecX;
  std::vector<double>vecY;
  std::vector<double>vecZ;
// reads in data from calibration curve file
  if(curve==NULL){
    std::cerr << "Failed to open input data file: \"" << strerror(errno) << "\"\n";
    return 1;
  }
  else{
    while(! curve.eof()){
      double x,y,z;
      curve >> x >> y >> z;
      vecX.push_back(x);
      vecY.push_back(y);
      vecZ.push_back(z);
    }
  }
  curve.close(); // closing the opened files
// modelled dates
  std::vector<double>vecUNMOD;
  std::vector<double>vecLIKELIHOOD;
// before setting the number of loops-count the number of data points.
// calibrating the radiocarbon dates
  std::vector<double>::iterator iX=vecX.begin();
  std::vector<double>::iterator iY=vecY.begin();
  std::vector<double>::iterator iZ=vecZ.begin();
  while(iX!=vecX.end()&&iY!=vecY.end()&&iZ!=vecZ.end()){
    double sigma=pow(*iZ,2)+pow(UNCERTAINTY,2);
    double b=exp(-(pow((*iY-DATE),2))/(2*sigma))/sqrt(sigma);
    if(b!=0){
      vecLIKELIHOOD.push_back(b);
      vecUNMOD.push_back(*iX);
    }
// increment
    ++ iX;
    ++ iY;
    ++ iZ;
  }
// output into files
  std::ofstream fout(filename,std::ios::app);
  if(!fout){
    std::cout << "Unable to open " << filename <<  "for appending.\n";
    return 1;
  }
  std::vector<double>::iterator iUNMOD=vecUNMOD.begin();
  std::vector<double>::iterator iLIKELIHOOD=vecLIKELIHOOD.begin();
  while(iUNMOD!=vecUNMOD.end()&&iLIKELIHOOD!=vecLIKELIHOOD.end()){
    fout << *iUNMOD << "\t" << *iLIKELIHOOD << std::endl;
    ++ iUNMOD;
    ++ iLIKELIHOOD;
  }
  fout.close();
}
```

## A.2 Trapezoidal phase prior

The code for the trapezoidal phase prior has been written to interact with the user. It is designed for modelling contiguous multiple phases, since it is the framework introduced in chapter 5, which was later used in sections 7.2 and 7.3. The program asks the user to input the number of phases, the number of events in each phase, and the name for each file for model parameter output, before running the analysis. In other case studies where overlapping, independent phases were used, individual phases

were modelled separately. The limits prior is not implemented in here because the trapezoidal phases implemented in this thesis were either contiguous, or independent. In a model with $n$ phases, there are $n + 1$ output files at the end of the model run, one for each set of trapezoidal model parameters (`boundary` and `transition`).

The program has a limit of two million iterations (a minimum of one million iterations were recommended by Karlsberg 2006). No convergence checker has been built into the program.

## Main program

```
#include "random.h"
#include "sampleNorm.h"
#include "trap.h"
#include <iostream>
#include <fstream>
#include <string>
#include <vector>
#include <map>
#include <algorithm>
#include <ctime>
#include <cmath>

typedef std::map<double,double>yearProb;
typedef std::pair<double,double>PAIR;
typedef std::vector<yearProb>group;
typedef std::vector<PAIR>vecPAIR;
typedef std::vector<vecPAIR>VECPAIR;

double getProbOfYear(yearProb&curve,double year);
double AcceptReject(double mh,double newValue,double old);
void updateDate(Trapezoid&Trap,dateCurve&curve,PAIR&phase,int p);

int main(){
  srand(CLOCKS_PER_SEC);
  std::vector <group>Phase;
  int nPHASES;
  std::cout << "Enter the number of phases: ";
  std::cin >> nPHASES;
  int nDATASET[nPHASES];
  for(int phase=0;phase<nPHASES;phase++){
    std::cout << "Enter the number of events in Phase " <<(phase+1) << ": ";
    std::cin >> nDATASET[phase];
  }

// open the calibrated data files
// calibrated ages are not needed for testing the trapezoidal model constraints.
// calibrated ages are also not needed for modelling tombstone simulation (chapter 5),
// instead, single data points are used.  Single data points are imported into the
// program using a vector.

  for(int phase=0;phase<nPHASES;phase++){
    group vecDATA;
    for(int k=0;k<nDATASET[phase];k++){
      char filename[30];
      std::cout << "Enter the name of file to be used in Phase " <<(phase+1) << ": ";
      std::cin >> filename;
      std::ifstream Data(filename);
      if(Data==NULL){
        std::cerr << "Failed to open input data file: \"" << strerror(errno) << "\"\n";
```

```
        return 1;
      }
      yearProb read;
      while(!Data.eof()){
        double year,prob;
        Data >> year >> prob;
        read.insert(std::pair<double,double>(year,prob));
      }
      Data.close();
      vecDATA.push_back(read);
    }
    Phase.push_back(vecDATA);
  }
/************* END OF PUTTING CALIBRATED DATA INTO VECTORS *****************/
// initiate Trapezoid for each phase
  FILE*TrapInit;
  TrapInit=fopen("INIT","w");
  Trapezoid Trap(nPHASES);
  for(int p=0;p<nPHASES;p++){Trap.initTrap(TrapInit,phase,nDATASET,p);}
  fclose(TrapInit);

// initiate individual events
// do not need to initiate events for modelling tombstone simulation (chapter 5)
// do not need to initiate events when testing model constraints with no events
  VECPAIR PHASE;
  for(int p=0;p<nPHASES;p++){
    vecPAIR GROUP;
    for(int k=0;k<nDATASET[p];k++){
      PAIR read;
      read.first=random(Phase.at(p).at(k).begin()->first,phase.at(p).at(k).end()->first);
      read.second=getProbOfYear(Phase.at(p)[k],read.first);
      GROUP.push_back(read);
    }
    PHASE.push_back(GROUP);
  }
  FILE*Boundary[nPHASES+1];
  char file[30];
  for(int p=0;p<(nPHASES+1);p++){
    if(p==0){
      std::cout << "Phase " <<(p+1) << " Front Boundary filename: ";
      std::cin >> file;
      Boundary[p]=fopen(file,"w");
    }
    else if(p==nPHASES){
      std::cout << "Phase " <<(p) << " End Boundary filename: ";
      std::cin >> file;
      Boundary[p]=fopen(file,"w");
    }
    else{
      std::cout << "Phase " << p << " / " <<(p+1) << " Boundary filename: ";
      std::cin >> file;
      Boundary[p]=fopen(file,"w");
    }
  }
  std::cout << "Please wait";
  for(int j=0;j<2000000;j++){
    if(j % 100000==0){std::cout << ".";}
// do not need to updateDate() when modelling with no events
// do not need to updateDate() when modelling tombstone simulation
    Trap.ModPara(Boundary[0],phase,nDATASET[0],0,j);
    for(int k=0;k<nDATASET[0];k++){updateDate(Trap,phase.at(0)[k],PHASE.at(0)[k],0);}
    for(int p=1;p<nPHASES;p++){
      Trap.ModPara(Boundary[p],PHASE,nDATASET[p-1],nDATASET[p],p-1,p,j);
      for(int k=0;k<nDATASET[p];k++){updateDate(Trap,phase.at(p)[k],PHASE.at(p)[k],p);}
    }
    Trap.ModPara(Boundary[nPHASES],PHASE,nDATASET[nPHASES-1],nPHASES-1,j);
  }// closes j loop
  for(int p=0;p<(nPHASES+1);p++){fclose(Boundary[p]);}
  return 0;
}
```

# Headers

```
// Header functions for random number generator random.h
double random();
double random(double a,double b);
double random(double a);

// Header functions for sampling from a normal distribution within 3 std
double sample(double mu,double sig);
double invert(double prob,double mu,double sig);

// Header functions for the trapezoidal prior model
#include <vector>
#include <map>
#include <algorithm>
#include <cmath>

typedef std::map<double,double>dateCurve;
typedef std::pair<double,double>PAIR;
typedef std::vector<dateCurve>group;
typedef std::vector<PAIR>vecPAIR;

class Trapezoid {
  public:
  Trapezoid(int n){
    Ta=new double [n];
    Tb=new double [n];
    Wa=new double [n];
    Wb=new double [n];
    nPHASES=n;
  }

  ~Trapezoid(){
    delete [] Ta;
    delete [] Tb;
    delete [] Wa;
    delete [] Wb;
  }

  void  initTrap(FILE*file,std::vector<group>&Phase,int nDATASET[],int p);
  void  updateT(FILE*file,VECPAIR&Date,int nDATASET,int p);
  void  updateT(FILE*file,VECPAIR&Date,int nP,int nQ,int p,int q);
  void  updateW(FILE*file,VECPAIR&Date,int nDATASET,int p);
  void  updateW(FILE*file,VECPAIR&Date,int nP,int nQ,int p,int q);
  void  ModPara(FILE*file,VECPAIR&Date,int nDATASET,int p,int k);
  void  ModPara(FILE*file,VECPAIR&Date,int nP,int nQ,int p,int q,int k);

  int  findMin(double*parameter);
  double  getFreq(double Date,int p);
  double  shape(double i,double height[],int p);
  double  sigmoid(double sig); // for the sigmoidal phase model
  double  frontCorner(int p){return(Ta[p]-Wa[p]);}
  double  backCorner(int p){return(Tb[p]+ Wb[p]);}

  private:
    int nPHASES;
    double*Ta;
    double*Tb;
    double*Wa;
    double*Wb;
    double T;
    double W;
};
```

# Functions

```
// functions for random(real) number generation
#include "random.h"
#include <cstdlib>

double random();
double random(double a,double b);
```

```
double random(double a);

double random(){return((double) rand() +0.5)/((double) RAND_MAX+1.0);}
double random(double a,double b){return(b-a)*random()+a;}
double random(double a){
  if(a<0){a=-a;}
  if(a==0){return 0};
  return long(random()*a)+1;
}

// functions for sampling from a normal distribution
#include "random.h"
#include "sampleNorm.h"
#include <cstdlib>

double sample(double mu,double sig);
double invert(double prob,double mu,double sig);

double sample(double mu,double sig){
  double z=random(-3.,3.); // sampling between 3 standard deviations
  double a=invert(z,mu,sig);
  return a;
}

double invert(double z,double mu,double sig){
  double x=z*sig+mu;
  return x;
}

// functions for the trapezoidal prior model
#include "random.h"
#include "trap.h"
#include "sampleNorm.h"
#include <cmath>
#include <map>
#include <vector>
#include <iostream>

typedef std::map<double,double>MAP;
typedef std::pair<double,double>PAIR;
typedef std::vector<MAP>group;
typedef std::vector<PAIR>vecPAIR;

double getDate(MAP&curve);
double getProbOfYear(MAP&curve,double year);
double findFrontDate(group&calDate,int&nDATASET);
double findDate(group&phaseFront,group&phaseBehind,int nFront,int nBehind);
double findEndDate(group&calDate,int&nDATASET);
void updateDate(Trapezoid&Trap,MAP&curve,PAIR&phase,int p);
double AcceptReject(double mh,double newValue,double old);

double getDate(MAP&curve){
// finds the year with the highest probability in each calibration
  MAP::const_iterator it;
  double highVal=0;
  double highDate;
  for(it=curve.begin();it !=curve.end();it++){
    if(it->second>highVal){
      highVal=it->second;
      highDate=it->first;
    }
  }
  return highDate;
}

double getProbOfYear(MAP&curve,double year){
  MAP::iterator it;
  it=curve.lower_bound(year);
  if(it->first==year){return it->second;}
  if(it==curve.end()||it==curve.begin()){return 0;}
//Now we're pointing to at least one into the list
//Not the start.
```

```
  double date=it->first;
  double freq=it->second;
  it++;
  double prob=(year-date)/((it->first)-date);
  prob=prob*((it->second)-freq);
  if(prob<0){prob=-prob;}
  prob=prob+freq;
  return prob;
}

double findFrontDate(group&calDate,int&nDATASET){
// compares the years with the highest prob and finds the earliest date
  double frontDate=2010;
  double curveDate[nDATASET];
  for(int j=0;j<nDATASET;j++){
    curveDate[j]=getDate(calDate[j]);
    if(curveDate[j]<frontDate){frontDate=curveDate[j];}
  }
  return frontDate;
}

double findDate(group&phaseFront,group&phaseBehind,int nFront,int nBehind){
  double frontDate=findFrontDate(phaseBehind,nBehind);
  double endDate=findEndDate(phaseFront,nFront);
  double midPoint=(frontDate+endDate)/2;
  return midPoint;
}

double findEndDate(group&calDate,int&nDATASET){
// compares the years with the highest prob and finds the latest date
  double endDate=-60000;
  double curveDate[nDATASET];
  for(int j=0;j<nDATASET;j++){
    curveDate[j]=getDate(calDate[j]);
    if(curveDate[j]>endDate){endDate=curveDate[j];}
  }
  return endDate;
}

void updateDate(Trapezoid&Trap,MAP&curve,PAIR&date,int p){
  double newDate=random(Trap.frontCorner(p),Trap.backCorner(p));
  double ratio=Trap.getFreq(newDate,p)/Trap.getFreq(date.first,p);
  double newProb=getProbOfYear(curve,newDate);
  double likelihoodRatio=newProb/date.second;
  double mh=ratio*likelihoodRatio;
  double a=random(0.0,1.0);
  if(a<mh){
    date.first=newDate;
    date.second=newProb;
  }
}

double AcceptReject(double mh,double newValue,double old){
  double a=random(0.0,1.0);
  if(a<mh){return newValue;}// acceptance
  return old;// rejection
}

void Trapezoid::initTrap(FILE*file,std::vector<group>&Phase,int nDATASET[],int p){
// in the first phase
  if(p==0){Ta[0]=findFrontDate(Phase.at(p),nDATASET[p]);}
// in the last phase
  if(p==(nPHASES-1)){Tb[nPHASES-1]=findEndDate(Phase.at(p),nDATASET[p]);}
  else{// not the first/last phase
    Tb[p]=findDate(Phase.at(p),Phase.at(p+1),nDATASET[p],nDATASET[p+1]);
    Ta[p+1]=Tb[p];
  }

// in the first phase
  if(p==0){Wa[p]=random(0,(Tb[p]-Ta[p]));}
  else{
    if((Ta[p]-Ta[p-1]-Wa[p-1])<(Tb[p]-Ta[p])){Wa[p]=random(0,(Ta[p]-Ta[p-1]-Wa[p-1]));}
```

```
    else{Wa[p]=random(0,(Tb[p]-Ta[p]));}
    Wb[p-1]=Wa[p];
  }
// in the last phase
  if(p==(nPHASES-1)){Wb[p]=random(0,(Tb[p]-Ta[p]-Wa[p]));}
  T=Ta[0];
  W=Wa[0];
  fprintf(file,"%f \t %f \t %f \t %f \n",Ta[p],2*Wa[p],Tb[p],2*Wb[p]);
}

void Trapezoid::updateT(FILE*file,std:: vector<vecPAIR>&Date,int nDATASET,int p){
  double freq[nDATASET];
  double D=0,Dj=0,Top=0,Topj=0;
  for(int k=0;k<nDATASET;k++){freq[k]=getFreq(Date.at(p)[k].first,p);}

  for(int i=0;i<nPHASES;i++){D=D+Wa[i];}
  D=2*(D+Wb[nPHASES-1]);
  Top=Tb[nPHASES-1]+Wb[nPHASES-1]-Ta[0]+Wa[0]-D;
  double utp=pow(D,nPHASES)*pow(Top,(nPHASES-1))*(D+Top);

  double newT=sample(T,25);
  enum SIDE{FRONT,END };
  SIDE side;
  if(T==Ta[0]){
    Ta[0]=newT;
    side=FRONT;
  }
  else{
    Tb[nPHASES-1]=newT;
    side=END;
  }

  for(int i=0;i<nPHASES;i++){Dj=Dj+Wa[i];}
  Dj=2*(Dj+Wb[nPHASES-1]);
  Topj=Tb[nPHASES-1]+Wb[nPHASES-1]-Ta[0]+Wa[0]-Dj;
  utp=utp /(pow(Dj,nPHASES)*pow(Topj,(nPHASES-1))*(Dj+Topj));
  enum CONSTRAINT{REJECT,ACCEPT };
  CONSTRAINT constraint;
  if((Tb[p]-Ta[p])<(Wa[p]+Wb[p])){constraint=REJECT;}
  if(constraint==REJECT){newT=T;}
  else{
    double ratio=1;
    for(int k=0;k<nDATASET;k++){ratio*=(getFreq(Date.at(p)[k].first,p)/freq[k]);}
// calculates the Metropolis Hastings ratio
    double t_mh=ratio*utp;
    newT=AcceptReject(t_mh,newT,T);
  }
  fprintf(file,"%f \t",newT);
  if(side==FRONT){
    Ta[0]=newT;
    T=Tb[nPHASES-1];
  }
  else{
    Tb[nPHASES-1]=newT;
    T=Ta[0];
  }
}

void Trapezoid::updateT(FILE*file,VECPAIR&Date,int nP,int nQ,int p,int q){
  double freqP[nP],freqQ[nQ];
  for(int k=0;k<nP;k++){freqP[k]=getFreq(Date.at(p)[k].first,p);}
  for(int k=0;k<nQ;k++){freqQ[k]=getFreq(Date.at(q)[k].first,q);}
  double oldT=Tb[p];
  double newT=sample(oldT,25);
  Tb[p]=newT;
  Ta[q]=newT;

  enum CONSTRAINT{REJECT,ACCEPT };
  CONSTRAINT constraint;
  if(((Tb[p]-Ta[p])<(Wa[p]+Wb[p]))||
   ((Tb[q]-Ta[q])<(Wa[q]+Wb[q]))){
    constraint=REJECT;
```

```
  }
  if(constraint==REJECT){newT=oldT;}
  else{
    double ratioP=1;
    double ratioQ=1;
    for(int k=0;k<nP;k++){ratioP*=(getFreq(Date.at(p)[k].first,p)/freqP[k]);}
    for(int k=0;k<nQ;k++){ratioQ*=(getFreq(Date.at(q)[k].first,q)/freqQ[k]);}
// calculates the Metropolis Hastings ratio
    double t_mh=ratioP*ratioQ;
    newT=AcceptReject(t_mh,newT,oldT);
  }
  fprintf(file,"%f \t",newT);
  Tb[p]=newT;
  Ta[q]=newT;
}

// There are no transition parameters in the uniform phase model so the following 2
// updateW(); functions are redundant in the listings for the uniform phase model.
void Trapezoid::updateW(FILE*file,VECPAIR&Date,int nDATASET,int p){
  double freq[nDATASET];
  double Dur=0,Durj=0,Top=0,Topj=0;
  for(int k=0;k<nDATASET;k++){freq[k]=getFreq(Date.at(p)[k].first,p);}
  for(int i=0;i<nPHASES;i++){Dur=Dur+Wa[i];}
  Dur=2*(Dur+Wb[nPHASES-1]);
  Top=Tb[nPHASES-1]+Wb[nPHASES-1]-Ta[0]+Wa[0]-Dur;

  double utp=(pow(Dur,nPHASES)*pow(Top,(nPHASES-1))*(Dur+Top));
  double newW=sample(W,25);

  enum SIDE{FRONT,END};
  SIDE side;
  if(W==Wa[0]){
    Wa[0]=newW;
    side=FRONT;
  }
  else{
    Wb[nPHASES-1]=newW;
    side=END;
  }

  for(int i=0;i<nPHASES;i++){Durj=Durj+Wa[i];}
  Durj=2*(Durj+Wb[nPHASES-1]);
  Topj=Tb[nPHASES-1]+Wb[nPHASES-1]-Ta[0]+Wa[0]-Durj;

  enum CONSTRAINT{REJECT,ACCEPT};
  CONSTRAINT constraint;
  if((newW<0)||((Wb[p]+Wa[p])>(Tb[p]-Ta[p])))
    constraint=REJECT;
  if(constraint==REJECT) newW=W;
  else{
    utp=utp /(pow(Durj,nPHASES)*pow(Topj,(nPHASES-1))*(Durj+Topj));
    double ratio=1;
    for(int k=0;k<nDATASET;k++){ratio*=(getFreq(Date.at(p)[k].first,p)/freq[k]);}
// calculates the Metropolis Hastings ratio
    double w_mh=ratio*utp;
    newW=AcceptReject(w_mh,newW,W);
  }
  fprintf(file,"%f \t",2*newW);
  if(side==FRONT){
    Wa[0]=newW;
    W=Wb[nPHASES-1];
  }
  else{
    Wb[nPHASES-1]=newW;
    W=Wa[0];
  }
}

void Trapezoid::updateW(FILE*file,VECPAIR&Date,int nP,int nQ,int p,int q){
  double freqP[nP],freqQ[nQ];
  double Dur=0,Durj=0,Top=0,Topj=0;
```

```
  for(int k=0;k<nP;k++){freqP[k]=getFreq(Date.at(p)[k].first,p);}
  for(int k=0;k<nQ;k++){freqQ[k]=getFreq(Date.at(q)[k].first,q);}
  for(int i=0;i<nPHASES;i++){Dur=Dur+Wa[i];}
  Dur=2*(Dur+Wb[nPHASES-1]);
  Top=Tb[nPHASES-1]+Wb[nPHASES-1]-Ta[0]+Wa[0]-Dur;

  double utp=(pow(Dur,nPHASES)*pow(Top,(nPHASES-1))*(Dur+Top));
  double oldW=Wb[p];
  double newW=sample(oldW,25);
  enum CONSTRAINT{REJECT,ACCEPT};
  CONSTRAINT constraint;
  if((newW<0)||((newW+Wa[p])>(Tb[p]-Ta[p]))||((Wb[q]+newW)>(Tb[q]-Ta[q])))
    constraint=REJECT;
  if(constraint==REJECT){newW=oldW;}
  else{
    Wb[p]=newW;
    Wa[q]=newW;
    for(int i=0;i<nPHASES;i++){Durj=Durj+Wa[i];}
    Durj=2*(Durj+Wb[nPHASES-1]);
    Topj=Tb[nPHASES-1]+Wb[nPHASES-1]-Ta[0]+Wa[0]-Durj;
    utp=utp /(pow(Durj,nPHASES)*pow(Topj,(nPHASES-1))*(Durj+Topj));
    double ratioP=1;
    double ratioQ=1;
    for(int k=0;k<nP;k++){ratioP*=(getFreq(Date.at(p)[k].first,p)/freqP[k]);}
    for(int k=0;k<nQ;k++){ratioQ*=(getFreq(Date.at(q)[k].first,q)/freqQ[k]);}

// calculates the Metropolis Hastings ratio
    double w_mh=ratioP*ratioQ*utp;
    newW=AcceptReject(w_mh,newW,oldW);
  }
  fprintf(file,"%f \t",2*newW);
  Wb[p]=newW;
  Wa[q]=newW;
}

void Trapezoid::ModPara(FILE*file,VECPAIR&Date,int nDATASET,int p,int k){
  updateT(file,date,nDATASET,p);
  updateW(file,date,nDATASET,p);
  fprintf(file,"\n");
}

void Trapezoid::ModPara(FILE*file,VECPAIR&Date,int nP,int nQ,int p,int q,int k){
  updateT(file,date, nP, nQ, p,q);
  updateW(file,date, nP, nQ, p,q);
  fprintf(file,"\n");
}

double Trapezoid::getFreq(double Date,int p){
  double h,density;

  if(!(Tb[p]-Ta[p])==0){h=1 /(Tb[p]-Ta[p]);}
  else{h=0;}
// for the trapezoidal phase prior
  double height[4]={0,h,h,0};
  if((Wa[p]+Wb[p])<(Tb[p]-Ta[p])){density=shape(Date,height,p);}
// for the uniform phase prior
  if(Ta[p]<=Date&&Tb[p] >Date)
    return h;
  else{density=0;}
  return density;
}

double Trapezoid::shape(double i,double height[],int q){
  double z,ans;
  double *p;
  p=new double [5];
  p[1]=Ta[q]-Wa[q];
  p[2]=Ta[q]+Wa[q];
  p[3]=Tb[q]-Wb[q];
  p[4]=Tb[q]+Wb[q];

  while(true){
```

```
    if(p[1]<p[2]&&p[2]<p[3]&&p[3]<p[4]){
      if(!((p[1]<=i)&&(i<=p[4]))){ans=0;}
      else{
        for(int c=1;c<4;c++){ // (Karlsberg, 2006)
          if(p[c]<=i&&p[c+1]>i){
// for the trapezoidal phase model
            z=(height[c]-height[c-1])/(p[c+1]-p[c]);
            ans=height[c-1]+z*(i-p[c]);
// for the sigmoidal phase model
//          if(c==1){ans=height[c]*sigmoid((i-p[c])/(p[c+1]-p[c]));}
//          else if(c==2){density=height[c];}
//          if(c==3){density=height[c-1]*sigmoid((p[c]-i)/(p[c+1]-p[c]));}
          }
        }
      }
    }
    else{ans=0;}
    delete [] p;
    return ans;
    break;
  }
}

int Trapezoid::findMin(double*parameter){
  double min=parameter[0];
  int where=0;
  for(int k=0;k<nPHASES;k++){
    if(min<parameter[k]){
      min=parameter[k];
      where=k;
    }
  }
  return where;
}

double Trapezoid::sigmoid(double sig){
       double shape=pow(sig,2)/(pow(sig,2)+pow((1-sig),2));
       return shape;
}
```

# Appendix B

# Data

## B.1 British Bronze Age Metalwork

| Sub-division | Lab. no. | $^{14}$C deetermination | Uncertainty |
|---|---|---|---|
| Acton & Taunton | OxA-5948 | 3225 | 65 |
| | OxA-5196 | 3035 | 40 |
| | OxA-4651 | 3220 | 80 |
| | OxA-6177 | 3055 | 50 |
| | OxA-5949 | 3110 | 50 |
| Penard | OxA-5187 | 3045 | 55 |
| | OxA-5959 | 2965 | 45 |
| | OxA-1526 | 3030 | 100 |
| | OxA-5183 | 2930 | 40 |
| | OxA-5953 | 3015 | 45 |
| | OxA-4653 | 2910 | 55 |
| | OxA-5951 | 2980 | 45 |
| | OxA-5950 | 2910 | 45 |
| | OxA-4504 | 2965 | 65 |
| | HAR-2940 | 3020 | 70 |
| | OxA-5952 | 2965 | 45 |
| Wilburton | OxA-4656 | 3005 | 75 |
| | OxA-5955 | 2900 | 45 |
| | OxA-4503 | 2930 | 55 |
| | OxA-5035 | 2900 | 45 |
| | OxA-4502 | 2925 | 50 |
| | OxA-5034 | 2890 | 45 |
| | OxA-5036 | 2920 | 50 |
| | OxA-5956 | 2850 | 50 |
| | OxA-5197 | 2910 | 50 |
| | OxA-5198 | 2820 | 70 |
| Blackmoor | OxA-5186 | 2840 | 40 |
| | OxA-5184 | 2830 | 65 |
| | OxA-5185 | 2770 | 50 |
| Ewart Park | OxA-5957 | 2810 | 45 |
| | OxA-4716 | 2780 | 50 |
| | OxA-4654 | 2765 | 45 |
| | OxA-5976 | 2740 | 45 |
| | OxA-4652 | 2720 | 45 |
| | BM-798 | 2704 | 45 |
| | OxA-5962 | 2685 | 60 |
| | OxA-6176 | 2655 | 50 |
| | OxA-5977 | 2620 | 45 |

Table B.1: Radiocarbon determinations of the organic materials and their associated Bronze age assemblages from Needham et al. (1997).

## B.2 Early Bronze Age Irish bowls

| Site | Lab. no. | $^{14}$C determination | Uncertainty | Material | Reference |
|---|---|---|---|---|---|
| Lug | GrA-24309 | 3575 | 40 | Collagen | Waddell (1990) |
| Ardballymore | GrA-24175 | 3695 | 40 | Carbonate | |
| Stonepark | GrN-11356 | 3665 | 35 | Collagen | |
| Treanmacmurtagh | GrN-12274 | 3550 | 40 | Collagen | |
| Altanagh | GrN-11450* | 2900 | 100 | Charcoal | |
| Donaghanie | GrA-14793 | 3690 | 40 | Carbonate | |
| Dungate | GrN-13581 | 3670 | 30 | Collagen | |
| Ballybrennan | GrA-24139 | 3650 | 40 | Collagen | |
| | GrA-24179 | 3660 | 40 | Carbonate | |
| Milltown | GrN-11903 | 3755 | 35 | Collagen | |
| Rathbennett | GrA-14822 | 3550 | 40 | Carbonate | |
| Redmondstown | GrA-24154* | 3310 | 80 | Unspecified | |
| Riverstown | GrN-9322 | 3645 | 30 | Collagen | |
| Sonnagh Demesne | GrA-24192 | 3580 | 70 | Carbonate | |
| Bolinready | GrN-9321 | 3620 | 60 | Collagen | |
| Dillonsdown | GrA-13330* | 3730 | 50 | Carbonate | |
| | OxA-2672 | 3660 | 70 | Collagen | |
| Haylands | OxA-2669 | 3580 | 70 | Collagen | |
| | GrN-11901* | 4095 | 30 | Collagen | |
| Grange | GrA-14751 | 3620 | 40 | Carbonate | Ríordáin et al. (1997) |
| | GrA-13331* | 3600 | 40 | Carbonate | |
| | OxA-2761 | 3620 | 80 | Collagen | |
| | GrA-13332* | 3770 | 70 | Carbonate | |
| | OxA-1664 | 3770 | 70 | Colagen | |
| | GrA-14752 | 3700 | 40 | Carbonate | |
| | GrA-14753 | 3740 | 40 | Carbonate | |
| Corkey | GrA-5409 | 3680 | 50 | Collagen | Waddell (1990) |
| Rathlin Island | OxA-2675 | 3560 | 70 | Collagen | Wiggins et al. (2000) |
| | GrN-14616* | 4460 | 60 | Collagen | |
| Rathlin | OxA-2677 | 3690 | 70 | Collagen | |
| Kilinane | GrA-14801 | 3610 | 40 | Carbonate | Moore (1984) |
| Siguff | OxA-2671 | 3570 | 70 | Collagen | Waddell (1990) |
| | GrN-11352* | 3475 | 35 | Collagen | |
| Vermont | GrA-24158 | 3575 | 40 | Collagen | |
| Straid | GrN-15491* | 3810 | 40 | Collagen | Brannon et al. (1990) |
| | GrA-14825 | 3690 | 40 | Carbonate | |
| | GrN-15492* | 3840 | 35 | Collagen | |
| | GrN-15493* | 3845 | 40 | Collagen | |
| Bohullion | GrA-14641 | 3680 | 50 | Carbonate | Brindley (2007) |
| Lisnamulligan | OxA-2667 | 3640 | 70 | Collagen | |
| Glassamucky | GrN-11899 | 3765 | 40 | Collagen | Waddell (1990) |
| Rush | GrA-14071 | 3440 | 35 | Carbonate | |
| | GrA-24157 | 3670 | 40 | Collagen | |
| Anaghkeen | GrN-11355 | 3660 | 25 | Collagen | Waddell (1990) |
| Blackhil | OxA-2668 | 3770 | 70 | Collagen | |
| Halverstown | GrN-12958* | 3820 | 40 | Collagen | |
| Hartwell Upper | GrA-24152* | 935 | 35 | Collagen | |
| Oldtown | GrN-11902 | 3655 | 35 | Collagen | Mount et al. (1998) |
| Ploopluck | GrN-11353 | 3735 | 35 | Collagen | |
| Newtownbalregan | GrN-14613 | 3685 | 35 | Collagen | Manning (1987) |
| Timolin | GrN-11364 | 3700 | 30 | Collagen | Brindley (2007) |
| Baggotstown | GrA-24177 | 3495 | 40 | Carbonate | |
| Corrower | GrA-14794 | 3610 | 40 | Carbonate | Waddell (1990) |
| Betaghstown | GrN-11357 | 3745 | 30 | Collagen | |
| Keenoge | GrN-12272 | 3685 | 45 | Collagen | Mount and Buckley (1997) |
| | GrA-2133 | 3585 | 35 | Collagen | |
| | GrA-2132 | 3565 | 35 | Collagen | |
| | GrA-17385 | 3640 | 50 | Carbonate | |
| | GrA-2134 | 3610 | 35 | Collagen | |
| | GrN-9323* | 2790 | 35 | Collagen | Brindley (2007) |
| Shanco | GrN-14342 | 3675 | 30 | Collagen | Williams (1987) |
| Martinstown | GrA-24155 | 3670 | 40 | Collagen | Waddell (1990) |
| Tara | GrA-17195 | 3570 | 60 | Carbonate | O'Sullivan et al. (2005) |
| | GrA-17193 | 3600 | 60 | Carbonate | |
| Lehinch | GrA-24193* | 3360 | 45 | Carbonate | Brindley (2007) |

Table B.2: (continued)

| Site | Lab. no. | $^{14}$C determination | Uncertainty | Material | Reference |
|---|---|---|---|---|---|
| New Newry | GrN-11363* | 3240 | 30 | Collagen | Ó Ríordáin and Waddell (1993) |
| Graney West | UB-3987* | 3638 | 46 | Collagen | Mount et al. (1998) |
| | UB-3988* | 3595 | 34 | Collagen | |
| | UB-3989* | 1430 | 32 | Collagen | |
| Oldtown | UB-3985* | 3666 | 41 | Collagen | |
| | UB-3986* | 3565 | 43 | Collagen | |

Table B.2: Radiocarbon determinations of bones associated with the Early Bronze Age Irish bowl tradition (Brindley, 2007, Chap. 4). Rejected radiocarbon determinations are marked with an *.

## B.3 Iron Age in Israel

| Site | Stratum | Lab. no. | $^{14}$C determination | Uncertainty | Material | Reference |
|---|---|---|---|---|---|---|
| Megiddo | K/6 (=VIIA?) | RT-4501.3 | 2790 | 40 | Olive pits | Sharon et al. (2007) |
| | | RT-4501.4 | 2764 | 50 | | |
| | | RT-4501.5 | 2767 | 40 | | |
| | | RT-4499.3 | 2880 | 40 | | |
| | | RT-4499.4 | 2865 | 45 | | |
| | | RT-4499.5 | 2925 | 40 | | |
| | | RT-4499a | 2907 | 40 | | |
| | | RT-4499aa | 2876 | 40 | | |
| | | RT-5080 | 2965 | 30 | | Finkelstein and Piasetzky (2010b,c) |
| | | RT-5081 | 2955 | 35 | | |
| | | RT-5082 | 2975 | 55 | | |
| | | RT-5083 | 3030 | 150 | | |
| | | RT-5084 | 2980 | 60 | | |
| Tel Mique | VIIb | RT-4286.3 | 2950 | 55 | Seeds | Sharon et al. (2007) |
| | | RT-4286.4 | 2900 | 40 | | |
| | | RT-4286.5 | 2870 | 60 | | |
| Tell Keisan | | RT-3804.3 | 2960 | 35 | Charcoal | Sharon et al. (2007) |
| | | RT-3804.4 | 2997 | 35 | | |
| | | RT-3804.5 | 2996 | 35 | | |
| | | RT-3804a | 3022 | 50 | | |
| | | RT-3804aa | 2985 | 40 | | |
| Lachish | VI | RT-2912 | 2915 | 25 | Olive pits | Carmi and Ussishkin (2004) |
| | | RT-2755 | 2955 | 25 | | |
| | | RT-1417 | 2810 | 100 | Seeds | |
| Tel Rehov | D-6 | RT-3119* | 2685 | 40 | Olive stones | Mazar (2005) |
| | | GrN-26118 | 2920 | 30 | | |
| | | GrA-18826 | 2950 | 50 | | |
| | | GrA-19034 | 2935 | 45 | | |
| | | GrN-26120 | 2880 | 30 | | |

Table B.3: Radiocarbon determinations of samples from the Iron IA strata. Rejcted radiocarbon determinations are marked with *.

| Site | Stratum | Lab. no. | $^{14}$C determination | Uncertainty | Material | Reference |
|---|---|---|---|---|---|---|
| Tel Mique | VIB | RT-4283.3 | 2915 | 45 | Olive pits | Sharon et al. (2007) |
| | | RT-4283.4 | 2960 | 45 | | |
| | | RT-4283.5 | 2880 | 45 | | |
| | VB | RT-4284.3 | 2835 | 45 | Seeds | |
| | | RT-4284.4 | 2830 | 45 | | |
| Beth Shemesh | 6 | RT-3934.3 | 2830 | 50 | Olive pits | Sharon et al. (2007) |
| | | RT-3934.4 | 2925 | 50 | | |
| | | RT-3934.5 | 2810 | 50 | | |
| | 5 | RT-3935.3 | 2830 | 53 | | |
| | | RT-3935.4 | 2750 | 55 | | |
| | | RT-3935.5 | 2770 | 65 | | |
| | | RT-3936.3 | 2810 | 50 | | |
| | | RT-3936.4 | 2850 | 55 | | |
| | | RT-3936.5 | 2855 | 65 | | |
| Tel Dor | D2/13 | RT-4528.3 | 2883 | 47 | Olive pits | Sharon et al. (2007) |
| | | RT-4528.4 | 2910 | 39 | | |
| | | RT-4528.5 | 2930 | 42 | | |
| | D2/12 | RT-4522.3 | 2868 | 50 | | |
| | | RT-4522.4 | 2855 | 38 | | |
| | | RT-4522.5 | 2850 | 43 | | |
| | | RT-4525.3 | 2857 | 38 | | |
| | | RT-4525.4 | 2869 | 38 | | |
| | | RT-4525.5 | 2811 | 40 | | |
| Tel Rehov | D-4 | GrN-26121 | 2890 | 30 | Olive stones | Mazar (2005) |
| | | GrA-18825 | 2870 | 50 | | |
| | | RT-3809.4 | 2830 | 34 | | Sharon et al. (2007) |
| | | RT-3809.5 | 2861 | 35 | | |
| | | RT-3809a | 2889 | 35 | | |
| | | GrA-21046 | 2905 | 35 | Seeds | Mazar (2005) |
| | | GrA-21057 | 2945 | 35 | | |

Table B.4: (continued)

| Site | Stratum | Lab. no. | $^{14}$C determination | Uncertainty | Material | Reference |
|---|---|---|---|---|---|---|
| Tel Rehov | D-4 | GrA-21184 | 2920 | 50 | Seeds | Mazar (2005) |
| | | RT-3121* | 2800 | 40 | Olive stones | |
| | D-3 | RT-3120* | 2670 | 40 | | Sharon et al. (2007) |
| | | RT-3805.3 | 2774 | 35 | | |
| | | RT-3805.4 | 2811 | 34 | | |
| | | RT-3805.5 | 2816 | 35 | | |
| | | GrA-16757 | 2820 | 50 | | |
| | | GrA-19033 | 2835 | 45 | | Mazar (2005) |
| | | GrN-26119* | 2720 | 30 | | |
| | | GrA-12889 | 2870 | 70 | | |
| | | GrA-16848 | 2895 | 40 | Charcoal | |
| | | GrA-21044 | 2845 | 35 | Olive stones | |
| | | GrA-21056 | 2825 | 35 | | |
| | | GrA-21183 | 2820 | 50 | | |
| | | GrA-22302a | 2730 | 50 | | |
| | | GrA-22302b | 2820 | 40 | | |
| | | GrA-22329a | 2810 | 50 | | |
| | | GrA-22329b | 2760 | 40 | | |
| | | RT-5230 | 2884* | 34 | | Boaretto et al. (unpublished) |
| | | RT-5228 | 2836* | 35 | | |
| | | RT-5237 | 2782* | 66 | | |
| El-Akhwat | | RT-4270.3 | 2828 | 40 | Olive pits | Sharon et al. (2007) |
| | | RT-4270.4 | 2807 | 40 | | |
| | | RT-4270.5 | 2809 | 40 | | |
| | | RT-4271.3 | 2809 | 40 | | |
| | | RT-4271.4 | 2858 | 40 | | |
| | | RT-4271.5 | 2868 | 40 | | |
| | | RT-4272.3 | 2822 | 40 | | |
| | | RT-4272.4 | 2838 | 40 | | |
| | | RT-4272.5 | 2935 | 40 | | |
| | | RT-4273.3 | 2847 | 40 | | |
| | | RT-4273.4 | 2819 | 40 | | |
| | | RT-4273.5 | 2780 | 40 | | |
| Shiloh | V | RT-3928.3 | 2925 | 50 | Raisins | Sharon et al. (2007) |
| | | RT-3928.4 | 2885 | 35 | | |
| | | RT-3928.5 | 2895 | 40 | | |
| | | RT-3929.3 | 2965 | 40 | Seeds | |
| | | RT-3929.4 | 2935 | 65 | | |
| | | RT-3929.5 | 2965 | 50 | | |
| Tel Hevron | VII | RT-4147.1 | 3095 | 50 | Charcoal | Sharon et al. (2007) |
| | | RT-4147.3 | 3013 | 56 | | |
| | | RT-4147.4 | 2917 | 65 | | |
| | | RT-4147.5 | 2852 | 65 | | |
| | | RT-4148.1 | 3010 | 40 | | |
| | | RT-4148.3 | 3010 | 35 | | |
| | | RT-4148.4 | 2910 | 55 | | |
| | | RT-4148.5 | 3025 | 40 | | |
| | | RT-4148.6 | 2935 | 35 | | |
| Tel Minque | Vb | RT-4282.3 | 2895 | 55 | Olive pits | Sharon et al. (2007) |
| | | RT-4282.4 | 2835 | 40 | | |
| | | RT-4282.5 | 2900 | 50 | | |
| | | RT-4282a | 2872 | 40 | | |
| | | RT-4282aa | 2895 | 40 | | |
| Tel Dor | D2/9-10 | RT-4532.3 | 2788 | 38 | | Sharon et al. (2007) |
| | | RT-4532.4 | 2771 | 39 | | |
| | | RT-4532.5 | 2789 | 38 | | |
| | | RT-4531.3 | 2756 | 38 | | |
| | | RT-4531.4 | 2808 | 38 | | |
| | | RT-4531.5 | 2849 | 38 | | |
| | | GrA-25543 | 2769 | 40 | | |
| | | GrA-25712 | 2807 | 38 | | |
| | | GrA-25772 | 2832 | 45 | | |
| Megiddo | K/4 (=VIA) | RT-3939.3 | 2910 | 45 | Seeds | Sharon et al. (2007) |
| | | RT-3939.4 | 2790 | 40 | | |
| | | RT-3939.5 | 2735 | 40 | | |
| | | RT-3940.3 | 2760 | 40 | | |
| | | RT-3940.4 | 2770 | 40 | | |
| | | RT-3940.5 | 2775 | 55 | | |

Table B.4: (continued)

| Site | Stratum | Lab. no. | $^{14}$C determination | Uncertainty | Material | Reference |
|---|---|---|---|---|---|---|
| Megiddo | K/4 (=VIA) | RT-3943.3 | 3045 | 40 | Seeds | Sharon et al. (2007) |
| | | RT-3943.4 | 2860 | 40 | | |
| | | RT-3943.5 | 2845 | 40 | | |
| | | RT-3944.3 | 2975 | 60 | | |
| | | RT-3944.4 | 2980 | 50 | | |
| | | RT-3944.5 | 2905 | 60 | | |
| | | RT-3944a | 2865 | 40 | | |
| | | RT-3945a | 2858 | 40 | | |
| | | RT-3945aa | 2912 | 45 | | |
| | | RT-3946a | 2910 | 35 | | |
| | | RT-3946aa | 2904 | 40 | | |
| | | RT-3942.3 | 2845 | 37 | Olive pits | |
| | | RT-3942.4 | 2832 | 43 | | |
| | | RT-3942.5 | 2856 | 42 | | |
| | | RT-3942.6 | 2949 | 36 | | |
| Qasile | X | RT-3853.3 | 2680 | 35 | Lathyrus | Sharon et al. (2007) |
| | | RT-3853.4 | 2747 | 35 | | |
| | | RT-3853-1 | 2884 | 45 | | |
| | | RT-3931.1 | 2853 | 20 | | |
| | | RT-3931.3 | 3830 | 55 | | |
| | | RT-3931.4 | 2930 | 56 | | |
| | | RT-3931.5 | 2936 | 41 | | |
| | | RT-3931-1 | 2852 | 45 | | |
| | | GrA-25535 | 2864 | 40 | | |
| | | GrA-25710 | 2818 | 38 | | |
| | | GrA-25768 | 2897 | 44 | | |
| | | RT-3932.3 | 2745 | 50 | | |
| | | RT-3932.4 | 2765 | 75 | | |
| | | RT-3932.5 | 2685 | 50 | | |
| | | RT-3932.6 | 2650 | 40 | | |
| | | RT-3932a | 2780 | 35 | | |
| | | RT-3932aa | 2862 | 40 | | |
| Tel Hadar | IV | RT-3795.3 | 2791 | 52 | Seeds | Sharon et al. (2007) |
| | | RT-4291.3 | 2800 | 50 | | |
| | | RT-4291.4 | 2745 | 45 | | |
| | | RT-4291.5 | 2780 | 50 | | |
| | | RT-4291-3.1a | 2856 | 30 | | |
| | | RT-4291-3.1b | 2852 | 30 | | |
| | | RT-4291-3.2 | 2815 | 60 | | |
| | | RT-4291-5.1 | 2901 | 30 | | |
| | | RT-4291-4.1 | 2924 | 35 | | |
| Tell Keisan | 9a | RT-3803.1 | 2893 | 35 | Charcoal | Sharon et al. (2007) |
| | | RT-3803.3 | 2817 | 50 | | |
| | | RT-3803.4 | 2840 | 50 | | |
| | | RT-3803.6 | 2870 | 45 | | |
| | | RT-3803.7 | 2800 | 40 | | |
| | | RT-3803.8 | 2800 | 40 | | |
| | | RT-3803a | 2938 | 35 | | |
| | | RT-3803aa | 2862 | 65 | | |
| | | RT-3803.5 | 2997 | 35 | | |
| | | RT-3796.3 | 2870 | 40 | Seeds | |
| | | RT-3796.4 | 2875 | 70 | | |
| | | RT-3796.5 | 2820 | 50 | | |
| | 9a-b | RT-3802.3 | 2820 | 50 | Charcoal | |
| | | RT-3802.4 | 2820 | 50 | | |
| | | RT-3802.5 | 2885 | 50 | | |
| | 9b | RT-3801.1 | 2935 | 35 | | |
| | | RT-3801.3 | 2640 | 50 | | |
| | | RT-3801.4 | 2720 | 50 | | |
| | | RT-3801.5 | 1655 | 60 | | |
| Yoqneam | XVII(a) | RT-3779.1 | 2926 | 30 | Charcoal | Sharon et al. (2007) |
| | | RT-3779.3 | 2815 | 45 | | |
| | | RT-3779.4 | 2870 | 60 | | |
| | | RT-3779.5 | 2800 | 55 | | |
| | XVII(b) | RT-3777.1 | 2866 | 15 | Olive pits | |
| | | RT-3777.3 | 2830 | 60 | | |
| | | RT-3777.4 | 2910 | 45 | | |
| | | RT-3777.5 | 2790 | 80 | | |

| Site | Stratum | Lab. no. | $^{14}$C determination | Uncertainty | Material | Reference |
|---|---|---|---|---|---|---|
| Yoqneam | XVII(b) | RT-3778.1 | 2776 | 15 | Olive pits | Sharon et al. (2007) |
| | | RT-3778.3 | 2780 | 45 | | |
| | | RT-3778.4 | 2865 | 45 | | |
| | | RT-3778.5 | 2800 | 45 | | |
| | | RT-3778a | 2780 | 45 | | |
| | | RT-3778aa | 2855 | 40 | | |
| | | GrA-25534 | 2925 | 38 | | |
| | | GrA-25708 | 2897 | 38 | | |
| | | GrA-25767 | 2929 | 54 | | |

Table B.4: Radiocarbon determinations of samples from the Iron IB strata. Rejected radiocarbon determinations are marked with *.

| Site | Stratum | Lab. no. | $^{14}$C determination | Uncertainty | Material | Reference |
|---|---|---|---|---|---|---|
| Tel Mique | IV | RT-4288.3 | 2615 | 40 | Olive pits | Sharon et al. (2007) |
| | | RT-4288.4 | 2550 | 40 | | |
| | | RT-4288.5 | 2642 | 40 | | |
| Tel Dor | D2/8c | RT-4540.3 | 2724 | 49 | Olive pits | Sharon et al. (2007) |
| | | RT-4540.4 | 2772 | 43 | | |
| | | RT-4540.5 | 2756 | 39 | | |
| | | GrA-25544 | 2741 | 38 | | |
| | | GrA-25714 | 2776 | 39 | | |
| | | GrA-25787 | 2792 | 76 | | |
| | | RT-4541.3 | 2796 | 38 | | |
| | | RT-4541.4 | 2773 | 38 | | |
| | | RT-4541.5 | 2772 | 38 | | |
| | | RT-4542.3 | 2801 | 38 | | |
| | | RT-4542.4 | 2757 | 38 | | |
| | | RT-4542.5 | 2777 | 54 | | |
| | | RT-2960 | 2710 | 20 | | Gilboa and Sharon (2003) |
| Tel Rehov | VI | GrN-27366 | 2761 | 14 | Cereal grains | Mazar (2005) |
| | | GrA-21943 | 2755 | 35 | Fine charcoal | |
| | | GrA-21054 | 2805 | 35 | | |
| | | GrA-21182 | 2800 | 50 | | |
| | | GrA-21417 | 2840 | 45 | Bone | |
| | | RT-5236 | 2807 | 23 | Olive pits | Boretto et al. (unpublished) |
| | | RT-5233 | 2767 | 13 | | |
| Khirbet Qeiyafa | | OxA-19425 | 2851 | 31 | Charred olive pits | Garfinkel and Ganor (2008) |
| | | OxA-19426 | 2837 | 29 | | |
| | | OxA-19588 | 2799 | 31 | | |
| | | OxA-19589 | 2883 | 29 | | |
| | | OxA-19127 | 2910 | 26 | | |
| | | OxA-22044 | 2858 | 33 | | |
| | | OxA-22045 | 2830 | 30 | | |

Table B.5: Radiocarbon determinations of samples from the Early Iron IIA strata.

| Site | Stratum | Lab. no. | $^{14}$C determination | Uncertainty | Material | Reference |
|---|---|---|---|---|---|---|
| Tel Rehov | VI or V | RT-5236 | 2807 | 23 | Olive pits | Boaretto et al. (unpublished) |
| | | RT-5233 | 2767 | 13 | | |
| | | GrN-26113 | 2760 | 30 | | Mazar (2005) |
| | | GrA-19030 | 2750 | 50 | | |
| | | GrN-26112 | 2805 | 15 | | |
| | | RT-3806.3 | 2728 | 35 | | Sharon et al. (2007) |
| | | RT-3806.5 | 2779 | 34 | | |
| | | RT-3807.1a | 2760 | 30 | | |
| | | RT-3807.1b | 2783 | 35 | | |
| | | RT-3807.3 | 2763 | 35 | | |
| | | RT-3807.4 | 2716 | 35 | | |
| | | RT-3807.5 | 2793 | 36 | | |
| | V | GrA-24455 | 2775 | 45 | | Mazar (2005) |
| | | GrA-24456 | 2750 | 45 | | |
| | | GrA-24497 | 2745 | 45 | | |
| | | GrN-27361 | 2764 | 11 | Charred grains | |
| | | GrN-26116 | 2810 | 20 | | |

Table B.6: (continued)

| Site | Stratum | Lab. no. | $^{14}$C determination | Uncertainty | Material | Reference |
|---|---|---|---|---|---|---|
| Tel Rehov | V | GrN-26117 | 2775 | 25 | Charred grains | Mazar (2005) |
| | | GrN-27362 | 2777 | 13 | | |
| | | GrN-27412 | 2785 | 28 | | |
| | | GrN-27363 | 2745 | 15 | | |
| | | GrN-27385 | 2771 | 15 | | |
| | | GrN-27386 | 2761 | 15 | | |
| | | RT-5232* | 2953 | 30 | | Boaretto et al. (unpublished) |
| | | GrA-45623 | 2775 | 40 | | Mazar, pers. comm. |
| | | GrA-45624 | 2690 | 40 | | |
| | | GrA-45650 | 2735 | 25 | | |
| | | OxA-24784 | 2690 | 30 | | |
| | | Beta-284753* | 2850 | 40 | | |
| | | | 2810 | 40 | | |
| | | Beta 287772 | 2720 | 30 | | |
| | IV | GrN-27364 | 2764 | 11 | Cereal grains | Mazar (2005) |
| | | GrN-27413 | 2866 | 21 | | |
| | | GrN-26114 | 2775 | 20 | | |
| | | GrN-26115 | 2800 | 20 | | |
| | | RT-3122A | 2700 | 20 | | |
| | | RT-3122A1 | 2655 | 25 | | |
| | | RT-31222A2 | 2655 | 25 | | |
| | | RT-3122B | 2720 | 20 | | |
| | | RT-3122B1 | 2700 | 25 | | |
| | | RT-3122B2 | 2650 | 30 | | |
| | | RT-3122BB | 2725 | 15 | | |
| | | RT-3122C | 2860 | 20 | | |
| | | RT-3122D | 2710 | 20 | | |
| | | AA30431 U3-11 | 2830 | 55 | | |
| | | AA30431 U3-12 | 2745 | 50 | | |
| | | AA30431 U3-13 | 2730 | 45 | | |
| | | AA30431 U3-21 | 2815 | 50 | | |
| | | AA30431 U3-22 | 2770 | 50 | | |
| | | AA30431 U3-23 | 2710 | 45 | | |
| | | AA30431 U3-31 | 2685 | 45 | | |
| | | AA30431 U3-32 | 2760 | 60 | | |
| | | AA30431 U3-33 | 2740 | 50 | | |
| | | VERA-3223 | 2715 | 35 | | Mazar, pers. comm. |
| | IV | GrA-21152 | 2770 | 50 | | Mazar (2005) |
| | | GrA-21154 | 2730 | 50 | | |
| | | GrA-21267 | 2760 | 35 | | |
| | | GrA-22301$^a$ | 2710 | 45 | | |
| | | GrA-22301$^b$ | 2775 | 40 | | |
| | | GrA-22330$^a$ | 2760 | 50 | | |
| | | GrA-22330$^b$ | 2785 | 40 | | |
| | | Beta-284754 | 2920* | 40 | Charred grains | Mazar, pers. comm. |
| | | | 2890 | 40 | | |
| | | Beta-287773 | 2770 | 30 | | |
| | | GrA-45626 | 2705 | 40 | | |
| | | GrA-45627 | 2690 | 40 | | |
| | | GrA-45651 | 2680 | 35 | | |
| | V or IV | GrA-17260 | 2745 | 40 | Olive stones | Mazar (2005) |
| | | RT-3808.3 | 2693 | 35 | | Sharon et al. (2007) |
| | | RT-3808.4 | 2671 | 35 | | |
| | | RT-3808.5 | 2669 | 35 | | |
| | | RT-3808a | 2671 | 35 | | |
| | | RT-3808aa | 2700 | 40 | | |
| | | GrA-24108 | 2765 | 45 | Seeds | Mazar (2005) |
| | | GrA-24109 | 2770 | 45 | | |
| | | GrA-24111 | 2780 | 45 | | |
| | | GrA-24112 | 2750 | 45 | | |
| | | GrN-28368 | 2735 | 30 | | |
| | | VERA-3221 | 2725 | 35 | | Mazar, pers. comm. |
| | | GrN-27365 | 2765 | 15 | Olive stones | Mazar (2005) |
| | | GrA-21034 | 2760 | 35 | | |
| | | GrA-21047 | 2820 | 35 | | |
| | | GrA-21179 | 2770 | 50 | | |

Table B.6: (continued)

| Site | Stratum | Lab. no. | $^{14}$C determination | Uncertainty | Material | Reference |
|---|---|---|---|---|---|---|
| Tel Rehov | V or IV | GrA-21042 | 2765 | 35 | Charcoal | mazar2005 |
| | | GrA-21053 | 2750 | 35 | | |
| | | GrA-21180 | 2690 | 50 | | |
| Bethsaida | 6 | RT-4281.1a | 2820 | 35 | Seeds | Sharon et al. (2007) |
| | | RT-4281.1b | 2866 | 35 | | |
| | | RT-4281.3 | 2775 | 50 | | |
| | | RT-4281.4 | 2800 | 40 | | |
| | | RT-4281.5 | 2780 | 40 | | |
| Rosh Zayit | 23 | RT-3797.3 | 2597 | 63 | Seeds | Sharon et al. (2007) |
| | | RT-3797.4 | 2766 | 65 | | |
| | | RT-3797.5 | 2695 | 44 | | |
| | | RT-3797.6 | 2660 | 40 | | |
| | | RT-3797.7 | 2762 | 40 | | |
| | | RT-3797.8 | 2750 | 40 | | |
| | | RT-3797-1.1 | 2670 | 50 | | |
| | | RT-3797-1.2 | 2715 | 45 | | |
| | | RT-3797-1.3 | 2725 | 45 | | |
| | 53 | RT-3798.1 | 2745 | 30 | | |
| | | RT-3798.3 | 2760 | 40 | | |
| | | RT-3798.4 | 2755 | 40 | | |
| | | RT-3798.5 | 2750 | 40 | | |
| | | RT-3798a | 2687 | 35 | | |
| | | RT-3798aa | 2693 | 50 | | |
| | 52 | RT-3799.1 | 2745 | 30 | | |
| | | RT-3799.3 | 2730 | 40* | | |
| | | RT-3799a | 2683 | 35 | | |
| | | RT-3799aa | 2728 | 70 | | |
| Sulem | 108 | RT-3989.3 | 2837 | 40 | Charcoal | Sharon et al. (2007) |
| | | RT-3989.4 | 2839 | 40 | | |
| | | RT-3990.3 | 2915 | 40 | | |
| | | RT-3990.4 | 2821 | 40 | | |
| | | RT-3990.5 | 2857 | 45 | | |
| | 111 | RT-3991.3 | 2642 | 35 | | |
| | | RT-3991.4 | 2629 | 35 | | |
| | | RT-3991.5 | 2758 | 40 | | |
| Hazor | Xa | RT-3782.3 | 2680 | 55 | Charcoal | Sharon et al. (2007) |
| | | RT-3782.4 | 2570 | 50 | | |
| | | RT-3782.5 | 2710 | 60 | | |
| | | RT-3783.3 | 2822 | 40 | | |
| | | RT-3783.4 | 2680 | 50 | | |
| | | RT-3783.5 | 2796 | 40 | | |
| | | RT-3783a | 2731 | 40 | | |
| | | RT-3783aa | 2674 | 35 | | |
| | | RT-3784.3 | 2620 | 80 | Olive pits | |
| | | RT-3784.4 | 2570 | 50 | | |
| | | RT-3784.5 | 2680 | 50 | | |
| | | RT-3784.6 | 2650 | 50 | | |
| | | RT-3786.4 | 2450 | 50 | | |
| | | RT-3786.3 | 2615 | 80 | | |
| | | RT-3786.5 | 2695 | 50 | | |
| | | RT-3786a | 2576 | 66 | | |
| | | RT-3786aa | 2656 | 35 | | |
| | | RT-3785.4 | 2675 | 50 | | |
| | | RT-3785.5 | 2710 | 50 | | |
| | | RT-3785.6 | 2680 | 50 | | |
| | | RT-3785a | 2693 | 35 | | |
| | | RT-3785aa | 2705 | 35 | | |
| Megiddo | IVB–VA | RT-3949.3 | 2820 | 50 | Seeds | Boaretto (2006) |
| | | RT-3949.4 | 2900 | 50 | | |
| | | RT-3949a | 2788 | 40 | | |
| | | RT-3949aa | 2775 | 50 | | |
| | | RT-3948a | 2695 | 50 | | |
| Tel Dor | D2/8b | RT-4556.3 | 2765 | 43 | Olive pits | Sharon et al. (2007) |
| | | RT-4556.4 | 2777 | 38 | | |
| | | RT-4556.5 | 2712 | 38 | | |

| Site | Stratum | Lab. no. | $^{14}$C determination | Uncertainty | Material | Reference |
|---|---|---|---|---|---|---|
| Tel el Har | Mid L117 | RT-4411.1a | 2830 | 35 | | Sharon et al. (2007) |
| | | RT-4411.1b | 2785 | 50 | | |
| | | RT-4414.3 | 2652 | 40 | | |
| | | RT-4414.4 | 2640 | 40 | | |
| | | RT-4414.5 | 2653 | 40 | | |
| | | RT-4415.5 | 2653 | 40 | | |
| | | RT-4415.3 | 2648 | 40 | | |
| | | RT-4415.4 | 2607 | 40 | | |
| | | RT-4418.3 | 2700 | 40 | | |
| | | RT-4418.4 | 2765 | 40 | | |
| | | RT-4418.5 | 2695 | 45 | | |
| | | RT-4423.3 | 2710 | 35 | Semolina | |
| | | RT-4423.4 | 2665 | 35 | | |
| | | RT-4425.3 | 2740 | 35 | | |
| | | RT-4425.4 | 2680 | 45 | | |
| | | RT-4425.5 | 2675 | 35 | | |
| | Mid L119 | RT-4412.3 | 2663 | 40 | Seeds | |
| | | RT-4412.4 | 2611 | 35 | | |
| | | RT-4412.5 | 2565 | 35 | | |
| | | RT-4419.3 | 2715 | 40 | Seeds | |
| | | RT-4419.4 | 2740 | 40 | | |
| | | RT-4420.3 | 2725 | 40 | | |
| | | RT-4420.4 | 2630 | 40 | | |
| | | RT-4420.5 | 2670 | 40 | | |
| | | RT-4424.3 | 2700 | 35 | Semolina | |
| | | RT-4424.4 | 2685 | 35 | | |
| | | RT-4424.5 | 2675 | 35 | | |
| | Mid L466 | RT-4413.3 | 2576 | 40 | Seeds | |
| | | RT-4413.4 | 2601 | 40 | | |
| | | RT-4413.5 | 2584 | 40 | | |
| | Upper L205 | RT-4422.3 | 2654 | 35 | Seeds + sediment | |
| | | RT-4422.4 | 2565 | 35 | | |
| | | RT-4422.5 | 2545 | 35 | | |
| Yoqueam | XIVb | RT-3780.1 | 2735 | 30 | Charcoal | Sharon et al. (2007) |
| | | RT-3780.1a | 2716 | 25 | | |
| | | RT-3780.3 | 2635 | 45 | | |
| | | RT-3780.4 | 2657 | 55 | | |
| | | RT-3780.5 | 2665 | 70 | | |
| | | RT-3780a | 2740 | 35 | | |
| | | RT-3780aa | 2725 | 45 | | |
| Moza | | RT-4583.3 | 2857 | 40 | Charcoal | Sharon et al. (2007) |
| | | RT-4583.4 | 2865 | 40 | | |
| | | RT-4583.5 | 2830 | 55 | | |
| | | RT-4584.3 | 2908 | 40 | | |
| | | RT-4584.4 | 2885 | 40 | | |
| | | RT-4584.5 | 2902 | 40 | | |
| | | RT-4586.3 | 2813 | 40 | | |
| | | RT-4586.4 | 2819 | 40 | | |
| | | RT-4586.5 | 2817 | 40 | | |
| | | RT-4587.3 | 2873 | 40 | | |
| | | RT-4587.4 | 2938 | 40 | | |
| Aphek | X8 | RT-4511.3 | 2685 | 35 | Seeds | Sharon et al. (2007) |
| | | RT-4511.4 | 2680 | 35 | | |
| | | RT-4511.5 | 2635 | 35 | | |
| Tel es-Safi | IV | RT-4409.3 | 2630 | 45 | Seeds | Sharon et al. (2007) |
| | | RT-4409.4 | 2693 | 60 | | |
| | | RT-4409.5 | 2679 | 55 | | |
| | | RT-4410.3 | 2748 | 60 | | |
| | | RT-4410.4 | 2671 | 45 | | |
| | | RT-4410.5 | 2712 | 45 | | |
| | | GrA-25536 | 2700 | 42 | | |
| | | GrA-25711 | 2733 | 38 | | |
| | | GrA-25770 | 2780 | 44 | | |

Table B.6: Radiocarbon determinations of samples from the Late Iron IIA strata. Rejected radiocarbon determinations are marked with *.

| Site | Stratum | Lab. no. | $^{14}$C determination | Uncertainty | Material | Reference |
|---|---|---|---|---|---|---|
| Tel Zayit | I | RT-4275-1.3 | 2640 | 40 | Seeds + charcoal | Sharon et al. (2007) |
| | | RT-4275-1.4 | 2646 | 45 | | |
| | | RT-4275-1.5 | 2745 | 55 | | |
| | | RT-4275-2.3 | 2616 | 40 | | |
| | | RT-4275-3.3 | 2573 | 40 | | |
| | | RT-4275-3.4 | 2605 | 40 | | |
| | | RT-4275-3.5 | 2600 | 40 | | |
| | | RT-4278.3 | 1400 | 35 | Olive pits | |
| | | RT-4278.4 | 1390 | 35 | | |
| | | RT-4278.5 | 1455 | 35 | | |
| | | RT-4279.4 | 2681 | 35 | Charcoal | |
| | | RT-4279.5 | 2683 | 35 | | |
| | | RT-4280.3 | 2615 | 40 | | |
| | | RT-4280.4 | 2653 | 40 | | |
| Beth Shemesh | 3 | RT-3937.1 | 2500 | 35 | Olive pits | Sharon et al. (2007) |
| | | RT-3937.3 | 2524 | 36 | | |
| | | RT-3937.4 | 2427 | 35 | | |
| | | RT-3937.5 | 2478 | 34 | | |
| | | RT-3938.3 | 2390 | 65 | | |
| | | RT-3938.4 | 2425 | 40 | | |
| | | RT-3938.5 | 2505 | 40 | | |

Table B.7: Radiocarbon determinations of samples from the Iron IIB strata.

## B.4 The Cape Riva tephra

| | Lab. no. | $^{14}$C determination | Uncertainty | Depth (m) | Material |
|---|---|---|---|---|---|
| ML00 sequence | SUERC-5863 | 23523 | 428 | 2.201 | Bulk sediment |
| | Beta-147750 | 24460 | 150 | 2.604 | |
| | SUERC-5862 | 27167 | 686 | 3.076 | |
| | SUERC-3019 | 30762 | 1085 | 3.957 | |
| | Beta-202262 | 32150 | 800 | 4.26 | |
| | SUERC-5864 | 31717 | 1225 | 4.653 | |
| | Beta-147749 | 32750 | 330 | 4.75 | |
| | SUERC-3020 | 34975 | 1848 | 5.647 | |
| | SUERC-3022 | 42083 | 4506 | 6.169 | |
| | SUERC-3023 | 38879 | 3017 | 6.582 | |
| | Beta-145632 | 38390 | 690 | 6.959 | |
| | SUERC-3026 | 43259 | 5219 | 7.441 | |
| | Beta–145631 | 37910 | 660 | 7.713 | |
| | SUERC-3027 | >43000 | | | |
| | Beta-145630 | 42400 | 2720 | 8.675 | |
| ML01 sequence | SUERC-1287 | 1538 | 28 | 0.645 | Mixed plant cuticles & seeds |
| | SUERC-5857 | 19072 | 237 | 1.836 | Bulk sediments |
| | SUERC-5858 | 21225 | 316 | 2.678 | |
| | SUERC-5859 | 20933 | 309 | 3.974 | |
| | SUERC-5860 | 27781 | 743 | 5.474 | |
| | SUERC-3027 | 32304 | 1319 | 6.677 | |
| | SUERC-3029 | >43000 | | | |
| | SUERC-3029 | >43000 | | | |
| | SUERC-3032 | 41384 | 4128 | 11.628 | |

Table B.8: Data from the Megali Limni basin on Lesvos Island from Margari et al. (2007, 2009). The Y-2 tephra was found at 1.81 m in the ML01 sequence and the Campanian Ignimbrite was found at 5.565 m in the ML00 sequence and 7.52 m in the ML01 sequence.

| Lab. no. | $^{14}$C determination | Uncertainty | Depth (m) | Material |
|---|---|---|---|---|
| Poz-15890 | 1950 | 30 | 0.76 | *Viviparus contectus* |
| Poz-15891 | 4200 | 40 | 1.79 | *Oxyloma elegans* |
| Poz-15894 | 5790 | 40 | 3.41 | |
| Beta-244646 | 6350 | 50 | 4.2 | Wood |
| Beta-244647 | 7600 | 50 | 4.59 | |
| Beta-244650 | 8820 | 50 | 5.56 | |
| Beta-244651 | 9890 | 60 | 6.15 | |
| Beta-244654 | 13570 | 70 | 6.98 | Bulk sediment |
| Beta-244655 | 16560 | 90 | 7.18 | |
| Beta-244637 | 20220 | 100 | 8.2 | |
| Poz-16295 | 23330 | 150 | 8.86 | |
| Beta-244638 | 24310 | 160 | 9.3 | |
| Beta-244639 | 25120 | 150 | 9.85 | |
| Beta-244640 | 27760 | 190 | 10.6 | |
| Beta-244641 | 28680 | 230 | 11.25 | |
| Beta-244642 | 32390 | 260 | 11.85 | |
| Beta-244643 | 35290 | 350 | 13.3 | |
| Beta-244644 | 36520 | 400 | 13.83 | |
| Beta-244645 | 39570 | 570 | 14.65 | |
| Beta-246628 | 43100 | 1200 | 15.28 | |

Table B.9: Radiocarbon determinations from Tenaghi Philippon from Müller et al. (2011). The Y-2 tephra was found at 7.61 m, and the Campanian Ignimbrite was found at 12.755 m.

## B.5 Taforalt chronology

| Unit | Lab. no. | $^{14}$C determination | Uncertainty | Depth (m) | Species |
|---|---|---|---|---|---|
| Yellow Series | OxA-16277 | 29160 | 160 | 5.77 | *Cupressus sempervirens* |
| | OxA-16278 | 29310 | 160 | 5.77 | |
| | OxA-16276 | 26550 | 140 | 5.63 | *Pinus sp.* |
| | OxA-13556# | 25760 | 140 | 5.61 | *Quercus sp.* |
| | OxA-16244 | 25860 | 150 | 5.48 | *Pinus sp.* |
| | OxA-16243 | 22890 | 120 | 5.34 | *Juniperus sp.* |
| | OxA-13607# | 22200 | 90 | 5.24 | *Taxus sp.* |
| | OxA-24110 | 20800 | 120 | 5.17 | *Panthera* |
| | OxA-16275 | 20560 | 90 | 5.16 | *Pinus sp.* |
| | OxA-16274 | 20630 | 90 | 5.11 | *Conifer* unidentified |
| | OxA-22910 | 20030 | 90 | 5.08 | *cf Cedrus* |
| | OxA-16271 | 20420 | 90 | 4.96 | *Pinus sp.* |
| | OxA-16273## | 17515 | 75 | 4.9 | |
| | OxA-16242## | 16630 | 75 | 4.77 | *Dicot* unidentified |
| | OxA-13518# | 17085 | 65 | 4.72 | *Quercus sp.* |
| | OxA-16270## | 16285 | 65 | 4.68 | *Pinus sp.* |
| | OxA-14351* | 16695 | 70 | 4.63 | *Struthio* (Ostrich eggshell) |
| | OxA-16269## | 15790 | 60 | 4.55 | *Juniperus sp.* |
| | OxA-14350* | 16660 | 70 | 4.55 | *Struthio* (Ostrich eggshell) |
| | OxA-16272## | 14630 | 60 | 4.36 | *Quercus sp.* |
| | OxA-22909 | 14140 | 55 | 4.35 | *Conifer* |
| | OxA-13519# | 13905 | 55 | 4.3 | *Juniperus / Tetraclinus* |
| | OxA-16268## | 14515 | 60 | 4.26 | *Tetraclinus articulata* |
| | OxA-22908 | 14110 | 55 | 4.25 | *cf Arbutus* |
| | OxA-22906 | 14135 | 55 | 4.18 | *Conifer* |
| | OxA-22907 | 14230 | 55 | 4.17 | *cf Juniperus* |
| | OxA-16267# | 14005 | 60 | 4.16 | *Tetraclinus articulata* |
| | OxA-22788 | 12850 | 55 | 4.12 | *Conifer* |
| | OxA-22905 | 12665 | 50 | 4.08 | *cf Arbutus* |
| | OxA-14349* | 12690 | 55 | 4.08 | *Struthio* (Ostrich eggshell) |
| | OxA-22903 | 13045 | 50 | 4.05 | *cf Cedrus* |
| | OxA-22786 | 12200 | 55 | 4.02 | *cf Juniperus* |
| Grey Series | OxA-24109 | 12605 | 55 | 3.98 | *Bos* |
| | OxA-22784 | 12660 | 70 | 3.97–3.88 | *cf Juniperus* |
| | OxA-22785 | 12500 | 55 | 3.97–3.88 | |
| | OxA-22787 | 12545 | 55 | 3.97–3.88 | *Conifer* |
| | OxA-22902 | 12370 | 50 | 3.97–3.88 | *Conifer* |
| | OxA-22904 | 12490 | 50 | 3.97–3.88 | *Conifer* |
| | OxA-13478# | 12495 | 50 | 3.88 | *Juniperus/Tetraclinus* |
| | OxA-23411 | 13060 | 65 | 3.51 | |
| | OxA-13477# | 12675 | 50 | 3.5 | *Conifer* |
| | OxA-23410 | 12405 | 55 | 2.96 | *Juniperus / Tetraclinus* |
| | OxA-23409 | 11890 | 55 | 1.56 | *Pinus sp.* |
| | OxA-23408 | 11545 | 55 | 1.14 | |
| | OxA-23406 | 11445 | 55 | 0.94 | *Juniperus/Tetraclinus* |
| | OxA-23407 | 11465 | 50 | 0.94 | |
| | OxA-24113 | 11540 | 50 | 0.69–0.61 | *Gazella* |
| | OxA-23405 | 11615 | 50 | 0.69–0.61 | *Juniperus/Tetraclinus* |
| | OxA-13517# | 10990 | 45 | 0.54 | *Dicotyledonous* |
| | OxA-24112 | 11165 | 45 | 0.53 | *Ammotragus* |
| | OxA-13516# | 11065 | 45 | 0.48 | *Pinus sp.* |
| | OxA-23404 | 10870 | 45 | 0.36–0.48 | *Pinus sp.* |
| | OxA-13480# | 10950 | 45 | 0.36–0.48 | |
| | OxA-13479# | 10935 | 40 | 0.36 | |
| | OxA-24111 | 10680 | 45 | 0.22 | *Ammotragus* |

Table B.10: Radiocarbon determinations from Grotte des Pigeons cave (Sector 8) at Taforalt, Morocco, provided by Professor Nick Barton. Determinations marked with # and ## were previously published in Barton et al. (2007) and Bouzouggar et al. (2008), respectively. Depths were provided by Dr. Simon Cullcutt, where ranges indicate samples that were from sediment blocks. Ostrich eggshells are marked with * and are excluded from the model.

# B.6 Mid-Holocene elm decline

Data for the mid-Holocene elm decline and posterior for individual models are included here. All dates ranges quoted are in units of cal BP.

## England

| | |
|---|---|
| Site: | Abbotsway |
| Model: | `P_Sequence` |
| Date: | SRR-541 |
| 95.4% range: | 5475–5293 |
| Outliers: | - |
| Lat: | 51.18 |
| Long: | -2.83 |
| Data source: | Beckett and Hibbert (1979); Harkness (1981) |

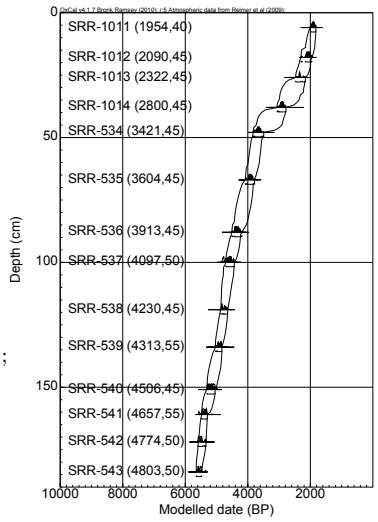


(a) Chronology

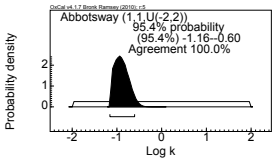


(b) Step-size parameter

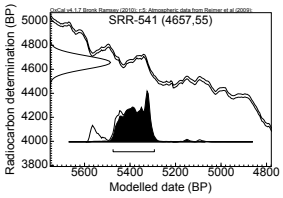


(c) Date of elm decline

| | |
|---|---|
| Site: | Alport Moor |
| Model: | `P_Sequence` |
| Date: | Q-2432 |
| 95.4% range: | 5645–5332 |
| Outliers: | Q-2433 (6%) |
| Lat: | 53.45 |
| Long: | -1.84 |
| Data source: | Tallis and Switsur (1990) |

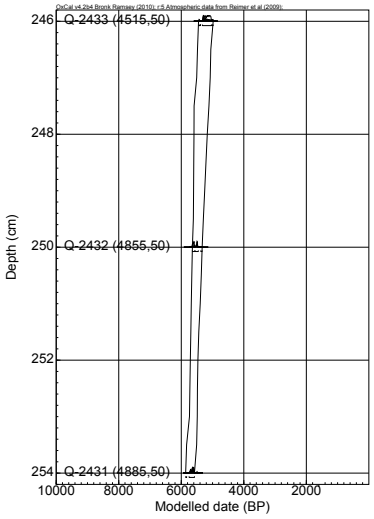


(a) Chronology

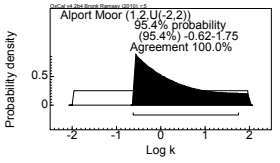


(b) Step-size parameter

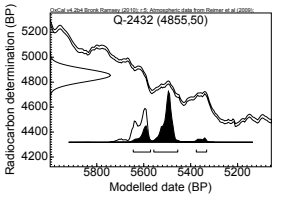


(c) Date of elm decline

Site: Bishop Middleham
Model: P_Sequence
Date: GaK-2071
95.4% range: 6263–5663
Outliers: GaK-2072 (8%)
Lat: 54.83
Long: -1.5
Data source: Bartley et al. (1976); Kigoshi et al. (1973)

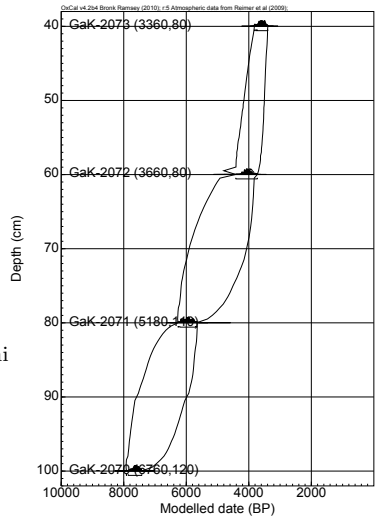


(a) Chronology

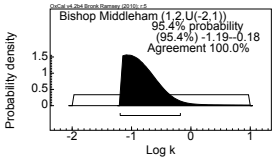


(b) Step-size parameter

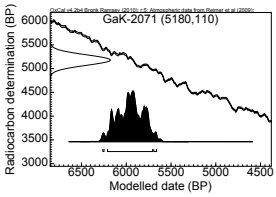


(c) Date of elm decline

Site: Blea Tarn
Model: P_Sequence
Date: SRR-17
95.4% range: 5865–5586
Outliers: -
Lat: 54.43
Long: -3.09
Data source: Pennington and Lishman (1984); Harkness and Wilson (1973)

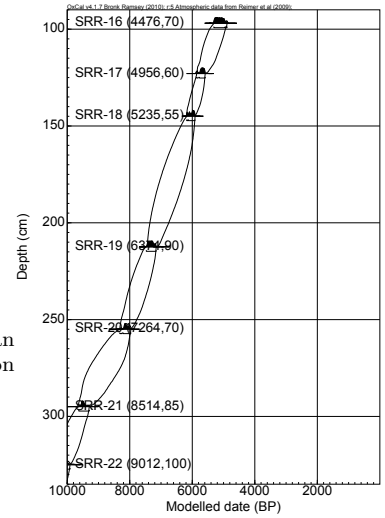


(a) Chronology

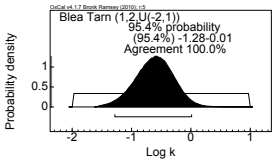


(b) Step-size parameter

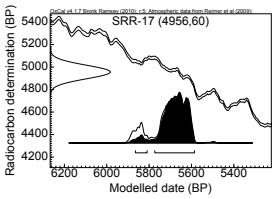


(c) Date of elm decline

Site: Blelham Tarn
Model: P_Sequence
Date: SRR-261
95.4% range: 5742–5468
Outliers: SRR-264 (7%); SRR-263 (14%); SRR-255 (8%)
Lat: 54.4
Long: -2.98
Data source: Pennington and Lishman (1984); Harkness and Wilson (1979)

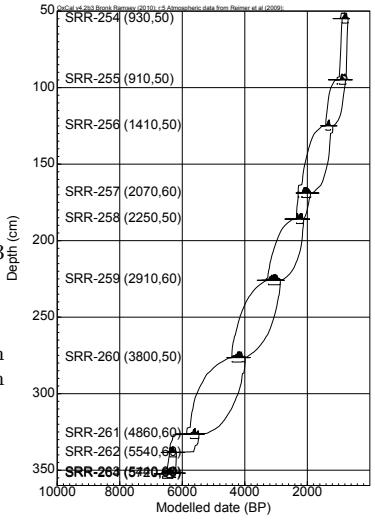


(a) Chronology

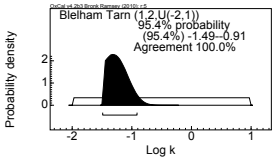


(b) Step-size parameter

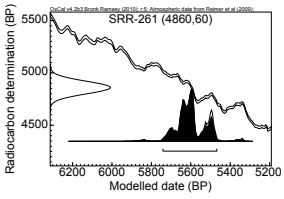


(c) Date of elm decline

| | |
|---|---|
| Site: | Bonfield Gill head |
| Model: | `P_Sequence` |
| Date: | HAR-4229 |
| 95.4% range: | 5885–5334 |
| Outliers: | - |
| Lat: | 54.35 |
| Long: | -1.08 |
| Data source: | Simmons and Innes (1988) |

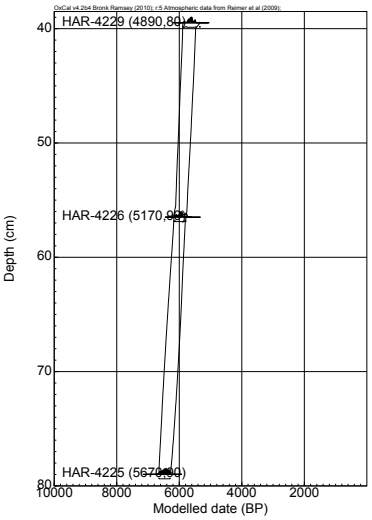


(a) Chronology

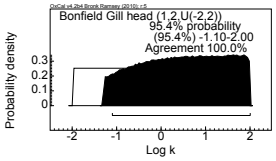


(b) Step-size parameter

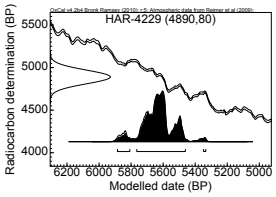


(c) Date of elm decline

| | |
|---|---|
| Site: | Broadness Marsh |
| Model: | `Sequence` |
| Date: | Q-1341 |
| 95.4% range: | 6184–5766 |
| Outliers: | Q-1340 (8%) |
| Lat: | 51.47 |
| Long: | 0.31 |
| Data source: | Devoy (1979) |

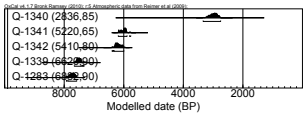


(a) Chronology

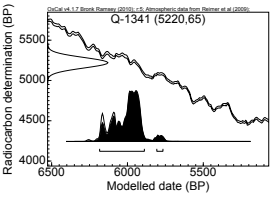


(b) Date of elm decline

| | |
|---|---|
| Site: | Crose Mere |
| Model: | `P_Sequence` |
| Date: | Q-1235 |
| 95.4% range: | 6409–5750 |
| Outliers: | Q-1240 (7%) |
| Lat: | 52.87 |
| Long: | -2.85 |
| Data source: | Beales (1980) |

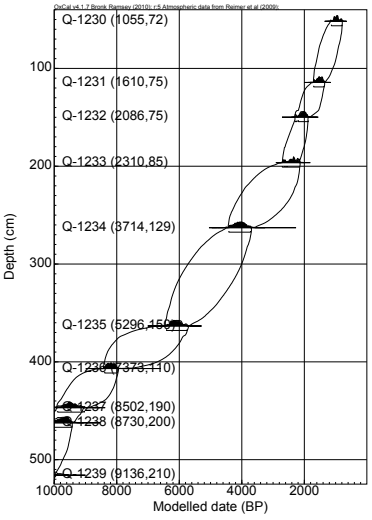


(a) Chronology

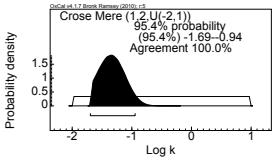


(b) Step-size parameter

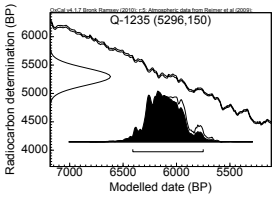


(c) Date of elm decline

| | |
|---|---|
| Site: | Daisybanks Fen |
| Model: | `P_Sequence` |
| Position: | 95 cm |
| 95.4% range: | 6189–4598 |
| Outliers: | OxA-4556 (6%) |
| Lat: | 51.68 |
| Long: | -1.26 |
| Data source: | Parker (1995) |

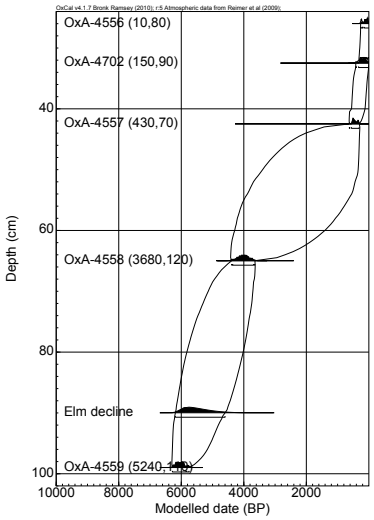


(a) Chronology

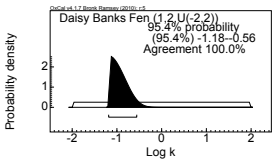


(b) Step-size parameter

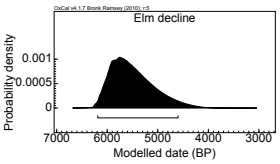


(c) Date of elm decline

| | |
|---|---|
| Site: | Dufton Moss |
| Model: | `P_Sequence` |
| Date: | SRR-510 |
| 95.4% range: | 6282–5922 |
| Outliers: | SRR-510 (6%) |
| Lat: | 54.66 |
| Long: | -2.2 |
| Data source: | Harkness (1981) |

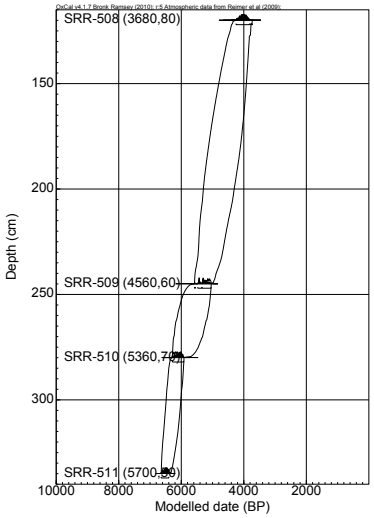


(a) Chronology

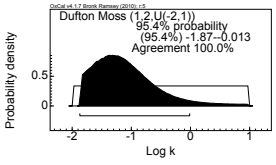


(b) Step-size parameter

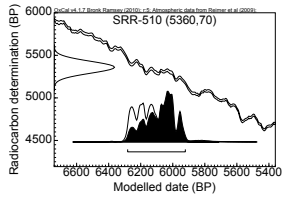


(c) Date of elm decline

| | |
|---|---|
| Site: | Ennerdale Water |
| Model: | `P_Sequence` |
| Date: | SRR-309 |
| 95.4% range: | 6190–5773 |
| Outliers: | SRR-309 (10%); SRR-308 (14%) |
| Lat: | 54.52 |
| Long: | -3.38 |
| Data source: | Harkness and Wilson (1974, 1979) |

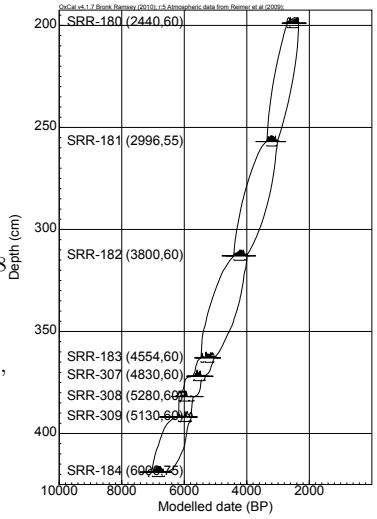


(a) Chronology

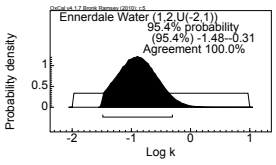


(b) Step-size parameter

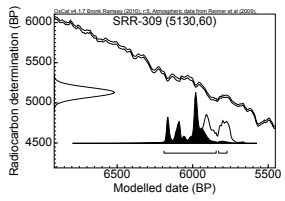


(c) Date of elm decline

| | |
|---|---|
| Site: | Eshton Tarn |
| Model: | `Sequence` |
| Date: | Birm-663 |
| 95.4% range: | 5990–5483 |
| Outliers: | - |
| Lat: | 54.01 |
| Long: | -2.13 |
| Data source: | Bartley et al. (1990); Williams and Johnson (1976) |

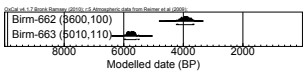


(a) Chronology

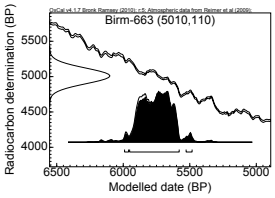


(b) Date of elm decline

| | |
|---|---|
| Site: | Fen Bogs |
| Model: | `P_Sequence` |
| Date: | T-1084 |
| 95.4% range: | 5643–4983 |
| Outliers: | T-1150 (17%) |
| Lat: | 54.37 |
| Long: | -0.69 |
| Data source: | Atherden (1976a,b) |

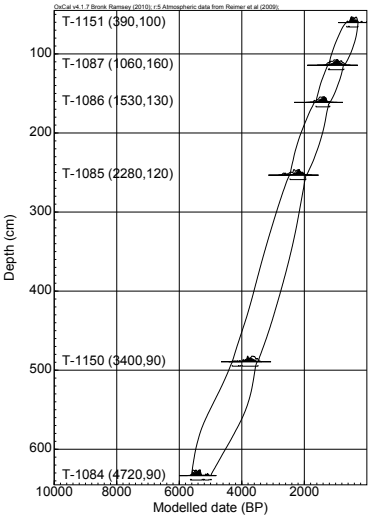


(a) Chronology

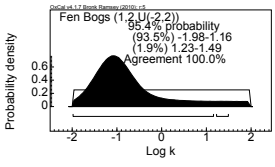


(b) Step-size parameter

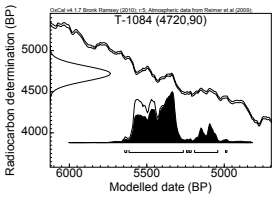


(c) Date of elm decline

| | |
|---|---|
| Site: | Fox Earth Gill |
| Model: | `P_Sequence` |
| Date: | SRR-397 |
| 95.4% range: | 5646–5327 |
| Outliers: | - |
| Lat: | 54.65 |
| Long: | -2.25 |
| Data source: | Harkness (1981) |

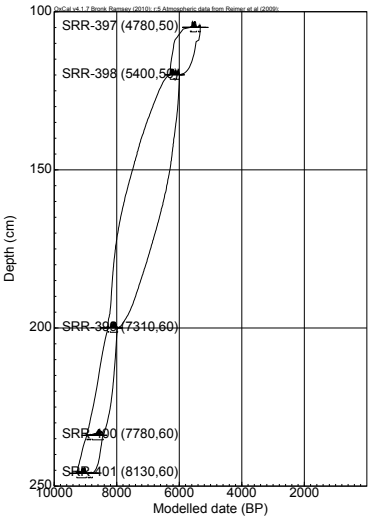


(a) Chronology

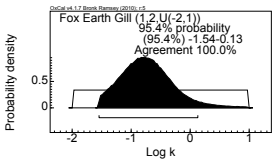


(b) Step-size parameter

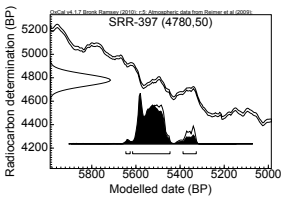


(c) Date of elm decline

| | |
|---|---|
| Site: | Gatcombe |
| Model: | `Sequence` |
| Date: | SRR-1338 |
| 95.4% range: | 5709–5471 |
| Outliers: | - |
| Lat: | 50.66 |
| Long: | -1.3 |
| Data source: | Scaife (1987b) |

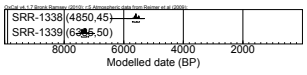


(a) Chronology

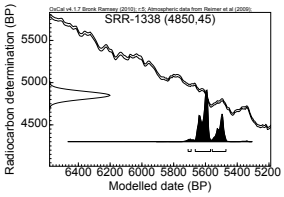


(b) Date of elm decline

| | |
|---|---|
| Site: | Gransmoor |
| Model: | Sequence |
| Date: | SRR-229 |
| 95.4% range: | 5985–5721 |
| Outliers: | - |
| Lat: | 54.02 |
| Long: | -0.3 |
| Data source: | Beckett (1981); Harkness and Wilson (1979) |

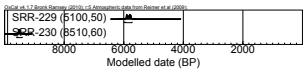


(a) Chronology

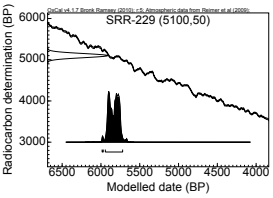


(b) Date of elm decline

| | |
|---|---|
| Site: | Haddenham Ouse Channel |
| Model: | P_Sequence |
| Date: | Q-2814 |
| 95.4% range: | 6413–5944 |
| Outliers: | - |
| Lat: | 52.34 |
| Long: | -0.07 |
| Data source: | Peglar and Waller (1994) |

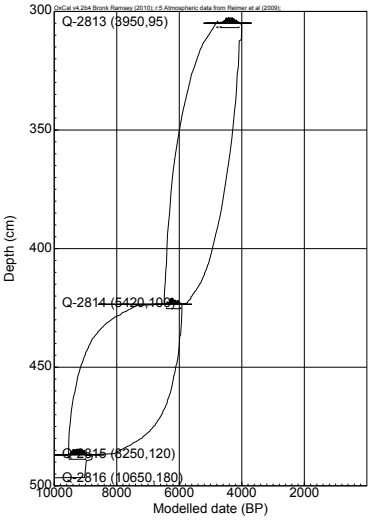


(a) Chronology

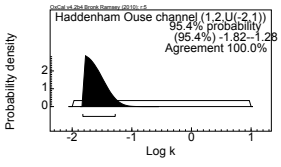


(b) Step-size parameter

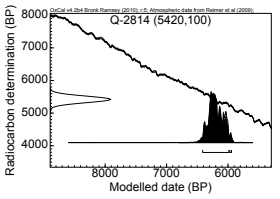


(c) Date of elm decline

| | |
|---|---|
| Site: | Hallowell Moss |
| Model: | P_Sequence |
| Date: | SRR-419 |
| 95.4% range: | 5890–5488 |
| Outliers: | SRR-413 (7%) |
| Lat: | 54.61 |
| Long: | -1.63 |
| Data source: | Harkness (1981); Donaldson and Turner (1977) |

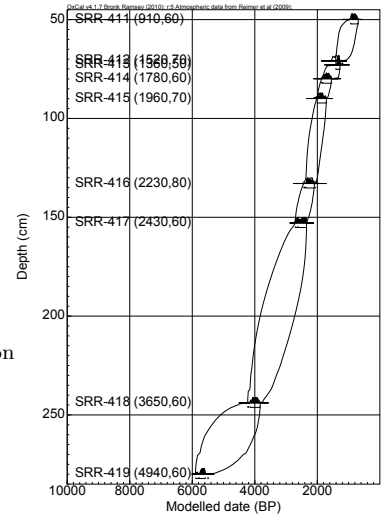


(a) Chronology

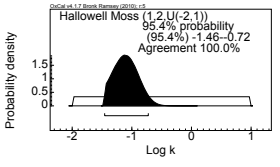


(b) Step-size parameter

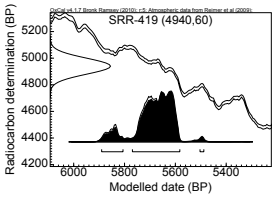


(c) Date of elm decline

| | |
|---|---|
| Site: | Hockham Mere |
| Model: | `P_Sequence` |
| Date: | Q-1048 |
| 95.4% range: | 5898–5595 |
| Outliers: | Q-1087 (6%) |
| Lat: | 52.51 |
| Long: | 0.85 |
| Data source: | Switsur and West (1973); Sims (1973) |

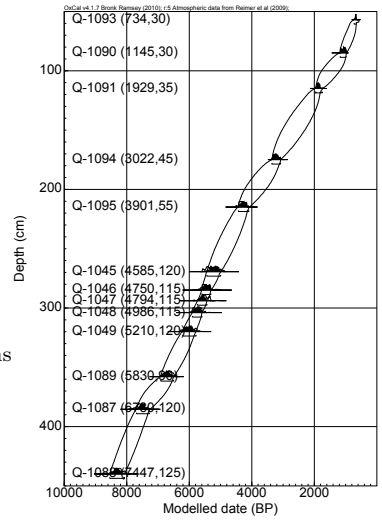


(a) Chronology

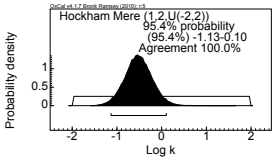


(b) Step-size parameter

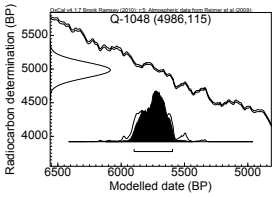


(c) Date of elm decline

| | |
|---|---|
| Site: | Knowsley Park |
| Model: | `P_Sequence` |
| Date: | Birm-1191 |
| 95.4% range: | 6266–5928 |
| Outliers: | - |
| Lat: | 53.45 |
| Long: | -2.82 |
| Data source: | Innes (1994) |

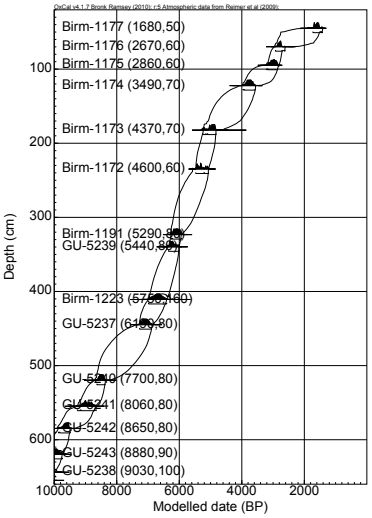


(a) Chronology

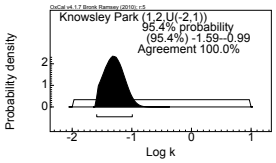


(b) Step-size parameter

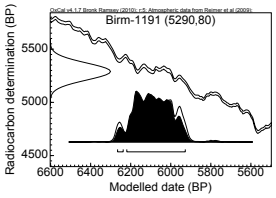


(c) Date of elm decline

| | |
|---|---|
| Site: | Mar Dyke |
| Model: | `Sequence` |
| Date: | HAR-4523 |
| 95.4% range: | 5588–5053 |
| Outliers: | - |
| Lat: | 51.51 |
| Long: | 0.33 |
| Data source: | Scaife (1987a,b) |

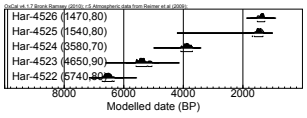


(a) Chronology

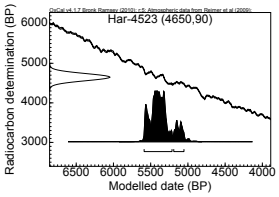


(b) Date of elm decline

Site: Mordon Carr
Model: P_Sequence
Date: SRR-475
95.4% range: 6182–5934
Outliers: -
Lat: 54.62
Long: -1.5
Data source: Bartley et al. (1976); Harkness and Wilson (1979)

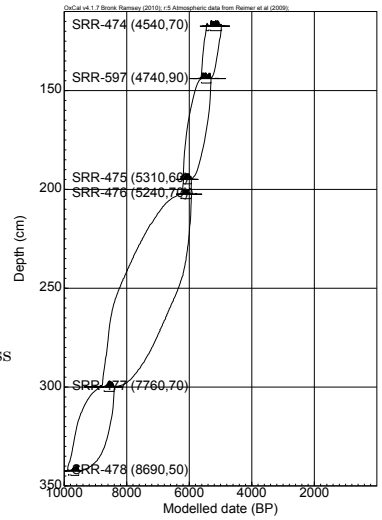


(a) Chronology

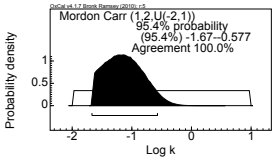


(b) Step-size parameter

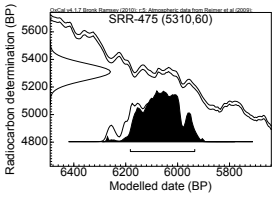


(c) Date of elm decline

Site: Neasham Fen
Model: Sequence
Date: SRR-102
95.4% range: 6432–6003
Outliers: -
Lat: 54.5
Long: -1.49
Data source: Bartley et al. (1976); Harkness and Wilson (1974)

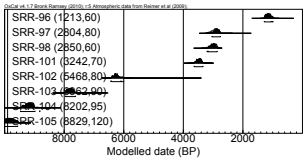


(a) Chronology

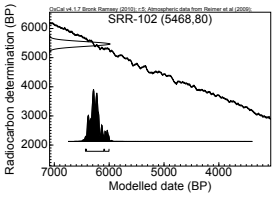


(b) Date of elm decline

Site: New Dartford Tunnel
Model: Sequence
Date: Q-1336
95.4% range: 5920–5333
Outliers: -
Lat: 51.46
Long: 0.25
Data source: Devoy (1979)

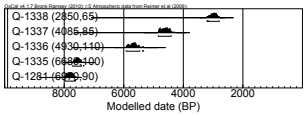


(a) Chronology

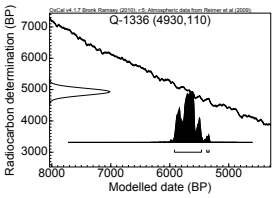


(b) Date of elm decline

Site: North Gill 1A
Model: P_Sequence
Date: SRR-3632
95.4% range: REJECTED
Outliers: SRR-3869 (100%); SRR-3634 (100%); SRR-3633 (100%); SRR-3868 (99%)
Lat: 54.4
Long: -0.88
Data source: Turner et al. (1993)

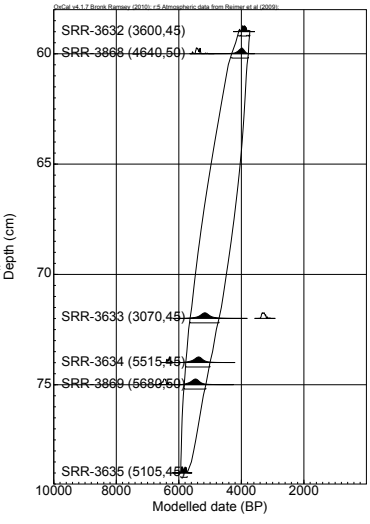


Chronology

| | |
|---|---|
| Site: | North Gill 4 |
| Model: | `P_Sequence` |
| Date: | SRR-3638 |
| 95.4% range: | 6135–5935 |
| Outliers: | - |
| Lat: | 54.4 |
| Long: | -0.88 |
| Data source: | Turner et al. (1993) |

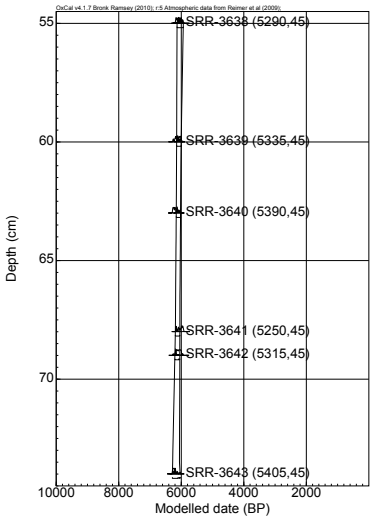


(a) Chronology

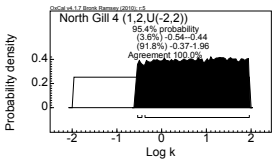


(b) Step-size parameter

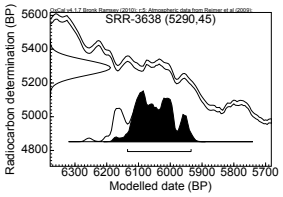


(c) Date of elm decline

| | |
|---|---|
| Site: | North Gill 5B |
| Model: | `P_Sequence` & `Sequence` |
| Date: | HAR-6620 |
| 95.4% range: | 5620–5326 |
| Outliers: | SRR-3648 (11%); SRR-3647 (69%); HAR-6619 (11%) |
| Lat: | 54.4 |
| Long: | -0.88 |
| Data source: | Turner et al. (1993) |

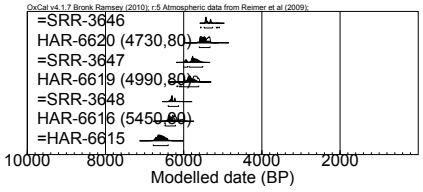


(a) Chronology (`Sequence`)

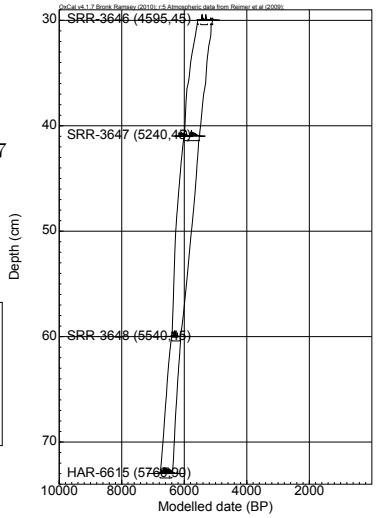


(b) Chronology (`P_Sequence`)

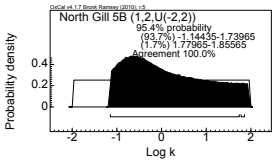


(c) Step-size parameter

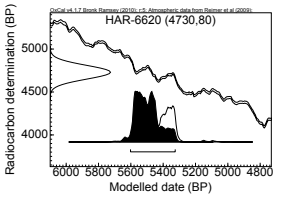


(d) Date of elm decline

| | |
|---|---|
| Site: | North Gill 6 |
| Model: | `P_Sequence` |
| Date: | SRR-3649 |
| 95.4% range: | 3876–3640 |
| Outliers: | - |
| Lat: | 54.4 |
| Long: | -0.88 |
| Data source: | Turner et al. (1993) |

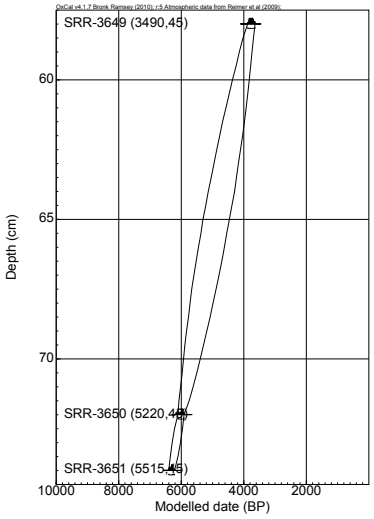


(a) Chronology

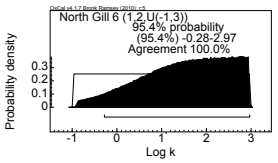


(b) Step-size parameter

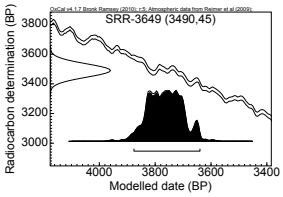


(c) Date of elm decline

| | |
|---|---|
| Site: | North Gill 7 |
| Model: | `P_Sequence` |
| Date: | SRR-3653 |
| 95.4% range: | 5576–5077 |
| Outliers: | SRR-3656 (6%) |
| Lat: | 54.4 |
| Long: | -0.88 |
| Data source: | Turner et al. (1993) |

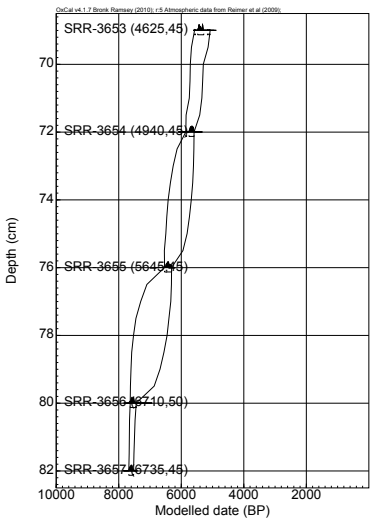


(a) Chronology

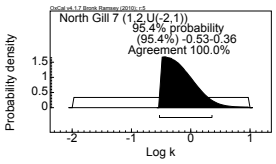


(b) Step-size parameter

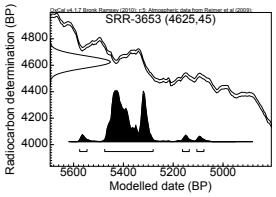


(c) Date of elm decline

| | |
|---|---|
| Site: | North Gill 8 |
| Model: | `P_Sequence` |
| Date: | SRR-3870 |
| 95.4% range: | 4142–3843 |
| Outliers: | - |
| Lat: | 54.4 |
| Long: | -0.88 |
| Data source: | Turner et al. (1993) |

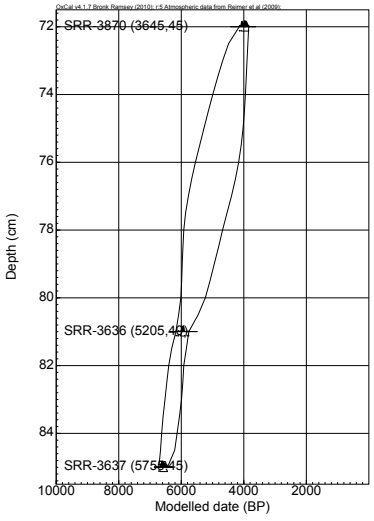


(a) Chronology

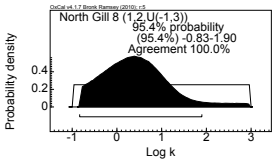


(b) Step-size parameter

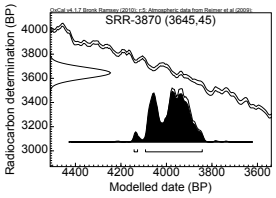


(c) Date of elm decline

| | |
|---|---|
| Site: | North Gill 9 |
| Model: | `P_Sequence` |
| Date: | SRR-3872 |
| 95.4% range: | 6508–6328 |
| Outliers: | SRR-3871 (6%) |
| Lat: | 54.4 |
| Long: | -0.88 |
| Data source: | Turner et al. (1993) |

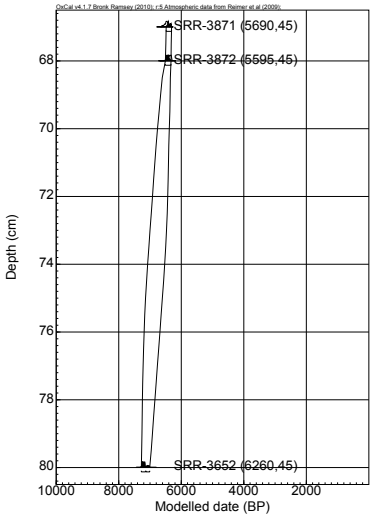


(a) Chronology

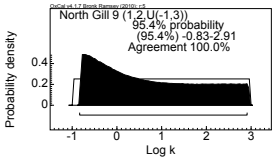


(b) Step-size parameter

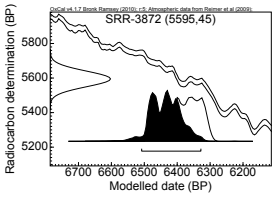


(c) Date of elm decline

| | |
|---|---|
| Site: | Pannel Valley |
| Model: | `P_Sequence` |
| Date: | SRR-2888 |
| 95.4% range: | 5934–5610 |
| Outliers: | SRR-2886 (100%) |
| Lat: | 50.91 |
| Long: | -0.7 |
| Data source: | Waller (1993) |

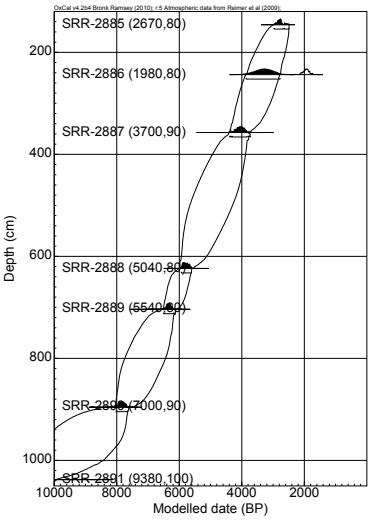


(a) Chronology

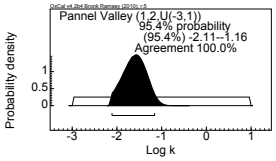


(b) Step-size parameter

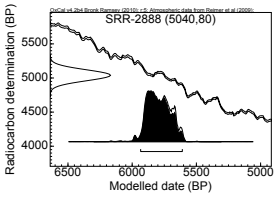


(c) Date of elm decline

| | |
|---|---|
| Site: | Quick Moss |
| Model: | `P_Sequence` |
| Position: | 190 cm |
| 95.4% range: | 5744–5485 |
| Outliers: | - |
| Lat: | 54.77 |
| Long: | -2.23 |
| Data source: | Rowell and Turner (1985) |

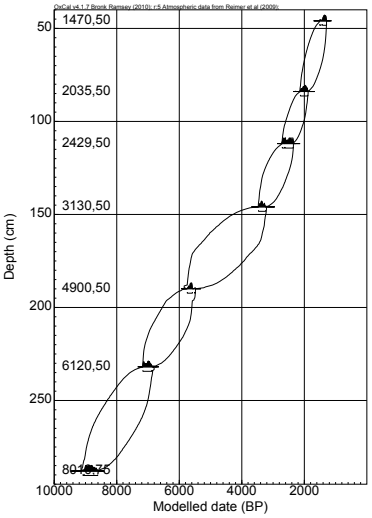


(a) Chronology

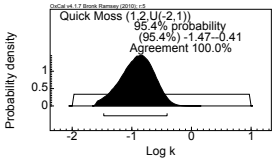


(b) Step-size parameter

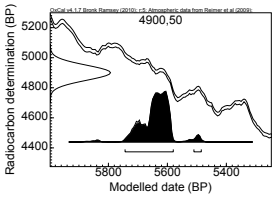


(c) Date of elm decline

| | |
|---|---|
| Site: | Raper Lodge |
| Model: | `P_Sequence` |
| Date: | Beta-64033 |
| 95.4% range: | 6173–5725 |
| Outliers: | Beta-64033 (6%) |
| Lat: | 53.18 |
| Long: | -1.69 |
| Data source: | Taylor et al. (1994) |

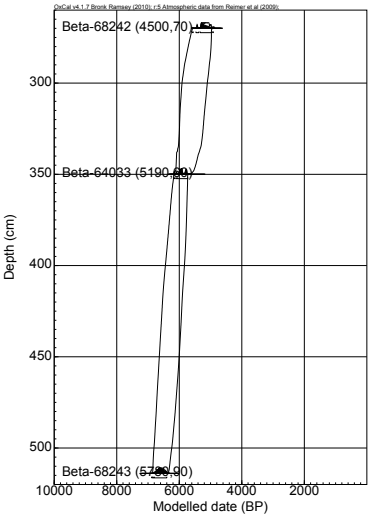


(a) Chronology

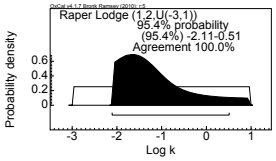


(b) Step-size parameter

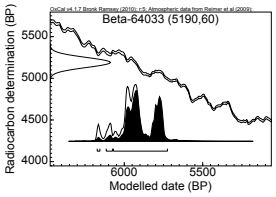


(c) Date of elm decline

| | |
|---|---|
| Site: | Red Moss |
| Model: | P_Sequence |
| Date: | Q-913 |
| 95.4% range: | 5927–5680 |
| Outliers: | Q-919 (6%) |
| Lat: | 52.69 |
| Long: | -2.55 |
| Data source: | Hibbert et al. (1971); Switsur et al. (1970) |

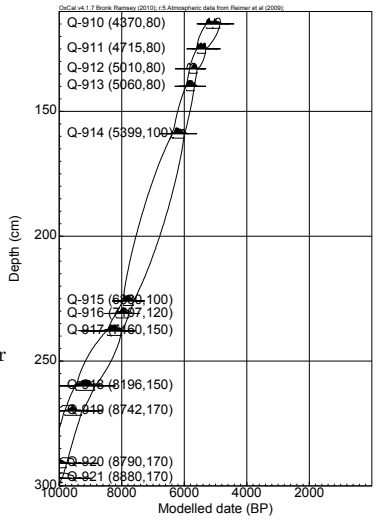


(a) Chronology

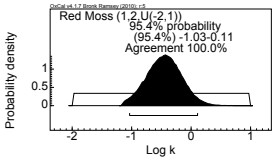


(b) Step-size parameter

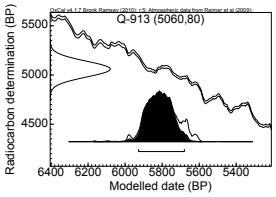


(c) Date of elm decline

| | |
|---|---|
| Site: | Rishworth Moor |
| Model: | P_Sequence |
| Date: | GaK-2822 |
| 95.4% range: | 6557–5917 |
| Outliers: | - |
| Lat: | 53.65 |
| Long: | -2.02 |
| Data source: | Bartley et al. (1976) |

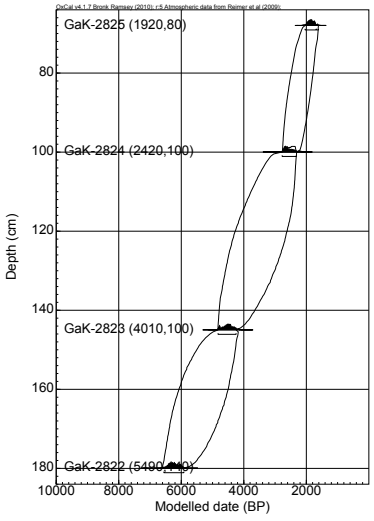


(a) Chronology

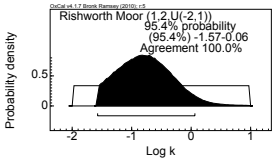


(b) Step-size parameter

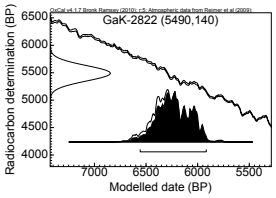


(c) Date of elm decline

| | |
|---|---|
| Site: | Robinsons Moss |
| Model: | P_Sequence |
| Date: | Q-2435 |
| 95.4% range: | 5720–5479 |
| Outliers: | Q-2273 (7%) |
| Lat: | 53.5 |
| Long: | -1.93 |
| Data source: | Tallis and Switsur (1990) |

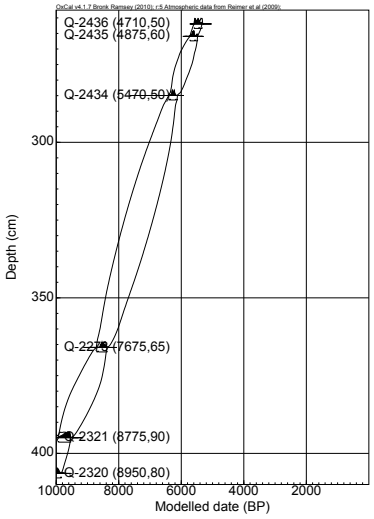


(a) Chronology

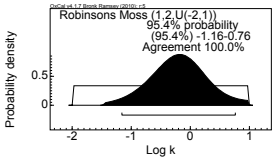


(b) Step-size parameter

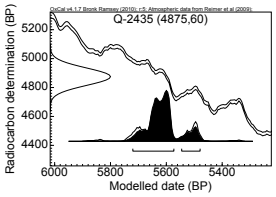


(c) Date of elm decline

Site: Scaleby Moss
Model: `P_Sequence`
Date: Q-171
95.4% range: 5900–5596
Outliers: Q-166 (8%)
Lat: 54.96
Long: -2.89
Data source: Switsur et al. (1970); Godwin and Willis (1959); Godwin et al. (1957)

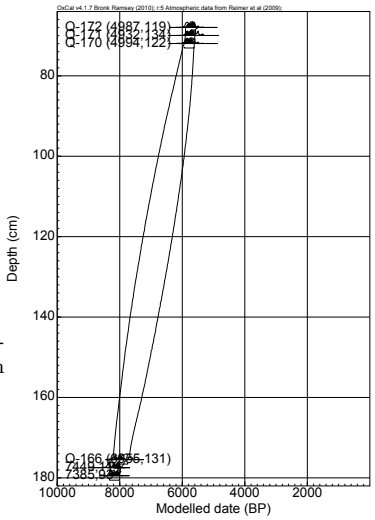


(a) Chronology

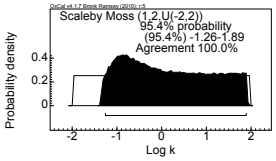


(b) Step-size parameter

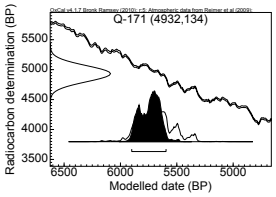


(c) Date of elm decline

Site: Shippea Hill
Model: `Sequence`
Date: Q-585
95.4% range: 6476–6071
Outliers: Q-588 (6%); Q-585 (6%)
Lat: 52.44
Long: -0.45
Data source: Clark and Godwin (1962); Godwin and Willis (1961); Godwin (1962)

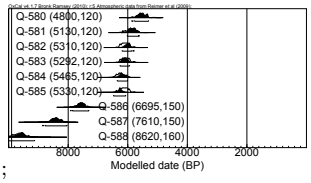


(a) Chronology

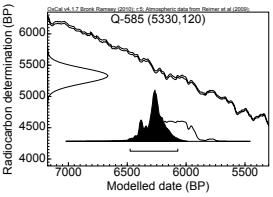


(b) Date of elm decline

Site: Sidlings Copse
Model: `P_Sequence`
Date: OxA-3560
95.4% range: 6269–5890
Outliers: -
Lat: 51.78
Long: -1.19
Data source: Day (1991); Hedges et al. (1990, 1994)

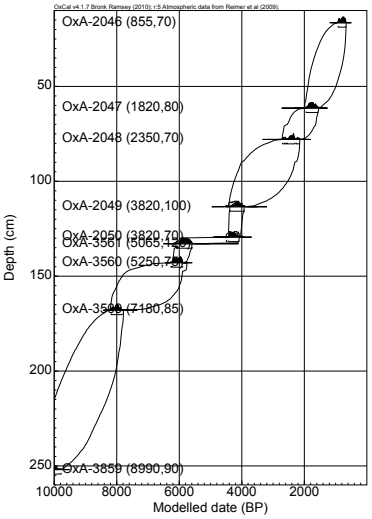


(a) Chronology

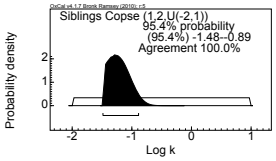


(b) Step-size parameter

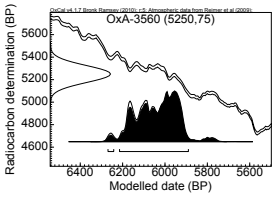


(c) Date of elm decline

| | |
|---|---|
| Site: | Soham Mere |
| Model: | `P_Sequence` |
| Date: | Q-2281 |
| 95.4% range: | 6436–6209 |
| Outliers: | - |
| Lat: | 52.58 |
| Long: | 0.81 |
| Data source: | Bennett (1988) |

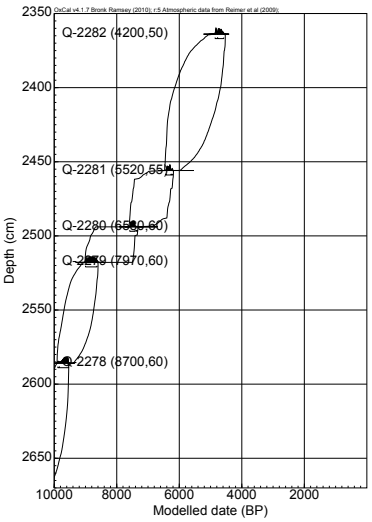


(a) Chronology

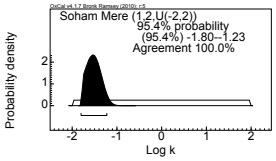


(b) Step-size parameter

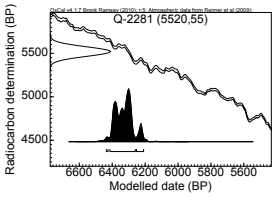


(c) Date of elm decline

| | |
|---|---|
| Site: | Soyland Moor |
| Model: | `Sequence` |
| Date: | Q-2386 |
| 95.4% range: | 5720–5475 |
| Outliers: | Q-2389 (100%) |
| Lat: | 53.67 |
| Long: | -2.04 |
| Data source: | Williams and Switsur (1985) |

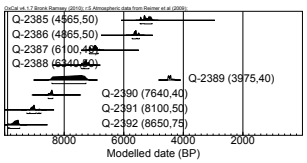


(a) Chronology

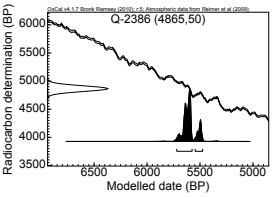


(b) Date of elm decline

| | |
|---|---|
| Site: | Spartum Fen |
| Model: | `P_Sequence` |
| Position: | 62 cm |
| 95.4% range: | 6391–4531 |
| Outliers: | AA-11607 (9%); AA-11606 (13%) |
| Lat: | 51.71 |
| Long: | -1.07 |
| Data source: | Parker (1995) |

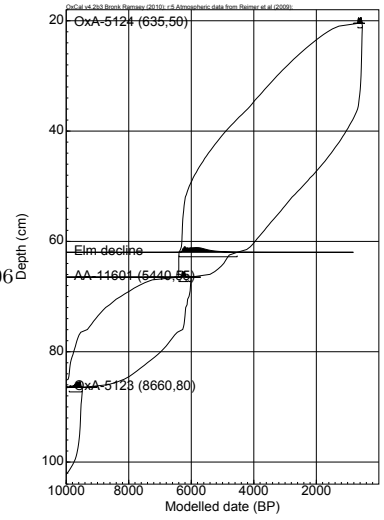


(a) Chronology

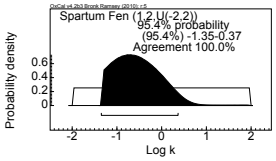


(b) Step-size parameter

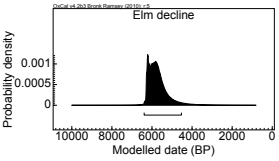


(c) Date of elm decline

| | |
|---|---|
| Site: | Stone Marsh |
| Model: | `Sequence` |
| Date: | Q-1336 |
| 95.4% range: | 5920–5333 |
| Outliers: | - |
| Lat: | 51.46 |
| Long: | 0.25 |
| Data source: | Devoy (1979) |

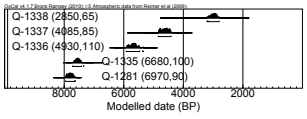


(a) Chronology

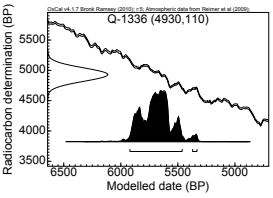


(b) Date of elm decline

| | |
|---|---|
| Site: | Sweet Track |
| Model: | `P_Sequence` |
| Position: | 70 cm |
| 95.4% range: | 5514–5039 |
| Outliers: | SRR-678 (6%) |
| Lat: | 51.16 |
| Long: | -2.82 |
| Data source: | Beckett and Hibbert (1979); Harkness (1981) |

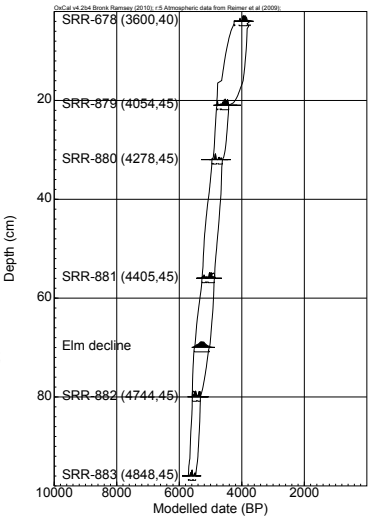


(a) Chronology

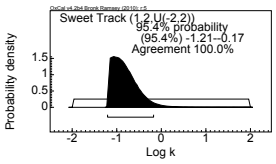


(b) Step-size parameter

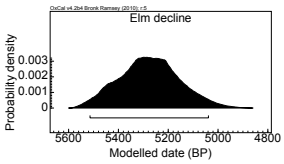


(c) Date of elm decline

| | |
|---|---|
| Site: | Tilbury |
| Model: | `P_Sequence` |
| Position: | 830 cm |
| 95.4% range: | 5798–4229 |
| Outliers: | Q-1427 (6%); Q-1431 (10%) |
| Lat: | 51.45 |
| Long: | 0.37 |
| Data source: | Devoy (1979) |

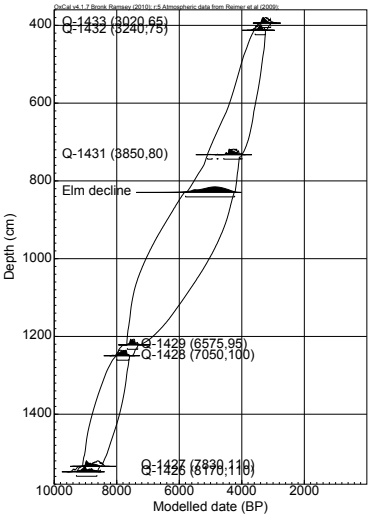


(a) Chronology

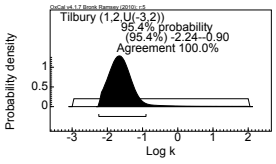


(b) Step-size parameter

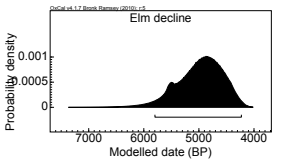


(c) Date of elm decline

| | |
|---|---|
| Site: | Vale of Gordano |
| Model: | `P_Sequence` |
| Date: | SRR-3200 |
| 95.4% range: | 6003–5333 |
| Outliers: | - |
| Lat: | 51.46 |
| Long: | -2.79 |
| Data source: | Gilbertson et al. (1990) |

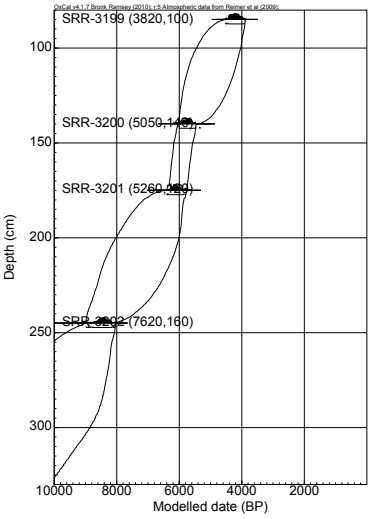


(a) Chronology

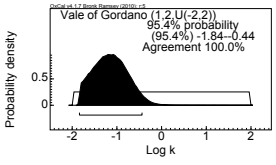


(b) Step-size parameter

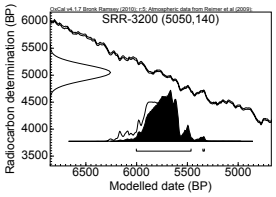


(c) Date of elm decline

| | |
|---|---|
| Site: | Valley Bog |
| Model: | `Sequence` |
| Date: | SRR-91 |
| 95.4% range: | 5645–5329 |
| Outliers: | - |
| Lat: | 54.69 |
| Long: | -2.37 |
| Data source: | Harkness and Wilson (1973) |

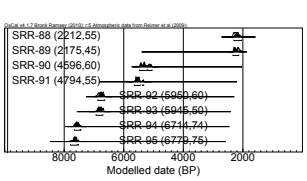


(a) Chronology

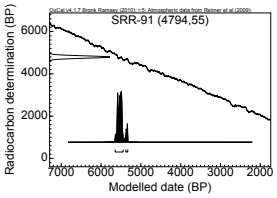


(b) Date of elm decline

| | |
|---|---|
| Site: | Wheelhead Moss |
| Model: | `P_Sequence` |
| Date: | GaK-2915 |
| 95.4% range: | 6409–5790 |
| Outliers: | GaK-2915 (6%) |
| Lat: | 54.69 |
| Long: | -2.33 |
| Data source: | Turner et al. (1973) |

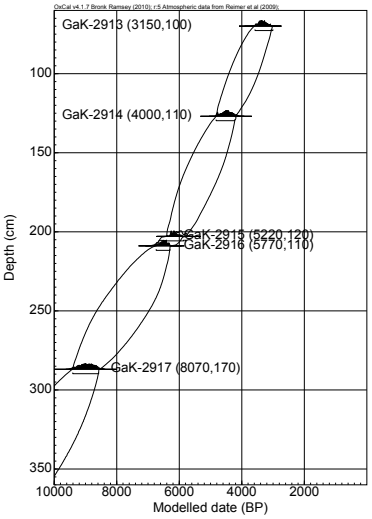


(a) Chronology

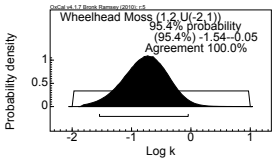


(b) Step-size parameter

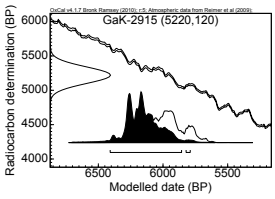


(c) Date of elm decline

| | |
|---|---|
| Site: | White Moss |
| Model: | `P_Sequence` |
| Date: | Birm-665 |
| 95.4% range: | 6005–5490 |
| Outliers: | - |
| Lat: | 53.99 |
| Long: | -2.32 |
| Data source: | Bartley et al. (1990); Williams and Johnson (1976) |

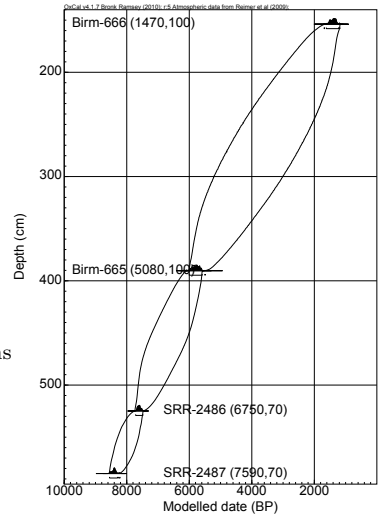


(a) Chronology

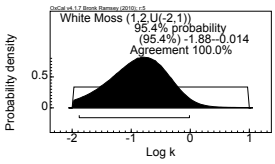


(b) Step-size parameter

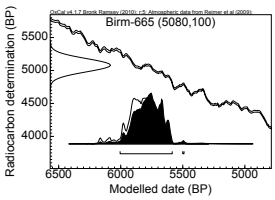


(c) Date of elm decline

| | |
|---|---|
| Site: | Wilden Marsh |
| Model: | `P_Sequence` |
| Date: | SRR-2829 |
| 95.4% range: | 6307–6016 |
| Outliers: | - |
| Lat: | 52.36 |
| Long: | -2.26 |
| Data source: | Brown (1988) |

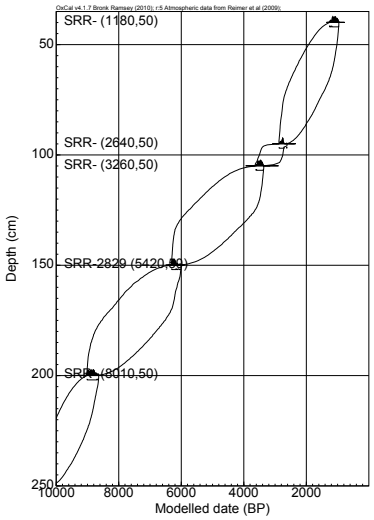


(a) Chronology

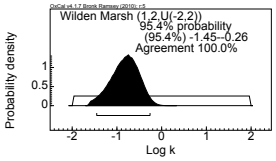


(b) Step-size parameter

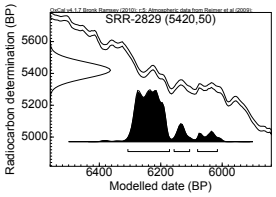


(c) Date of elm decline

| | |
|---|---|
| Site: | Williamsons Moss |
| Model: | `P_Sequence` |
| Date: | SRR-3065 |
| 95.4% range: | 6209–5661 |
| Outliers: | - |
| Lat: | 54.32 |
| Long: | -3.41 |
| Data source: | Harkness (1981); Tipping (1994) |

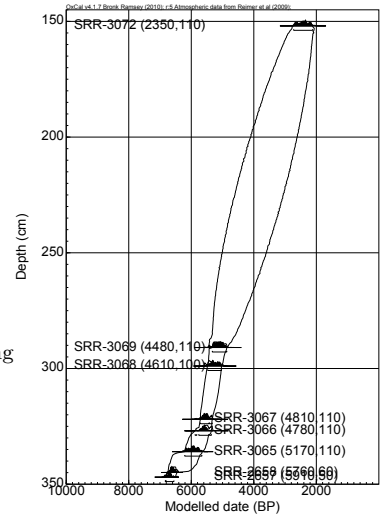


(a) Chronology

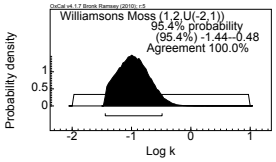


(b) Step-size parameter

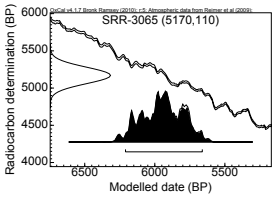


(c) Date of elm decline

# Ireland

| | |
|---|---|
| Site: | Altar Lough |
| Model: | `P_Sequence` |
| Date: | Q-2899 |
| 95.4% range: | 5711–5324 |
| Outliers: | Q-2901 (7%) |
| Lat: | 55.02 |
| Long: | -8.39 |
| Data source: | Fossitt (1994) |

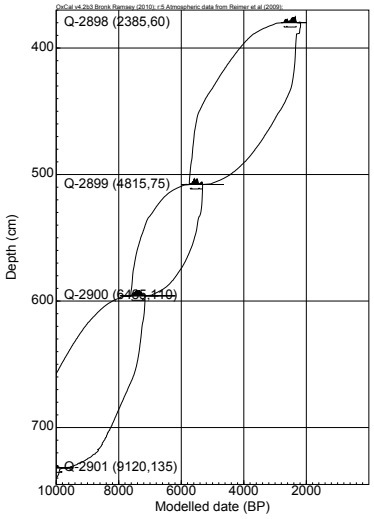


(a) Chronology

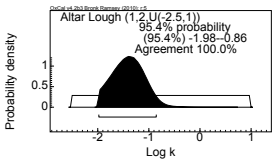


(b) Step-size parameter

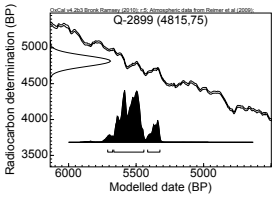


(c) Date of elm decline

| | |
|---|---|
| Site: | Altnahinch |
| Model: | P_Sequence |
| Date: | UB-423 |
| 95.4% range: | 5919–5367 |
| Outliers: | - |
| Lat: | 54.94 |
| Long: | -6.08 |
| Data source: | Smith et al. (1973) |

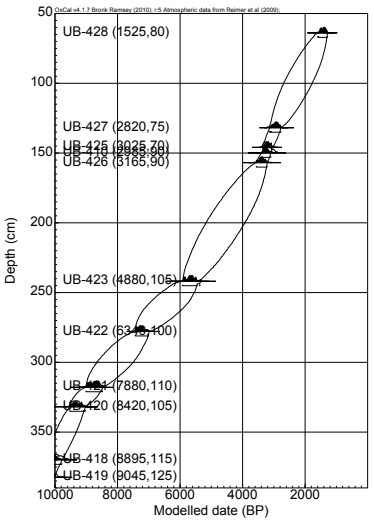


(a) Chronology

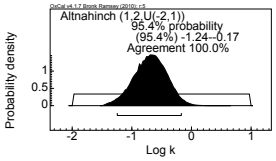


(b) Step-size parameter

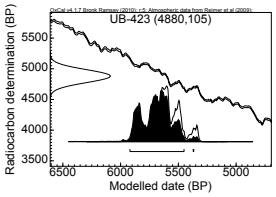


(c) Date of elm decline

| | |
|---|---|
| Site: | Ballynagilly |
| Model: | P_Sequence |
| Date: | UB-253 |
| 95.4% range: | 6112–5746 |
| Outliers: | - |
| Lat: | 54.7 |
| Long: | -6.84 |
| Data source: | Pilcher et al. (1971); Smith et al. (1970, 1971a) |

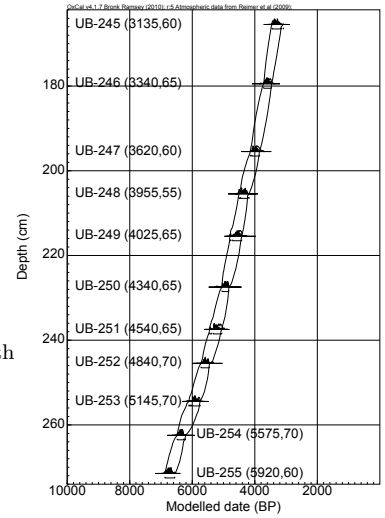


(a) Chronology

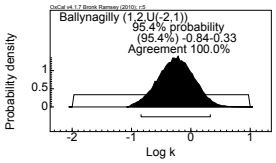


(b) Step-size parameter

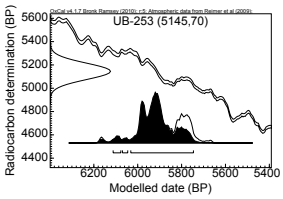


(c) Date of elm decline

| | |
|---|---|
| Site: | Ballyscullion |
| Model: | P_Sequence |
| Date: | UB-114 |
| 95.4% range: | 5785–5645 |
| Outliers: | UB-109 (8%) |
| Lat: | 54.8 |
| Long: | -6.45 |
| Data source: | Pilcher et al. (1971); Smith et al. (1971a) |

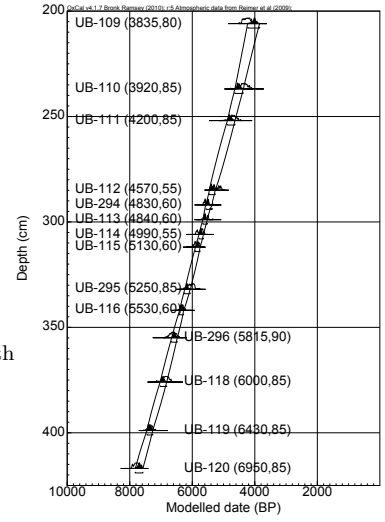


(a) Chronology

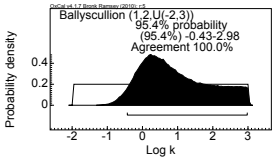


(b) Step-size parameter

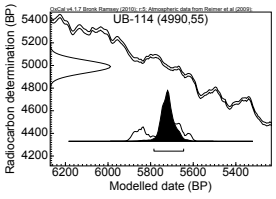


(c) Date of elm decline

| | |
|---|---|
| Site: | Beaghmore |
| Model: | `P_Sequence` |
| Date: | UB-98 |
| 95.4% range: | 5896–5610 |
| Outliers: | UB-94 (6%) |
| Lat: | 54.7 |
| Long: | -6.94 |
| Data source: | Pilcher et al. (1971); Smith et al. (1970, 1971a); Pilcher (1969) |

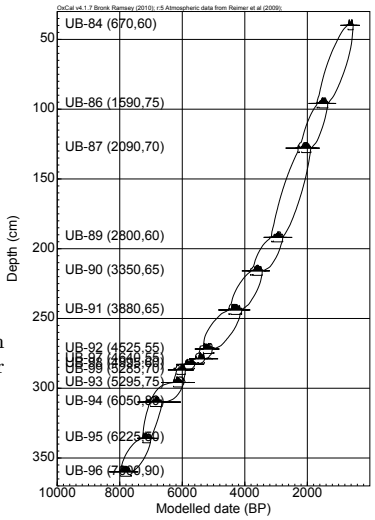


(a) Chronology

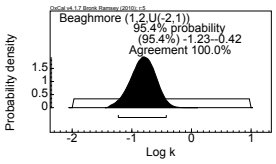


(b) Step-size parameter

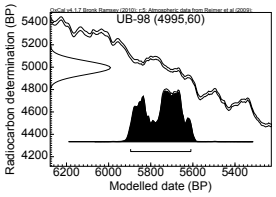


(c) Date of elm decline

| | |
|---|---|
| Site: | Carrivmoragh |
| Model: | `P_Sequence` |
| Date: | UB-870 |
| 95.4% range: | 5644–5305 |
| Outliers: | UB-869 (9%) |
| Lat: | 54.31 |
| Long: | -5.98 |
| Data source: | Pearson and Pilcher (1975) |

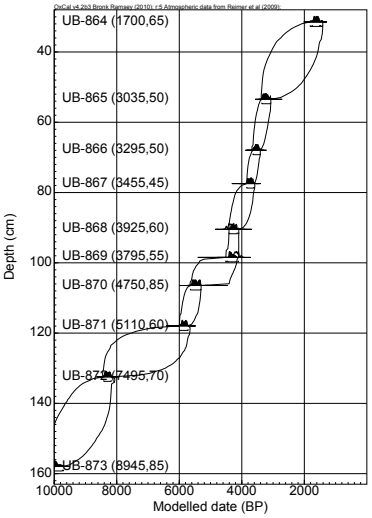


(a) Chronology

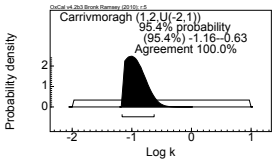


(b) Step-size parameter

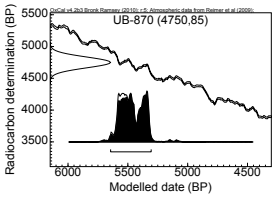


(c) Date of elm decline

| | |
|---|---|
| Site: | Connemara Nat Pk |
| Model: | `Sequence` |
| Date: | ? |
| 95.4% range: | 5455–5053 |
| Outliers: | - |
| Lat: | 53.54 |
| Long: | -9.88 |
| Data source: | O'Connell (1990) |

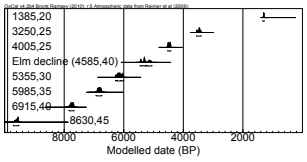


(a) Chronology

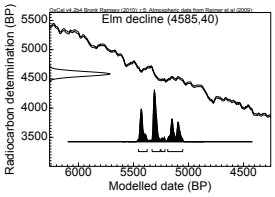


(b) Date of elm decline

| | |
|---|---|
| Site: | Fallahogy |
| Model: | P_Sequence |
| Date: | Q-555 |
| 95.4% range: | 6284–5990 |
| Outliers: | - |
| Lat: | 54.91 |
| Long: | -6.55 |
| Data source: | Godwin (1962); Smith and Willis (1961/1962) |

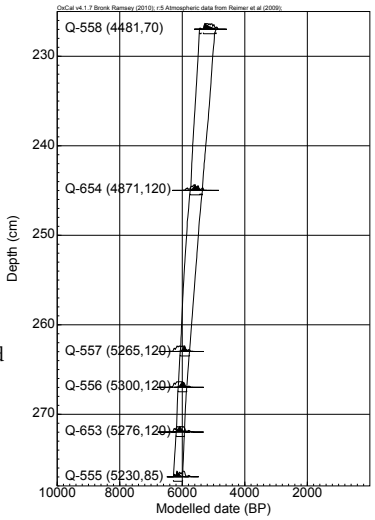


(a) Chronology

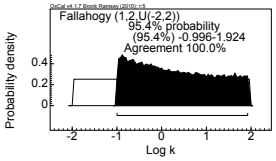


(b) Step-size parameter

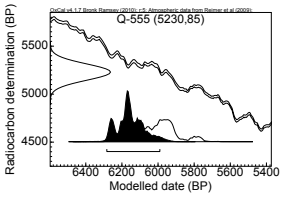


(c) Date of elm decline

| | |
|---|---|
| Site: | Garry Bog |
| Model: | P_Sequence |
| Date: | UB-2191 |
| 95.4% range: | 5579–5045 |
| Outliers: | UB-2196 (38%); UB-2195 (35%) |
| Lat: | 55.1 |
| Long: | -6.55 |
| Data source: | Pearson (1979); Pilcher and Larmour (1982) |

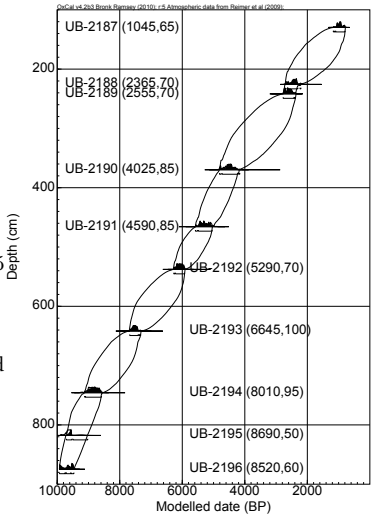


(a) Chronology

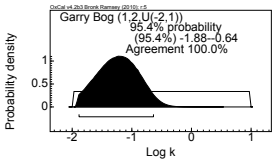


(b) Step-size parameter

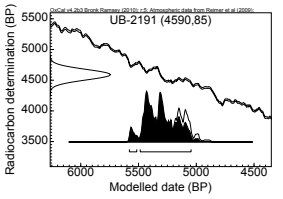


(c) Date of elm decline

| | |
|---|---|
| Site: | Killymaddy Lough |
| Model: | Sequence |
| Date: | UB-2475 |
| 95.4% range: | 5994–5615 |
| Outliers: | - |
| Lat: | 54.5 |
| Long: | -6.79 |
| Data source: | Hirons and Edwards (1986) |

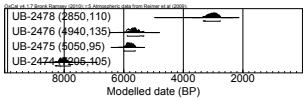


(a) Chronology

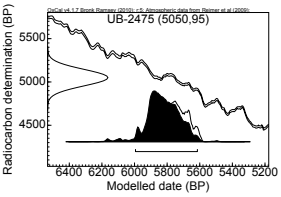


(b) Date of elm decline

Site: Lackan
Model: P_Sequence
Date: UB-801
95.4% range: 5925–5719
Outliers: UB-806 (6%)
Lat: 54.27
Long: -6.09
Data source: Pearson and Pilcher (1975)

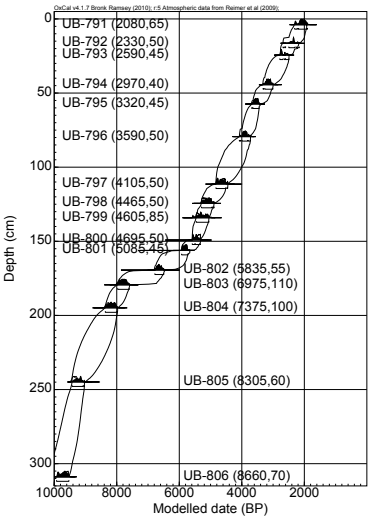


(a) Chronology

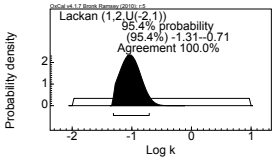


(b) Step-size parameter

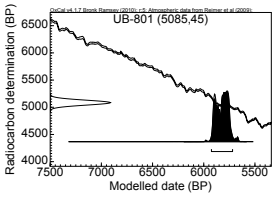


(c) Date of elm decline

Site: Lough Catherine II
Model: P_Sequence
Date: UB-2266
95.4% range: 6271–5912
Outliers: UB-2314 (6%)
Lat: 54.7
Long: -7.43
Data source: Hirons and Edwards (1986)

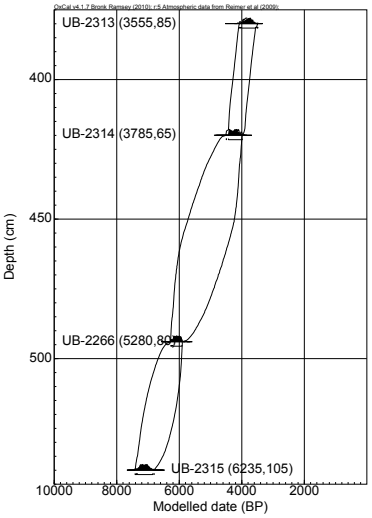


(a) Chronology

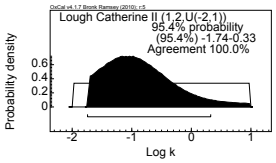


(b) Step-size parameter

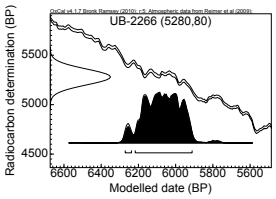


(c) Date of elm decline

Site: Lough Catherine VI
Model: P_Sequence
Date: UB-2389
95.4% range: 6269–5793
Outliers: -
Lat: 54.7
Long: -7.43
Data source: Hirons and Edwards (1986)

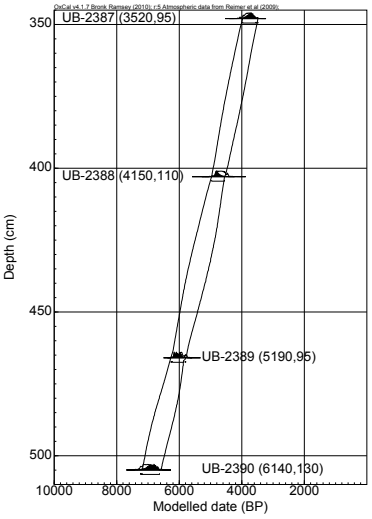


(a) Chronology

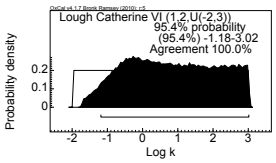


(b) Step-size parameter

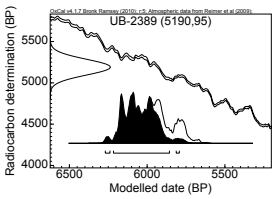


(c) Date of elm decline

| | |
|---|---|
| Site: | Lough Doo |
| Model: | `P_Sequence` |
| Date: | GrN-11737b |
| 95.4% range: | 6175–5307 |
| Outliers: | GrN-11738 (100%); GrN-11738b (100%); GrN-11739 (22%); GrN-11739b (39%) |
| Lat: | 54.05 |
| Long: | -9.1 |
| Data source: | O'Connell et al. (1987) |

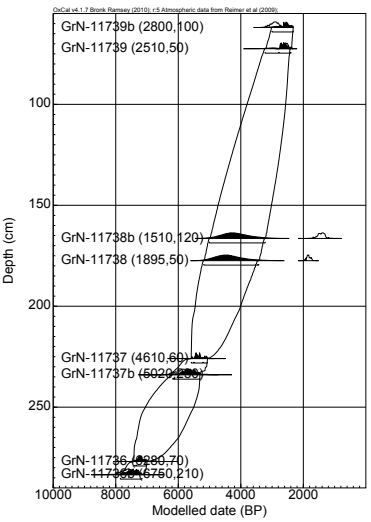


(a) Chronology

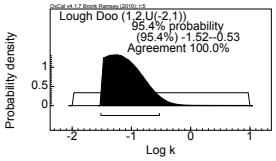


(b) Step-size parameter

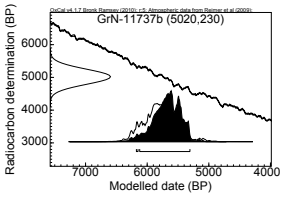


(c) Date of elm decline

| | |
|---|---|
| Site: | Lough Mullaghlahan |
| Model: | `Sequence` |
| Date: | Q-2849 |
| 95.4% range: | 6262–5937 |
| Outliers: | - |
| Lat: | 54.78 |
| Long: | -8.47 |
| Data source: | Fossitt (1994) |

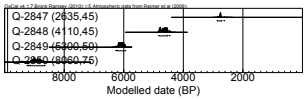


(a) Chronology

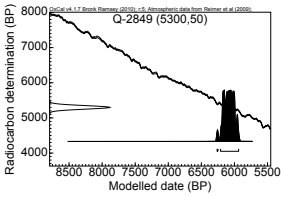


(b) Date of elm decline

| | |
|---|---|
| Site: | Lough Namackanberg |
| Model: | `Sequence` |
| Date: | ? |
| 95.4% range: | 6407–5939 |
| Outliers: | - |
| Lat: | 53.28 |
| Long: | -9.3 |
| Data source: | O'Connell (1990) |

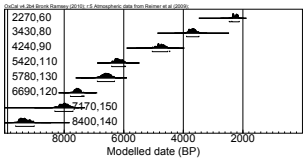


(a) Chronology

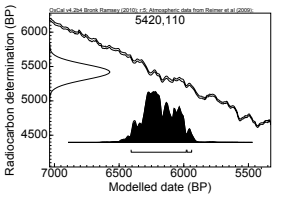


(b) Date of elm decline

| | |
|---|---|
| Site: | Lough Sheeauns |
| Model: | `Sequence` |
| Date: | GrN-14041 |
| 95.4% range: | 5741–5597 |
| Outliers: | - |
| Lat: | 53.56 |
| Long: | -10.08 |
| Data source: | Molloy and O'Connell (1987) |

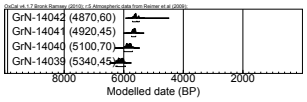


(a) Chronology

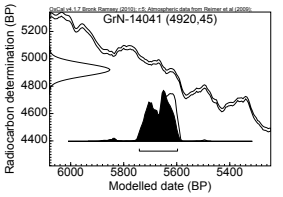


(b) Date of elm decline

| | |
|---|---|
| Site: | Meenadoan |
| Model: | P_Sequence |
| Date: | UB-2110 |
| 95.4% range: | 5885–5086 |
| Outliers: | UB-2142 (7%) |
| Lat: | 54.59 |
| Long: | -7.62 |
| Data source: | Pearson (1979); Pilcher and Larmour (1982) |

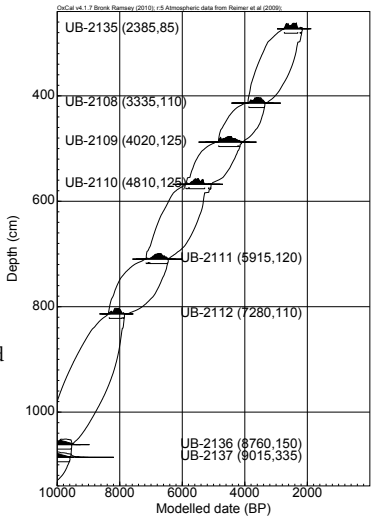


(a) Chronology

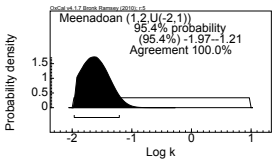


(b) Step-size parameter

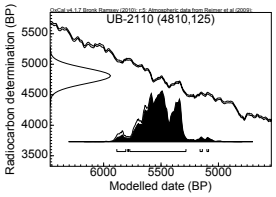


(c) Date of elm decline

| | |
|---|---|
| Site: | Redbog |
| Model: | P_Sequence |
| Date: | D-4 |
| 95.4% range: | 6211–5327 |
| Outliers: | - |
| Lat: | 53.97 |
| Long: | -6.42 |
| Data source: | McAulay and Watts (1961); Mitchell (1954-1956) |

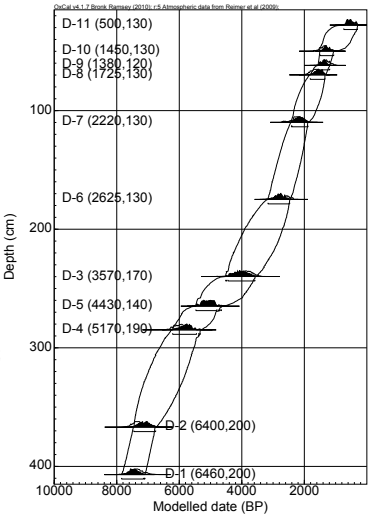


(a) Chronology

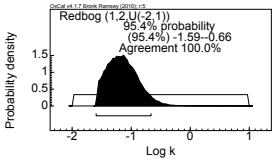


(b) Step-size parameter

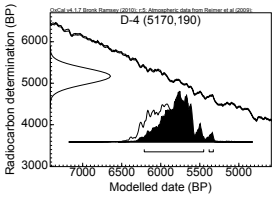


(c) Date of elm decline

| | |
|---|---|
| Site: | Slieve Croob |
| Model: | P_Sequence |
| Date: | UB-833 |
| 95.4% range: | 5576–4826 |
| Outliers: | UB-833 (13%) |
| Lat: | 54.34 |
| Long: | -5.97 |
| Data source: | Pearson and Pilcher (1975) |

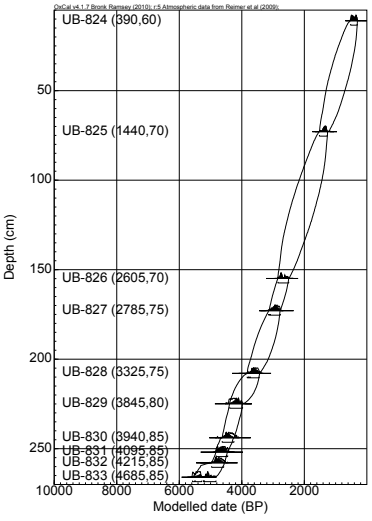


(a) Chronology

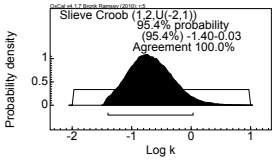


(b) Step-size parameter

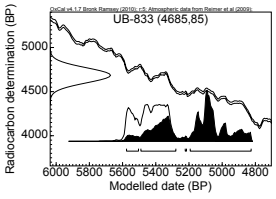


(c) Date of elm decline

Site: Slieve Gallion
Model: P_Sequence
Date: UB-275
95.4% range: 5872–5476
Outliers: UB-298 (6%)
Lat: 54.75
Long: -6.75
Data source: Pilcher (1973); Smith et al. (1971a)

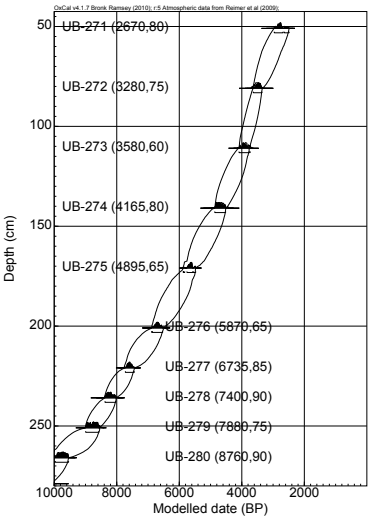


(a) Chronology

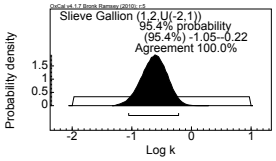


(b) Step-size parameter

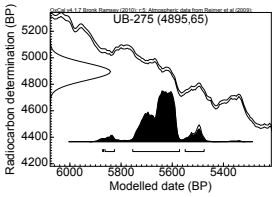


(c) Date of elm decline

Site: Sluggan Bog
Model: P_Sequence
Date: UB-441
95.4% range: 5896–5475
Outliers: UB-448 (64%); UB-447 (7%); UB-445(99%); UB-442 (6%); UB-219d (6%)
Lat: 54.77
Long: -6.43
Data source: Smith et al. (1971a,b); Smith and Goddard (1991)

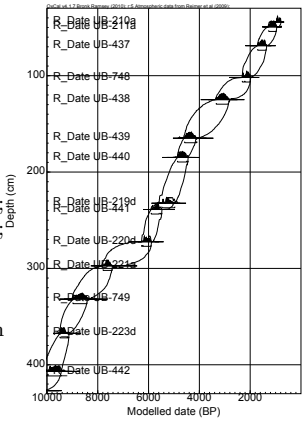


(a) Chronology

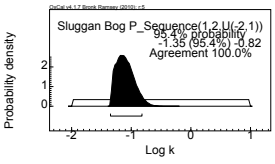


(b) Step-size parameter

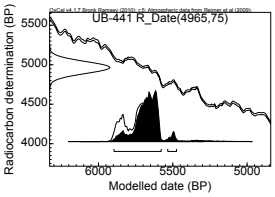


(c) Date of elm decline

Site: Treanscrabbagh
Model: Sequence
Date: D-13
95.4% range: 6180–5291
Outliers: D-17 (92%); D-16 (10%)
Lat: 54.05
Long: -8.38
Data source: Mitchell (1950); McAulay and Watts (1961); Smith and Pilcher (1973)

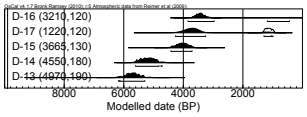


(a) Chronology

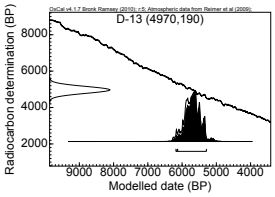


(b) Date of elm decline

Site: Union Wood
Model: Sequence
Date: ARL-188
95.4% range: 6391–4891
Outliers: -
Lat: 54.52
Long: -8.43
Data source: Dodson and Bradshaw (1987)

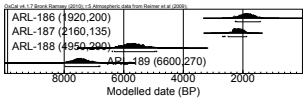


(a) Chronology

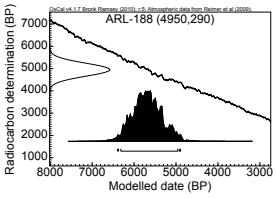


(b) Date of elm decline

| | |
|---|---|
| Site: | Weir's Lough |
| Model: | `P_Sequence` |
| Date: | UB-2488 |
| 95.4% range: | 6177–5919 |
| Outliers: | - |
| Lat: | 54.49 |
| Long: | -6.62 |
| Data source: | Hirons and Edwards (1986) |

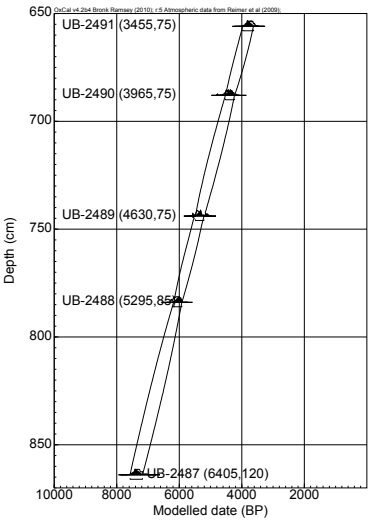


(a) Chronology

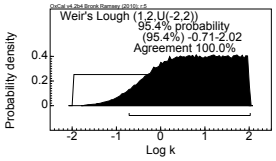


(b) Step-size parameter

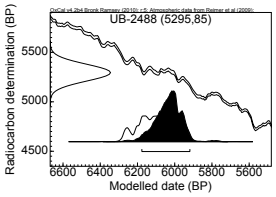


(c) Date of elm decline

# Scotland

| | |
|---|---|
| Site: | Aukurn |
| Model: | `Sequence` |
| Date: | GU-1840 |
| 95.4% range: | 5610–5319 |
| Outliers: | - |
| Lat: | 58.56 |
| Long: | -3.16 |
| Data source: | Robinson (1987) |

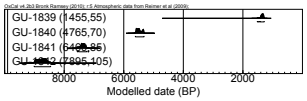


(a) Chronology

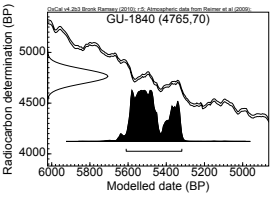


(b) Date of elm decline

| | |
|---|---|
| Site: | Black Loch |
| Model: | `P_Sequence` |
| Date: | SRR-2618 |
| 95.4% range: | 5658–5345 |
| Outliers: | SRR-2614 (6%) |
| Lat: | 56.32 |
| Long: | -3.2 |
| Data source: | Whittington et al. (1991) |

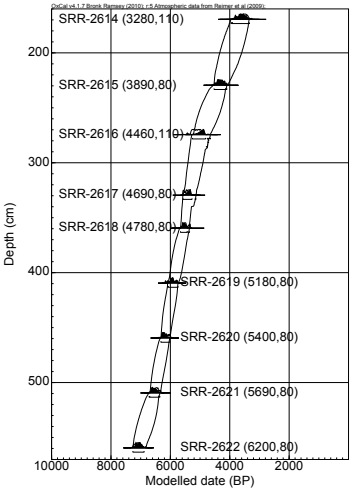


(a) Chronology

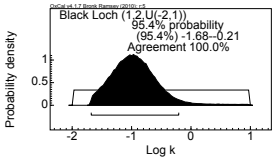


(b) Step-size parameter

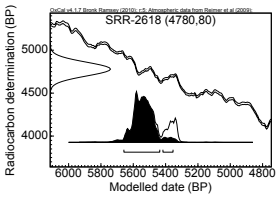


(c) Date of elm decline

Site: Burnfoothill Moss
Model: P_Sequence
Date: SRR-3755
95.4% range: 5651–5470
Outliers: SRR-3756 (6%)
Lat: 55.05
Long: -3.15
Data source: Tipping (1995a,b)

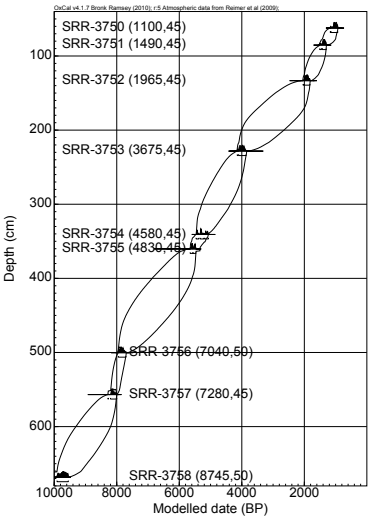


(a) Chronology

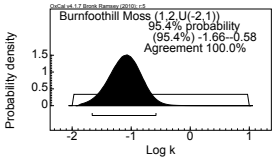


(b) Step-size parameter

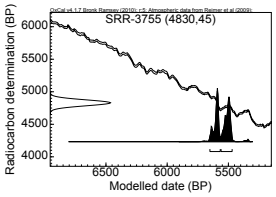


(c) Date of elm decline

Site: Caenlochan Glen
Model: P_Sequence
Date: Q-1447
95.4% range: 5642–5313
Outliers: -
Lat: 56.87
Long: -3.36
Data source: Huntley (1981); Switsur (1981)

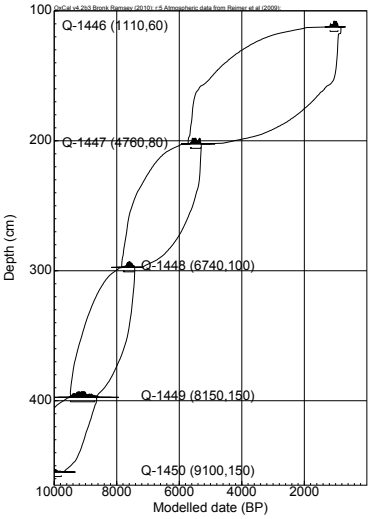


(a) Chronology

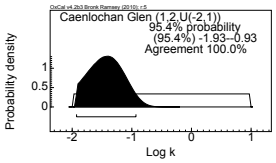


(b) Step-size parameter

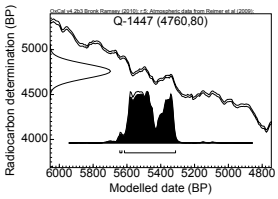


(c) Date of elm decline

Site: Carn Dubh
Model: P_Sequence
Date: GU-3370
95.4% range: 5889–5579
Outliers: -
Lat: 56.73
Long: -3.66
Data source: Tipping (1995c)

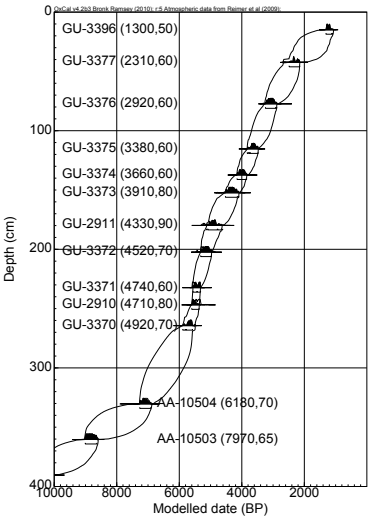


(a) Chronology

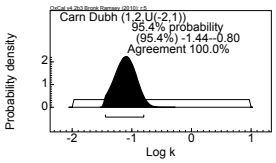


(b) Step-size parameter

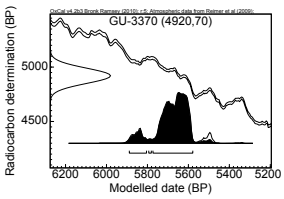


(c) Date of elm decline

| | |
|---|---|
| Site: | Coire Fee |
| Model: | P_Sequence |
| Date: | Q-1421 |
| 95.4% range: | 5470–4963 |
| Outliers: | - |
| Lat: | 56.87 |
| Long: | -3.23 |
| Data source: | Huntley (1981); Switsur (1981) |

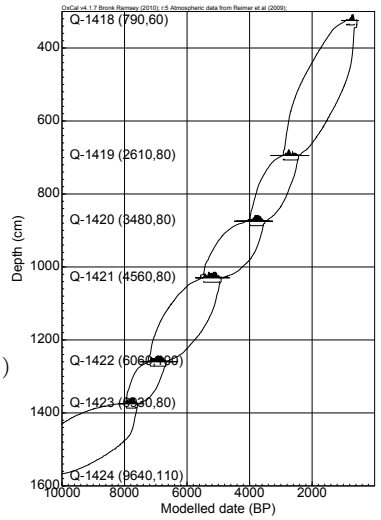


(a) Chronology

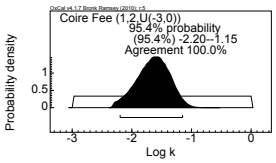


(b) Step-size parameter

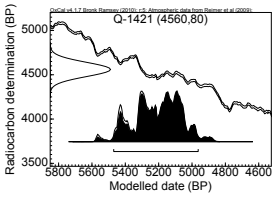


(c) Date of elm decline

| | |
|---|---|
| Site: | Creag na Caillach |
| Model: | P_Sequence |
| Date: | GU-2976 |
| 95.4% range: | 4965–4656 |
| Outliers: | - |
| Lat: | 56.5 |
| Long: | -4.34 |
| Data source: | Tipping et al. (1993) |

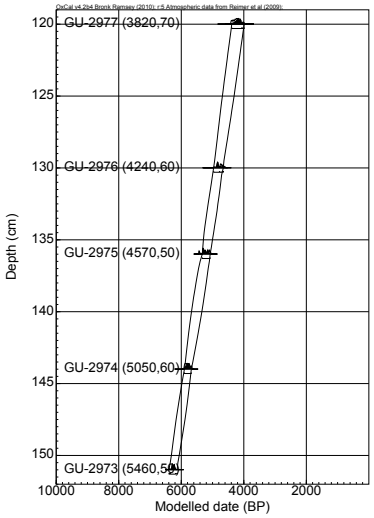


(a) Chronology

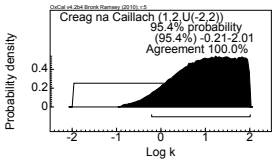


(b) Step-size parameter

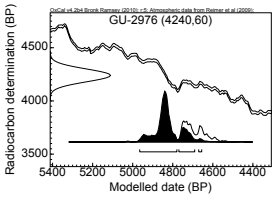


(c) Date of elm decline

| | |
|---|---|
| Site: | Dalican Ness |
| Model: | P_Sequence |
| Date: | Q-2758 |
| 95.4% range: | 5999–5604 |
| Outliers: | - |
| Lat: | 60.39 |
| Long: | -1.1 |
| Data source: | Bennett et al. (1992) |

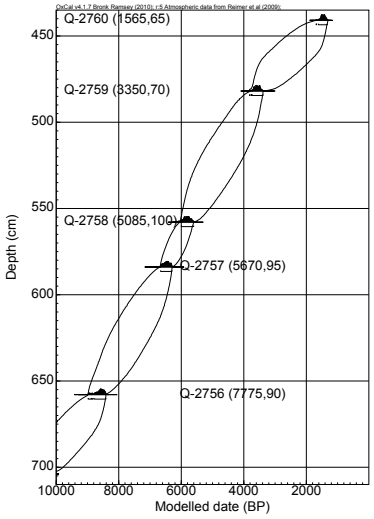


(a) Chronology

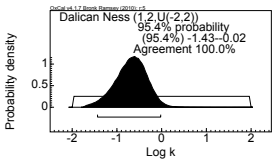


(b) Step-size parameter

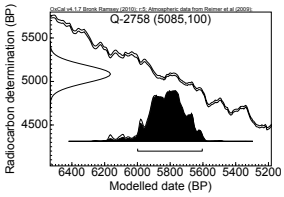


(c) Date of elm decline

Site: Din Moss
Model: P_Sequence
Date: Q-1063
95.4% range: 6291–6022
Outliers: Q-1080 (6%); Q-1069 (6%)
Lat: 55.58
Long: -2.31
Data source: Hibbert and Switsur (1976)

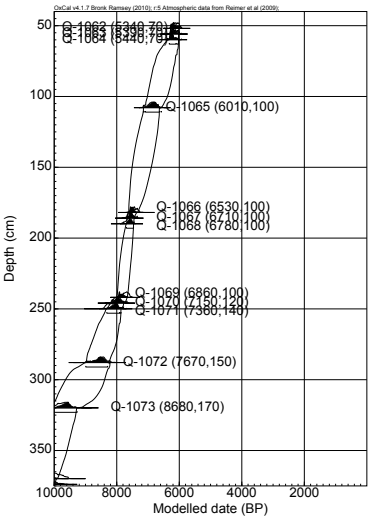


(a) Chronology

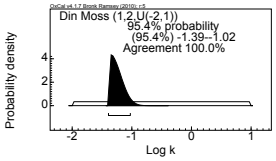


(b) Step-size parameter

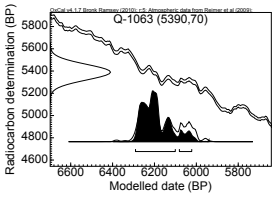


(c) Date of elm decline

Site: Duartbeg
Model: Sequence
Date: Q-741
95.4% range: 4800–4079
Outliers: -
Lat: 58.3
Long: -5.13
Data source: Moar (1969); Godwin et al. (1965)

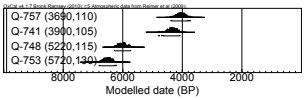


(a) Chronology

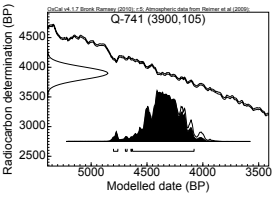


(b) Date of elm decline

Site: Dubh Lochan
Model: Sequence
Date: SRR-1219
95.4% range: 5898–5472
Outliers: -
Lat: 56.13
Long: -4.61
Data source: Stewart et al. (1984)

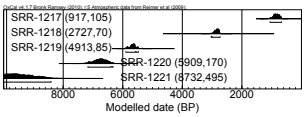


(a) Chronology

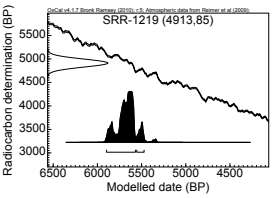


(b) Date of elm decline

Site: Flanders Moss
Model: Sequence
Date: Q-578
95.4% range: 6101–5616
Outliers: Q-575 (6%); Q-570 (6%)
Lat: 56.13
Long: -4.33
Data source: Turner (1965); Godwin (1962)

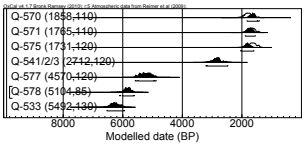


(a) Chronology

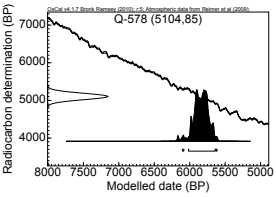


(b) Date of elm decline

| | |
|---|---|
| Site: | Glen Carron |
| Model: | `P_Sequence` |
| Date: | RCD-2185 |
| 95.4% range: | 5436–4966 |
| Outliers: | - |
| Lat: | 57.56 |
| Long: | -5.37 |
| Data source: | Anderson (1996) |

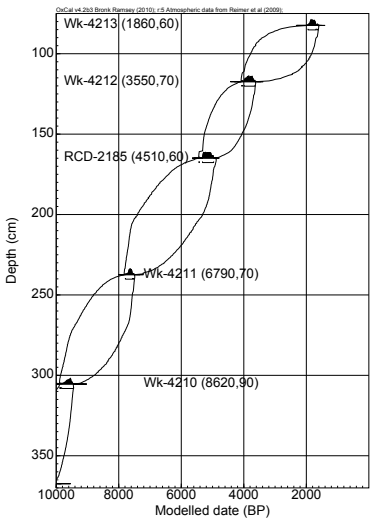


(a) Chronology

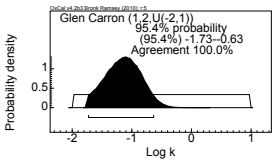


(b) Step-size parameter

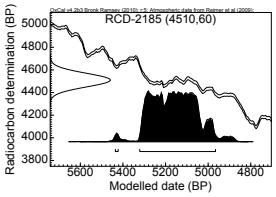


(c) Date of elm decline

| | |
|---|---|
| Site: | Glen Torridan |
| Model: | `P_Sequence` |
| Date: | SRR-5600 |
| 95.4% range: | 6270–5943 |
| Outliers: | - |
| Lat: | 57.53 |
| Long: | -5.15 |
| Data source: | Anderson (1996) |

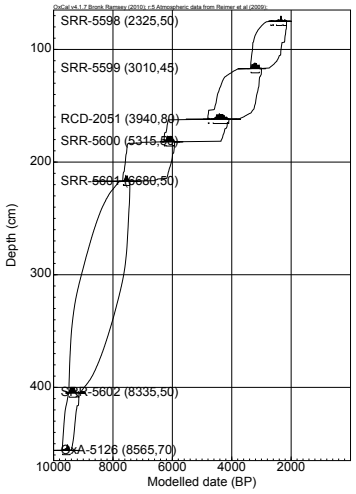


(a) Chronology

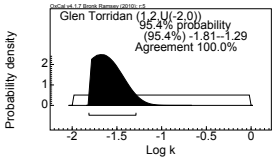


(b) Step-size parameter

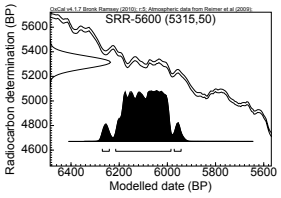


(c) Date of elm decline

| | |
|---|---|
| Site: | Loch a'Mhuilinn |
| Model: | `Sequence` |
| Date: | SRR-2578 |
| 95.4% range: | 6390–5916 |
| Outliers: | SRR-2775 (24%); SRR-2576 (34%) |
| Lat: | 55.7 |
| Long: | -5.28 |
| Data source: | Boyd and Dickson (1987) |

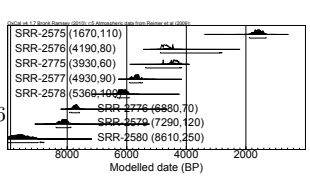


(a) Chronology

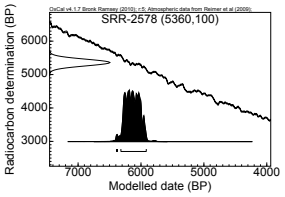


(b) Date of elm decline

Site: Loch Ashik
Model: P_Sequence
Date: SRR-807
95.4% range: 5468–5036
Outliers: -
Lat: 57.24
Long: -5.83
Data source: Harkness (1981)

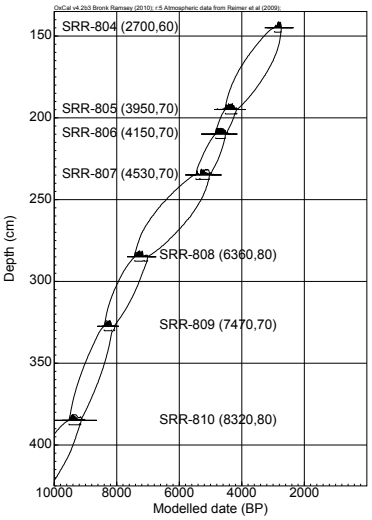


(a) Chronology

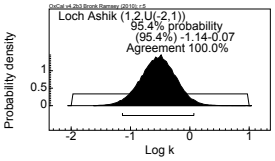


(b) Step-size parameter

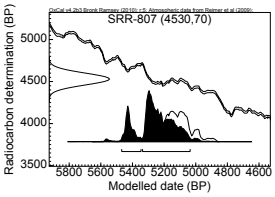


(c) Date of elm decline

Site: Loch Assynt
Model: P_Sequence
Date: Q-1275
95.4% range: 6297–5774
Outliers: -
Lat: 58.17
Long: -5.07
Data source: Switsur (1981)

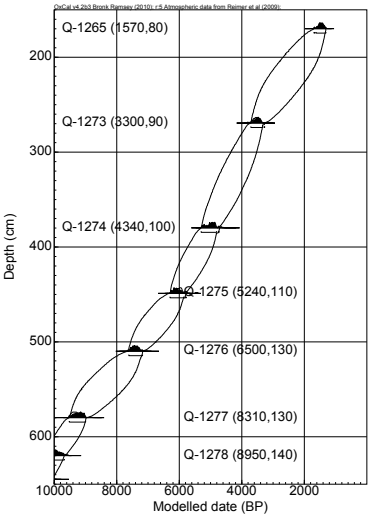


(a) Chronology

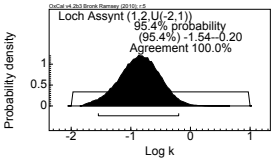


(b) Step-size parameter

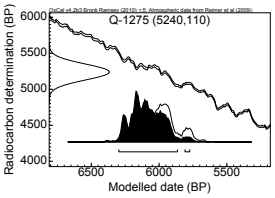


(c) Date of elm decline

Site: Loch Cill an Aonghais
Model: P_Sequence
Date: Q-1414
95.4% range: 6207–5751
Outliers: -
Lat: 55.8
Long: -5.55
Data source: Switsur (1981)

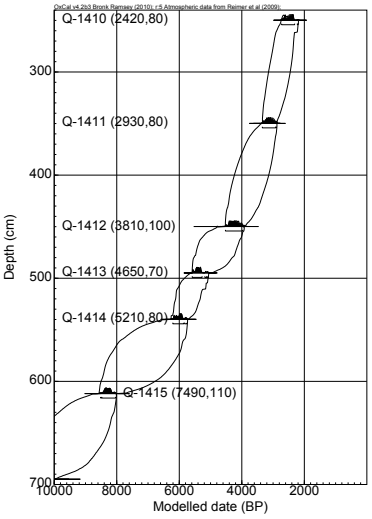


(a) Chronology

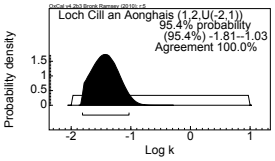


(b) Step-size parameter

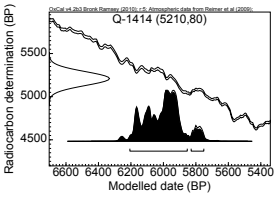


(c) Date of elm decline

Site: Loch Clair
Model: P_Sequence
Date: I-4814
95.4% range: 6392–5917
Outliers: I-4967 (6%)
Lat: 57.67
Long: -5.43
Data source: Pennington et al. (1972)

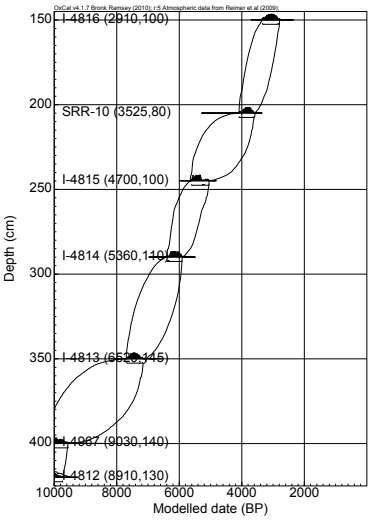


(a) Chronology

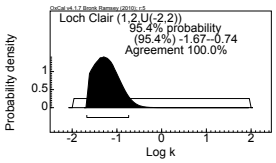


(b) Step-size parameter

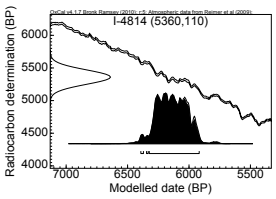


(c) Date of elm decline

Site: Loch Cleat
Model: P_Sequence
Date: SRR-935
95.4% range: 5870–5324
Outliers: -
Lat: 57.68
Long: -6.33
Data source: Harkness (1981)

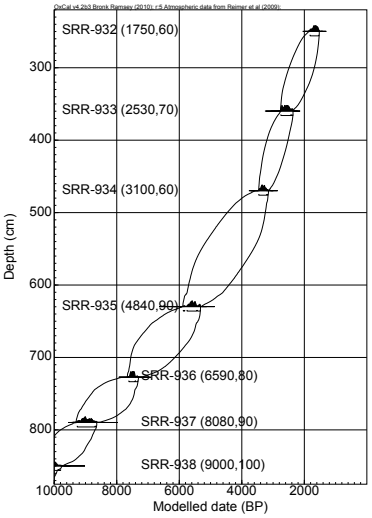


(a) Chronology

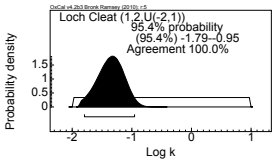


(b) Step-size parameter

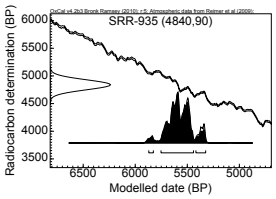


(c) Date of elm decline

Site: Loch Coultrie
Model: P_Sequence
Date: Q-1514
95.4% range: 6267–5891
Outliers: Q-1518 (6%); Q-1513 (10%)
Lat: 57.46
Long: -5.58
Data source: Switsur (1981)

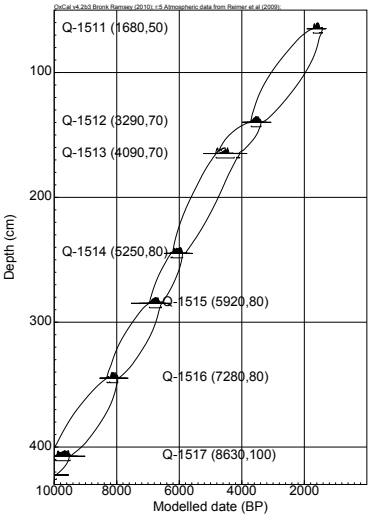


(a) Chronology

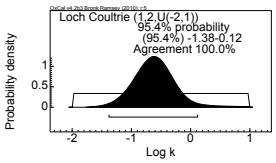


(b) Step-size parameter

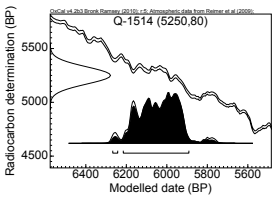


(c) Date of elm decline

| | |
|---|---|
| Site: | Loch Maree |
| Model: | P_Sequence |
| Date: | Q-1006 |
| 95.4% range: | 6001–5751 |
| Outliers: | - |
| Lat: | 57.68 |
| Long: | -5.5 |
| Data source: | Birks (1972); Switsur and West (1973) |

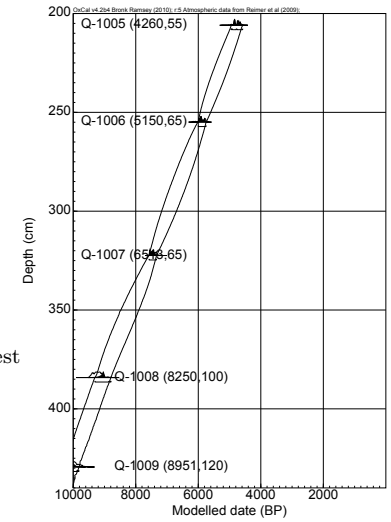


(a) Chronology

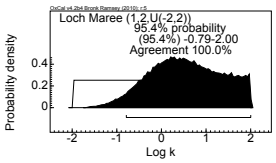


(b) Step-size parameter

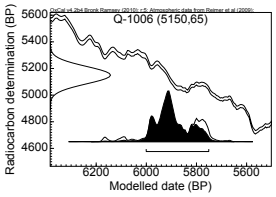


(c) Date of elm decline

| | |
|---|---|
| Site: | Loch Meodal |
| Model: | P_Sequence |
| Date: | Q-1305 |
| 95.4% range: | 6265–5715 |
| Outliers: | - |
| Lat: | 57.13 |
| Long: | -5.87 |
| Data source: | Switsur (1981) |

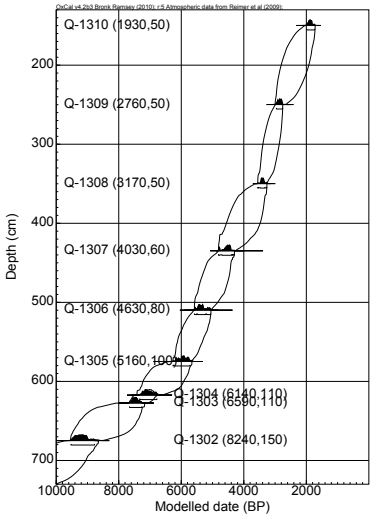


(a) Chronology

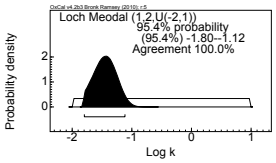


(b) Step-size parameter

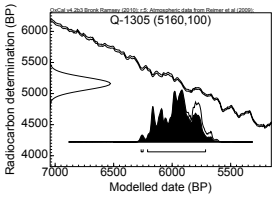


(c) Date of elm decline

| | |
|---|---|
| Site: | Loch of Winless |
| Model: | P_Sequence |
| Date: | Q-1443 |
| 95.4% range: | 5844–5320 |
| Outliers: | - |
| Lat: | 58.48 |
| Long: | -3.32 |
| Data source: | Peglar (1979); Switsur (1981) |

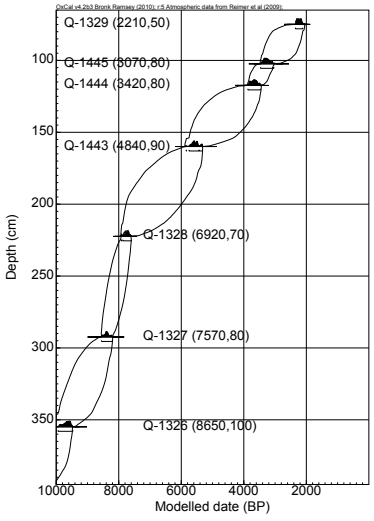


(a) Chronology

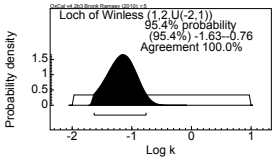


(b) Step-size parameter

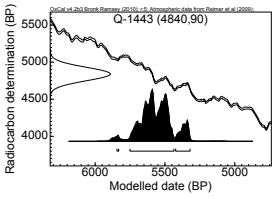


(c) Date of elm decline

| | |
|---|---|
| Site: | Loch Pityoulish |
| Model: | Sequence |
| Date: | SRR-459 |
| 95.4% range: | 6445–6224 |
| Outliers: | - |
| Lat: | 57.2 |
| Long: | -3.79 |
| Data source: | Harkness (1981); O'Sullivan (1976) |

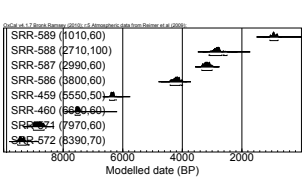


(a) Chronology

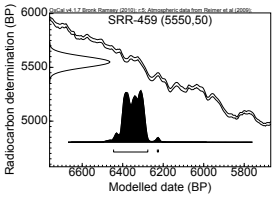


(b) Date of elm decline

| | |
|---|---|
| Site: | Loch Sionascaig |
| Model: | P_Sequence |
| Date: | SRR-12 |
| 95.4% range: | 5328–4905 |
| Outliers: | - |
| Lat: | 58.07 |
| Long: | -5.2 |
| Data source: | Pennington et al. (1972) |

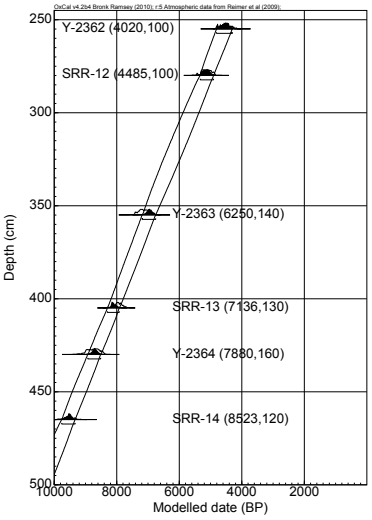


(a) Chronology

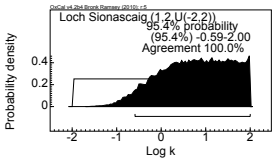


(b) Step-size parameter

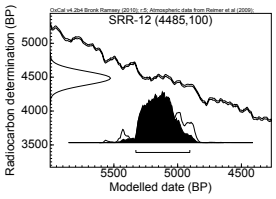


(c) Date of elm decline

| | |
|---|---|
| Site: | Lochan Doilead |
| Model: | P_Sequence |
| Date: | SRR-768 |
| 95.4% range: | 5572–5056 |
| Outliers: | - |
| Lat: | 56.99 |
| Long: | -5.8 |
| Data source: | Harkness (1981) |

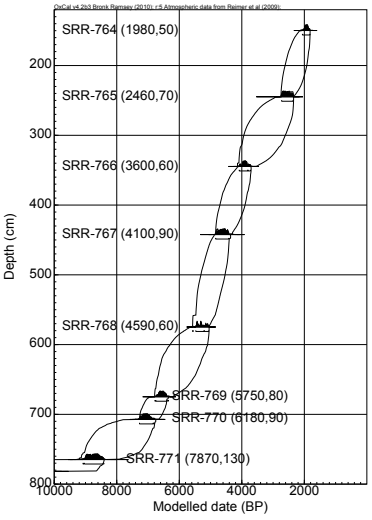


(a) Chronology

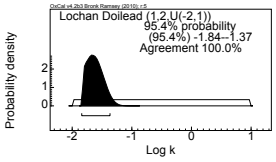


(b) Step-size parameter

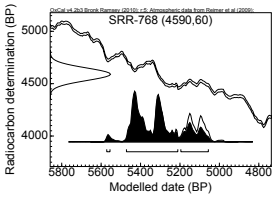


(c) Date of elm decline

Site: Machrie Moor
Model: P_Sequence
Date: GU-1346
95.4% range: 5641–5304
Outliers: -
Lat: 55.53
Long: -5.32
Data source: Robinson and Dickson (1988)

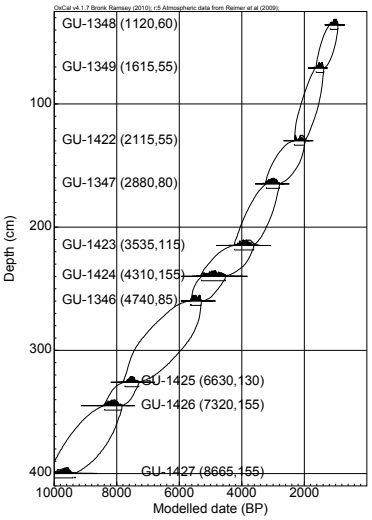


(a) Chronology

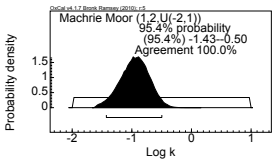


(b) Step-size parameter

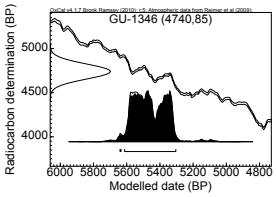


(c) Date of elm decline

Site: Moorlands
Model: Sequence
Date: GrN-13880
95.4% range: 5890–5476
Outliers: -
Lat: 55.44
Long: -5.68
Data source: Edwards and McIntosh (1988)

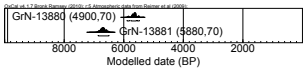


(a) Chronology

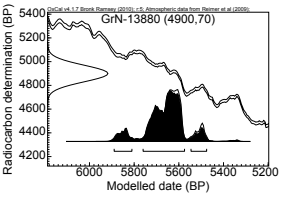


(b) Date of elm decline

Site: Pickletillem
Model: P_Sequence
Date: SRR-3356
95.4% range: 5894–5595
Outliers: GU-1845 (10%)
Lat: 56.4
Long: -2.89
Data source: Whittington et al. (1991)

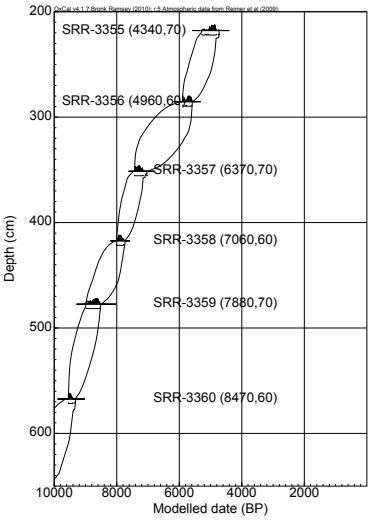


(a) Chronology

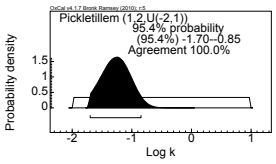


(b) Step-size parameter

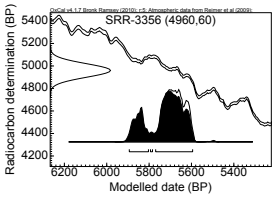


(c) Date of elm decline

| | |
|---|---|
| Site: | Red Moss |
| Model: | `P_Sequence` |
| Date: | SRR-6636 |
| 95.4% range: | 5745–5582 |
| Outliers: | - |
| Lat: | 57.1 |
| Long: | -2.42 |
| Data source: | Clark and Edwards (2004) |

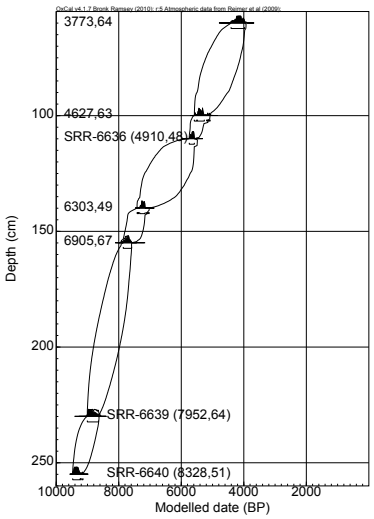


(a) Chronology

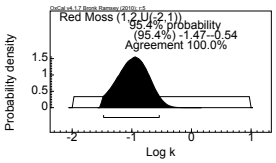


(b) Step-size parameter

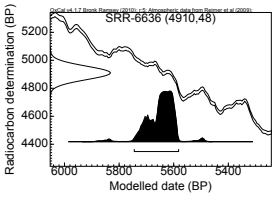


(c) Date of elm decline

| | |
|---|---|
| Site: | Rhoin Farm |
| Model: | `Sequence` |
| Date: | GrN-13882 |
| 95.4% range: | 5878–5466 |
| Outliers: | - |
| Lat: | 55.45 |
| Long: | -5.67 |
| Data source: | Edwards and McIntosh (1988) |

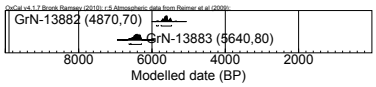


(a) Chronology

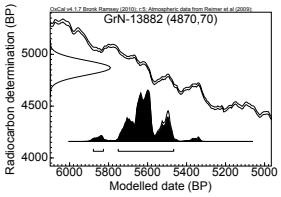


(b) Date of elm decline

| | |
|---|---|
| Site: | St Fergus Moss |
| Model: | `P_Sequence` |
| Date: | SRR-6629 |
| 95.4% range: | 6287–6006 |
| Outliers: | - |
| Lat: | 57.57 |
| Long: | -1.91 |
| Data source: | Clark and Edwards (2004) |

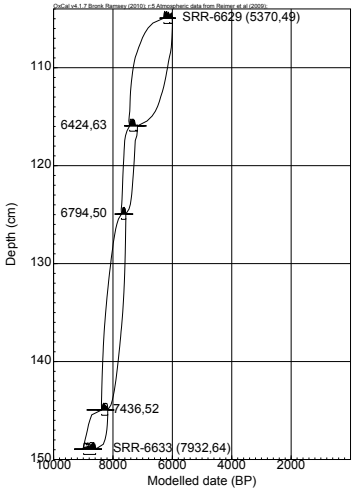


(a) Chronology

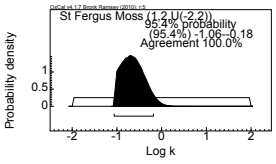


(b) Step-size parameter

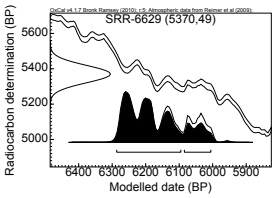


(c) Date of elm decline

# Wales

| | |
|---|---|
| Site: | Breidden Pond |
| Model: | P_Sequence |
| Date: | CAR-143 |
| 95.4% range: | 5285–4855 |
| Outliers: | - |
| Lat: | 52.72 |
| Long: | -3.04 |
| Data source: | Dresser (1985) |

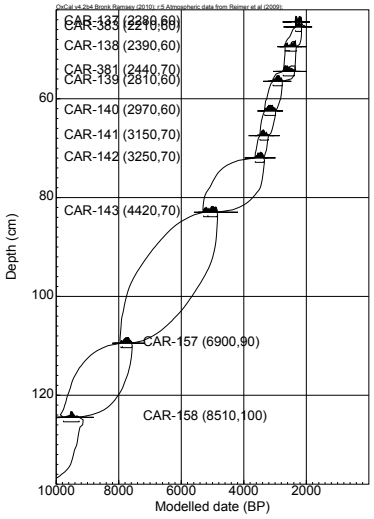


(a) Chronology

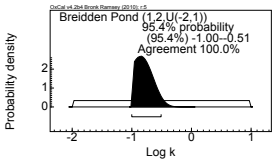


(b) Step-size parameter

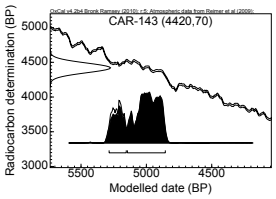


(c) Date of elm decline

| | |
|---|---|
| Site: | Cefn Graeanog Bog |
| Model: | P_Sequence |
| Position: | 127 cm |
| 95.4% range: | 6026–5337 |
| Outliers: | CAR-109 (7%) |
| Lat: | 53.01 |
| Long: | -4.31 |
| Data source: | Dresser (1985) |

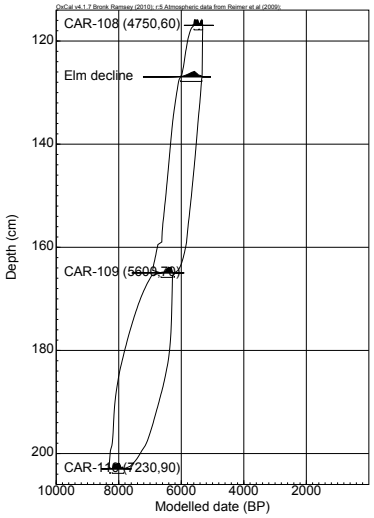


(a) Chronology

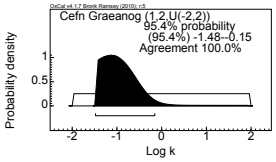


(b) Step-size parameter

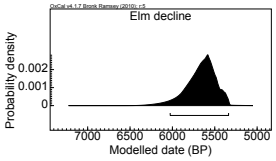


(c) Date of elm decline

| | |
|---|---|
| Site: | Cefn Gwernffrwd |
| Model: | P_Sequence |
| Date: | CAR-45 |
| 95.4% range: | 5903–5475 |
| Outliers: | CAR-97 (29%); CAR-98 (9%) |
| Lat: | 52.13 |
| Long: | -3.84 |
| Data source: | Chambers (1982); Dresser (1985) |

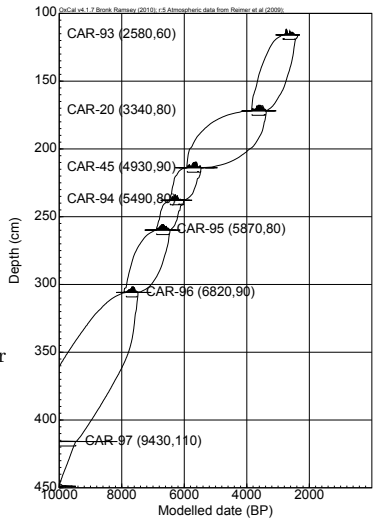


(a) Chronology

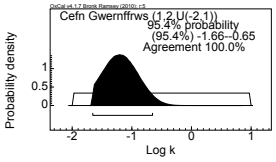


(b) Step-size parameter

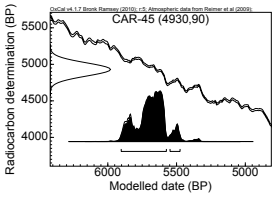


(c) Date of elm decline

Site: Clarach Bay
Model: Sequence
Date: ?
95.4% range: 6002–5611
Outliers: -
Lat: 52.43
Long: -4.08
Data source: Heyworth et al. (1985)

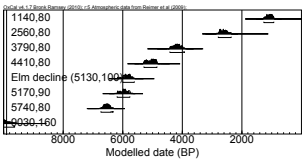


(a) Chronology

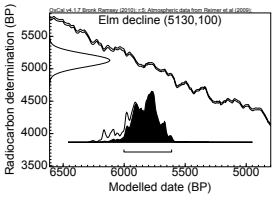


(b) Date of elm decline

Site: Coed Taf
Model: P_Sequence
Date: CAR-91
95.4% range: 5580–5050
Outliers: -
Lat: 51.79
Long: -3.47
Data source: Chambers (1983); Dresser (1985)

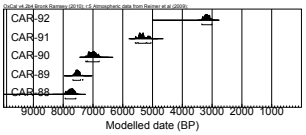


(a) Chronology

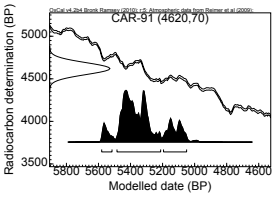


(b) Date of elm decline

Site: Goldcliff
Model: Sequence
Date: CAR-652
95.4% range: 5798–5440
Outliers: CAR-653 (28%); CAR-652 (14%)
Lat: 51.53
Long: -2.9
Data source: Smith and Morgan (1989)

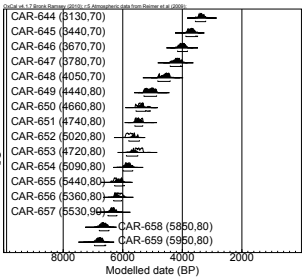


(a) Chronology

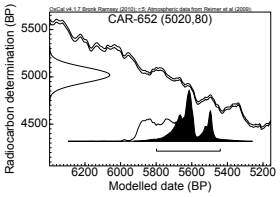


(b) Date of elm decline

Site: Melynllyn Tarn
Model: P_Sequence
Date: SRR-638
95.4% range: 5662–5306
Outliers: -
Lat: 53.17
Long: -3.94
Data source: Walker (1978); Harkness (1981)

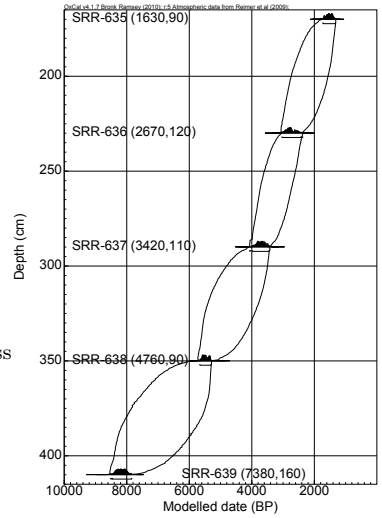


(a) Chronology

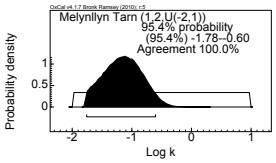


(b) Step-size parameter

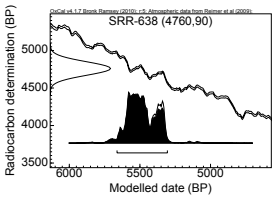


(c) Date of elm decline

Site: Moel Y Gerddi
Model: P_Sequence
Date: CAR-642
95.4% range: 6180–5748
Outliers: -
Lat: 52.87
Long: -4.06
Data source: Chambers and Price (1985); Dresser (1985)

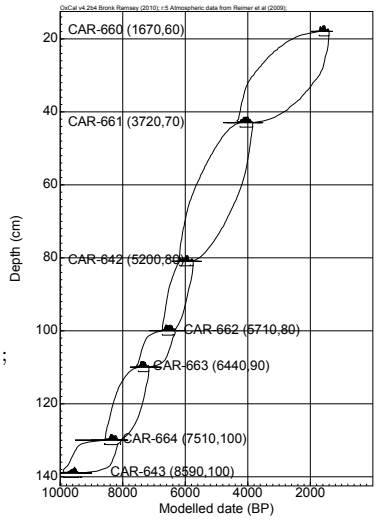


(a) Chronology

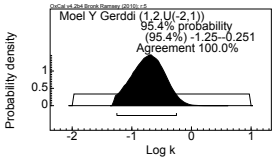


(b) Step-size parameter

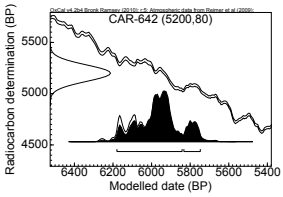


(c) Date of elm decline

Site: Nant Francon
Model: P_Sequence
Date: Q-904
95.4% range: 5911–5660
Outliers: -
Lat: 53.15
Long: -4.06
Data source: Hibbert and Switsur (1976)

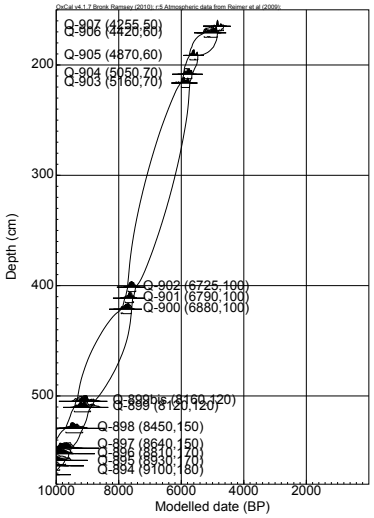


(a) Chronology

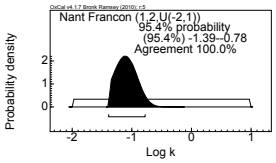


(b) Step-size parameter

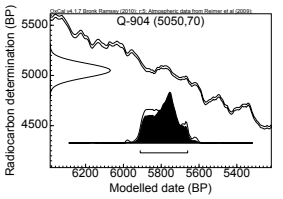


(c) Date of elm decline

Site: Pen Rhiw Wen L
Model: P_Sequence
Date: CAR-17
95.4% range: 5642–5307
Outliers: -
Lat: 51.85
Long: -3.84
Data source: Dresser (1985)

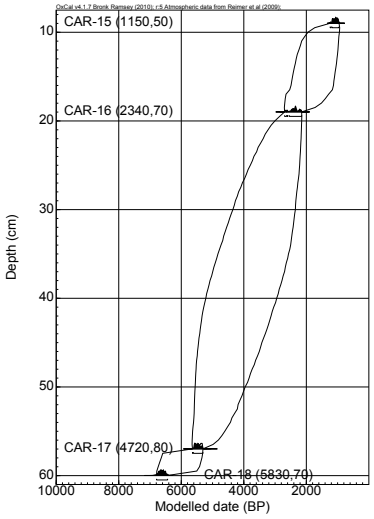


(a) Chronology

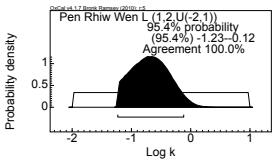


(b) Step-size parameter

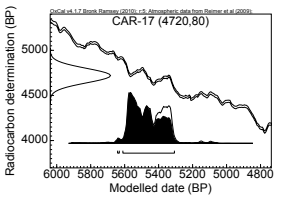


(c) Date of elm decline

Site: Pen Rhiw Wen M
Model: P_Sequence
Date: CAR-12
95.4% range: 5651–5324
Outliers: CAR-13 (7%)
Lat: 51.85
Long: -3.84
Data source: Dresser (1985)

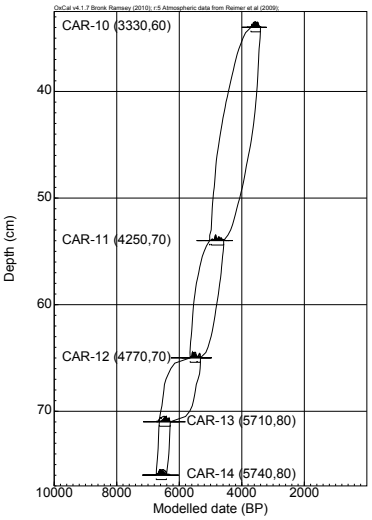


(a) Chronology

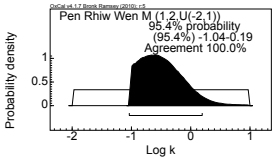


(b) Step-size parameter

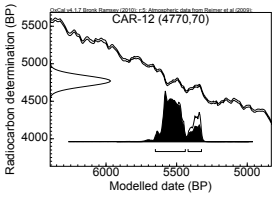


(c) Date of elm decline

Site: Tregaron
Model: P_Sequence
Date: Q-942
95.4% range: 5866–5609
Outliers: -
Lat: 52.24
Long: -3.93
Data source: Hibbert and Switsur (1976)

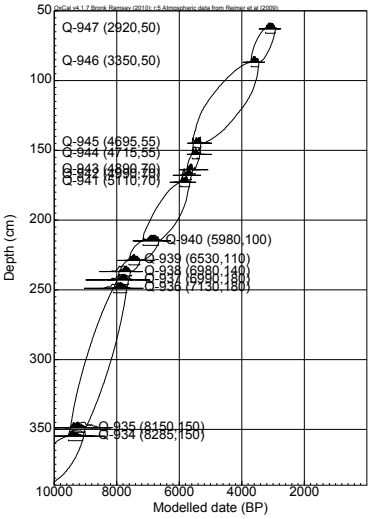


(a) Chronology

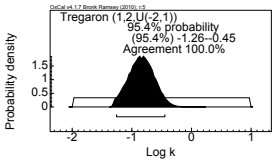


(b) Step-size parameter

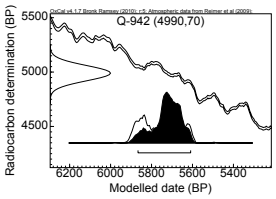


(c) Date of elm decline

Site: WFF A16W
Model: P_Sequence
Date: CAR-326
95.4% range: 6211–5766
Outliers: CAR-329 (6%)
Lat: 51.85
Long: -3.71
Data source: Smith and Cloutman (1988); Dresser (1985)

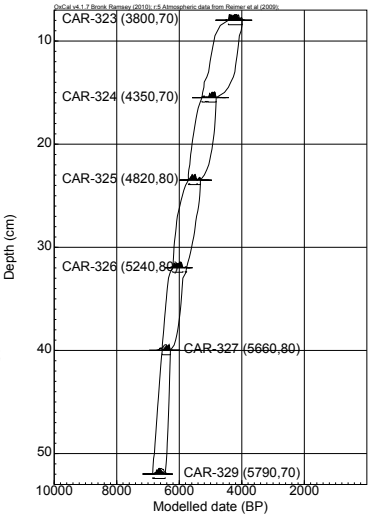


(a) Chronology

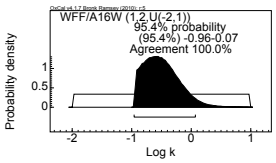


(b) Step-size parameter

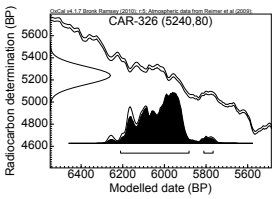


(c) Date of elm decline

| | |
|---|---|
| Site: | WFF B32S |
| Model: | P_Sequence |
| Date: | CAR-339 |
| 95.4% range: | 5750–5326 |
| Outliers: | CAR-342 (9%); CAR-338 (10%) |
| Lat: | 51.85 |
| Long: | -3.71 |
| Data source: | Smith and Cloutman (1988); Dresser (1985) |

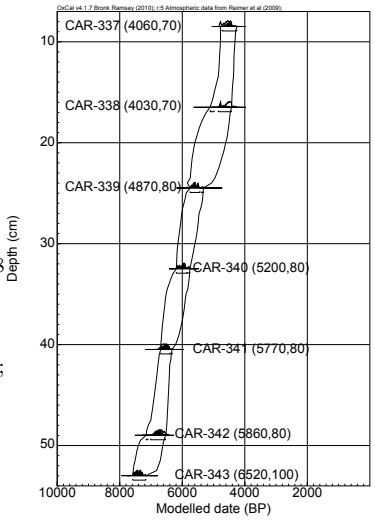


(a) Chronology

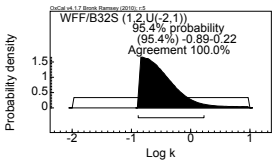


(b) Step-size parameter

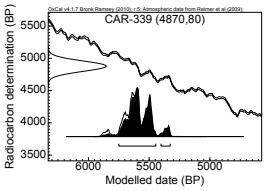


(c) Date of elm decline

| | |
|---|---|
| Site: | WFF B46 |
| Model: | P_Sequence |
| Date: | CAR-410 |
| 95.4% range: | 4237–3775 |
| Outliers: | - |
| Lat: | 51.85 |
| Long: | -3.71 |
| Data source: | Smith and Cloutman (1988); Dresser (1985) |

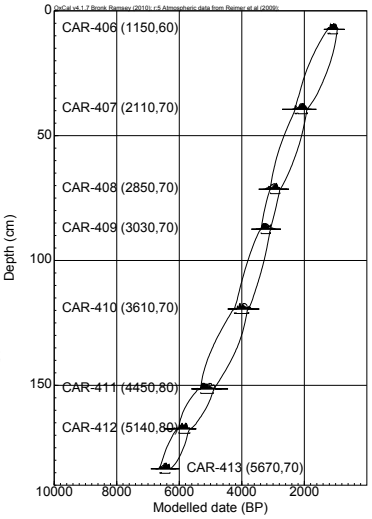


(a) Chronology

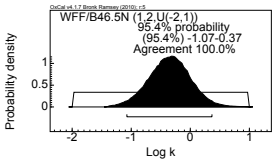


(b) Step-size parameter

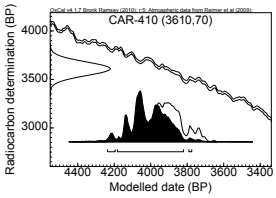


(c) Date of elm decline

| | |
|---|---|
| Site: | WFF B90S |
| Model: | P_Sequence |
| Date: | CAR-500 |
| 95.4% range: | 6185–5757 |
| Outliers: | CAR-501 (8%) |
| Lat: | 51.85 |
| Long: | -3.71 |
| Data source: | Smith and Cloutman (1988); Dresser (1985) |

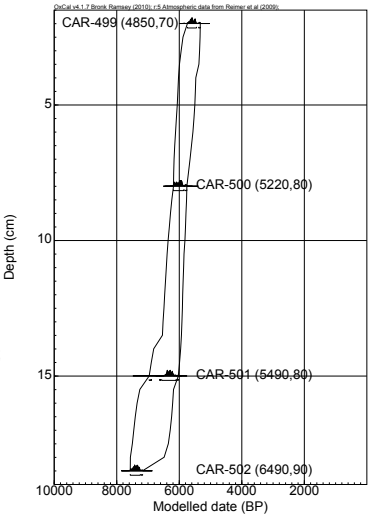


(a) Chronology

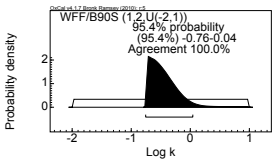


(b) Step-size parameter

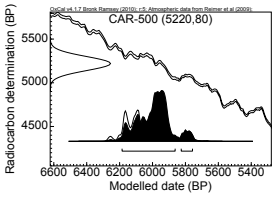


(c) Date of elm decline

Site: WFF E13N
Model: P_Sequence
Date: CAR-638
95.4% range: 6275–5918
Outliers: -
Lat: 51.85
Long: -3.71
Data source: Smith and Cloutman (1988); Dresser (1985)

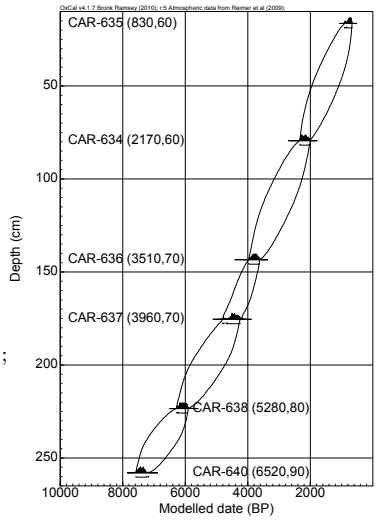


(a) Chronology

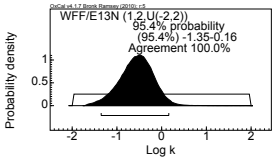


(b) Step-size parameter

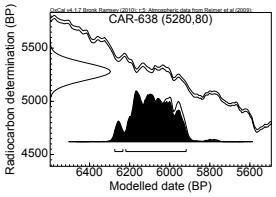


(c) Date of elm decline

Site: WFF E1N
Model: P_Sequence
Date: CAR-427
95.4% range: 5885–5491
Outliers: -
Lat: 51.85
Long: -3.71
Data source: Smith and Cloutman (1988); Dresser (1985)

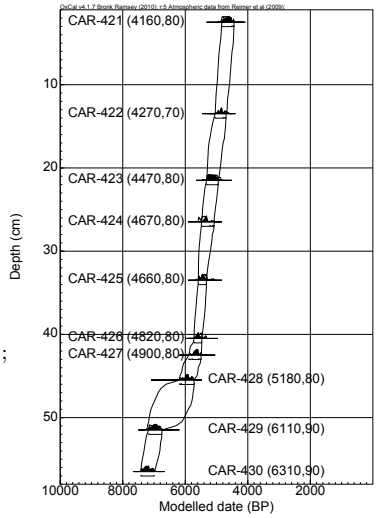


(a) Chronology

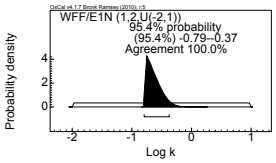


(b) Step-size parameter

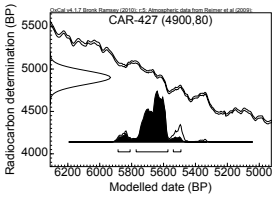


(c) Date of elm decline

Site: WFF EE17E
Model: P_Sequence
Date: CAR-623
95.4% range: 5710–5322
Outliers: CAR-622 (6%)
Lat: 51.85
Long: -3.71
Data source: Smith and Cloutman (1988); Dresser (1985)

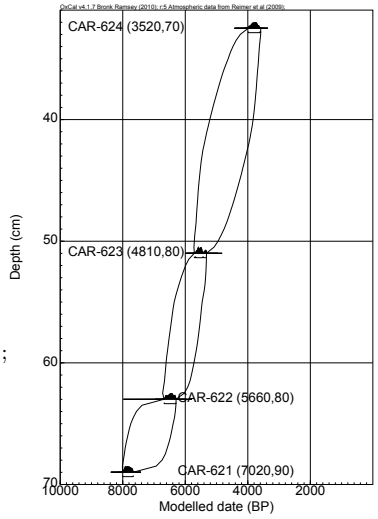


(a) Chronology

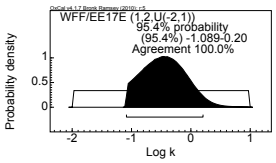


(b) Step-size parameter

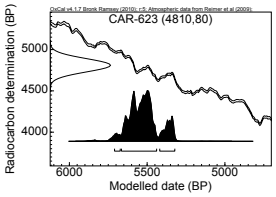


(c) Date of elm decline

| | |
|---|---|
| Site: | WFF G00 |
| Model: | P_Sequence |
| Date: | CAR-687 |
| 95.4% range: | 5928–5621 |
| Outliers: | CAR-692 (6%) |
| Lat: | 51.85 |
| Long: | -3.71 |
| Data source: | Smith and Cloutman (1988); Dresser (1985) |

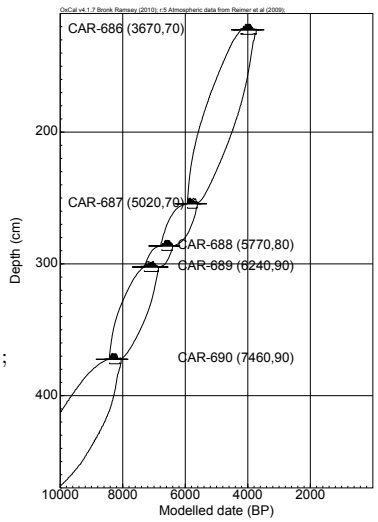


(a) Chronology

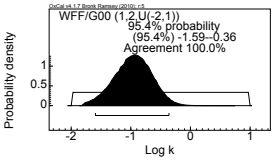


(b) Step-size parameter

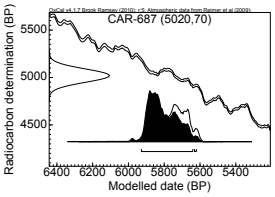


(c) Date of elm decline

# Appendix C

# CQL listings

The chronology building software, OxCal was used to build the majority of models described in this thesis and the CQL codes outlining the structure of various models are listed here. Data for individual models are available in Appendix B and are not included in the listings below.

## C.1 Iron Age in Israel

The Iron Age chronology In Israel was modelled using a contiguous trapezoidal phase model.

```
Options(){
  Resolution=1;
  UniformSpanLimits=0;
};
Plot(){
  Outlier_Model("RScaled",T(5),U(0,4),"r");
  Outlier_Model("General",T(5),U(0,4),"t");
  Sequence(){
    Boundary("Start IA"){
      Transition();
      Start();
      End();
    };
    Phase("Iron IA"){
    ... data attributed to Iron IA in here ...
    ... in the form of ...
      R_Combine("RT-4501"){
        Outlier("General", 0.05);
        R_Date("RT-4501.3", 2790, 40){ Outlier("RScaled", 0.05); };
        R_Date("RT-4501.4", 2764, 50){ Outlier("RScaled", 0.05); };
        R_Date("RT-4501.5", 2767, 40){ Outlier("RScaled", 0.05); };
      };
      ... for radiocarbon determinations belonging to the same sample or stratum ...
    };
    Boundary("End IA/Start IB"){
      Transition("",U(0,100));
      Start();
      End();
    };
    Phase("Iron IB"){
    ... data attributed to Iron IB in here ...
    };
    Boundary("End IB/Start Early Iron IIA"){
      Transition("",U(0,100));
      Start();
      End();
    };
    Phase("Early Iron IIA"){
```

```
    ... data attributed to Early Iron IIA in here ...
    };
    Boundary("End Early Iron IIA/Start Late Iron IIA"){
      Transition("",U(0,100));
      Start();
      End();
    };
    Phase("Late Iron IIA"){
    ... data attributed to Late Iron IIA in here ...
    };
    Boundary("End Late Iron IIA/Start Iron IIB"){
      Transition("",U(0,100));
      Start();
      End();
    };
    Phase("Iron IIB"){
    ... data attributed to Iron IIB in here ...
    };
    Boundary("End IIB"){
      Transition();
      Start();
      End();
    };
  };
};
```

## C.2 The Cape Riva tephra

The age of the Y-2 tephra was estimated using a combination of `P_Sequence` and `Sequence` functions, and phase models.

```
Options(){
  BCAD=FALSE;
};
Plot(){
  P_Sequence("Tenaghi Philippon",1,20,U(-1,2)){
    Boundary();
    R_Date("Beta-246628",43100,1200){ ... };
    ...
    C_Date("CI",39280,110){ ... };
    ...
    Date("CR"){ ... };
    ...
    R_Date("Poz-15890",1950,30){ ... };
    Boundary();
  };
  P_Sequence("ML01",1,20,U(-1,2)){
    Boundary();
    R_Date("SUERC-3032",41384,4128){ ... };
    Date("=CI"){ ... };
    ...
    Boundary("=CR"){ ... };
  };
  Sequence(){
    Tau_Boundary();
    Phase(){
      R_Date("DEM-650", 18527, 145);
      R_Date("DEM-653", 18244, 143);
    };
    Boundary("=CR");
  };
};
```

## C.3 Taforalt chronology

The Taforalt chronology was constructed using a combination of `P_Sequence` and `Sequence` functions.

```
Plot(){
  Outlier_Model("General",T(5),U(0,4),"t");
  Outlier_Model("RScaled",T(5),U(0,4),"r");
  P_Sequence("yellow 3",1,10,U(1,2)){
    Boundary();
    R_Combine("OxA-16277/78"){ ... };
    ...
    R_Date("OxA-16275",20560,90){ ... };
    R_Date("OxA-16274",20630,90){ ... };
    ...
    Boundary("MSA");
  };
  P_Sequence("yellow 2",1,10,U(1,4)){
    Boundary();
    R_Date("OxA-16273",17515,75){ ... };
    ...
    R_Date("OxA-16267",14005,60){ ... };
    Boundary();
  };
  P_Sequence("yellow Y1",1,10,U(1,4)){
    Boundary();
    R_Date("OxA-22788",12850,55){ ... };
    ...
    Boundary("YG"){ z=4; };
  };
  P_Sequence("grey",1,10,U(0,2)){
    Boundary("=YG"){ z=4; };
    ...
    Date("C"){ z=3.97; };
    R_Date("OxA-13478",12495,50){ ... };
    ...
    Date("B"){ z=0.69; };
    Date("A"){ z=0.61; };
    ...
    R_Date("OxA-13516",11065,45){ ... };
    R_Date("OxA-13479",10935,40){ ... };
    ...
    Boundary();
  };
  Sequence(){
    Boundary("=OxA-16275");
    R_Date("OxA-22910",20030,90){ ... };
    Boundary("=OxA-16274");
    Date("=C");
    Phase(){
      R_Combine("OxA-22784/85"){
        Outlier("General", 0.05);
        R_Date("OxA-22784",12660,70){ ... };
        R_Date("OxA-22785",12500,55){ ... };
      };
      R_Date("OxA-22787",12545,55){ ... };
      R_Date("OxA-22902",12370,50){ ... };
      R_Date("OxA-22904",12490,50){ ... };
    };
    Date("=OxA-13478");
    Date("=B");
    Phase(){
      R_Date("OxA-24113",11540,50){ ... };
      R_Date("OxA-23405",11615,50){ ... };
    };
    Date("=A");
    Date("=OxA-13516");
    Phase(){
      R_Date("OxA-23404",10870,45){ ... };
      R_Date("OxA-13480",10950,45){ ... };
    };
```

```
    Date("=OxA-13479");
  };
};
```

## C.4 Mid-Holocene elm decline

A two-stage approach was employed to investigate the mid-Holocene elm decline. Firstly, `P_Sequence` and `Sequence` functions were used to construct individual site chronology. Secondly, the trapezoidal phase model was used to investigate the timings of the elm decline, and also the relative order of events in different regions.

```
Plot(){
  P_Sequence("",1,20,U(-2,2)){
    Boundary();
    ...
    Boundary();
  };
};
// for a P_Sequence model

Plot(){
  Sequence(){
    Boundary();
    ...
    Boundary();
  };
};
// for a Sequence model

Plot(){
  Sequence(){
    Boundary(){
      Start("A");
      Transition();
      End("B");
    };
    Phase(){ ... };
    Boundary(){
      Start("C");
      Transition();
      End("D");
    };
  };
};
// for a single phase.  See text for details on the using an order matrix to determine the relative
// order of events in different regions.
```